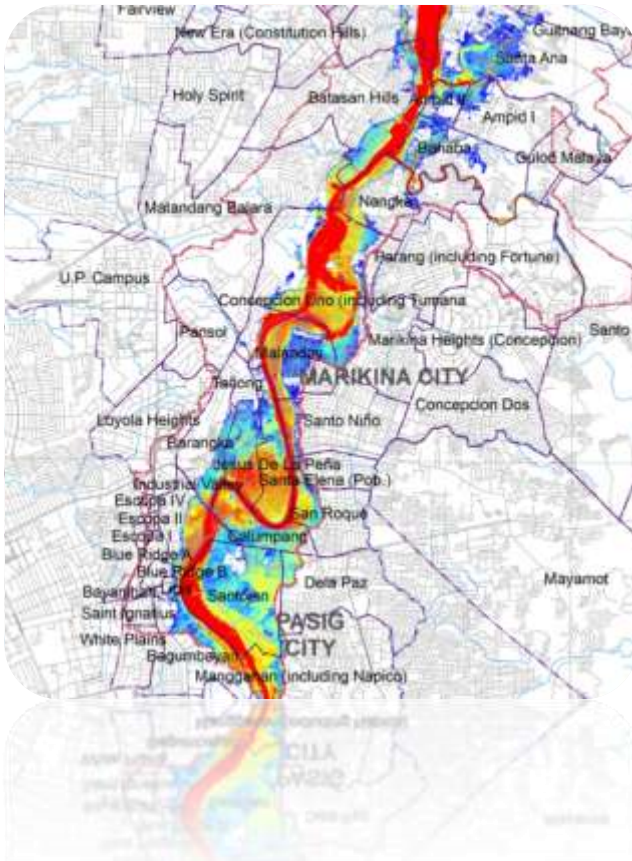# TERMINAL REPORT

Surveys and Measurement Technologies for Flood Control, Mitigation and Management Systems

Project 3: Modeling of Flashflood Events Using Integrated GIS and Hydrological Simulations

June 2013

Summary

Program Title: Surveys and Measurement Technologies for Flood Control, Mitigation and Management Systems (SMTFCMMS)

Project Title: Project 3: Modeling of Flash-flood Events using Integrated GIS and Hydrological Simulations

Project Leader: Engr. Jojene R. Santillan

Program Leader: Dr. Enrico C. Paringit

Research Staff:
- Engr. Roseanne V. Ramos (SRAssist.: May – Nov. 2011; SRS I: Nov. 2011 – March 2012; SRS II: April 2012 – March 2013; RAssoc. I: April – June 2013)
- Ms. Girlie David (URA I: July 2012 – March 2013)
- Ms. Sabrina M. Recamadas (URA I: July 2012 – March 2013)
- Engr. Rudolph L. Peralta (URA I: July 2012 – March 2013)
- Engr. Edgardo Macatulad (SRS I: May – Nov. 2011)

L2 Project Staff: Ms. Ellen Cruz-Ignacio (May 2012 – March 2013)
                        Engr. Jessie Linn P. Ablao (May 2011 – May 2012)
                        Engr. Louie P. Balicanta (May 2011 – May 2012)

Implementing Agency: Training Center for Applied Geodesy and Photogrammetry
                        University of the Philippines
                        Diliman, Quezon City

Duration of the Project:
        Year 1:   April 1, 2011 – March 30, 2012
        Year 2:   April 1, 2012 – March 30, 2013; extended until June 30, 2013

Source of Fund: Philippine Council for Industry, Energy and Emerging Technology Research and Development, Department of Science and Technology (PCIEERD DOST)

Acknowledgements

Table of Contents

List of Abbreviations

ASTER	Advanced Spaceborne Thermal Emission and Reflection Radiometer
GDEM	Global Digital Elevation Model
DEM	Digital Elevation Model
DOST	Department of Science and Technology
GPS	Global Positioning System
HEC HMS	Hydrologic Engineering Center Hydrologic Modeling System
HEC RAS	Hydrologic Engineering Center River Analysis System
LIDAR	Light Detection and Ranging
MBES	Multi-Beam Echosounder System
MRB	Marikina River Basin
MSL	Mean Sea Level
NAMRIA	National Mapping and Resource Information Authority
PAGASA	Philippine Atmospheric, Geophysical and Astronomical Services Administration
PHIVOLCS	Philippine Institute of Volcanology and Seismology
SBES	Single-Beam Echosounder System
SJRB	San Juan River Basin
UTM 51	Universal Transverse Mercator Zone 51
WGS 1984	World Geodetic System 1984

List of Tables

List of Figures

Abstract

The September 2009 flash floods caused by Tropical Storm (TS) Ketsana (Local Name: *Ondoy*) that devastated Metro Manila and its surroundings exemplified the need for an accurate and reliable flood forecasting tool for determining the possible duration and extents of floods and for assessing the risks due to this disaster. This project was proposed and implemented in response for this need. Using the Marikina River Basin as pilot area, a flood model was developed using a framework that utilized field observations, Remote Sensing (RS), Geographic Information System (GIS), and numerical modeling. The flood model consists of two components. The first component deals with the upstream watershed hydrology, wherein a hydrological model based on HEC HMS was developed to estimate how much runoff is produced during a rainfall event. The second component deals with the river and flood plain hydraulics which aims to determine the behavior of water coming from the upstream watershed as it enters the main river and travels downstream towards the sea. This was done using HEC RAS. The combination of HEC HMS and HEC RAS resulted into a flood model that can be used for a variety of purposes: (1) for water level forecasting and flood inundation extent monitoring, (2) for reconstruction of actual flood events, (3) for simulation of flooding due to hypothetical extreme rainfall events, and (4) for flood hazard mapping and assessment. To explore the usefulness and the repeatability of the methodology developed and utilized in this project, it has been applied in the San Juan River Basin.

The project's major outputs are available online at http://dge.upd.edu.ph/proj3/. Two online applications have been developed through the project: I aM AWaRE and Marikina RELiEF. **I aM AWaRe** (or **I**nund**a**tion **M**onitoring **A**nd **W**ater Level Forec**a**sting in **Ri**ve**r**s, http://iamawareph.wordpress.com) is an online geo-visualization tool for monitoring flood inundation and forecasting of water levels in rivers as applied to the Marikina, San Juan and Pasig Rivers in Metro Manila, Philippines. On the other hand, Marikina RELiEF (http://mrbforecast.wordpress.com) is an online application that provides water level forecasts at three locations along Marikina River. The information displayed in these applications are results of flood models developed by the project.

The project was also a contributor to Project NOAH (Nationwide Operational Assessment of Hazards, http://noah.dost.gov.ph) through uploading of near-real time flood inundation extents to its website. The flood inundation extent information which are updated every 10-minutes (depending on data availability) is similar to the ones displayed in the I aM AWaRe application.

Chapter 1. Introduction

Background

Floods are a persistent problem that needs to be addressed in a more scientific way in order to mitigate its costly impacts to properties and human lives. Flashfloods, in particular, are among the most destructive natural disasters that strike people and infrastructures, and it is not surprising that forecasting such events has increasingly become a high priority in many countries [1].

Figure 1. Flooding in Marikina River during the August 2012 *Habagat* event. (*Photo credits: Google Earth; newsinfo.inquirer.net*)

In the Philippines, the September 2009 flooding caused by Tropical Storm (TS) Ketsana (Local Name: *Ondoy*) that devastated Metro Manila and its surroundings [2] exemplified the need for an accurate and reliable flood forecasting tool for determining the possible duration and extents of floods and for assessing the risks due to this disaster. It can be recalled that on September 26, 2009, TS Ketsana dumped a month's worth of rain in less than 24 hours and caused flooding in Metro Manila, killing at least 300 people and displacing another 700,000 [3]. The need for an accurate and reliable flood monitoring and water level forecasting tools for the Marikina River has again been exemplified in August 2012 when an eight-day period of torrential rain and thunderstorms brought about by the strong movement of the Southwest Monsoon caused the Marikina River to overflow and brought damages to places near the banks of the river. The intense, nonstop rains that occurred from August 1 to August 8, 2012 have been informally known as *Habagat*. The event caused the heaviest damage in Metropolitan Manila since TS Ketsana [4]. The same scenario happened again in August 2013 when heavy to torrential rains (7.5 mm/hr to as much as 30 mm/hr or more) were pouring over Metro Manila and nearby provinces. Raining continued for more

than 3 days and caused flooding in different areas, most especially in the vicinity of Marikina, San Juan and Pasig Rivers. As the flood plain is host to densely populated areas as well as commercial and industrial zones, flooding due to overflowing of the river resulted to significant damage to human lives and properties.

Statement of the Problem

In the case of Marikina River, several water level and rainfall monitoring stations are in place within and near the MRB and along the Marikina River that can provide up-to-date status of water levels at selected sections of the main river, and of rainfall depth at different locations. While these monitoring stations are helpful, what remains to be lacking is a system that can provide two levels of information during the occurrence of flood events: (1) near-real time information on the status of water levels all throughout the river, especially if one wanted to know the current extent of flooding along the river and the areas that are presently flooded, and (2) forecasts on how water level will rise (or recede) at different locations along the river as rainfall events occur in the MRB. Providing this kind of information is useful in informing the public as to the current extent and depth of flooding in the Marikina River that could then assist in preparation for evacuation. This will also aid in estimating the severity of damage as flooding progresses.

Objectives

The main objective of this research is the development of a flood model by utilizing field observations, Remote Sensing (RS), Geographic Information System (GIS), and hydrological simulations. The detailed objectives are:

1. To generate necessary data/information from different sources such as remotely sensed images, surveying and cartographic data, to form the basic inputs of the flood model;

2. To develop a flood simulation model suitable for Philippine setting, particularly the case of Marikina River flood plain as the area of interest; and

3. To incorporate all components into a Geographic Information System environment for the modeling, simulation, analysis and information retrieval tool for disaster response and prevention.

Significance

The model can be eventually applied at an operational scale by the flood forecasting and warning system (FFWS) program of PAGASA and the flood control offices in the area of interest.

This model can also provide the details necessary for the development of an accurate and reliable forecasting for assessing disaster risks. Examples of which are estimated extent, duration, degree (depths) of the flood that is about to occur at any given amount of rainfall, evacuation and relief operation route, cost estimate of damaged properties, etc.

The project can be a first step in the study of the characteristics of flooding events from extreme rainfall conditions. Such characteristics can be incorporated to the model through the use of Rainfall Intensity Duration Frequency Curves (RIDFs). RIDFs of extreme rainfall events in different areas in the country have been generated by the PAGASA-DOST through statistical analysis of historical data. If successful, the output will help us analyze and understand the characteristics of such floods caused by torrential rainfall, its risk implications for the community and its effects to the environment.

The Project Area

The pilot area for flood model development is the Marikina River Basin and its floodplains -- specifically those within the lower part of the Marikina-Pasig River Basin and the floodplain where the municipalities of Rodriguez, San Mateo, and the cities of Marikina and Pasig areas are located (Figure 2).
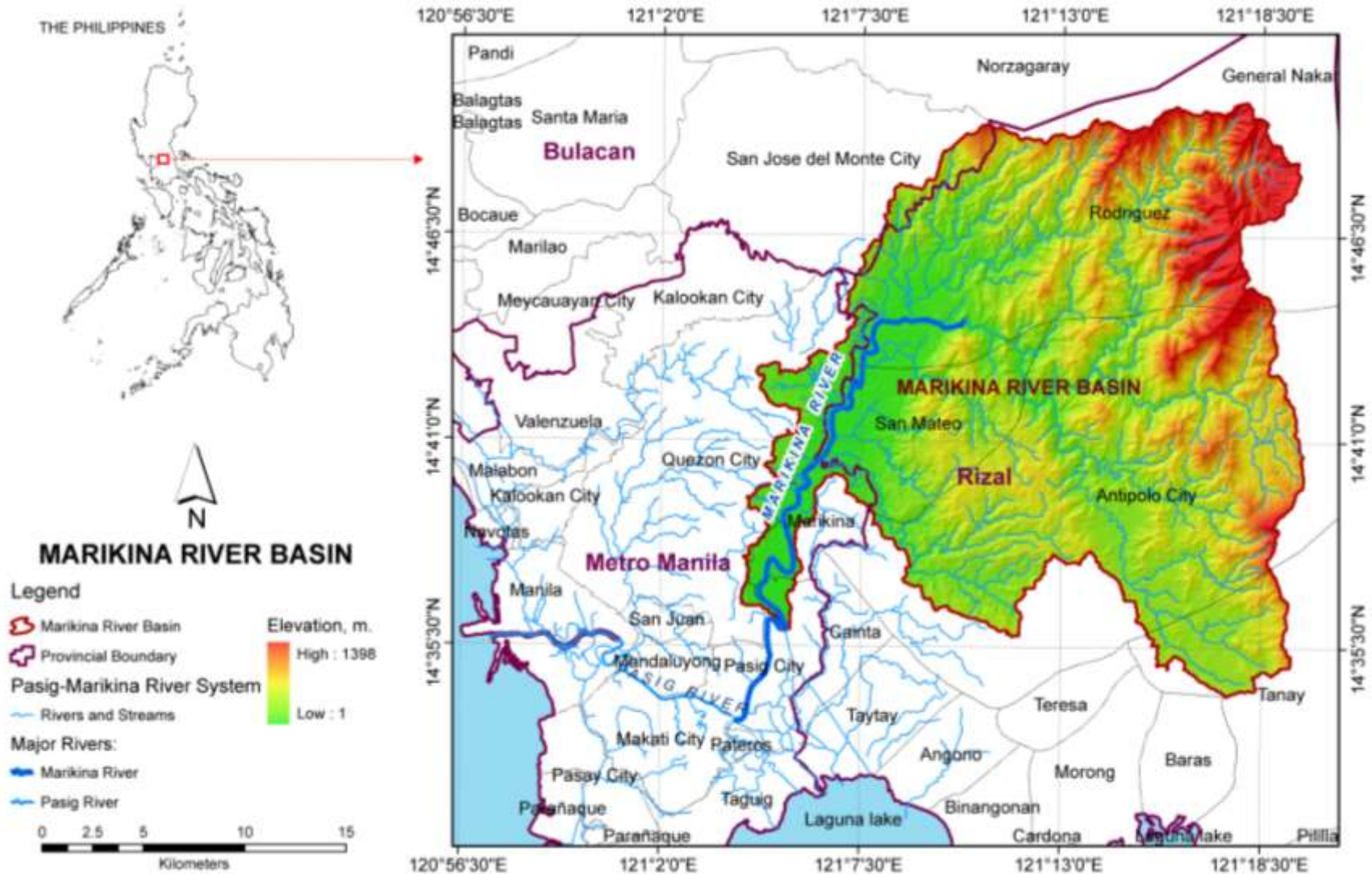
Figure 2. The Marikina River Basin, the project's pilot area.

Scientific Basis/Theoretical Framework

A simple modeling framework (Figure 3) is adapted to implement the project. A flood model is composed of two components. The first component deals with the upstream watershed hydrology, wherein a hydrological model is developed to estimate how much runoff is produced during a rainfall event. The second component deals with the river and flood plain hydraulics which aims to determine the behavior of water coming from the upstream watershed as it enters the main river and travels downstream towards the sea.
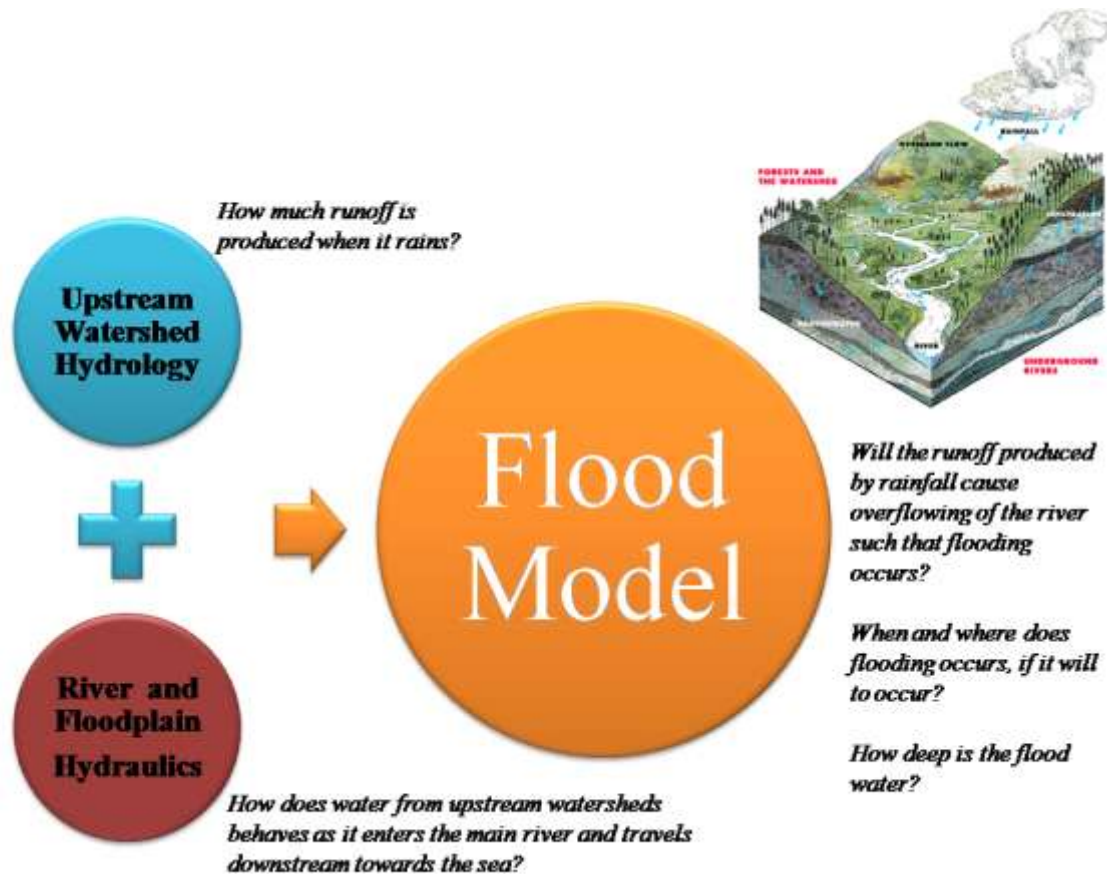
Figure 3. The theoretical framework adapted in project implementation.

With these two components combined, a flood forecasting tool is developed and this could be used to answer several flood-related questions. For example,

- Will the runoff produced by rainfall cause overflowing of the river such that flooding occurs?
- When and where does flooding occur, if it will to occur?
- How deep is the flood water?

The flood model can also be used to reconstruct past flood events. Reconstructing flood events caused by heavy/torrential rains can assist in understanding how flooding

occurs, and in mapping areas that were flooded. If an area has been flooded before, it is more likely that it will be flooded again in the near future. If this is known through flood reconstruction, then it is easy to pinpoint which areas are to be avoided should heavy/torrential rains will pour over the area.

Another application of the flood model is to generate flood hazard maps – maps that categorizes flood hazard based on depth of water (low: less than 0.5 m; medium: greater than or equal to 0.5 m but less than 1.5 m.; high: greater than or equal to 1.5 m). This can be done by simulating the effects of hypothetical, extreme rainfall events (e.g., rainfall events with different return periods) to the generation of runoff in upstream watersheds, and then determining the behavior of water coming from the upstream watershed as it enters the main river, including its overflow from the banks towards the flood plain.

For near-real time applications, the flood model can also be used to generate the latest flood inundation extent by using actual (recorded) water level from monitoring stations instead of discharge data simulated by the watershed hydrologic model.

To implement this framework, the study area needs to be schematized, i.e., we separate the flood plains from the upstream watersheds and look for the locations where water from the upstream watersheds enters the flood plain. This is illustrated in Figure 4.

Overview of Methodology

Figure 5 provides an overview of the project's methodology. Although the methodology consists of several sets of procedures, it can be summarized into three major components: field observations, secondary data collection, and flood model development and applications.

Field observations aim to gather primary topographic, hydrographic and hydrological data necessary for flood model development. This includes river and floodplain geometries (in terms of river profile, bed topography and river cross-sections), rainfall, water level and water velocity. River and flood plain geometries were collected using surveying instruments such as Global Positioning Systems (GPS), total station, digital levels, as well as single-beam and multi-beam echosounders (SBES/MBES). Hydrological data were collected through simultaneous installation of datalogging sensors (rain gauge, depth gauge, and velocity meters) in specific period of time.

In addition to field observations, collection of secondary data aims to compile spatial and hydrological datasets that are also required in developing the flood model. Such datasets include Digital Elevation Models (DEMs), digital elevation data (e.g., contours and spot heights), hydrological data (water level and rainfall) recorded by monitoring stations, satellite images, and administrative boundaries, among others.

All data that has been collected were then processed, analyzed and integrated through GIS to create a database of spatial and hydrological data. This database was then utilized in the development, calibration and validation of the flood model. The flood model consisted of upstream hydrological model based on the Hydrologic Engineering Center (HEC) –

Hydrological Modeling System (HMS), and the river and floodplain hydraulic model based on HEC – RAS (River Analysis System). After calibration and validation, the flood model was then applied to reconstruct actual flood events, to create flood hazard maps, and for near-real time inundation monitoring and water level forecasting. GIS is an important tool in the project's methodology as it made possible rapid flood model development, calibration, validation and application, including development of online visualization tools. However, it should be noted that the use of GIS in this project is not only as a software but more of a system for collecting, storing, retrieving at will, transforming, and displaying spatial data [5], including hydrological data, for flood modeling applications.
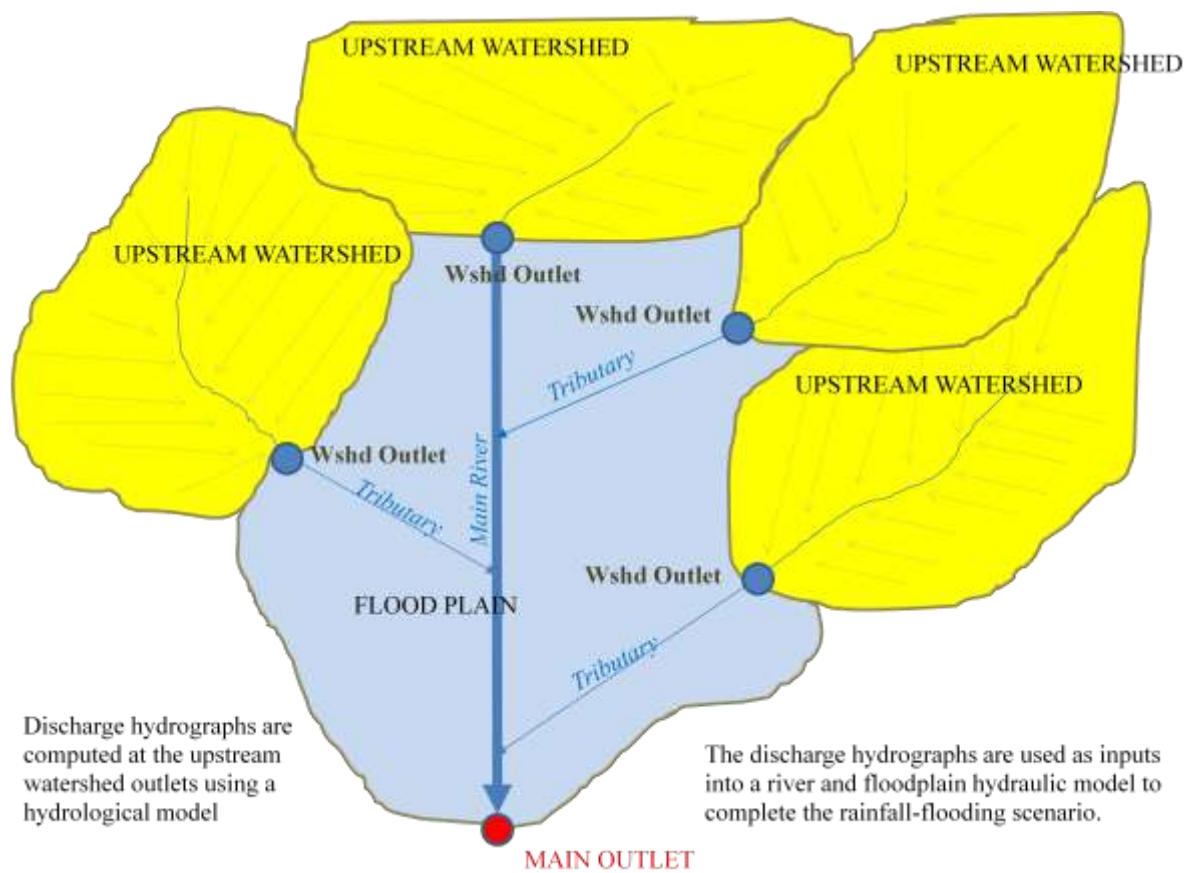
Figure 4. A schematization of a flood model domain wherein the upstream watersheds and the flood plains are identified.
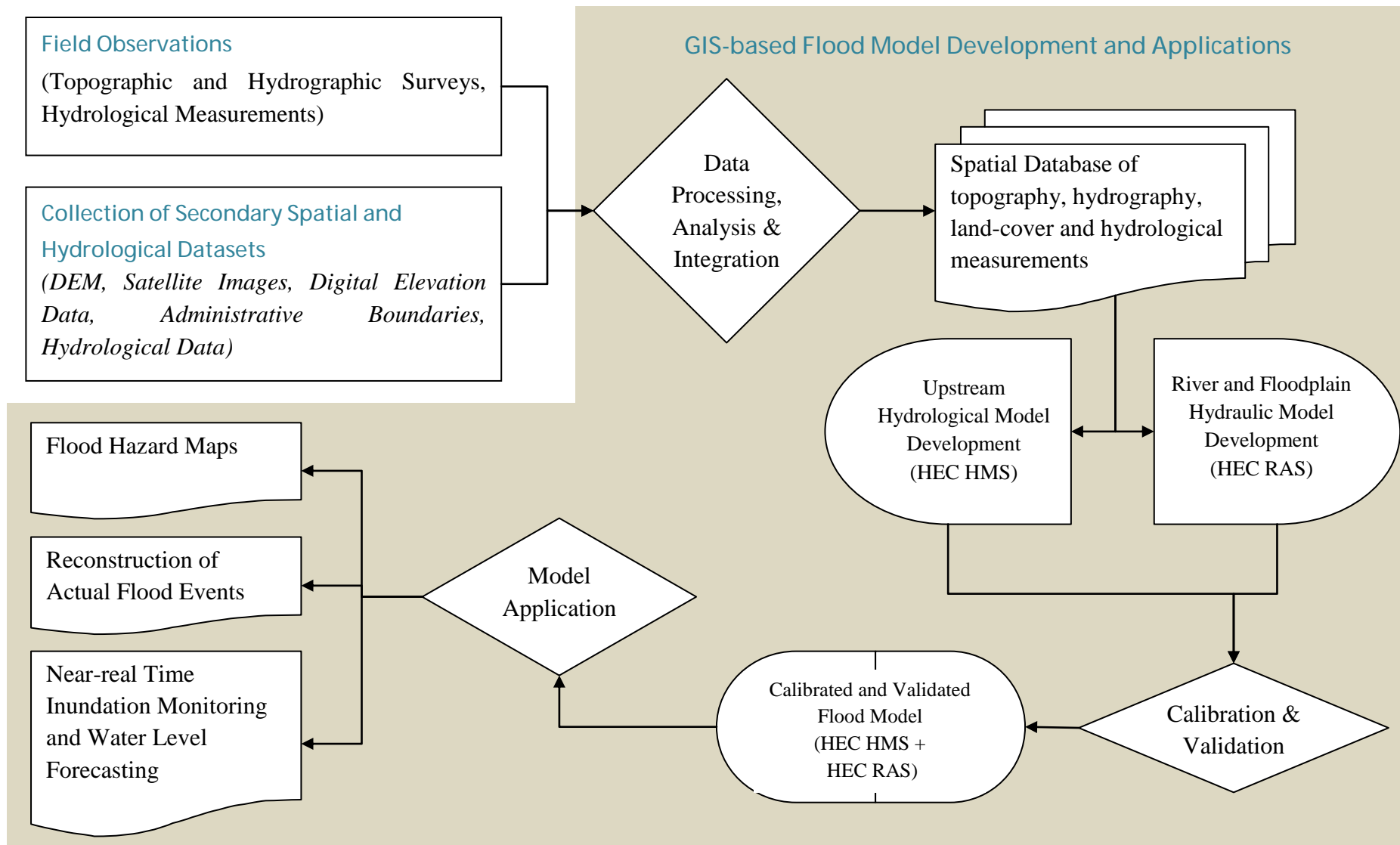
Figure 5. An overview of the project's methodology where GIS plays a major role from model development to application.

Datasets Used

Table 1 summarizes the datasets used in the project, some of which were obtained through field observation, and most are through secondary data collection.

Expected Outputs

The following are the expected outputs of the project for the pilot area which is the Marikina River and its floodplain:

1. Flood model consist of HEC HMS and HEC RAS
   a. for water level forecasting and flood inundation extent monitoring
   b. for reconstruction of actual flood events
   c. for simulation of flooding due to hypothetical, extreme rainfall events
2. Simulation of the flooding events that have occurred.
3. Flood extent and flood height information in the project area during the flooding event as simulated by the flood models (flood depth maps).
4. Flood hazard maps of the project area.

To explore the usefulness and the repeatability of the methodology developed and utilized in this project, it has been applied in the San Juan River Basin where the above list of outputs was also generated.

Structure of this Report

This report has 11 chapters. Chapter 1 (this chapter) has provided an introduction on why this project was conducted, its objectives, significance, methodology and expected outputs. Chapter 2 provides a review of related literature pertaining to the objectives of the project. The next chapters provide individual discussions on how the project objectives were attained for the Marikina River Basin, as well as reports on the application of the methodology in the San Juan River Basin. The two dimensional approach in modeling floods in Marikina River is discussed in Chapter 10. The findings, conclusions and recommendations are summarized in Chapter 11. An appendix of publishable and published reports is also included.

Table 1. Summary of datasets used in the project.

Type of Data	Dataset name	Purpose	Source/Method of Collection
River and Floodplain Geometry	Elevation profile	HEC HMS and HEC RAS model development and parameterization	Field observation
	Cross-section	HEC HMS and HEC RAS model development and parameterization	Field observation
	Bed topography	HEC HMS and HEC RAS model development and parameterization	Field observation
Hydrological Data	Water level	HEC HMS and HEC RAS model calibration and validation	Field observation and secondary data collection (from EFCOS and ASTI monitoring stations)
	Water velocity	HEC HMS model calibration and validation	Field observation
	Rainfall	HEC HMS model calibration and validation	Field observation and secondary data collection (from EFCOS and ASTI monitoring stations)
	RIDF Curves	Generation of time series of 24-hour hypothetical rainfall events with return periods of 2, 5, 10, 25, 50 and 100 years.	DOST PAGASA
Spatial Data	Metro Manila MMEIRS Elevation Data	HEC HMS model development and parameterization	PHIVOLCS
	NAMRIA 1:50,000 Topographic Maps	HEC HMS model development and parameterization	NAMRIA
	DEMs:		
	- ASTER GDEM	HEC HMS model development and parameterization	NASA Reverb http://reverb.echo.nasa.gov/
	- LIDAR DEM	HEC RAS model parameterization and flood inundation and hazard mapping	Collective Strengthening of Community Awareness for Natural Disasters (CSCAND)
	Satellite Images:		
	- ALOS AVNIR-2	Land-cover and surface roughness estimation for HEC HMS and HEC RAS	NAMRIA; SMTFCMMS-Project 4
	- Worldview-2	Land-cover and surface roughness estimation for HEC HMS and HEC RAS	Purchased
	- ALOS PALSAR	Validation of flood model generated inundation extents	Purchased
	- RADARSAT 2	Validation of flood model generated inundation extents	Purchased

Chapter 2. Literature Review

Floods and Flash-floods

Flood is an overflowing of the normal confines of a stream or other body of water, or the accumulation of water over areas that are not normally submerged [6]. Flooding may occur if there is an overflow of water from water bodies, such as river or lake, or it may occur due to an accumulation of rainwater on saturated ground [7]. Some floods develop slowly, while others such as flash floods can develop in just a few minutes and without visible signs of rain. According to the United Nations, floods have the greatest damage potential of all natural disasters worldwide and affect the greatest number of people [8].

The United Nations Economic and Social Commission for Asia and the Pacific have a simple yet informative description of the flooding process [9]. When heavy storm rainfall occurs, the precipitation will initially be intercepted on vegetation or infiltrated into the soil, where it will build up soil moisture levels and reduce infiltration capacity. When this capacity is exceeded, overland flow will commence and a build-up of surface run-off, flowing towards the nearest watercourse, will commence. Once this run-off reaches a watercourse, the rate of streamflow will commence to increase and, if the supply of run-off continues, to cause the stream to rise and perhaps overflow its banks. At the same time, precipitation which has infiltrated into the soil may move laterally as interflow or, at a deeper level, as groundwater flow, and eventually enter the watercourse and supplement the flood streamflow.

Floods have important characteristics which can help determine the magnitude and cost of their disastrous effects [9]:

a. The peak depth of inundation, which determines the extent and cost of damage to buildings and crops and the cost and feasibility of mitigation measures;
b. The areal extent of inundation, which determines similar factors;
c. The duration of flooding, which is an important factor in determining the degree of damage and inconvenience caused;
d. The rate of rise of the flood event, which determines the effectiveness of flood warning and evacuation procedures;
e. The velocity of flood flow, which determines the cost of flood damage and the feasibility and design of levees and flood proofing structures;
f. The frequency of flooding, which expresses the statistical characteristics of flood events of a given magnitude and determines the long-term average costs and benefits of flooding and flood mitigation;
g. The seasonability of flooding, which determines the cost of flood damages, particularly when agricultural areas are inundated.

According to these characteristics, two types of flooding can be distinguished: riverine flooding and flash flooding. Riverine flooding occurs when the flow in a river channel exceeds its bankfull capacity, overflowing the normal banks and inundating the adjacent floodplain. It is a phenomenon associated with hydrologically large catchments and

its most significant effect is the widespread, comparatively shallow inundation of large expanses of flat terrain [**9**]. On the other hand, flash flooding is a phenomenon principally associated with watersheds which are hydrologically small. It is commonly caused by intense convective storms of comparatively short duration but producing highly intense rates of rainfall. The severity of flooding is increased if the watershed is steep and its surface has low infiltration capacity. The duration of the flooding is short but the depth of flooding can be considerable and very extensive damage may result [**9**]. This exemplified by a study of Doswell [**10**] based on observations from the United States which showed that flash flooding was typically triggered when rainfall rates was at least 25 mm per hour sustained for at least 1 hour. Because they occur very rapidly and with little warning, flash floods can cause substantial injury and loss of life [**9**].

Flood Modeling and Forecasting

Ramirez [**11**] refers to flood modeling as the processes of transformation of rainfall (hydrology) into a flood hydrograph and to the translation of that hydrograph throughout a watershed or any other hydrologic system (hydraulics). In this manner, the flooding processes – which consist of upstream watershed hydrological processes and river and floodplain hydraulic processes – as described in [**9**], are approximated either physically or mathematically (through the use mathematical equations) where the relationships between system state, input and output are represented.

Based on a number of published literatures, Badilla [**12**] summarized the differences and applications of hydrological and hydraulic models in the context of flood modeling. A hydrologic model is a mathematical representation of hydrological processes in a watershed in a simplified form. It has been primarily used to understand and explain hydrological processes and for hydrological prediction. This model can be of different types depending on whether the approach is deterministic or stochastic. A hydrologic model is deterministic if it represents the physical processes in a watershed without consideration of randomness. It becomes a stochastic model when it incorporates in its mathematical representation random variables and their probability of distribution in the parameter space. In flood modeling, it is mainly used to simulate discharge in a watershed [**12**]. On the other hand, hydraulic models utilize discharge computed by the hydrologic models to simulate movement of flood water along waterways, storage elements and hydraulic structures. Using the continuity and momentum equations, it can simulate flood levels and flow patterns and can model the complex effects of backwater or tidal intrusion, overtopping of embankments, waterways confluences and diversions, bridge constrictions, weirs, culverts, and pumps and other obstructions on the flow in the river system [**12**].

One of the most commonly used hydrologic and hydraulic modeling systems are the Hydrologic Engineering Center Hydrologic Modeling System (HEC HMS) and HEC RAS (River Analysis System), respectively. HEC HMS is a generalized modeling system designed to simulate the precipitation-runoff processes of dendritic watershed systems with a wide

range of applicability large river basin water supply and flood hydrology, and small urban or natural watershed runoff [13]. Some applications of HEC HMS include examining rainfall-runoff processes in a small oil palm catchment in Malaysia [14]; event and continuous and hydrologic modeling to reveal quantity, variability, and sources of runoff in the Mona Lake watershed in West Michigan, USA [15]; modeling rainfall-runoff relations for a single rain event in Jordan [16]; and hydrological modeling of typhoon-induced extreme storm runoffs from Shihmen watershed to reservoir, Taiwan [17]. The study of De Silva et al. [18] demonstrated potential application of HEC HMS in disaster mitigation, flood control and water management in medium size river basins in tropical countries. In the Philippines, there are few studies that utilized HEC HMS in hydrological modeling. Santillan et al. [19] used HEC HMS to elucidate impacts of land-cover change on runoff generation during rainfall events in a Mindanao watershed. For flood studies, Catane et al. [20] utilized HEC HMS to determine peak discharges during the 2008 Panay Island landslide-amplified flashflood, while Abon et al. [2] used it to reconstruct the Tropical Storm Ketsana flood event in Marikina River, Philippines. Abon et al. [21] also used it as a major component of community-based monitoring for flood early warning system in central Bicol River basin.

On other hand, HEC RAS is an integrated system of software designed to perform one-dimensional hydraulic calculations for a full network of natural and constructed channels [22]. HEC RAS requires river cross-sections and Manning's roughness coefficients as its geometric parameters. The basic computational procedure is based on the solution of the one-dimensional energy equation with energy losses evaluated by friction through Manning's equation and contraction/expansion. HEC RAS utilizes the momentum equation in situations where the water surface profile is rapidly varied (e.g., in mixed flow regimes, flow in bridges and at river confluences). One of the most common use of HEC RAS is flood inundation mapping provided that inflow data is available (e.g., from hydrological simulations or actual flow measurements) to serve as the model's boundary conditions [23]. HEC RAS provide water surface levels at the cross-sections which can be converted into inundation extents by re-projecting the water levels onto a DEM through the use of GIS techniques [24]. The accuracy of HEC RAS in predicting flood inundation extents was found by [24] to be better than those of two-dimensional models provided that it is adequately calibrated on hydrometric data. An adequate prediction of flood extent is also possible when water free surfaces are extrapolated onto a high resolution DEM.

The work of Knebl et al. [25] exemplified the combined use of HEC HMS and HEC RAS for flood modeling in the San Antonio River Basin, Texas, USA which is a region subject to frequent occurrences of severe flash flooding. They utilized HEC HMS to convert precipitation excess to overland flow and channel runoff, and HEC RAS to model unsteady state flow through the river channel network based on the HEC-HMS-derived hydrographs. The HEC RAS model then provided outputs of floodplain polygons that show areas that were inundated due to bank overflows.

Pedsizai [26] reasons that the essence of modeling floods is to enhance forecasting that allows for effective prediction and rapid relay of communication to mitigate impending

or progressing flood hazard. At the core of flood warning systems is a flood forecasting procedure that essentially predicts stream flow using precipitation data and other relevant hydrometeorological parameters using rainfall-runoff models [27]. Provision of flood forecasting and warning systems can bring significant benefits through giving forewarning of imminent flooding, allowing timely evacuation, relocation of valuables, and management of affected infrastructure [28]. Being the most destructive natural disasters that strike people and infrastructures [8] and in a very frequent manner [29], it is not surprising that modeling of floods for forecasting purposes has increasingly become a high priority in many countries [1].

Remote Sensing and GIS in Flood Modeling, Forecasting and Hazard Assessment

The role of geospatial technologies - remote sensing and GIS - has been very important in flood modeling, forecasting and hazard assessment [29,30]. Flood modeling requires the analyst to acquire, maintain, and extensively utilize a spatially referenced database. Remote sensing and GIS are excellent tools that can fulfill these requirements [30].

Remote sensing's role in modeling watershed hydrology as part of the whole modeling process is due to its ability to provide spatially continuous data, its potential to provide measurements of hydrological variables not available through traditional techniques, and its ability to provide long term, global data, even for remote and generally inaccessible regions of the Earth [31]. As explained by Santillan et al. [19], it is perhaps for land-cover data derivation that RS has made its largest impact and comes closest to maximize its capabilities especially in hydrological research. Because of this it has prompted researchers and watershed planners to exploit land-cover in formation derived from remotely-sensed images in a variety of hydrological modeling studies, most especially in runoff predictions [32,33,34,35]. The addition of Geographic Information System (GIS) technology further enhanced the importance of remote sensing through improved the efficiency of the modeling process that leads to increased confidence in the accuracy of modeled watershed conditions, and increased the estimation capability of hydrologic models [35]. GIS is ideally suited for preparing, storing, updating, analyzing, and displaying flood modeling data and outputs for two reasons [30]. First, GIS can integrate data from different sources required by floodplain modeling and flood damages calculation. Secondly, GIS can create spatial relationships that are important in floodplain modeling and flood damages calculation.

Aside from fulfilling the data requirements in flood modeling, remote sensing is also useful as an independent tool to collect flood information which are necessary in calibration and validation of flood model outputs [24,36,37,38], as well as in flood mapping, monitoring and management [29,39]. The use of remotely-sensed maps of flood extent to validate flood models has strongly influenced the development of flood simulation models in recent years, and that the high resolution of remotely sensed data, especially from synthetic aperture radar (SAR) systems (typically a few tens of meters), has encouraged modeling at a higher spatial resolution than was previously impractical, and has also encouraged the integration of high resolution DEMs into hydraulic models [24].

Sanyal and Xu [**29**] remarked that remote sensing technology along with GIS has become the key tool for flood monitoring and management in recent years, most especially in Asia. They reported that development in this field has evolved from optical to radar remote sensing, which has provided all weather capability compared to the optical sensors for the purpose of flood mapping. The central focus in this field revolves around delineation of flood zones and preparation of flood hazard maps for the vulnerable areas. With this, they argued that flood depth is considered crucial for flood hazard mapping and a DEM is considered to be the most effective means to estimate flood depth from remotely sensed or hydrological data.

Floods and Flood Modeling Studies in Marikina River

Flooding in Marikina River and in areas downstream (e.g., Pasig and San Juan Rivers) has been reported by Badilla [**12**] as a recurring problem especially during rainy season or whenever rain bearing weather disturbance affects the country. To reduce the flood discharge in the Pasig River and avoid flooding in the drainage network in Metro Manila, the Manggahan floodway was built in 1986 in order to temporarily divert the flood water of the Marikina River to Laguna Lake [**40**]. Since the completion of this floodway, no floods have occurred in Metro Manila at least by over banking of the Pasig River but unfortunately, a big discharge from the floodway seems to amplify some flood problems in the low-lying shoreline villages of the Laguna de Bay Lake, especially when a Seiche or storm surge induced by a typhoon and the large discharge from the Floodway coincide [**40,41**]. Before the infamous September 2009 TS Ketsana (Ondoy) flood event [**3,21**], a massive flooding was experienced on August 2004 in areas of Metropolitan Manila and nearby provinces when two typhoons simultaneously affected the country [**12**]. This flood, with depths ranging from two to twelve feet, affected a total of 24,108 persons and killed 8 people in Metro Manila alone. Flooding and flood hazards in Metro Manila has been found to have differential impacts among street children, the urban poor and residents of wealthy neighborhoods, and have been argued that being poor is not the only reason why certain sectors are more vulnerable to floods or any environmental hazards; spatial isolation and lack of participation in decision making intensify their present and future vulnerability, as well [**42**].

The September 2009 flooding caused by Tropical Storm (TS) Ketsana (Local Name: *Ondoy*) that devastated Metro Manila and its surroundings [**2**] exemplified the need for an accurate and reliable flood forecasting tool for determining the possible duration and extents of floods and for assessing the risks due to this disaster. It can be recalled that on September 26, 2009, TS Ketsana dumped a month's worth of rain in less than 24 hours and caused flooding in Metro Manila, killing at least 300 people and displacing another 700,000 [**3**]. The need for an accurate and reliable flood monitoring and water level forecasting tools for the Marikina River has again been exemplified in August 2012 when an eight-day period of torrential rain and thunderstorms brought about by the strong movement of the Southwest Monsoon caused the Marikina River to overflow and brought damages to places near the banks of the river. The intense, nonstop rains that occurred from August 1 to August 8, 2012

have been informally known as *Habagat*. The event caused the heaviest damage in Metropolitan Manila since TS Ketsana [**4**]. The same scenario happened again in August 2013 when heavy to torrential rains (7.5 mm/hr to as much as 30 mm/hr or more) were pouring over Metro Manila and nearby provinces. Raining continued for more than 3 days and caused flooding in different areas, most especially in the vicinity of Marikina, San Juan and Pasig Rivers. As the flood plain is host to densely populated areas as well as commercial and industrial zones, flooding due to overflowing of the river resulted to significant damage to human lives and properties.

Flood modeling studies and the development of flood forecasting systems in Marikina River are very few. Earlier attempt to study and forecast flooding in Marikina River and nearby areas has been made by Madsen and Skotner [**43**] in 2005. They set-up a hydrologic and hydrodynamic forecasting model based on MIKE 11 in order to produce flow forecasts on the basis of precipitation, water level and gate level measurements collected at local telemetry stations and transmitted in real-time to a central data server. The modeled river basin covers an area of 621 km^2 and the river network consists of 10 branches with a total length of approximately 79 km, the main rivers being the San Juan, Marikina and Pasig Rivers. The forecasting model was found to provide accurate forecast results due to incorporation of a robust, accurate and efficient forecast updating technique. Although the authors reported that the developed forecasting system is highly suitable for real-time applications, no information is available on the usage of the said system in the present time.

In 2008, Badilla [**12**] did flood modeling in the Pasig-Marikina River Basin using HBV and DUFLOW in order to study the flood wave behavior and to come up with calibrated models which could be used as basis for the operation of Rosario Weir and Napindan Hydraulic Control Structure for effective flood control and early warning in Manggahan Floodway. HBV (or Hydrologiska Byrans Vattenbalansavdelning/Hydrological Bureau Waterbalance) is a conceptual hydrological model mostly used for the simulation of continuous runoff while DUFLOW (short for Dutch Flow) is a hydraulic model used for unsteady flow calculation in open water course systems. In Badilla's study, HBV was applied to simulate the runoff from Pasig-Marikina River Basin using hourly hydrometeorological data. The hydrographs from the HBV model was used as the upstream boundary condition of a calibrated DUFLOW model to provide water level forecast in the Marikina River and to increase the flood lead time which the author thinks could be beneficial for flood control and early warning purposes. The calibration and validation of the two models resulted to Nash-Sutcliffe efficiency coefficient of 0.79 and 0.76, respectively. As the results are satisfactory, Badilla concluded that the calibrated models can be applied for flood control and early warning system in Manggahan Floodway. However, no information is available if the models have been applied or being applied in the Manggahan Floodway.

Abon et al [**2**] reconstructed the September 2009 Tropical Storm Ketsana ("Ondoy") flood event in Marikina River through conduct of resident interviews in the absence of stream gauge data. They also carried out hydrologic modeling using HEC HMS to understand the mechanism that brought the flood. The results of their study showed that peak floods occurred at different hours along the river resulting from the transmission of water from the

main watershed to the downstream areas. Their analysis revealed that modeled peak flood and flood timing coincided well with actual observations as elucidated from interviews except for downstream stations where actual peak floods were observed to have occurred at a later time which they considered to be caused by compounding factors such as other flood sources and stream backflow. They concluded that prediction of flood heights and the use of the known time lag between the peak rainfall and the peak runoff could be utilized to issue timely flood forecasts to allow people to prepare for future flooding. They also suggested that the results of their study be used to generate flood risk maps when integrated with channel model and digital elevation data with sufficient resolution. However, the HEC HMS model they used was not sufficiently calibrated and validated and needs further refinement.

Chapter 3. Topographic and Hydrographic Data Collection, Processing and Analysis for Flood Model Development

Overview

Topographic and hydrographic data are important in the development of flood models. Without this data, it is impossible to develop models. In hydrologic model development, topographic and hydrographic data such as DEM, slope, river width, river cross-section and river profile are necessary to delineate the basin, sub-basin and watershed boundaries. With the addition of land-cover information to topographic data, the amount of runoff generated during a rainfall event and how much time it will took for this runoff to be generated and routed towards the outlets of the watersheds in a river basin can also be computed. The same data sets, also with addition of land-cover data, are necessary in developing the hydraulic model in order to geometrically represent the river and floodplain, and to compute for water surface profile necessary for flood inundation mapping.

In this chapter, the collection, processing and analysis of topographic and hydrographic datasets are presented. The dataset collected covers the Marikina River, Pasig River and San Juan River and their floodplains and upstream watersheds (Figure 6). This chapter is composed of three major parts consisting discussions of the following:

- Establishment of reference control points
- River and floodplain geometry data collection and processing and integration with LIDAR DEM
- Collection and processing of other elevation datasets

Table 2 provides a list of topographic and hydrographic datasets that were collected, processed, and analyzed in this project. The method of collection are also included and further explained in the next sections. Reference points as well as river and floodplain geometry data were obtained through field observations while the rest of the datasets were obtained from various agencies.
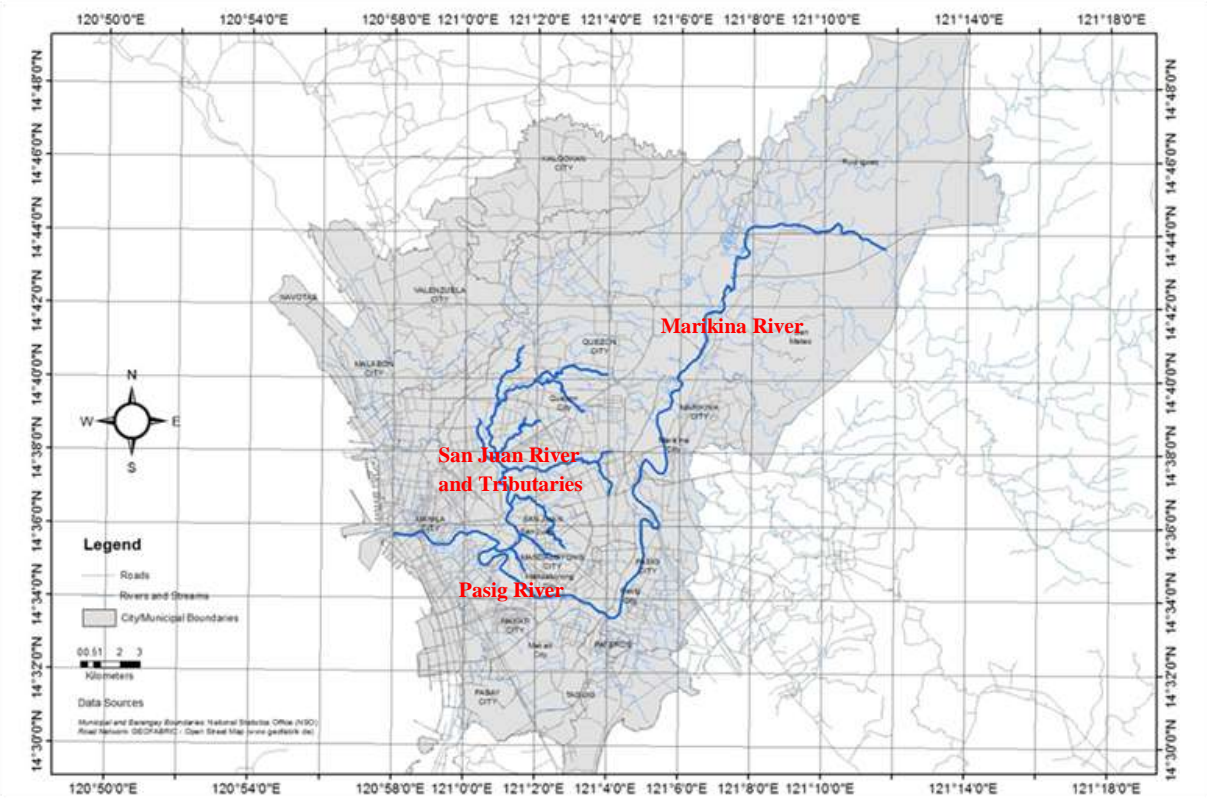
Figure 6. Scope of the topographic and hydrographic data collection, processing and analysis.

Table 2. List of topographic and hydrographic datasets, including their purpose.

Type of Data	Dataset name	Purpose	Source/Method of Collection
Reference Points	Horizontal and Vertical Control Points	Reference points used to adjust the topographic and hydrographic survey data into a common horizontal (UTM 51 WGS 1984) and vertical (MSL) datum	Field observation through 3rd order GPS observation and differential levelling
River and Floodplain Geometry	Elevation profile	HEC HMS and HEC RAS model development and parameterization	Field observation through topographic and hydrographic surveys
	Cross-section	HEC HMS and HEC RAS model development and parameterization	Field observation through topographic and hydrographic surveys
	Bed topography	HEC HMS and HEC RAS model development and parameterization	Field observation through topographic and hydrographic surveys
Elevation Data	Metro Manila MMEIRS Boundary and Elevation Data	HEC HMS model development and parameterization	PHIVOLCS
	NAMRIA 1:50,000 Topographic Maps	HEC HMS model development and parameterization	NAMRIA
	DEMs:		
	- ASTER GDEM	HEC HMS model development and parameterization	NASA Reverb http://*reverb.echo.nasa.gov/*
	- LIDAR DEM	HEC RAS model parameterization and flood inundation and hazard mapping	Collective Strengthening of Community Awareness for Natural Disasters (CSCAND)

Establishment of Reference Control Points

Procedures employed

Horizontal and vertical control points used as reference points for river hydrographic surveys were established in the project areas using 3rd order static GPS observations and 3rd order differential leveling. The control points were established and marked mostly in the bridges of the Marikina River, Pasig River and San Juan River (including its tributaries). The San Juan River tributaries that were covered for the surveys include San Francisco River, Talayan Creek, Mariblo Creek, Diliman Creek, Kamias Creek, Maytunas Creek, Ermitanio Creek and Kalentong Creek.

Prior to the GPS observations, reconnaissance surveys were conducted to inspect the areas where the control points are to be established. It also included the recovery of existing horizontal control points with known x and y coordinates and vertical control points or benchmarks with elevations referred from the mean sea level (MSL). Google Earth images and handheld GPS devices were utilized to navigate to the locations of the control points.

The locations of the control points were initially selected from available lists of horizontal and vertical control points in Metro Manila. The lists comprise of horizontal and vertical control points previously established by the NAMRIA, DPWH and the Effective Flood Control Operation System Project of the Metropolitan Manila Development Authority (EFCOS-MMDA). However, during the reconnaissance some of the control points no longer exist and some are located very far from the rivers. Hence, most of the control points established are new points.

The control points were marked on the ground using concrete nail, washer, cement and paint. Some points were marked permanently. They were selected and marked on locations with the least obstruction. They were placed on areas without trees or tall buildings in the vicinity. Most of the control points were located on bridges and the other points on roads near and within the extent of the rivers and tributaries.

The horizontal coordinates of the control stations were obtained through differential GPS technique. Most of the GPS observations utilized the 1st order NAMRIA control station MMA 5 at the rooftop of the Melchor Hall (College of Engineering, UP Diliman) as the base station while for some observations, existing NAMRIA control points and those points established by SMTFCMMS – Project 2[1] [**44**] were utilized. A Topcon Hiper GA survey grade GPS receiver was used as the base station. Another set consisting of Topcon Hiper GA and Spectra Precision Epoch 10 survey grade GPS receivers were used as to measure coordinates at the control points (rovers). These GPS devices are shown in Figure 11. At least 1 hour of fixed GPS observations (logging rate of 1 second) were conducted for each control point. The GPS observations were post-processed using the Topcon Tools software.

To obtain the mean sea level (MSL) elevations of the control points, a 3rd order closed-loop differential leveling (maximum elevation error of 12mm/km) using a Topcon

---

[1] Project 2: Establishment of spillover elevation along flood prone river systems: Marikina-Pasig River

DL-102C digital level was used. This instrument has a precision of 0.1mm. Leveling rods with bar code, turning plates, rod clippers and leveling bubbles were also included in the implementation of the surveys. NAMRIA benchmarks and benchmarks established by SMTFCMMS – Project 2 of 3rd order accuracy were recovered from the study area and used as reference stations in the leveling. Leveling routes were created based on the existing benchmarks within the area. The routes were designed using Google Earth images in which shortest distances were chosen along the roads connecting the available benchmark to the control point with unknown elevation.
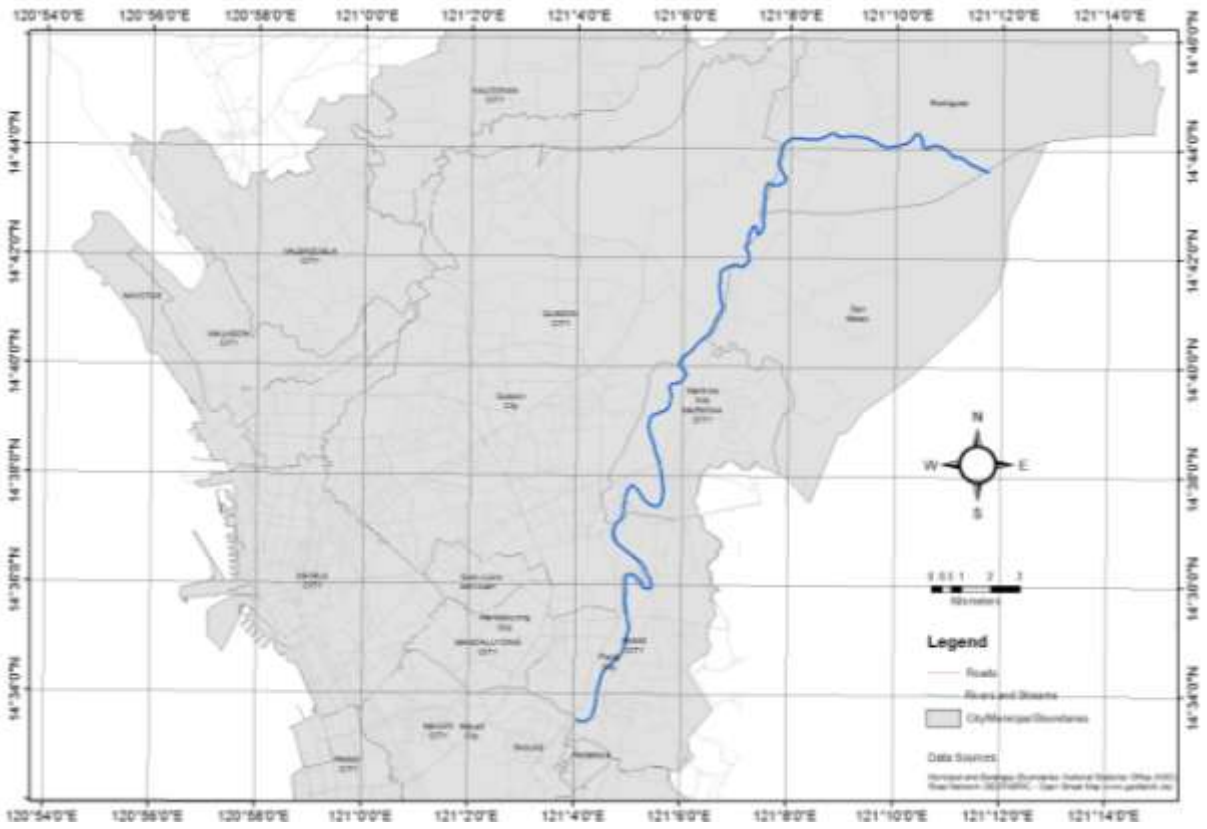
Figure 7. Vicinity map of Marikina River where the control points were established.
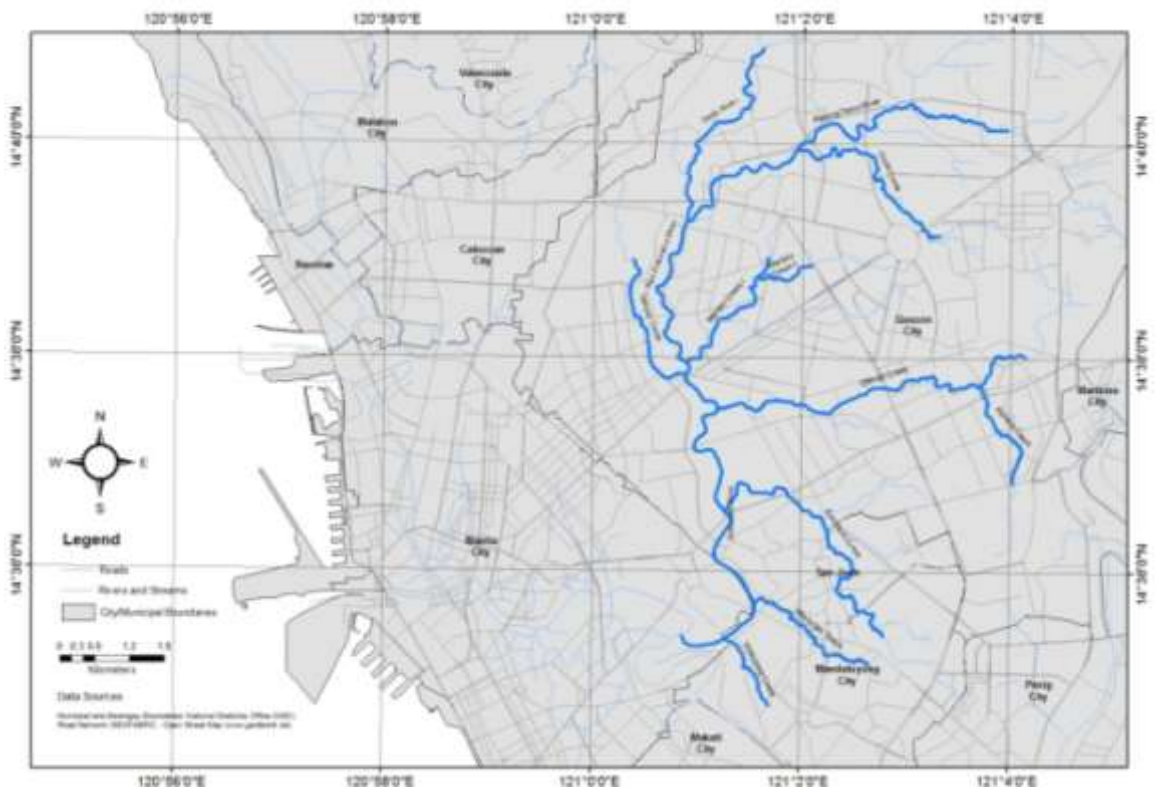
Figure 8. Vicinity map of San Juan River and its tributaries where the control points were established.

Figure 9. Markings of some control points in Marikina River.

Figure 10. Marking of some control points in San Juan River and its tributaries.

Figure 11. Survey-grade GPS receivers used in getting the horizontal coordinates of the control points.

Figure 12. Pictures showing the conduct of GPS observation in some of the control points in Marikina River.

Figure 13. Pictures showing the conduct of GPS observation in some of the control points in Pasig River.
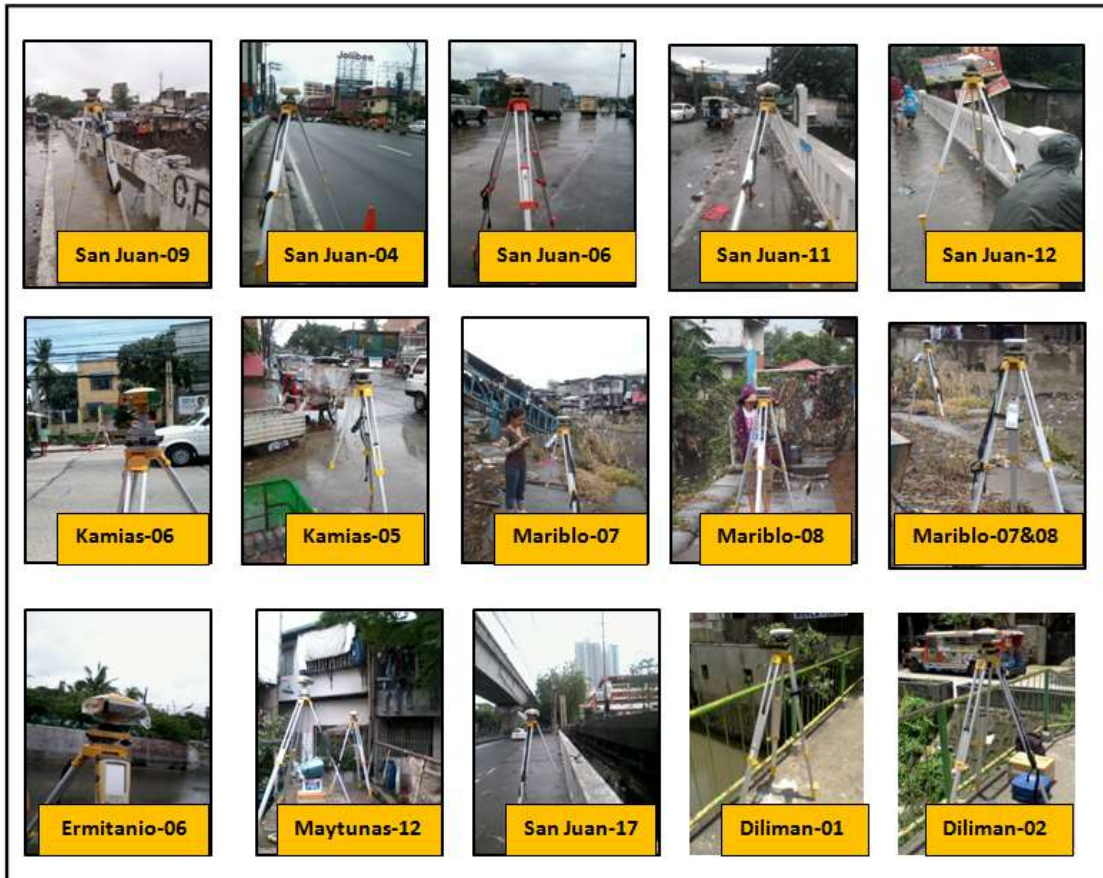
Figure 14. Pictures showing the conduct of GPS observation in some of the control points in San Juan River and its tributaries.

Figure 15. Set-up of equipments for a 3rd order leveling survey to obtain the MSL elevations of the control points.

Figure 16. Pictures showing the conduct of 3rd order leveling surveys in some of the control points in Marikina River.
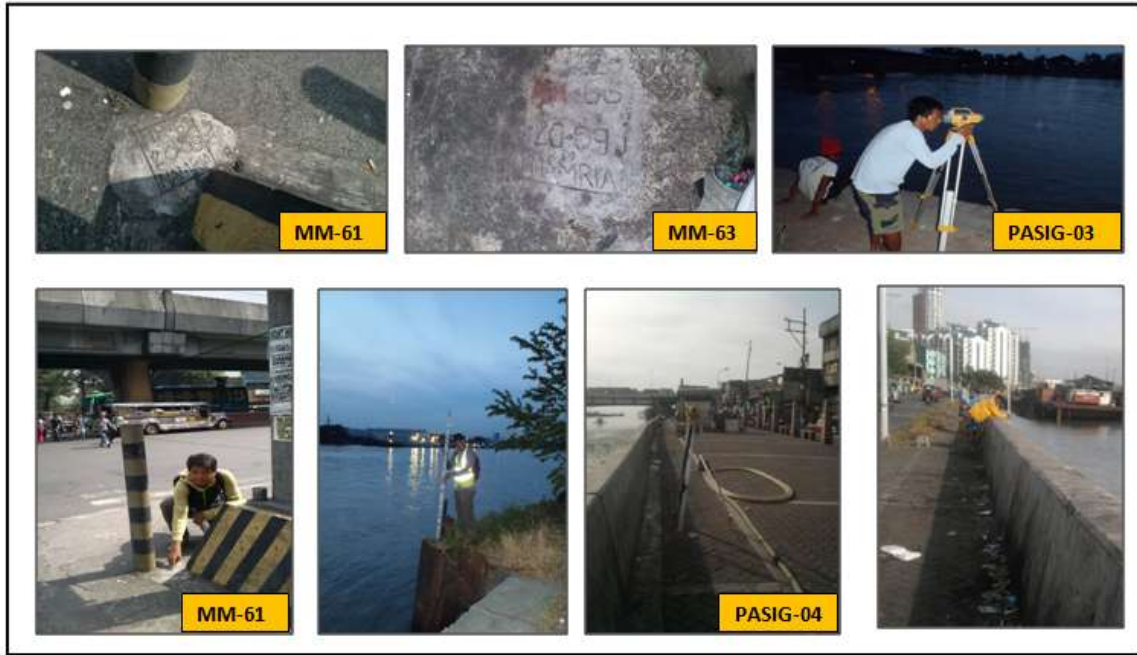
Figure 17. Pictures showing the conduct of 3rd order leveling surveys in some of the control points in Pasig River.
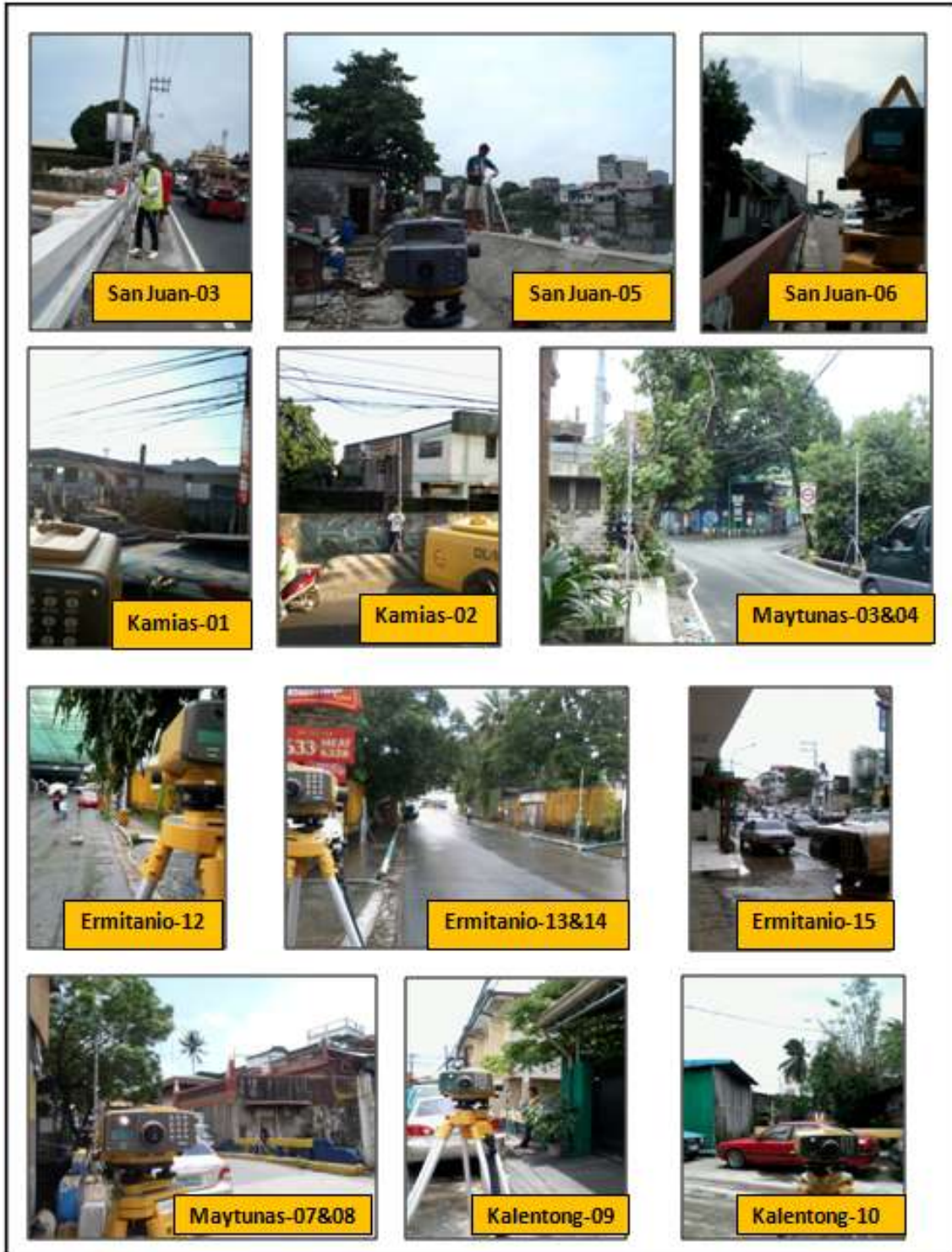
Figure 18. Pictures showing the conduct of 3rd order leveling surveys in some of the control points in San Juan River and its tributaries.

Results of control point establishment

A total of 105 reference control points were established and marked in the project areas. They are summarized in Table 3 and shown in the following figures. The coordinates of the established control points can be found in Table 4.

Table 3. Summary of established control points.

Main River	Tributary Name	No. of Established Control Points	Year Established
Marikina River	-	7	2011
Pasig River	-	3	2012
San Juan River	San Francisco River	8	2012
	Talayan Creek	18	2012
	Mariblo Creek	6	2012
	Diliman Creek	8	2012
	Kamias Creek	4	2012
	Ermitanio Creek	16	2012
	Maytunas Creek	12	2012
	Kalentong Creek	10	2012
	San Juan River	13	2012
TOTAL		105	

In San Juan River and its tributaries (as listed in Table 3), the control points were established in partnership with the Pasig River Tributaries Survey and Assessment Study (PRTSAS) Phase II – Hydrographic Surveys Component. PRTSAS Phase II is also implemented by the UP TCAGP. This project covers the San Juan River Basin which is also covered by the SMTFCMMS – Project 3. To avoid duplication of the activities, the SMTFCMMS Project 3 team conducted the GPS observations in the control points while the PRTSAS Phase II – Hydrographic Surveys Team conducted the 3rd order leveling. For tributaries not listed (e.g., Dario River, Pasong Tamo River, Culiat Creek), control points established by PRTSAS II – Hydrographic Surveys Component were utilized during the topographic and hydrographic surveys.
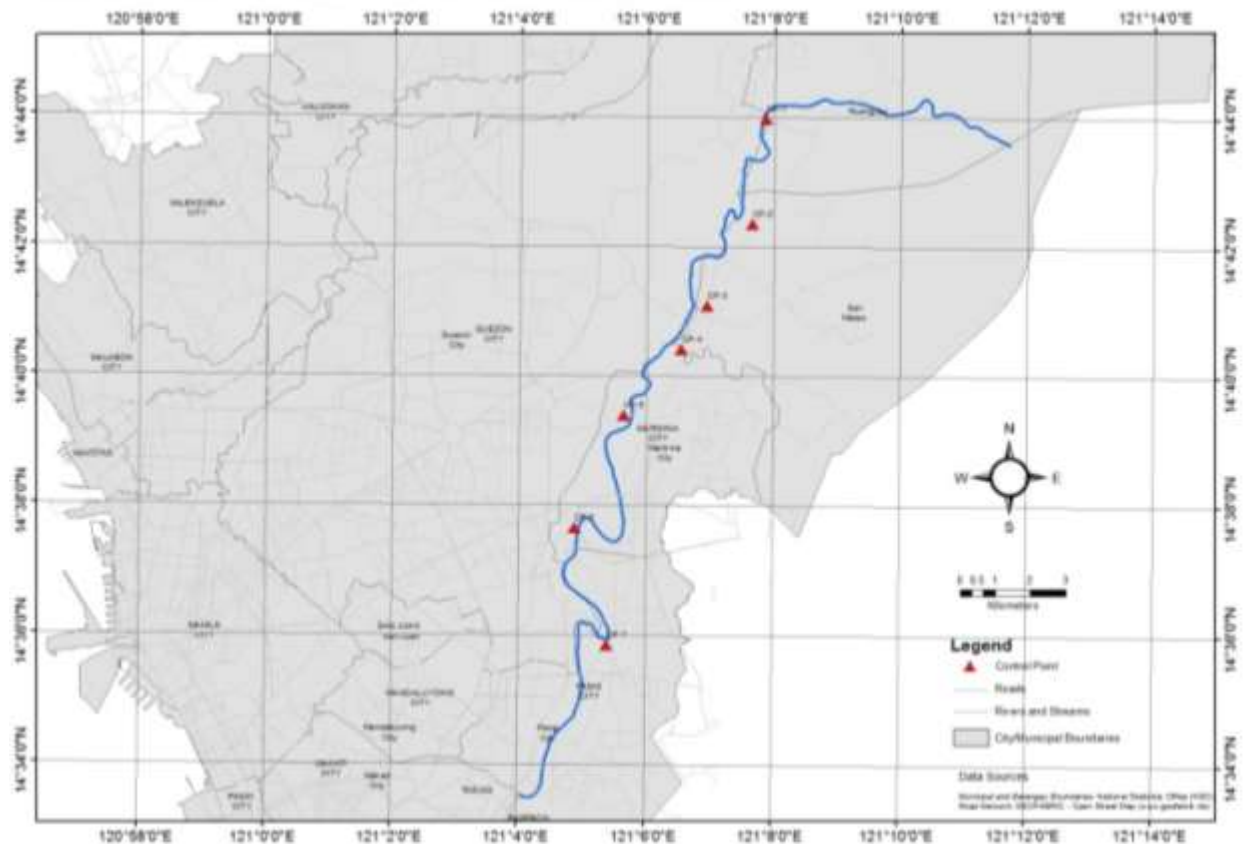
Figure 19. Map showing the control points established in Marikina River.
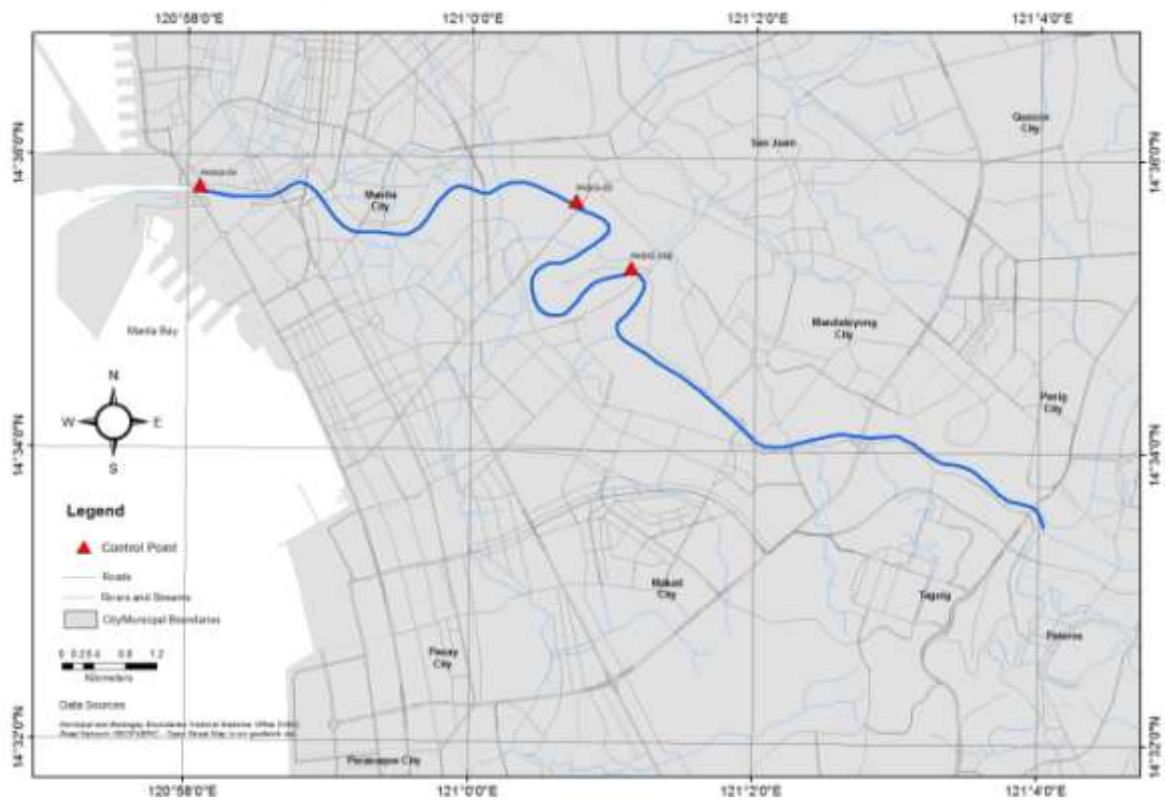
Figure 20. Map showing the control points established in Pasig River.
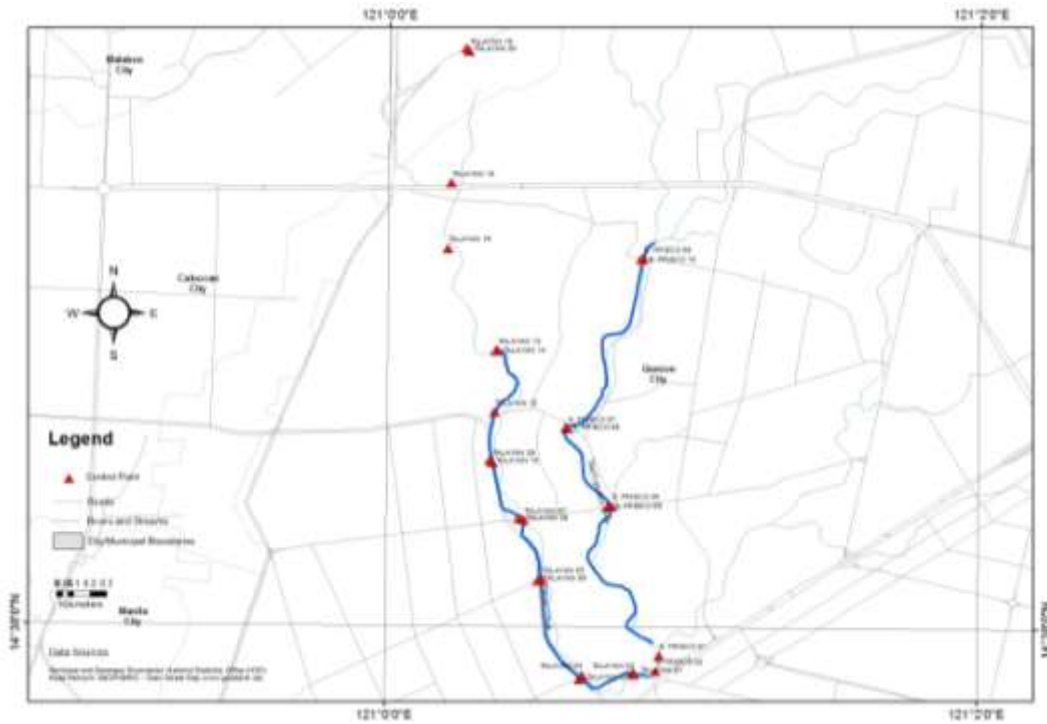
Figure 21. Map showing the control points established in Talayan Creek and San Francisco River (both tributaries of San Juan River).
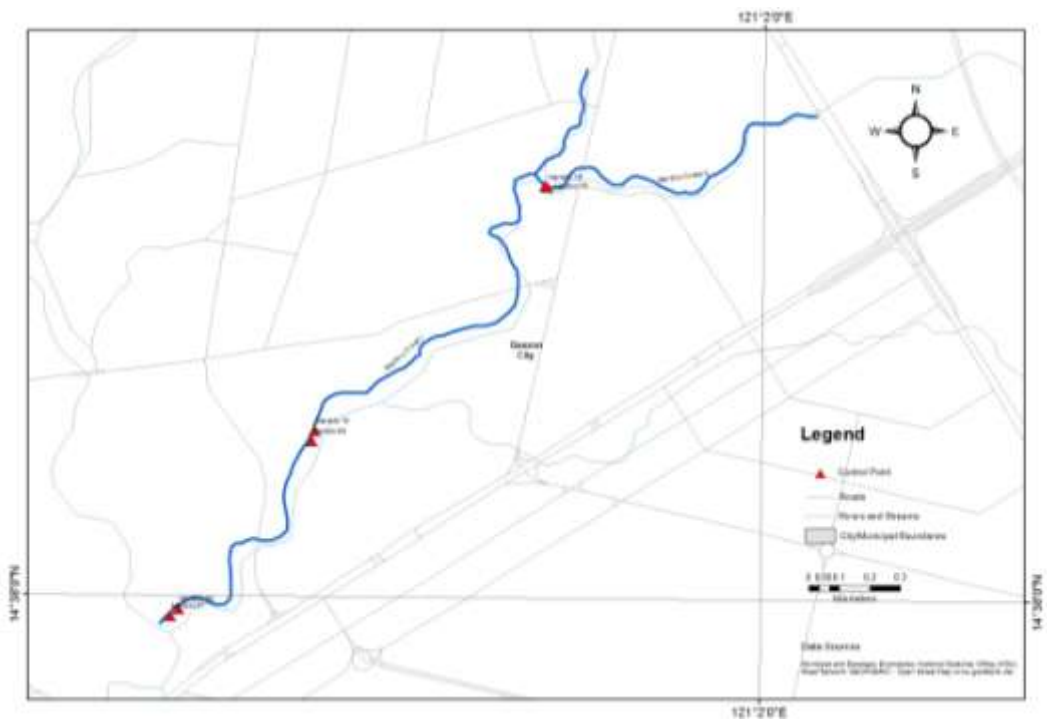
Figure 22. Map showing the control points established in Mariblo Creek (a tributary of San Juan River).
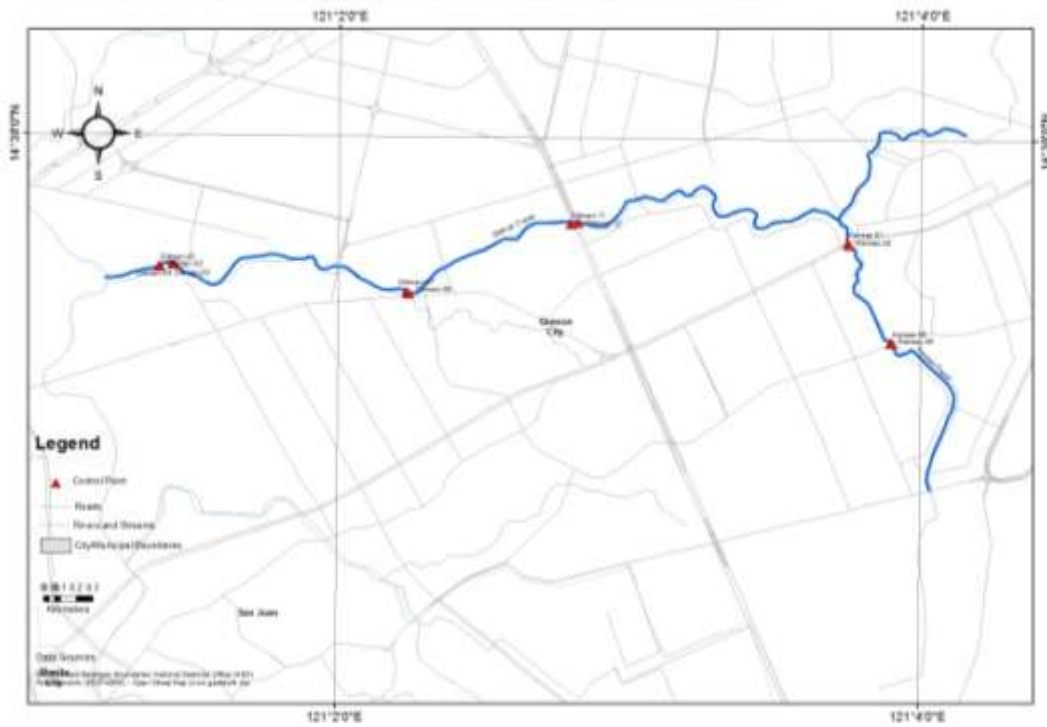
Figure 23. Map showing the control points established in Kamias Creek and Diliman Creek (both tributaries of San Juan River).
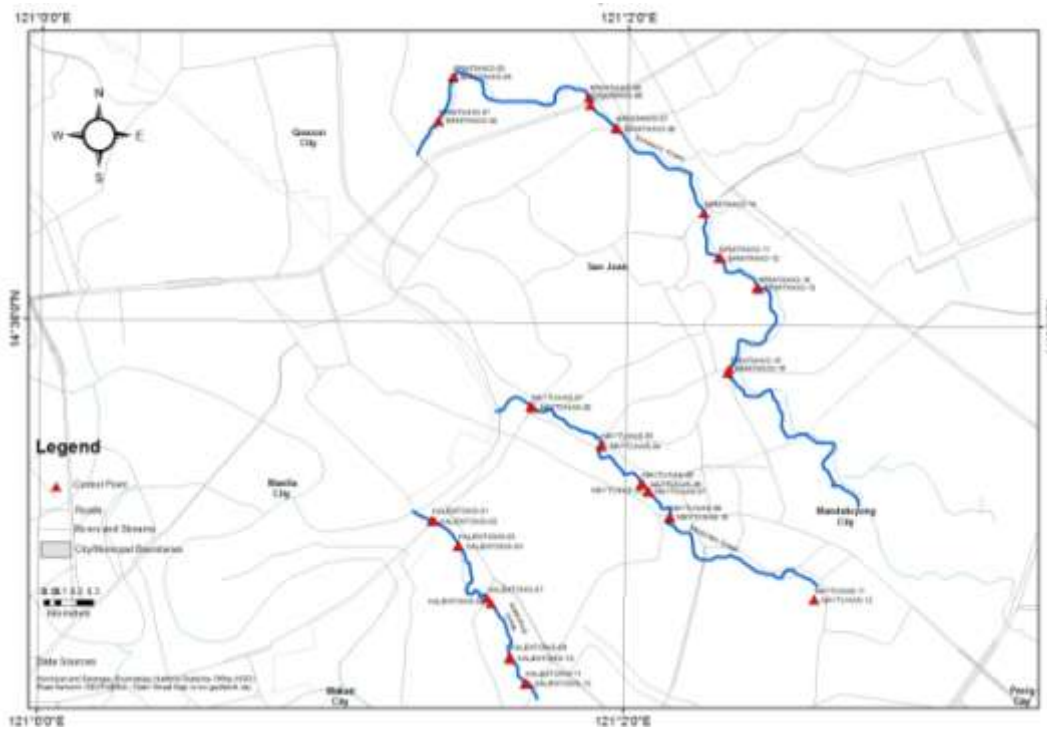
Figure 24. Map showing the control points established in Ermitanio, Maytunas and Kalentong Creeks (all are tributaries of San Juan River).
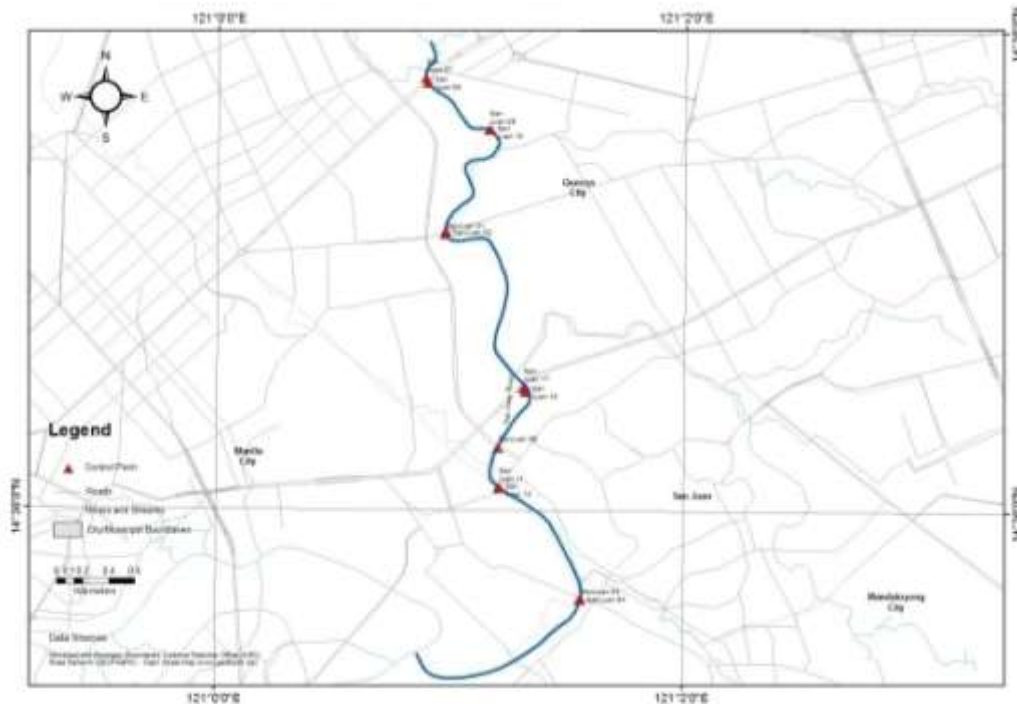
Figure 25. Map showing the control points established in San Juan River.

Table 4. Horizontal coordinates (in UTM 51 WGS 1984) and elevation (referred to Mean Sea Level) of established control points.

Main River Name	Tributary Name	Name of Control Point	UTM 51 WGS 1984 Grid Northing (m)	UTM 51 WGS 1984 Grid Easting (m)	Elevation MSL (m)
Marikina River	NA	CP1	1,629,623.045	298,810.675	23.044
Marikina River	NA	CP2	1,626,625.068	298,429.224	18.252
Marikina River	NA	CP3	1,624,299.558	297,131.398	17.562
Marikina River	NA	CP4	1,623,064.097	296,408.329	14.569
Marikina River	NA	CP5	1,621,203.393	294,757.184	11.100
Marikina River	NA	CP6	1,618,014.889	293,353.591	7.776
Marikina River	NA	CP7	1,614,660.721	294,265.935	8.982
Pasig River	NA	PASIG-03	1,614,484.347	285,864.430	1.7828
Pasig River	NA	PASIG-03B	1,613,629.797	286,559.922	2.40753
Pasig River	NA	PASIG-04	1,614,681.955	281,117.087	2.0752
San Juan River	San Francisco River	S FRISCO 01	1,618,596.316	286,234.873	4.238
San Juan River	San Francisco River	S FRISCO 02	1,618,574.579	286,241.822	4.179
San Juan River	San Francisco River	S FRISCO 05	1,619,437.894	285,965.366	9.656
San Juan River	San Francisco River	S FRISCO 06	1,619,432.732	285,924.697	9.307
San Juan River	San Francisco River	S FRISCO 07	1,619,909.159	285,707.004	11.070
San Juan River	San Francisco River	S FRISCO 08	1,619,920.283	285,688.667	11.077
San Juan River	San Francisco River	S FRISCO 09	1,620,940.245	286,146.526	10.704
San Juan River	San Francisco River	S FRISCO 10	1,620,944.549	286,165.077	10.700
San Juan River	Talayan Creek	TALAYAN 01	1,618,426.978	286,101.166	5.513
San Juan River	Talayan Creek	TALAYAN 02	1,618,418.833	286,102.861	5.517
San Juan River	Talayan Creek	TALAYAN 03	1,618,390.344	285,781.365	6.160
San Juan River	Talayan Creek	TALAYAN 04	1,618,407.928	285,775.625	6.165

34

San Juan River	Talayan Creek	TALAYAN 05	1,618,983.637	285,538.743	6.970
San Juan River	Talayan Creek	TALAYAN 06	1,619,003.908	285,537.601	6.926
San Juan River	Talayan Creek	TALAYAN 07	1,619,356.930	285,432.674	9.474
San Juan River	Talayan Creek	TALAYAN 08	1,619,368.971	285,413.521	9.427
San Juan River	Talayan Creek	TALAYAN 09	1,619,691.491	285,238.533	9.381
San Juan River	Talayan Creek	TALAYAN 10	1,619,726.729	285,240.991	9.466
San Juan River	Talayan Creek	TALAYAN 11	1,620,015.350	285,266.250	9.221
San Juan River	Talayan Creek	TALAYAN 12	1,620,018.766	285,259.826	8.932
San Juan River	Talayan Creek	TALAYAN 13	1,620,388.286	285,278.833	11.380
San Juan River	Talayan Creek	TALAYAN 14	1,620,394.052	285,273.469	11.410
San Juan River	Talayan Creek	TALAYAN 16	1,621,051.329	284,963.707	14.321
San Juan River	Talayan Creek	TALAYAN 18	1,621,402.281	285,001.497	14.722
San Juan River	Talayan Creek	TALAYAN 19	1,622,254.621	285,204.965	20.944
San Juan River	Talayan Creek	TALAYAN 20	1,622,265.681	285,197.260	20.928
San Juan River	Diliman Creek	DILIMAN−01	1,617,892.647	287,072.286	5.411
San Juan River	Diliman Creek	DILIMAN−02	1,617,887.229	287,076.352	5.482
San Juan River	Diliman Creek	DILIMAN−03	1,617,908.184	287,159.191	6.807
San Juan River	Diliman Creek	DILIMAN−04	1,617,900.494	287,161.554	6.753
San Juan River	Diliman Creek	DILIMAN−07	1,617,732.512	288,599.613	21.662
San Juan River	Diliman Creek	DILIMAN−08	1,617,716.665	288,611.416	21.641
San Juan River	Diliman Creek	DILIMAN−11	1,618,144.851	289,609.372	31.956
San Juan River	Diliman Creek	DILIMAN−12	1,618,152.582	289,656.975	31.846
San Juan River	Ermitanio Creek	ERMITANIO−01	1,616,243.549	286,996.616	2.183
San Juan River	Ermitanio Creek	ERMITANIO−02	1,616,247.442	286,999.436	2.217
San Juan River	Ermitanio Creek	ERMITANIO−03	1,616,514.254	287,087.836	2.309
San Juan River	Ermitanio Creek	ERMITANIO−04	1,616,519.492	287,090.901	2.479
San Juan River	Ermitanio Creek	ERMITANIO−05	1,616,392.433	287,922.730	5.989
San Juan River	Ermitanio Creek	ERMITANIO−06	1,616,345.471	287,929.970	8.759
San Juan River	Ermitanio Creek	ERMITANIO−07	1,616,205.984	288,086.756	9.882
San Juan River	Ermitanio Creek	ERMITANIO−08	1,616,197.940	288,092.543	9.885
San Juan River	Ermitanio Creek	ERMITANIO−09	1,617,135.496	286,324.006	15.011
San Juan River	Ermitanio Creek	ERMITANIO−10	1,615,216.477	288,958.531	15.027
San Juan River	Ermitanio Creek	ERMITANIO−11	1,615,405.278	288,715.176	13.021
San Juan River	Ermitanio Creek	ERMITANIO−12	1,615,405.567	288,727.976	13.016
San Juan River	Ermitanio Creek	ERMITANIO−13	1,615,224.372	288,951.887	13.916
San Juan River	Ermitanio Creek	ERMITANIO−14	1,615,681.119	288,626.076	13.918
San Juan River	Ermitanio Creek	ERMITANIO−15	1,614,720.299	288,779.444	17.052
San Juan River	Ermitanio Creek	ERMITANIO−16	1,614,699.525	288,770.589	17.021
San Juan River	Kalentong Creek	KALENTONG−01	1,613,797.322	286,957.335	3.458
San Juan River	Kalentong Creek	KALENTONG−02	1,613,790.506	286,969.051	4.113
San Juan River	Kalentong Creek	KALENTONG−03	1,613,639.677	287,120.039	2.932
San Juan River	Kalentong Creek	KALENTONG-04	1,613,637.434	287,125.538	2.932
San Juan River	Kalentong Creek	KALENTONG−07	1,613,317.124	287,293.242	2.586
San Juan River	Kalentong Creek	KALENTONG−08	1,613,288.215	287,318.747	3.000
San Juan River	Kalentong Creek	KALENTONG−09	1,612,959.585	287,437.156	3.048
San Juan River	Kalentong Creek	KALENTONG−10	1,612,947.497	287,436.489	3.071
San Juan River	Kalentong Creek	KALENTONG−11	1,612,797.404	287,528.418	3.094
San Juan River	Kalentong Creek	KALENTONG−12	1,612,794.190	287,543.176	3.145

San Juan River	Kamias Creek	KAMIAS−01	1,618,027.524	291,319.783	41.044
San Juan River	Kamias Creek	KAMIAS−02	1,618,011.695	291,329.610	41.210
San Juan River	Kamias Creek	KAMIAS−05	1,617,411.524	291,584.631	42.460
San Juan River	Kamias Creek	KAMIAS−06	1,617,402.220	291,590.344	42.501
San Juan River	Mariblo Creek	MARIBLO−07	1,618,625.710	286,233.593	4.525
San Juan River	Mariblo Creek	MARIBLO−08	1,618,617.171	286,226.580	4.495
San Juan River	Mariblo Creek	MARIBLO−09	1,619,211.894	286,705.321	7.956
San Juan River	Mariblo Creek	MARIBLO−10	1,619,230.758	286,715.472	8.028
San Juan River	Mariblo Creek	MARIBLO−15	1,620,043.273	287,480.574	22.248
San Juan River	Mariblo Creek	MARIBLO−16	1,620,039.671	287,484.542	22.241
San Juan River	Maytunas Creek	MAYTUNAS−01	1,614,495.291	287,564.919	3.002
San Juan River	Maytunas Creek	MAYTUNAS−02	1,614,488.516	287,576.710	3.826
San Juan River	Maytunas Creek	MAYTUNAS−03	1,614,257.239	287,996.124	3.539
San Juan River	Maytunas Creek	MAYTUNAS−04	1,614,250.989	288,000.901	3.671
San Juan River	Maytunas Creek	MAYTUNAS−05	1,614,019.672	288,244.241	4.682
San Juan River	Maytunas Creek	MAYTUNAS−06	1,614,018.426	288,249.921	4.719
San Juan River	Maytunas Creek	MAYTUNAS−07	1,613,974.998	288,281.016	4.839
San Juan River	Maytunas Creek	MAYTUNAS−08	1,613,972.154	288,289.332	4.829
San Juan River	Maytunas Creek	MAYTUNAS−09	1,613,814.362	288,415.078	5.291
San Juan River	Maytunas Creek	MAYTUNAS−10	1,613,814.582	288,416.612	5.324
San Juan River	Maytunas Creek	MAYTUNAS−11	1,613,306.691	289,300.941	18.028
San Juan River	Maytunas Creek	MAYTUNAS−12	1,613,307.210	289,299.220	18.077
San Juan River	San Juan River	SAN JUAN−01	1,617,135.496	286,324.006	4.937
San Juan River	San Juan River	SAN JUAN−02	1,617,158.874	286,329.574	4.923
San Juan River	San Juan River	SAN JUAN−03	1,614,331.299	287,355.649	3.860
San Juan River	San Juan River	SAN JUAN−04	1,614,347.379	287,367.026	3.847
San Juan River	San Juan River	SAN JUAN−06	1,615,486.698	286,726.128	7.194
San Juan River	San Juan River	SAN JUAN−07	1,618,283.293	286,187.427	9.188
San Juan River	San Juan River	SAN JUAN−08	1,618,328.046	286,178.888	9.329
San Juan River	San Juan River	SAN JUAN-09	1,617,939.367	286,683.040	8.134
San Juan River	San Juan River	SAN JUAN−10	1,617,944.158	286,675.896	8.156
San Juan River	San Juan River	SAN JUAN−11	1,615,184.721	286,730.537	5.096
San Juan River	San Juan River	SAN JUAN−12	1,615,182.623	286,740.551	5.224
San Juan River	San Juan River	SAN JUAN−17	1,615,999.765	286,928.171	5.638
San Juan River	San Juan River	SAN JUAN−18	1,615,988.272	286,941.603	5.631

River and Floodplain Geometry Data Collection and Processing

River and floodplain geometry of Marikina River, Pasig River and San Juan River (and its tributaries) were collected through conduct of bathymetric surveys and profile and cross-section surveys. The objective of these surveys is to collect elevation data points of river beds and the flood plains which will be integrated later on to a high resolution LIDAR DEM. The elevations are referred to MSL. Bathymetric surveys were done on deep portions of the rivers using GPS-integrated single- and multi-beam echosounders (to measure depth), together with total station, digital levels, and water level loggers (for tidal correction and conversion of depths to MSL elevation). For shallow portions of the river as well as in the flood plains, profile and cross-section surveys using total station and stop-and-go kinematic GPS surveys were implemented to collect elevation data points.

Bathymetric Surveys

Bathymetric Surveys Equipment Set-up

The bathymetric surveys were conducted using different types of echosounders and survey-grade GPS receivers. The devices measure simultaneously during each bathymetric survey. The echosounders measure depths, while the GPS receivers obtain the precise location of the points from network of satellites and signals at a specific time. The echosounders and GPS were attached to poles and frames to form a set-up in which both devices measure on a common point (echosounder for the depth, and the GPS for the position). The echosounders were connected to an external battery that supplies power during the surveys. The outputs of the surveys are (X, Y, depth) data where (X, Y) are UTM 51 WGS 1984 coordinates at the point of measurement, and depth is in meters.

Single-beam echosounders (Figure 26) were used for the Marikina River and the Pasig River because during the survey period only this kind of echosounder was available. The echosounders are the HiTarget HD-370 Digital VF Echosounder and Lowrance LCX-17M echosounder. The Lowrance echosounder has integrated GPS, mapping and sonar capabilities. It obtains depth samples at an interval of at least one second. The HiTarget echosounder, a single-beam echosounder, measured soundings one point at a time. The least interval it can measure is three seconds. Draft heights, the measurement from the sonar or transducer to the water surface, were noted and used correct the measured depths.

The single-beam echosounders (SBES) were paired with Topcon HiPer Ga dual-frequency GPS receivers for both real-time and post-processed kinematic positioning of depth measurements. This "rover" receiver was connected to the pole where the transducer is attached. A similar GPS receiver was placed on one of established control points on the ground to act as the base station that provides real-time correction to the rover receiver and at the same time logs data for post-processing of rover GPS data for surveys that real-time kinematic correction failed due to loss of signal between the base and the rover.

For the San Juan River, the ES3 Odom multi-beam echosounder system (MBES), as shown in Figure 27, was used. The transducer, motion sensor and sound velocity probe were integrated and enclosed in a metal frame. Two Trimble SPS64 GPS receivers were included in the system that also comprises a real-time appliance (RTA) and data acquisition and

processing computers. The RTA served as the device connecting all the cables and sensors and supplied power to each of them from an external source. The two computers, in a form of rugged laptops, were used separately for viewing the surveyed area and recording the depths. The processing software was installed in one of the computers. The MBES recorded numerous points that cover the riverbed, depending on the depth of the river at the survey location. It returned swaths, a fan-shaped coverage of the riverbed, in every interval or time of acquisition. The set-up of the MBES on boat included the installation of the wooden planks, metal frames and poles for the sonar head, the integrated transducer, motion sensor and sound velocity probe. Screws, ropes and cable ties were used as attachments. The two GPS antenna, one for the heading and the other as rover, were screwed to a metal bar attached horizontally above the pole of the sonar head. The metal bar is positioned parallel to the boat.

A rubber boat and motorized wooden bancas were used as vehicles during the bathymetric surveys.

Figure 26. Single-beam echosounders used in the bathymetric surveys of the Marikina and Pasig Rivers.
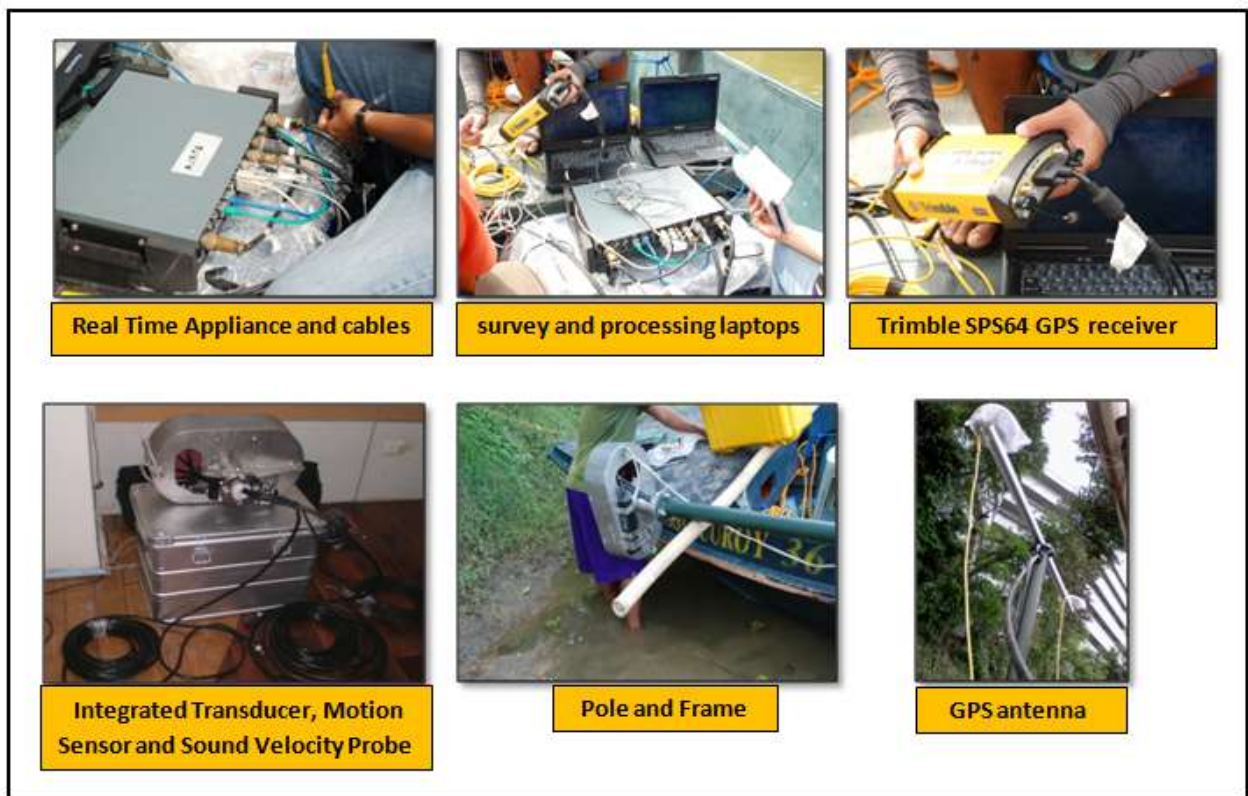
Figure 27. Multi-beam echosounder system used for the bathymetric survey of the San Juan River.

Figure 28. Set-up of rubber boat and echosounders.

Bathymetric Survey Implementation

The bathymetric surveys were implemented using pre-defined survey routes. The routes were selected based on the established control points in the vicinity of the rivers being surveyed. The control point nearest to each segment was used as the reference base station during the bathymetric surveys.

The bathymetric surveys in the Marikina River were executed on zigzag routes. The surveys were conducted by going downstream then back in an upstream direction. The profile of the river was also surveyed along its centerline. Figure 29 shows the survey routes while Figure 30 shows some pictures taken during the conduct of the surveys. The survey dates are shown in Table 5.
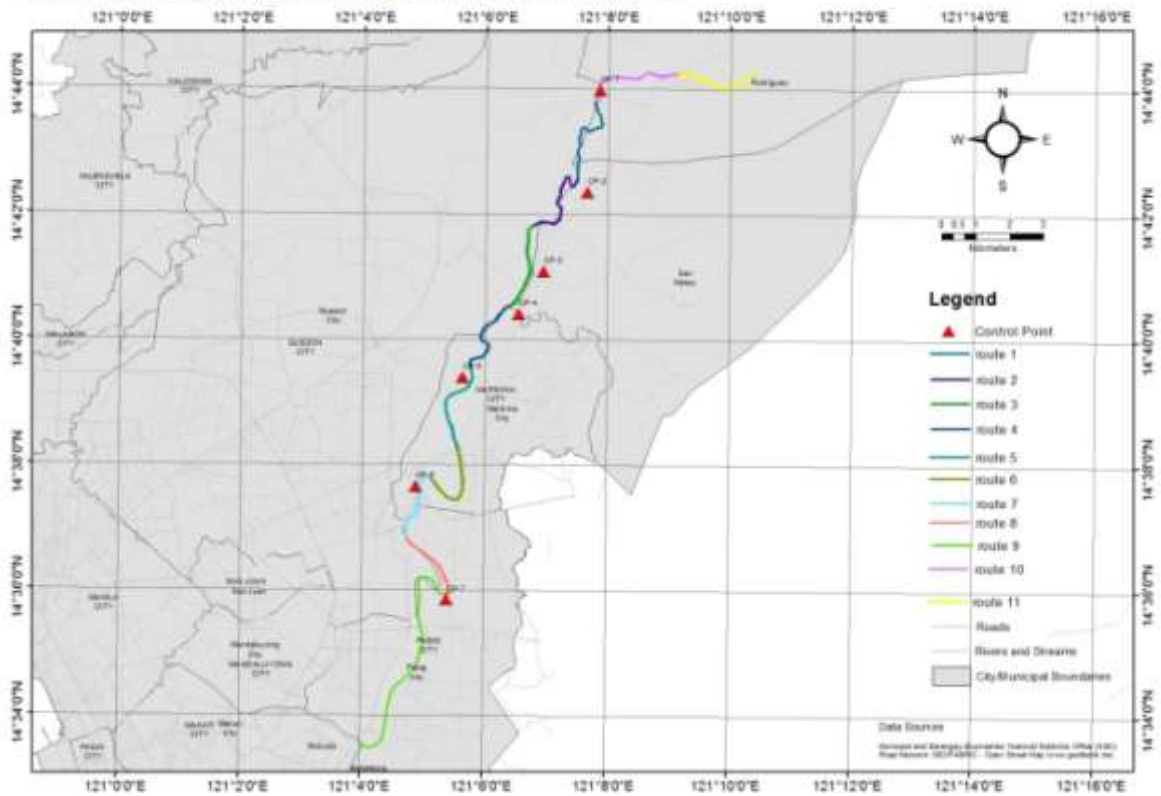
Figure 29. Bathymetric survey routes for Marikina River. The reference control points are indicated by red triangles.

Table 5. Dates of bathymetric surveys of Marikina River.

Dates of Survey	Survey Route Accomplished	Approximate length surveyed, km.
20-23 September 2011	routes 3 to 8	12
05-12 October 2011	routes 6 to 8	10
08-11 November 2011	route 2, 10 and 11	4
16-18 November 2011	route 1 and 2 to 4	6
13 -15 December 2011	route 9 and route 5	6.67

Figure 30. Bathymetric surveys in the Marikina River.

The bathymetric surveys in the San Juan River were conducted on July 5 to 6, 2012. The bathymetric surveys were implemented per segment of the river (Figure 31). The survey routes were executed on a straight path instead of the zigzag direction in order to take advantage of the multibeam echosounder that was used. The profile lines were located on each side of the centreline to obtain overlapping swaths from the multibeam data. The directions taken for the surveys were first going downstream then back upstream.

A total approximate length of 5.63 km of the San Juan River was surveyed (Table 6). The unsurveyed portions, with an approximate length of 1.65 km., were shallow and inaccessible by the motor boat. These portions were re-surveyed using conventional techniques (use of total station).

Figure 31. Bathymetric survey routes for the San Juan River.

Table 6. Dates of bathymetric surveys of San Juan River.

Dates of Survey	Survey Route Accomplished	Approximate length surveyed, km.
5 July 2012	route 1	2.85
6 July 2012	route 2	2.78

Figure 32. Bathymetric surveys in the San Juan River.

The bathymetric surveys in the Pasig River were executed in zigzag routes similar to the surveys done in Marikina River. Figure 33 shows the survey routes while Figure 34 shows some pictures taken during the conduct of the surveys. The survey dates are shown in Table 7.

Table 7. Dates of bathymetric surveys in the Pasig River.

Dates of Survey	Survey Route Accomplished	Approximate length surveyed, km.
6 December 2012	routes 1	5.68
7 December 2012	routes 2A	3.63
11 December 2012	route 3	6.74
12 December 2012	route 2B	7.17
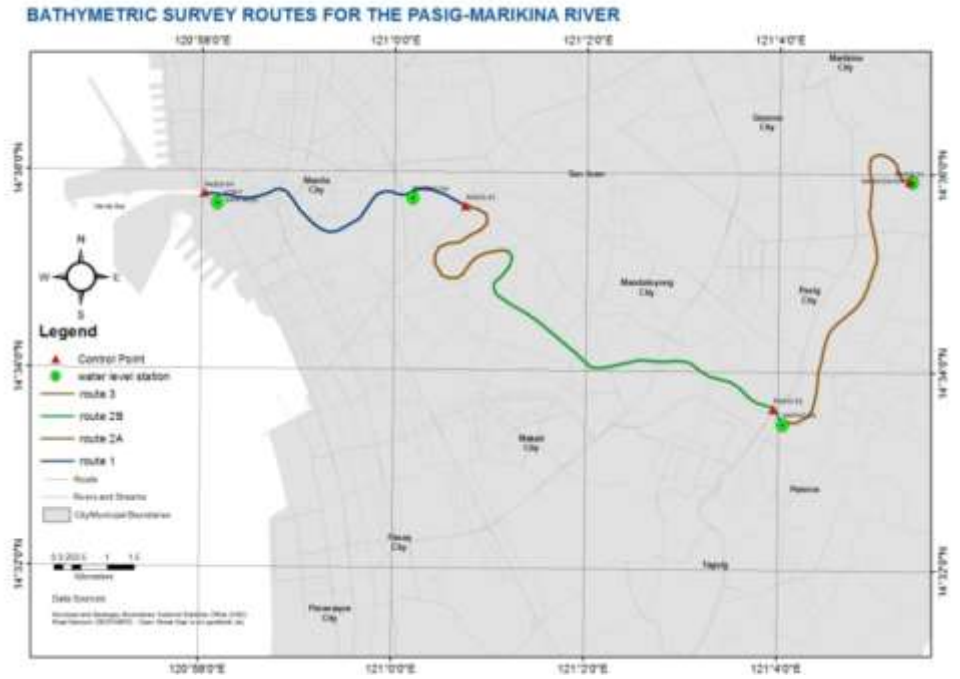
Figure 33. Bathymetric survey routes for the Pasig River.
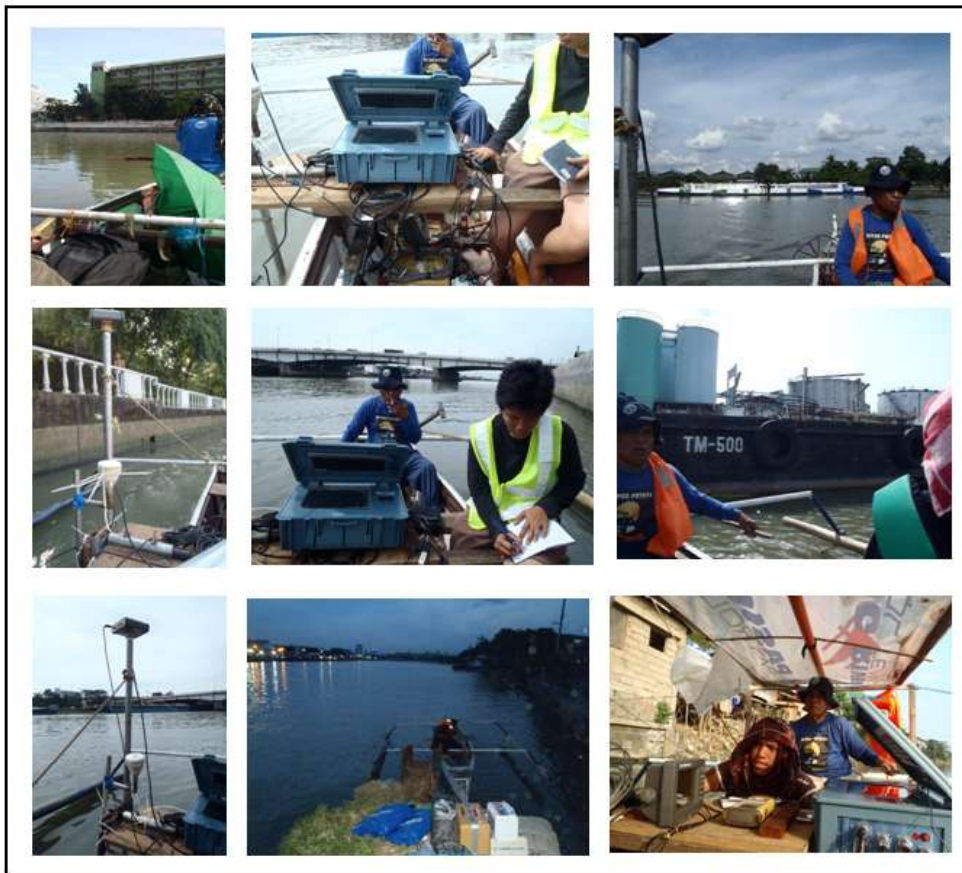
Figure 34. Bathymetric Surveys in the Pasig River.

As data recorded by echosounders are water depths it is necessary to convert these depths into river bed surface elevation referred to the MSL. This can be obtained by determining the water surface elevation at the point of measurement and then subtracting the depth to get the bed elevation (Figure 35). However, information on water surface elevation is usually not available or not measured simultaneously during a bathymetric survey. In some instances, it is possible to obtain the elevation of the water surface by configuring the GPS receiver so that elevation is simultaneously measured while the echosounder is measuring the depth. Unfortunately, the vertical datum used by the GPS receiver is either an ellipsoid or a geoid model (such as the Earth Gravitational Model (EGM) 2008) which is different from the MSL datum. Elevation measured by the GPS cannot be used directly as it still needs to be transformed using a relationship between the GPS-derived elevation (geoidal or ellipsoidal elevation) and the MSL elevation. This relationship can be obtained by using data from established control points. Moreover, the use of GPS may be considered an inappropriate means to measure water surface elevation considering that the boat is affected by wave movements and will make the elevation measurements erroneous.
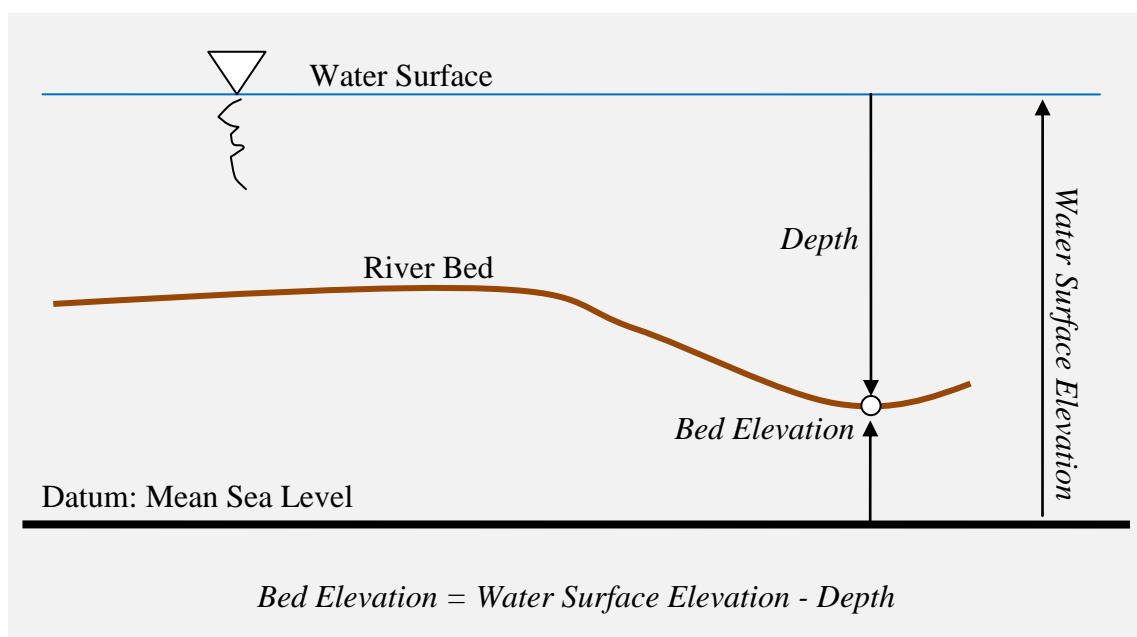
Figure 35. Illustration of computing bed elevation based on measured depth and water surface elevation.
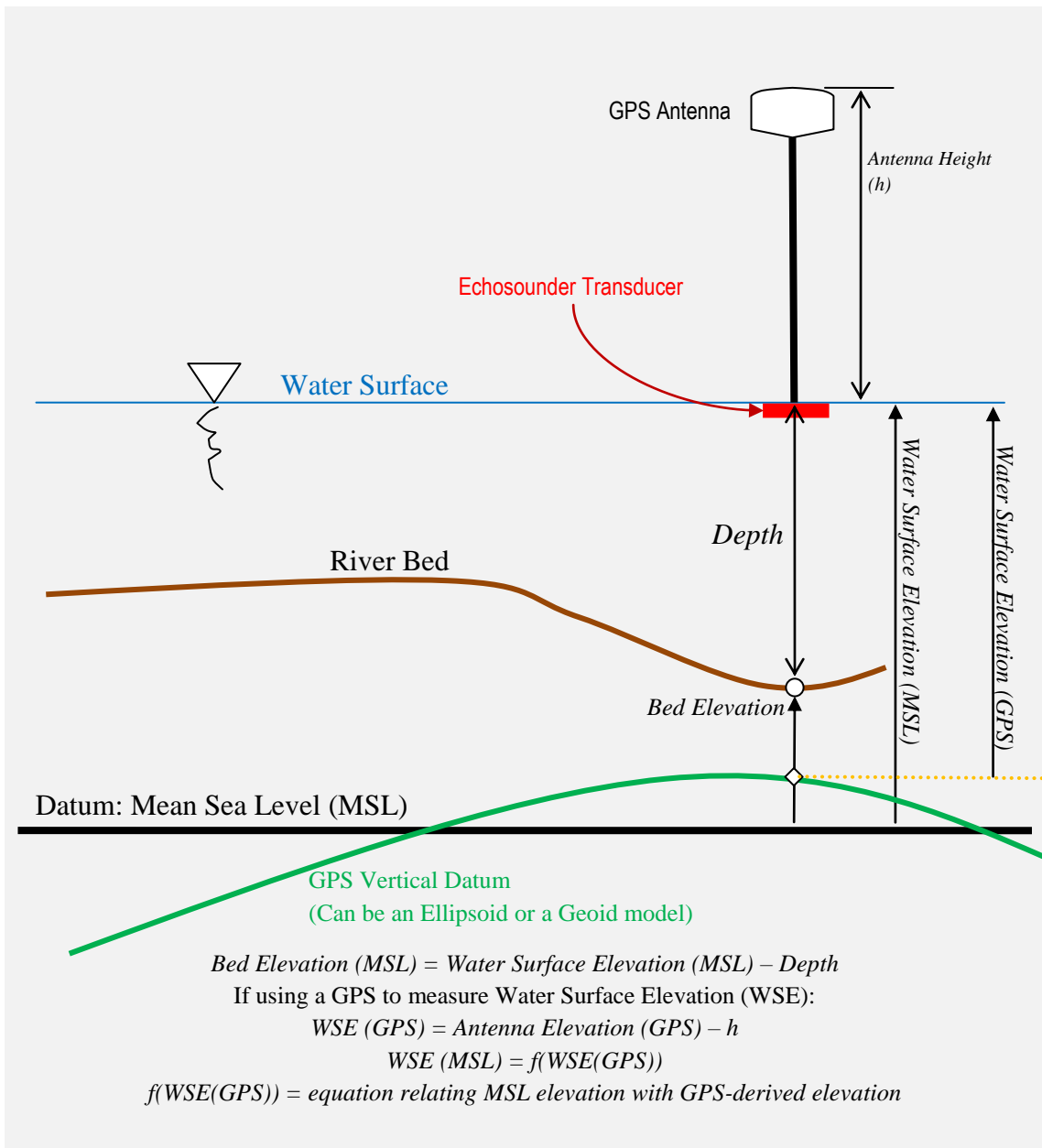
Figure 36. Illustration of getting bed elevation (MSL) using GPS-derived water surface elevation and depth.

In this project, we used an alternative means of converting the depths measured by the echosounders into bed elevations. The method uses time series of WSE measured by water level loggers during the time when the bathymetric surveys were implemented. Hobo water level loggers (Figure 37) were installed at the end points of each survey route to automatically measure time series of depths. The depth time series data is converted to water surface elevation by taking several reference measurements of the elevation of the water surface after the loggers have been deployed and have stabilized. A Total Station with prism and pole (Figure 38) were used to measure WSEs at least five times at each deployment station. After each deployment, the time series of depth data is downloaded from loggers and

processed using the Hoboware software wherein the reference WSE is utilized by the software to convert the depths into WSE referred to the MSL.

Figure 37. An picture of Hobo water level logger deployed during the bathymetric surveys to measure water surface elevation.
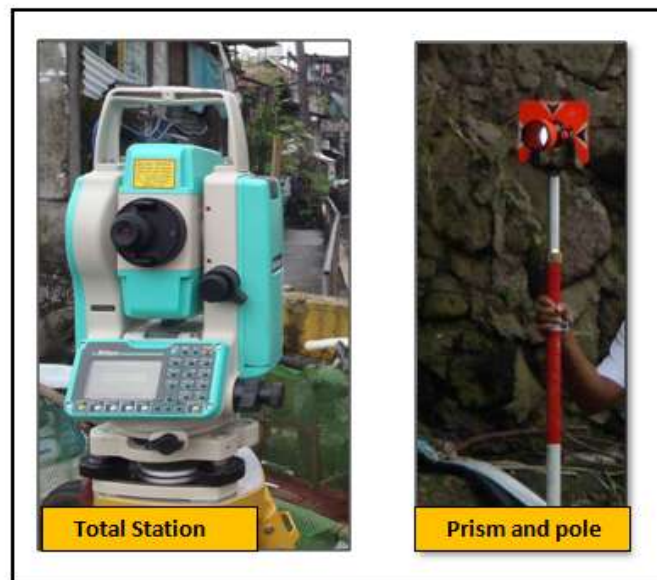
Figure 38. Total Station and accessories used for water surface elevation measurements at the location where the water level loggers were deployed.

The purpose of taking water surface elevation measurements at the end points of each survey route is to estimate the water surface profile (i.e., the slope of the water surface) between the end points. At any given time, the slope of the water surface is computed by getting the difference between the water surface elevations at the end points divided by the river centerline distance between the two points. Assuming that the slope is uniform between the two end points, then the water surface elevation at a bathymetric data point located between the two end points can be estimated by ratio-and-proportion provided that the centerline distance of the bathymetric data point to the two end points are known. This distance can be easily estimated because each bathymetric data point has (x,y) coordinates.

To facilitate faster computation of WSEs, the river centerline that connects the end points of a survey route was divided into 1-m segments with the vertex of the every segment considered as 1-m river center points. This was done using Arcview GIS 3.2 software. The centerline distance of each river center point to the two end points are calculated and assigned as an attribute. Using nearest neighbor analysis, each bathymetric data point is assigned the nearest 1-m center point for which it inherits the centerline distances to the end points of the survey route. By ratio-and-proportion, the WSE at this point can then be computed. This is illustrated in Figure 39. Since each bathymetric data point has a time stamp, the water surface slope during the time when the depth at the data point was measured is calculated using the time series of WSEs. This procedure was repeated for all the bathymetric points. After the WSEs have been computed, the bed elevation is also computed by subtracting the WSE with the measured depth (as shown earlier in Figure 35).

Water level data recorded by EFCOS monitoring stations installed along Marikina River, Pasig River and San Juan River were also utilized to supplement the WSE data measured by the Hobo water level loggers. However, the elevation datum of these stations is not MSL, and recorded water levels are more than 10 meters higher than the MSL. Hence, appropriate correction factors obtained by SMTFCMMS – Project 2 and the 1999 EFCOS Assessment Study were utilized. The water level data were downloaded from the Predict server of ASTI-DOST (http://repo.pscigrid.gov.ph/predict). The stations and their correction factors are listed in Table 8.

Table 8. List of EFCOS monitoring stations which provided supplemental water level data for bathymetric data reduction to MSL,

EFCOS Station Name	River Location	MSL Correction Factor for Water Level Data	Source of Correction Factor
MONTALBAN	Marikina River	- 10.43 m.	2011 SMTFCMMS – Project 2
STO. NINO	Marikina River	- 10.05 m.	
ROSARIO JS	Marikina River	- 10.55 m.	
NAPINDAN JS	Pasig River	-10.60	1999 EFCOS Assessment Study
PANDACAN	Pasig River	-10.60	
FORT SANTIAGO	Pasig River	-10.60	
SAN JUAN	San Juan River	-10.60	
SEVILLA	San Juan River	-10.60	
E. RODRIGUEZ	San Juan River	-10.60	

PLAN VIEW

1-m center point

River bank

A, B = end points of survey route
<u>a</u> = 1-meter center point
<u>b</u> = bathymetric data point

A

<u>a</u>

<u>b</u>

Centerline

River bank

bathymetric data point

Survey route

Water Level Logger

B

Water Level Logger

PROFILE VIEW

Water Surface

<u>b</u> <u>a</u>

WSE_B

WSE_A

$d_{\underline{a}}$

A

B

d_{AB}

Datum: Mean Sea Level (MSL)

$$WSE_{\underline{b}} = d_{\underline{a}} \times (WSE_B - WSE_A) / d_{AB}$$

Note: centerline distance of bathymetric data point <u>b</u> is made equal to centerline distance of 1-m centerpoint <u>a</u> because the data point is nearest to <u>a</u>.

Figure 39. Illustration of computing WSE at a bathymetric data point using measured WSE data measured at the end points of the survey route.

Bathymetric Data Processing

The sounding files of the HiTarget echosounder, in a form of text files, contain the time of acquisition, and depth values in meters. The files from the Lowrance echosounder, in form of charts, were viewed in SonarViewer Version 2.1.2 and the points were exported to a comma delimited (csv) file containing the coordinates, depth values in feet and time offset. Depths from Lowrance echosounder were converted to meter values and the time of acquisition was calculated based on the start times of surveys and the time offsets.

The raw data acquired using the MBES was in .RAW and .HSX format. The .RAW files correspond to the data logged by the Hypack Survey software while the .HSX files correspond to the data logged by the Hysweep Survey software. The Hypack Survey software was designed to take measurements like the single-beam echosounder while the Hysweep Survey software displayed multibeam data. Two editors in Hypack 2011 were used for processing the MBES data and these were the Single Beam Max editor and the Hysweep MBMax editor. The resulting table was exported and contained date, time, coordinates and depth values.

The processed data points from the SBES and MBES were merged and converted to shapefiles and the following attributes were included: date and time of measurement, UTM 51 WGS 1984 coordinates, and depth values.

The time series of water surface elevation data collected during the bathymetric surveys and from EFCOS water level monitoring stations were compiled into tabular files. Using ArcView GIS, these tables were then joined with the attribute tables of the bathymetric data point shapefiles based on the date and time that are common to both dataset. This procedure will assign the WSE to the bathymetric data points as discussed in the previous section. From this, the depth values were converted to bed surface elevations referred to MSL.

Bathymetric Survey Results

About 32.98 km of the Marikina River was surveyed using single-beam echosounders. The survey extent starts in the upstream in a portion of Wawa River in Brgy. San Rafael, Rodriguez, Rizal to the Napindan floodgate in Pateros as shown in Figure 40. Some portions on the upstream part of the Marikina River were not surveyed due to limited access on the area and also due to the strong current which posed danger during the field surveys.

The San Juan River's total surveyed length using the MBES is equal to 5.24 kilometers. The portions of the San Juan River that were surveyed and were accessible by boat were from the E. Rodriguez Bridge to its outlet which connects to the Pasig River (Figure 41).

The Pasig River's total surveyed length using single-beam echosounders is equal to 16.35 kilometers. The Pasig River was surveyed from the Del Pan Bridge, near the Fort Santiago WL station and the Manila Bay, to the Napindan floodgate (Figure 42).

BATHYMETRIC MAP OF THE MARIKINA RIVER
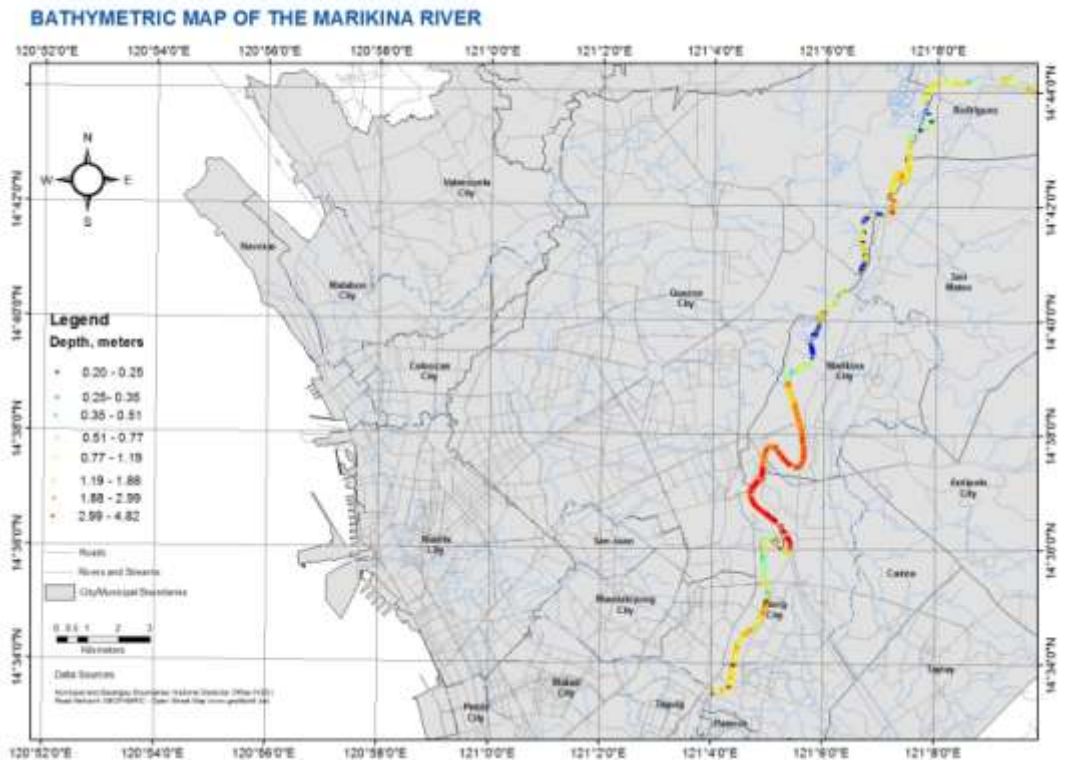
Figure 40. Map showing the bathymetric data points collected using SBES in Marikina River.

BATHYMETRIC MAP OF THE SAN JUAN RIVER

Figure 41. Map showing the bathymetric data points collected using MBES in San Juan River.
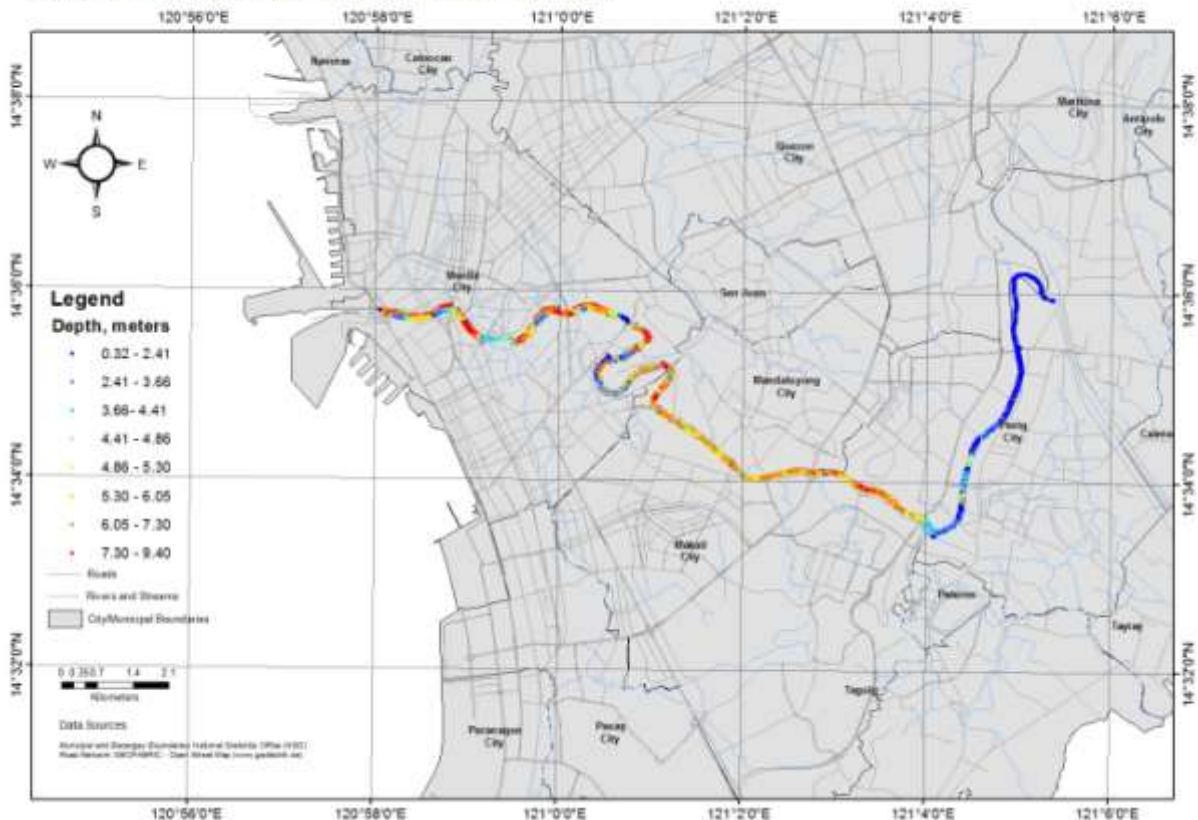
Figure 42. Map showing the bathymetric data points collected using MBES in Pasig River.

Profile and Cross-Section Surveys

Profile and cross-section surveys were conducted to supplement the bathymetric survey data points. These surveys were implemented in San Juan River and in the tributaries as well as in the tributaries of Marikina River. The data collected were cross-section points which include the floodplain, the top of banks, bottom of banks and river bed points.

Profile and Cross-section Surveys of Marikina River tributaries

For the tributaries of the Marikina River (Figure 43), dual frequency, survey-grade Topcon GPS receivers were used in the profile and cross-section measurements using stop-and-go kinematic technique since there are few obstructions present along the tributaries. Another receiver was set-up over one of the established control points and served as base station to log data that were used for post processing. The survey utilized several control points depending on which point is nearest to the survey area.

The rover GPS receivers were attached on poles with fixed heights. The epoch count, the number of measurements per point, was set to 10 seconds. One rover GPS measured on the left bank portion while the other rover measured on the right bank and on the river bed surface. All the rover GPS receivers were set to initialize for at least 15 minutes to obtain fixed solutions on the observations. The rover GPS receivers were placed on steady state and free from obstructions while initializing. The profile measurements were taken along the

banks at an interval of at least 10 meters. The floodplain portions were surveyed to an extent of at least 300 meters from each bank. The cross-sections were measured at an interval of at least 200 meters. The method used to traverse each tributary was in an endpoint-to-bank manner. From an approximate location of the endpoint of a cross-section line, the measurements were taken along roads or pathways until reaching the banks of the tributary. Existing walls were also taken in the measurements.
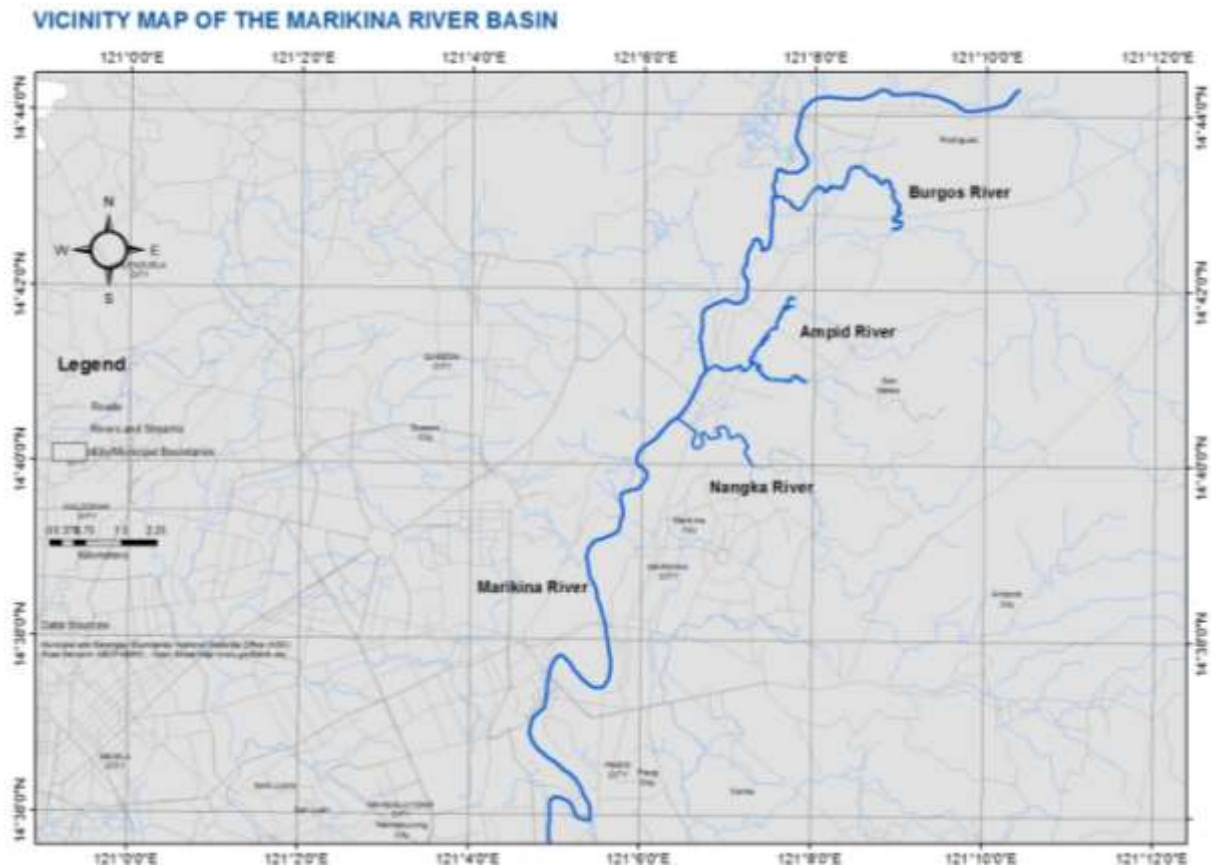
Figure 43. Map of Marikina River and its tributaries.

The elevation datum of the survey points collected using this technique are referred to the EGM 2008 geoid model [45] which were converted to MSL using a second order polynomial equation (Figure 44). This equation was developed through regression between elevation values of the six (out of seven) control points established along Marikina River. Cross-validation of this equation with all the seven control points resulted to an average absolute error of 0.209 m and root mean square error of 0.232 m. A 2nd order polynomial equation was used because it yielded the lowest error compared to a linear equation. Further validation of this equation using the established control points in Pasig and San Juan River was not done due to differences in topographic characteristics in these areas to that in Marikina River. Also, during the time when the regression equation was developed, control points in Pasig and San Juan Rivers were not yet established.

The profile and cross-section surveys were conducted per tributary (Table 9). The profile and cross-section surveys for the Burgos River were made on February 14-17, 2012.

The Burgos River was surveyed from its upstream portion to the downstream portion at the mouth of the Marikina River (Figure 45). The profile and cross-section surveys for the Ampid River were made on February 22-24 and March 19-20, 2012. The Ampid River was surveyed from its upstream portions, from southern part and then the northern part, to the downstream portion at the mouth of the Marikina River (Figure 46). The Nangka River was surveyed from its upstream portion to the downstream portion at the mouth of the Marikina River (Figure 47).
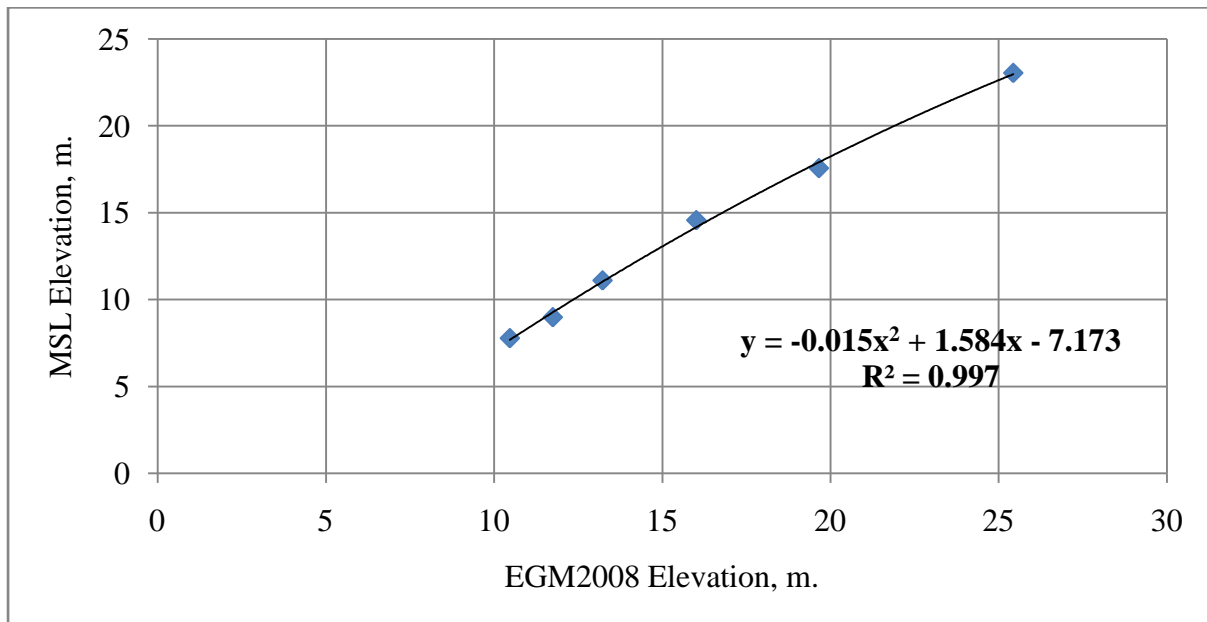
Figure 44. Second-order polynomial regression to convert EGM 2008 Elevation to MSL Elevation.

The chart shows a scatter plot of MSL Elevation (m.) versus EGM2008 Elevation (m.) with the equation $y = -0.015x^2 + 1.584x - 7.173$ and $R^2 = 0.997$.

Table 9. Implementation dates of profile and cross-section surveys of the tributaries of Marikina River.

Date of Survey	Tributary	Activity	Approximate length surveyed, km.
14-15 February 2012	Burgos River	Profile Surveys	4.75
16-17 February 2012	Burgos River	Cross-section Surveys	3.79
22-24 February 2012	Ampid River	Profile and Cross-Section Surveys	4.92
19-20 March 2012	Ampid River	Cross-section Surveys	1.58
21 March 2012	Nangka River	Cross-section Surveys	2.92
26-28 March 2012	Nangka River	Profile and Cross-Section Surveys	3.16

Figure 45. Pictures showing the conduct of profile and cross-section surveys in Burgos River which is a tributary of Marikina River.

Figure 46. Pictures showing the conduct of profile and cross-section surveys in Ampid River which is a tributary of Marikina River.

Figure 47. Pictures showing the conduct of profile and cross-section surveys in Nangka River which is a tributary of Marikina River.

Profile and Cross-section Surveys of San Juan River and its tributaries

For San Juan River and in some of its tributaries, conventional topographic surveying technique (traverse) using a total station with prism and pole was used instead of GPS receivers due to the presence of tall buildings and trees along the river network which could affect GPS signals. Elevation data obtained from these surveys are already referred to the MSL. These surveys utilized the previously established control points as reference stations.

It can be noticed that bathymetric surveys were earlier conducted in San Juan River. However, results of the bathymetric surveys showed incomplete coverage of the river due to inaccessibility problems. Hence resurveys were conducted as explained here.

The profile surveys were conducted on the San Juan River and Kamias Creek. Cross-section measurements were also taken on the San Juan River and Kamias Creek and other tributaries (Mariblo Creek and Diliman Creek). The profile and cross-section surveys were

conducted per river segment wherein established control points were used as reference stations. Additional control points were marked as traverse points in between long segments and in river bends. Resection method was used to obtain the location of the occupied stations using the traverse points as back sight stations. The implementation dates of the surveys are shown in Table 10.

Table 10. Implementation dates of profile and cross-section surveys of the San Juan River and tributaries.

Date of Survey	River/Tributary	Activity	Approximate length surveyed, km.
5-7 September 2012	San Juan River	Profile Surveys	1.72
10-14 September 2012	San Juan River	Profile Surveys	2.07
17 September 2012	San Juan River	Profile Surveys	1.58
19,21,24 September 2012	Mariblo Creek I	Cross-section Surveys	2.86
25 September 2012	Mariblo Creek II	Cross-section Surveys	1.15
26-28 September 2012	Diliman Creek	Cross-section Surveys	2.39
1-4 October 2012	Diliman Creek	Cross-section Surveys	4.18
9-11 October 2012	Kamias Creek	Profile and Cross-section Surveys	1.34
16-17 October 2012	San Juan River	Profile Surveys	1.62
12-13 November 2012	San Juan River	Profile Surveys	0.35
14 November 2012	Kamias Creek	Profile and Cross-section Surveys	0.84

Figure 48. Pictures showing the conduct of profile and cross-section surveys in San Juan River.

Figure 49. Pictures showing the conduct of profile and cross-section surveys in Mariblo Creek which is a tributary of San Juan River.

Figure 50. Pictures showing the conduct of profile and cross-section surveys in Diliman Creek which is a tributary of San Juan River.

Figure 51. Pictures showing the conduct of profile and cross-section surveys in Kamias Creek which is a tributary of San Juan River.

Profile and Cross-section Survey Results

The processed survey points for the tributaries of the Marikina River consist of elevations referred from the Earth Gravitation Model of 2008 (EGM 2008) geoid. The elevation values were converted to elevations referred from MSL using the 2nd order polynomial equation shown earlier in Figure 44.

The survey maps of the Burgos River (Figure 52), Ampid River (Figure 53) and Nangka River (Figure 54) consist of classified survey points that include floodplain points, top and bottom of bank points, riverbed points and walls.
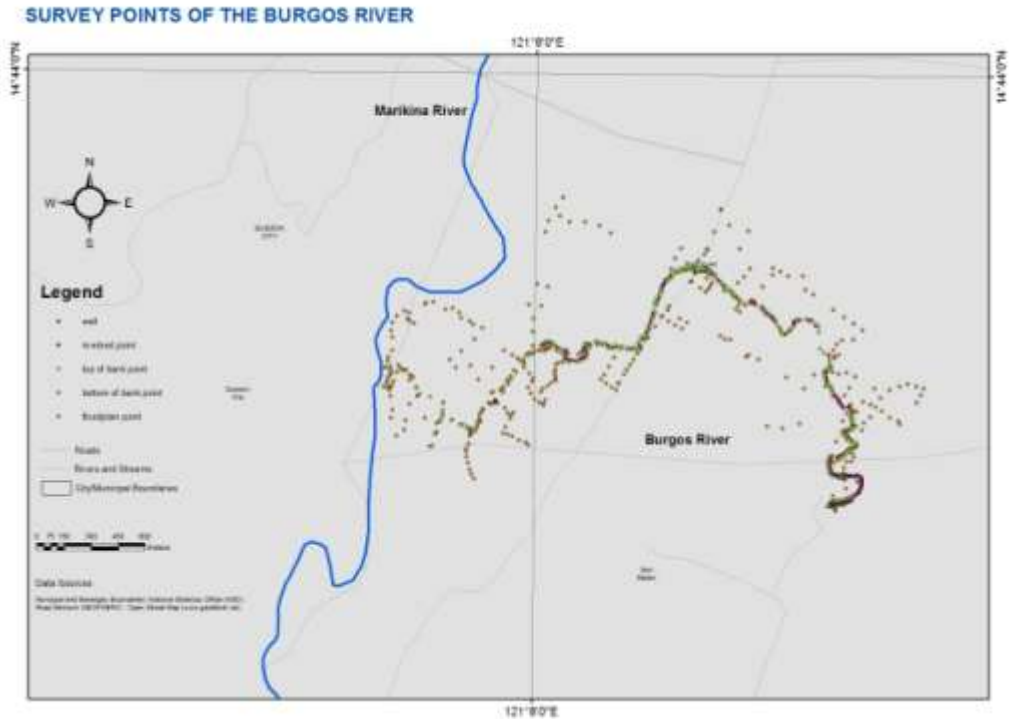
Figure 52. Map showing the profile and cross-section survey points collected in Burgos River which is a tributary of Marikina River.
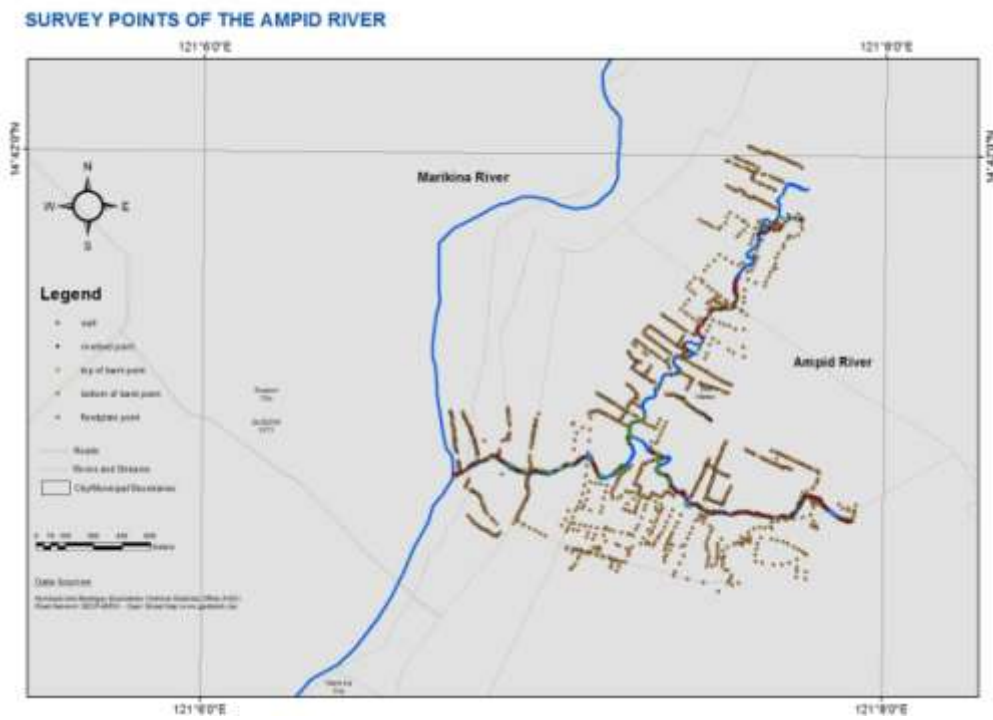
Figure 53. Map showing the profile and cross-section survey points collected in Ampid River which is a tributary of Marikina River.

Figure 54. Map showing the profile and cross-section survey points collected in Nangka River which is a tributary of Marikina River.

For San Juan River, profile and cross-section data were collected for a total river length of approximately 7.29 km. The cross-section points of the San Juan River (Figure 55) consist of riverbed points measured from an end of the bank to its opposite end. The measurements were taken at an interval of at least 80 meters. There were a total of 104 cross-section lines made on the San Juan River (Figure 56).

Figure 55. Map showing the profile survey points collected in San Juan River.
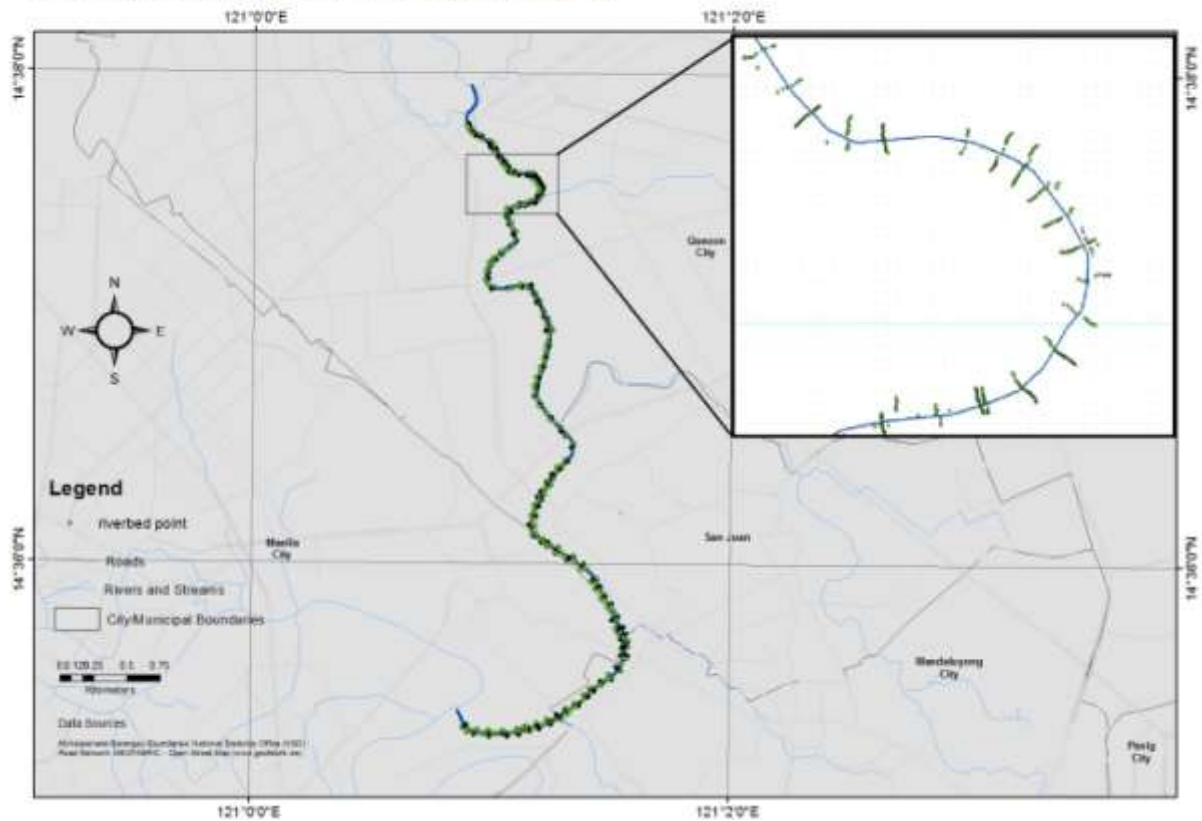
Figure 56. Map showing the cross-section survey points collected in San Juan River.

The survey points of the tributaries Mariblo Creek, Diliman Creek and Kamias Creek consist of top and bottom of bank points, water surface points, concrete walls, outfalls or drainage points and trees. The profile measurements were taken at an interval of at least 15 meters while cross-section measurements were taken at an interval of at least 80 meters.

In Diliman Creek, 72 cross-section lines were measured (Figure 57). In Mariblo Creek a total of 55 cross-section lines were measured (Figure 58). In Kamias Creek there were 87 cross-section lines measured (Figure 59).
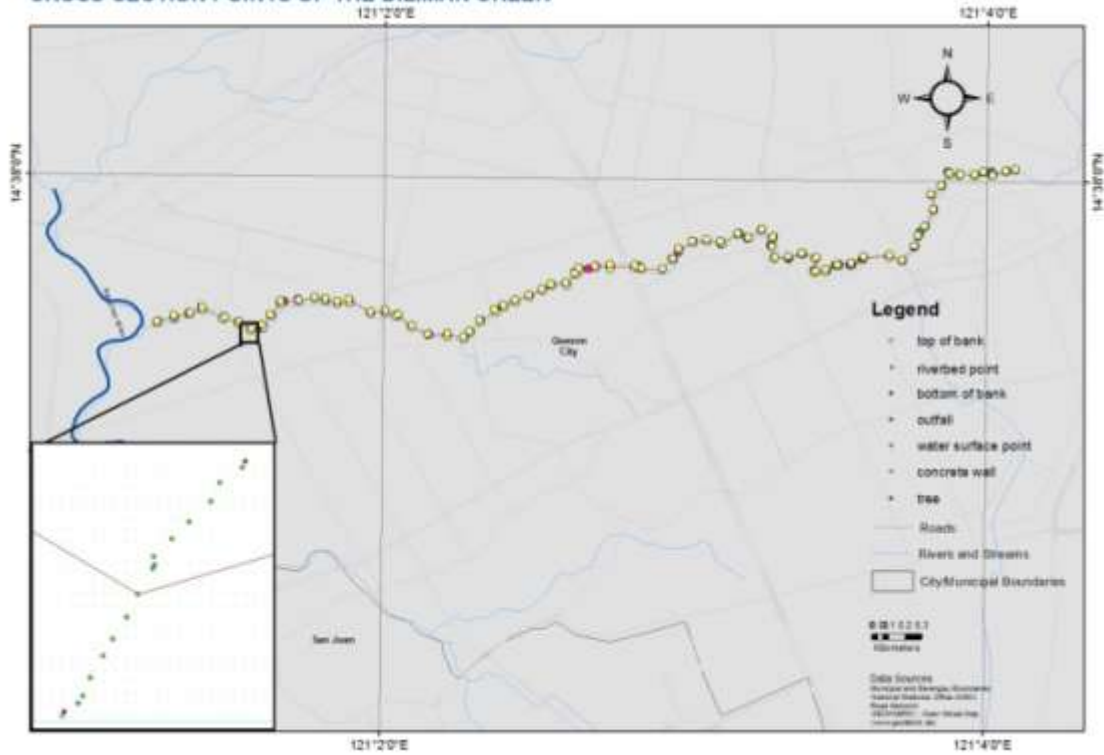
Figure 57. Map showing cross-section survey points collected in Diliman Creek.
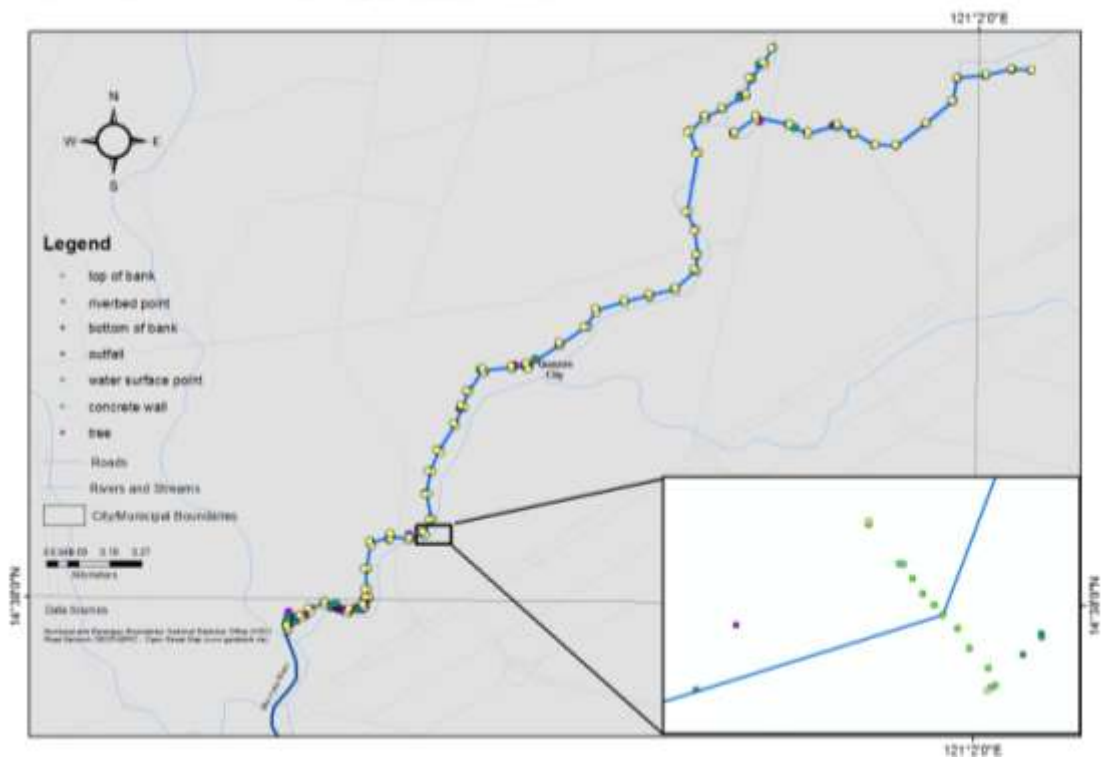
Figure 58. Map showing cross-section survey points collected in Mariblo Creek.
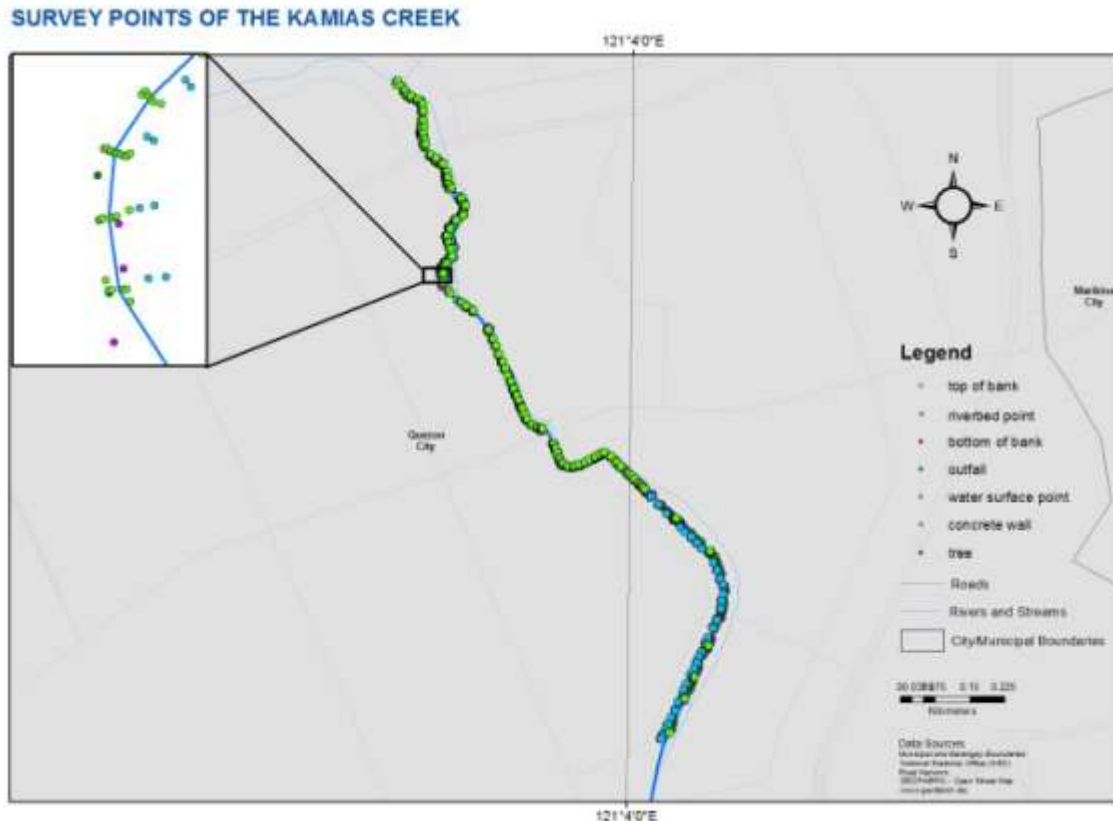
Figure 59. Map showing cross-section survey points collected in Kamias Creek.

All the data points collected and processed from the profile and cross-section surveys were compiled into a GIS shapefile and included the following attributes: type (e.g., river bed, top of bank or flood plain point), their UTM 51 WGS 1984 coordinates and elevation referred to the MSL.

River bed surface point data of San Juan River tributaries that were not surveyed under the project such as Pasong Tamo River, Culiat Creek, Dario River, Talayan Creek, San Francisco, Ermitanio Creek, Maytunas Creek and Kalentong Creek were obtained from the UP TCAGP PRTSAS Phase II – Hydrographic Surveys Components. During the project surveys in San Juan River Basin, the PRTSAS Phase II - Hydrographic Surveys Components were conducting detailed surveys of these tributaries. Instead of duplicating these surveys, the project opted to request selected river bed surface point data. In exchange, the project provided the profile and cross-section data of San Juan River, Mariblo Creek, Diliman Creek and Kamias Creek.

Riverbed Surface Generation and Integration with 1-m LiDAR DEM

The river bed elevation data points collected through conduct of bathymetric and profile and cross-section surveys and those from the UPTCAGP PRTSAS Phase II – Hydrographic Surveys Components were utilized to generate continuous river bed elevation surfaces/grids. These grids were then integrated into a 1-m "bare earth" LIDAR DEM of the major portions project areas.

The LiDAR DEM (Figure 60) was provided by the Collective Strengthening of Community Awareness of Natural Disasters (CSCAND) agencies under the National Disaster Risk Reduction and Management Council - Office of Civil Defense (NDRRMC-OCD) thru the National Mapping Resource and Information Authority (NAMRIA). The dataset is composed of six blocks which were mosaicked and used for the data integration. Originally, the DEM is in a Transverse Mercator projection and with the Philippine Reference System of 1992 (PRS92) as its datum. Using ArcGIS, the LiDAR DEM was re-projected to UTM 51 WGS 1984 to make it compatible with the project datasets.

The integration of field surveyed data into the DEM was necessary as the riverbed portions in the LIDAR DEM were poorly represented and not well defined (e.g., river beds are flat). This is due to the inability of lasers coming from the LIDAR equipment to penetrate water in rivers and other water bodies.
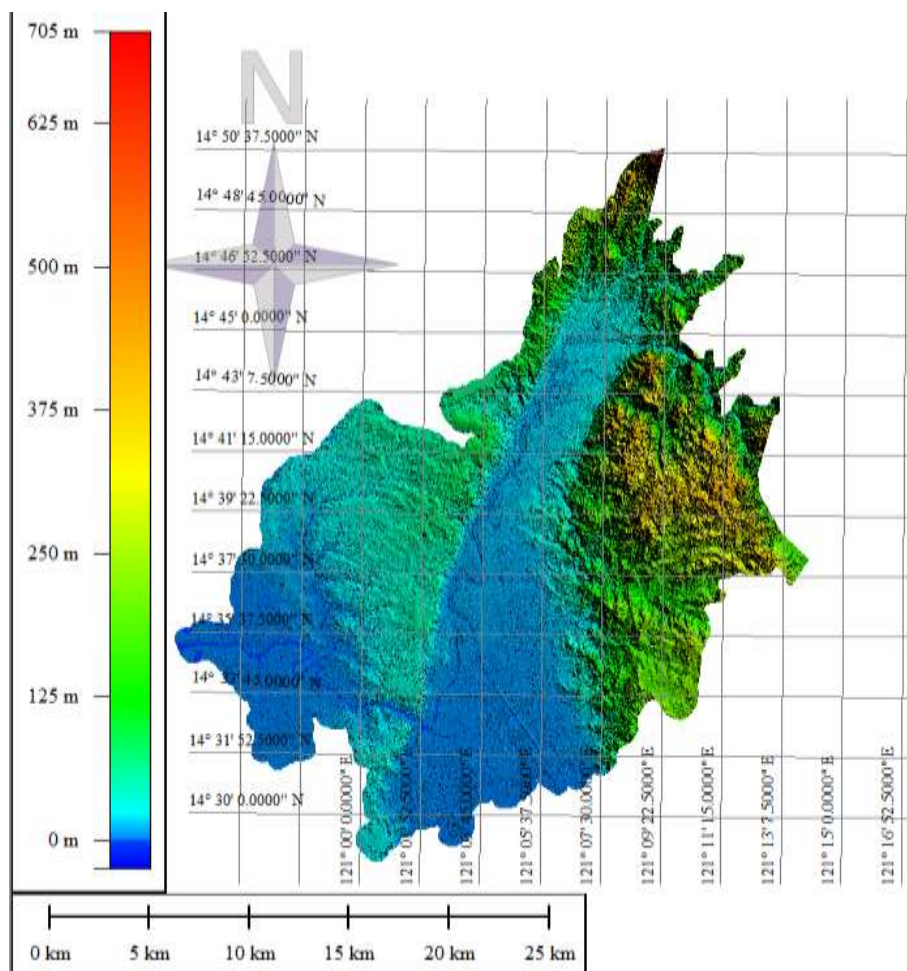
Figure 60. Map showing the 1-m "bare earth" LIDAR DEM of the major portions project areas.

For each river or creek, 1-m resolution bed surface elevation grids were generated through kriging interpolation of the riverbed surface points. Kriging is a geostatistical method used to predict the elevations of the unsurveyed portions given the samples of known

locations and elevations. The predicted values were estimated by their spatial distribution. The Kriging method uses a variogram to express the spatial variation and to minimize the error of predicted values. Prior to kriging interpolation, the bed surface point data was divided into prediction and validation points. Prediction points (consist of those points which are 95% of the full data) were used for the kriging interpolation of the bed surface. The remaining 5% of the full data were used to assess the accuracy of the interpolation. The validation points were randomly selected from the full data using the Random Points Generator extension of Arcview GIS 3.2 software.

Table 11 provides a summary of prediction and validation points used in river bed surface interpolation and accuracy assessment. The accuracies, in terms of average error and RMS Error, of the interpolated surfaces are provided as well.

An example of interpolated river bed surface elevation grid for Marikina River is shown in Figure 61. The river bed surface elevation grids were then integrated into the LIDAR DEM by first masking all the river bed portions in the DEM, and then adding the interpolated surfaces. Snapshots of the results are shown in Figure 62 and Figure 63, and Figure 64.

The LIDAR DEM integrated with river bed data, hereinafter referred to as the "updated LIDAR DEM", was used as primary source of topographic information for HEC RAS model development (river profile, cross-sections, river width) of Marikina River, San Juan River and Pasig River. It was also used as input DEM for HEC HMS model development of San Juan River Basin (watershed delineation, slope estimation, river width and river profile).
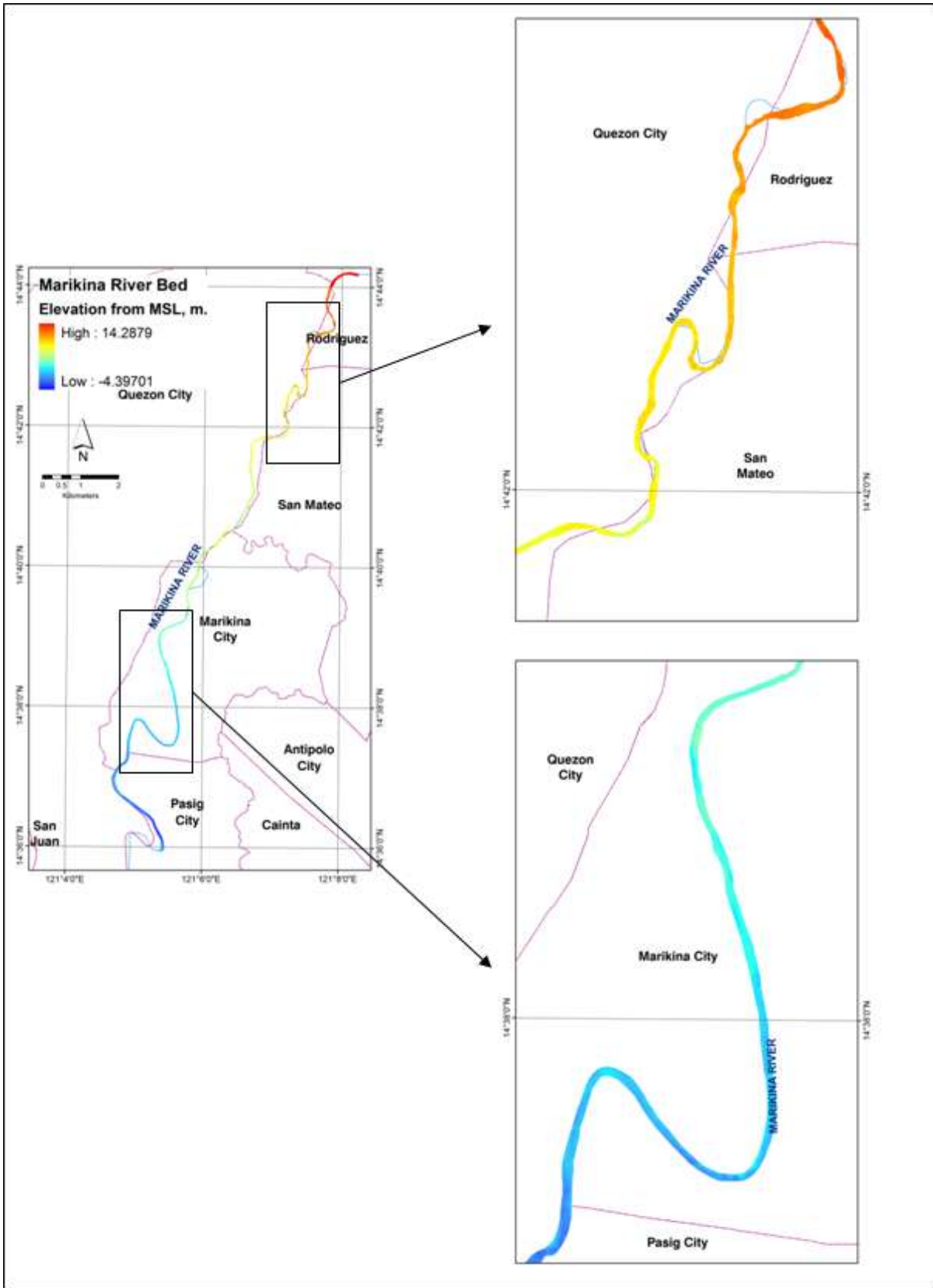
Figure 61. An example of interpolated river bed surface elevation grid for Marikina River.

Table 11. Summary of prediction and validation points used in river bed surface interpolation and accuracy assessment.

Main River	Tributary Name	Prediction Points	Validation Points	Accuracy of River Bed Elevation Interpolation	
				Average Error (m.)	RMS Error (m.)
Marikina River	Main River	74,939	3,948	0.003	0.258
	Burgos River	695	36	-0.005	0.866
	Ampid River	502	26	-0.029	1.324
	Nangka River	732	38	0.033	0.928
Pasig River	Main River	37,379	1,967	-0.077	1.290
San Juan River	Main River	3,227	170	-0.043	1.152
	Dario River	4,325	228	-0.015	0.387
	Pasong Tamo River	3,475	183	0.019	0.327
	Culiat Creek	1,473	78	0.007	0.097
	San Francisco River	2,202	115	-0.093	0.510
	Talayan Creek	3,423	181	0.033	0.910
	Mariblo Creek	2,670	138	-0.034	0.279
	Diliman Creek	4,708	248	-0.017	0.357
	Kamias Creek	692	37	0.080	0.181
	Ermitanio Creek	3,616	190	-0.016	0.264
	Maytunas Creek	1,224	65	0.013	0.171
	Kalentong Creek	856	45	-0.055	0.328
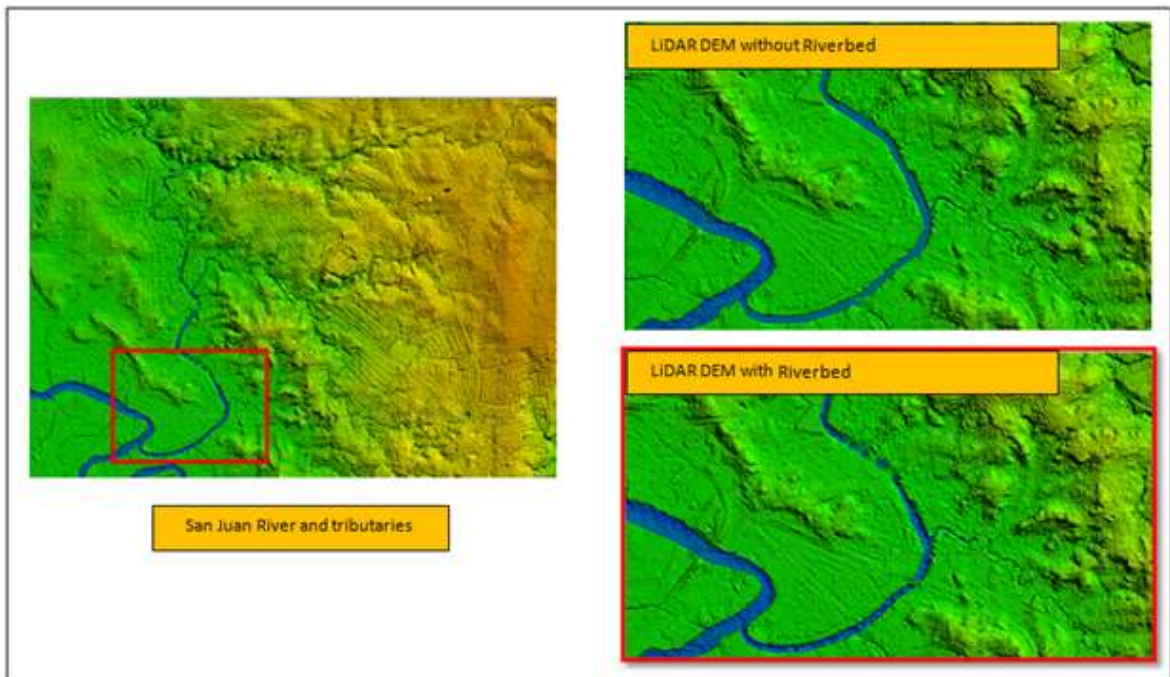
Figure 62. Snapshot of a portion of the San Juan River LIDAR DEM integrated with river bed surface elevation grids.
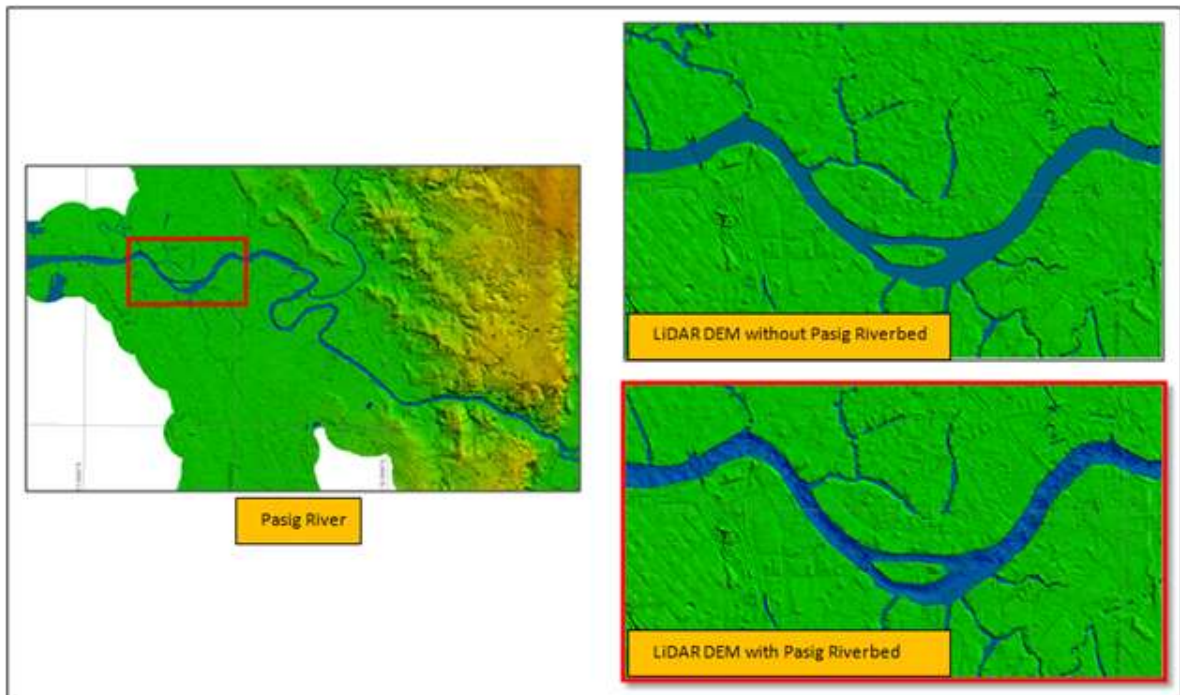
Figure 63. Snapshot of a portion of the Pasig River LIDAR DEM integrated with river bed surface elevation grids.
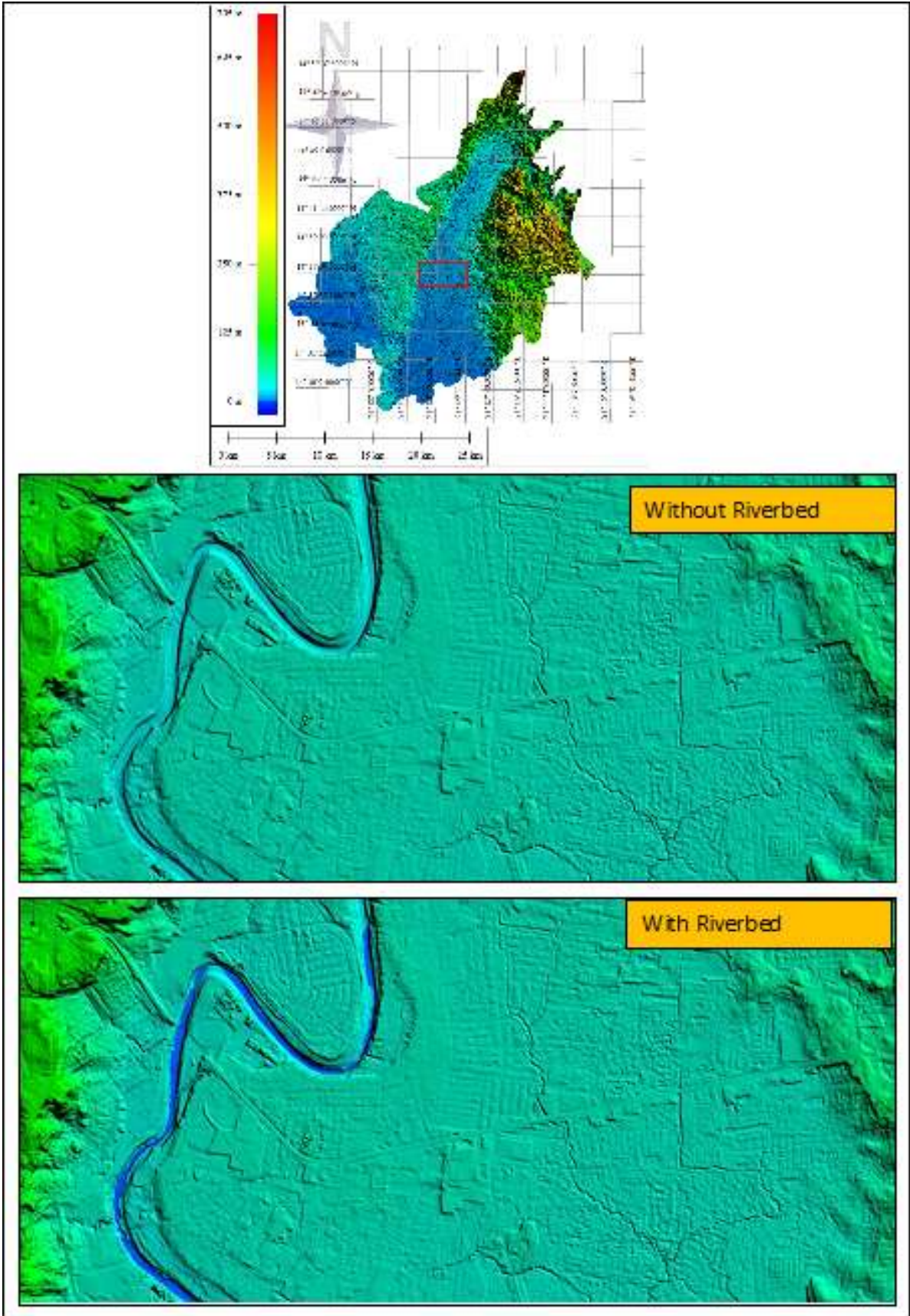
Figure 64. Snapshot of a portion of the Marikina River LIDAR DEM integrated with river bed surface elevation grids.

Collection and processing of other Elevation Datasets

The updated LIDAR DEM only includes a portion of the Marikina River Basin (MRB) but includes the whole of San Juan River Basin. It must be noted that during the hydrological model development of MRB, the LIDAR DEM are not yet available. Because of this, the hydrological model development of Marikina River Basin which requires a DEM relied on the use of other elevation datasets which includes the MMEIRS 2004 Metro Manila Elevation Data, 1:50,000 NAMRIA Topographic Map Vector Data, and ASTER GDEM Version 1. The 1-m interval elevation contour lines of MMEIRS data covers those portions of MRB that are within the cities of Marikina and Pasig. The 1:50,000 NAMRIA data covers the whole of MRB but too few contour lines (20-m intervals) are present in the Marikina River flood plains and in the flood plains of other major rivers, especially in the portions not covered by the MMEIRS data. To supplement this relatively incomplete elevation data, 1-m contour lines where extracted from the ASTER GDEM using contour line extraction tools in ArcGIS. Essentially, the sparse 1:50,000 NAMRIA contour lines in the river flood plains were replaced with contour lines from ASTER GDEM. The contour lines from the three datasets are shown in Figure 65.

Prior to the extraction of contour lines from the ASTER GDEM, consistency of elevation values between the ASTER GDEM with the MMEIRS and the NAMRIA elevation datasets were checked first. This was done by selecting nearby spot heights from both the MMEIRS and NAMRIA elevation datasets and then extracting the corresponding ASTER GDEM elevation. It must be noted that there were no available spot heights from MMEIRS and NAMRIA datasets in the portion where the ASTER GDEM is to be supplemented. This is the reason why nearby spot heights were utilized (selected in a random manner using Arcview GIS 3.2's Random Point Generator extension) in comparing the elevation values. The range of ASTER GDEM elevation values in the areas/portions of MRB to be supplemented is 2 to 55 meters.

The results of the comparisons, shown in Figure 66, indicates that the ASTER GDEM elevations are 16 meters lower than their elevations in 1:50,000 NAMRIA dataset. However, this comparison may not be representative of the topographic characteristics in the areas/portions of MRB to be supplemented because the ASTER GDEM elevation range of the spot heights is wider (between 2 to 475 m).

On the other hand, the comparison of MMEIRS spot height elevations with the ASTER GDEM elevation indicates a more realistic comparison as the elevation range is between 1 to 58 m – this is nearer to the elevation values in the areas/portions of MRB to be supplemented. Based on the comparison, the ASTER GDEM elevations are 3 meters lower than their elevations in the MMEIRS dataset. The linear equation to adjust the ASTER GDEM elevation values is represented by $y = 1.03x + 2.09$ where y = adjusted elevation and x = ASTER GDEM elevation. After adjusting the elevation values, contour lines were then extracted.

To create a DEM for the Marikina River Basin, first the contour lines from the three datasets were merged. Then, a TIN surface was generated based on the contour lines. After this, the TIN was converted into a 10-meter resolution grid. This grid became the MRB DEM which was used for HEC HMS model development. The DEM is shown in Figure 67.

This multi-source approach of generating the MRB DEM was adapted instead of utilizing a readily available DEM such as SRTM DEM and ASTER GDEM in order to make use of the consistent and detailed elevation datasets from the MMEIRS and 1:50,000 NAMRIA topographic maps. Here, consistency is with regards to the elevation datum which is the MSL. The project did not use SRTM DEM as the resolution is low (~ 90 m) and needs calibration such that the elevation values are referred to the MSL. On the other hand, only a portion of ASTER GDEM was utilized and not the whole because of some sinks/pits present in the data that needs correction, in addition to the need to calibrate the elevation values.
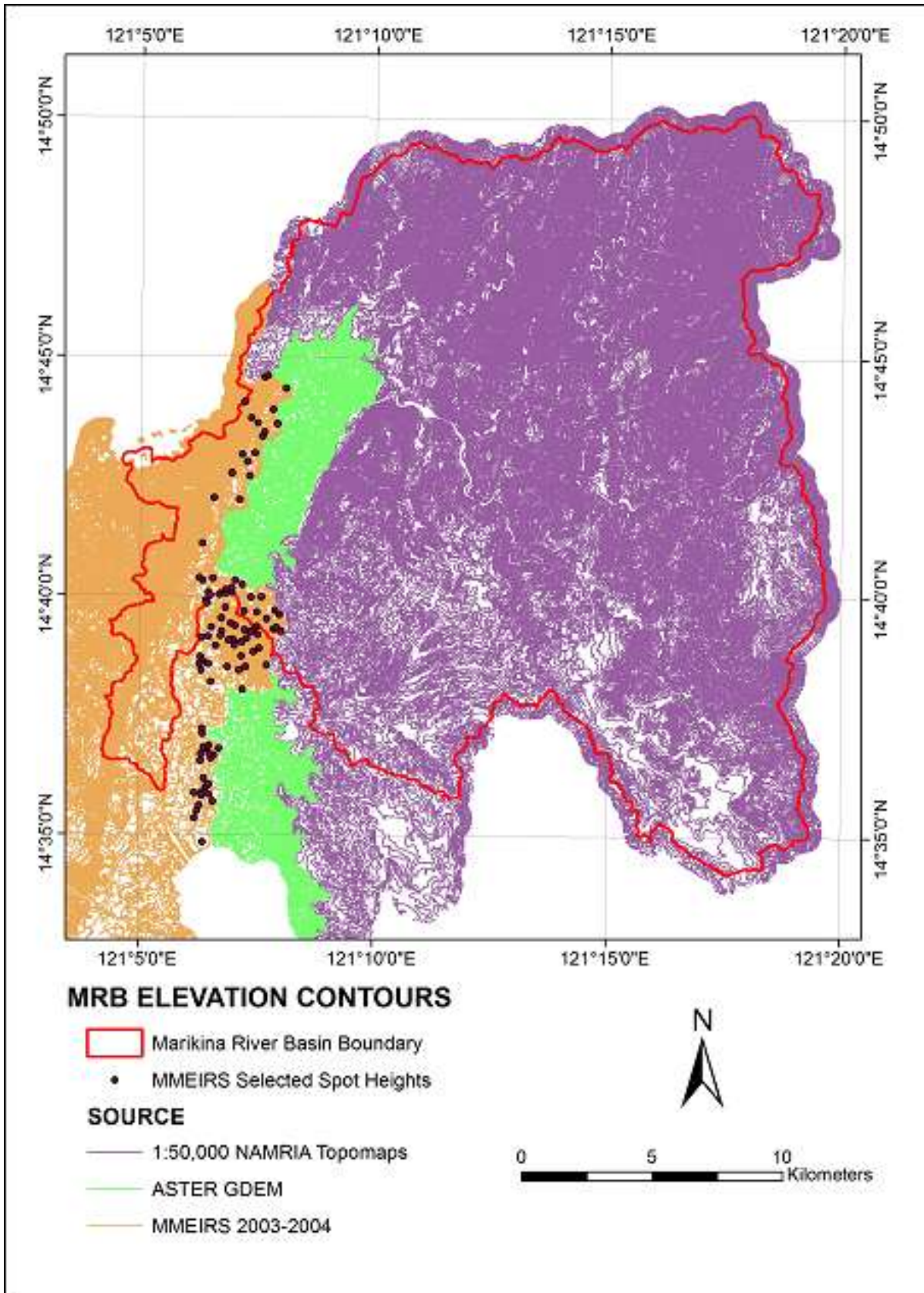
Figure 65. Map showing contour lines from MMEIRS, ASTER GDEM and 1:50,000 NAMRIA Topographic Maps that were used to generate the MRB DEM for hydrological model development. Spot heights used for ASTER GDEM calibration are also shown.
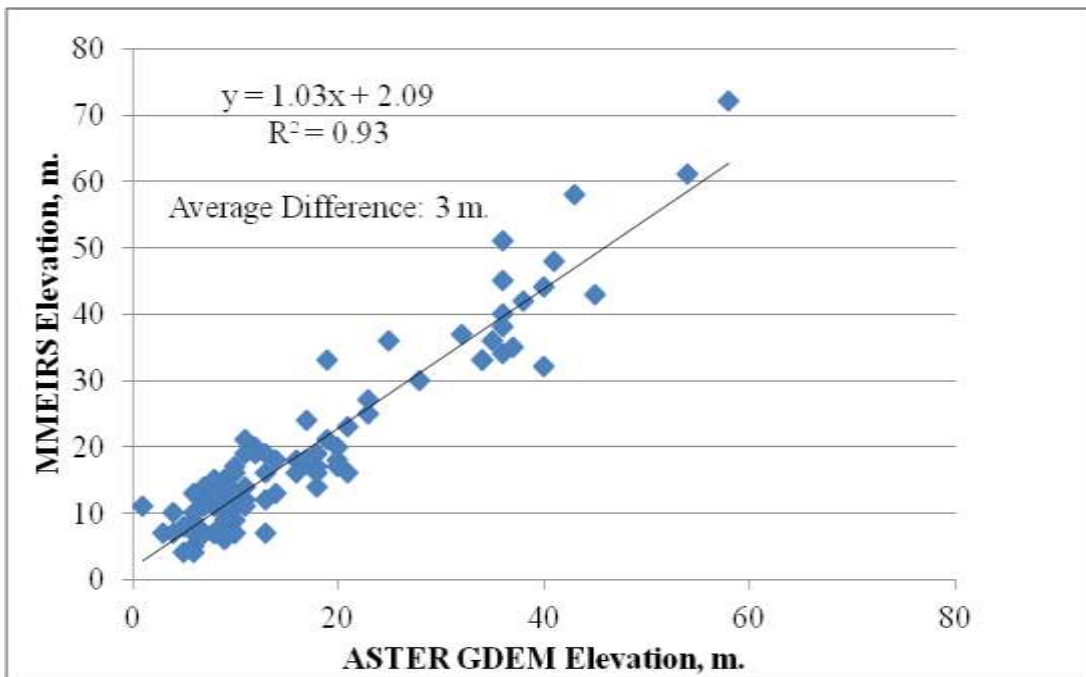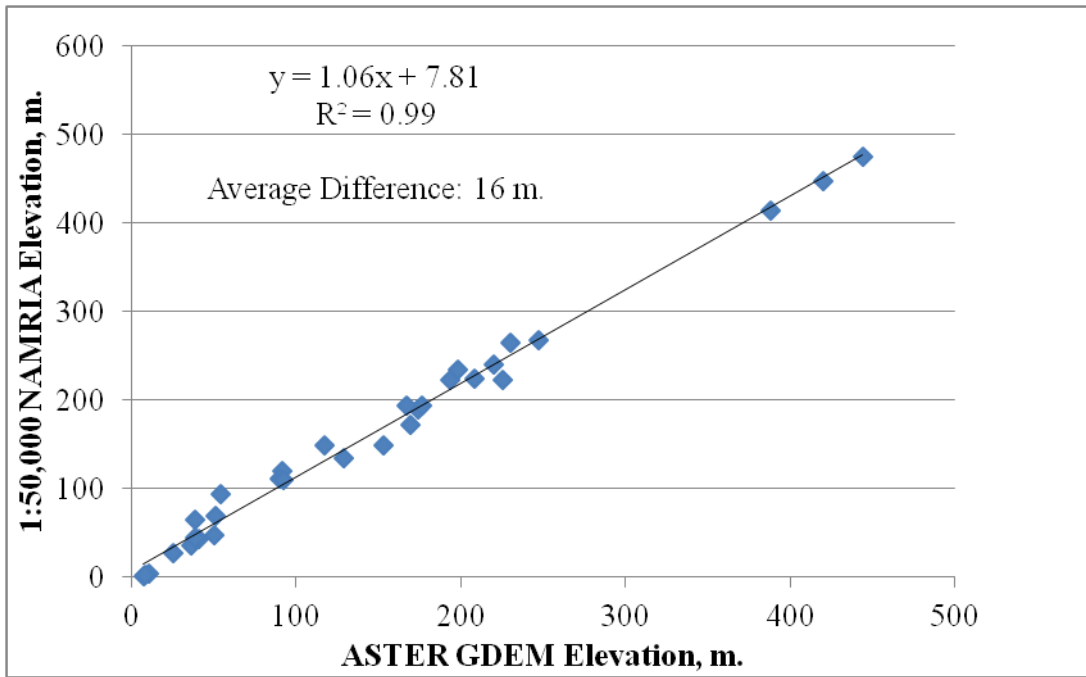
Figure 66. Result of comparing elevation of selected MMEIRS and NAMRIA spotheights with their corresponding elevation in an ASTER GDEM.
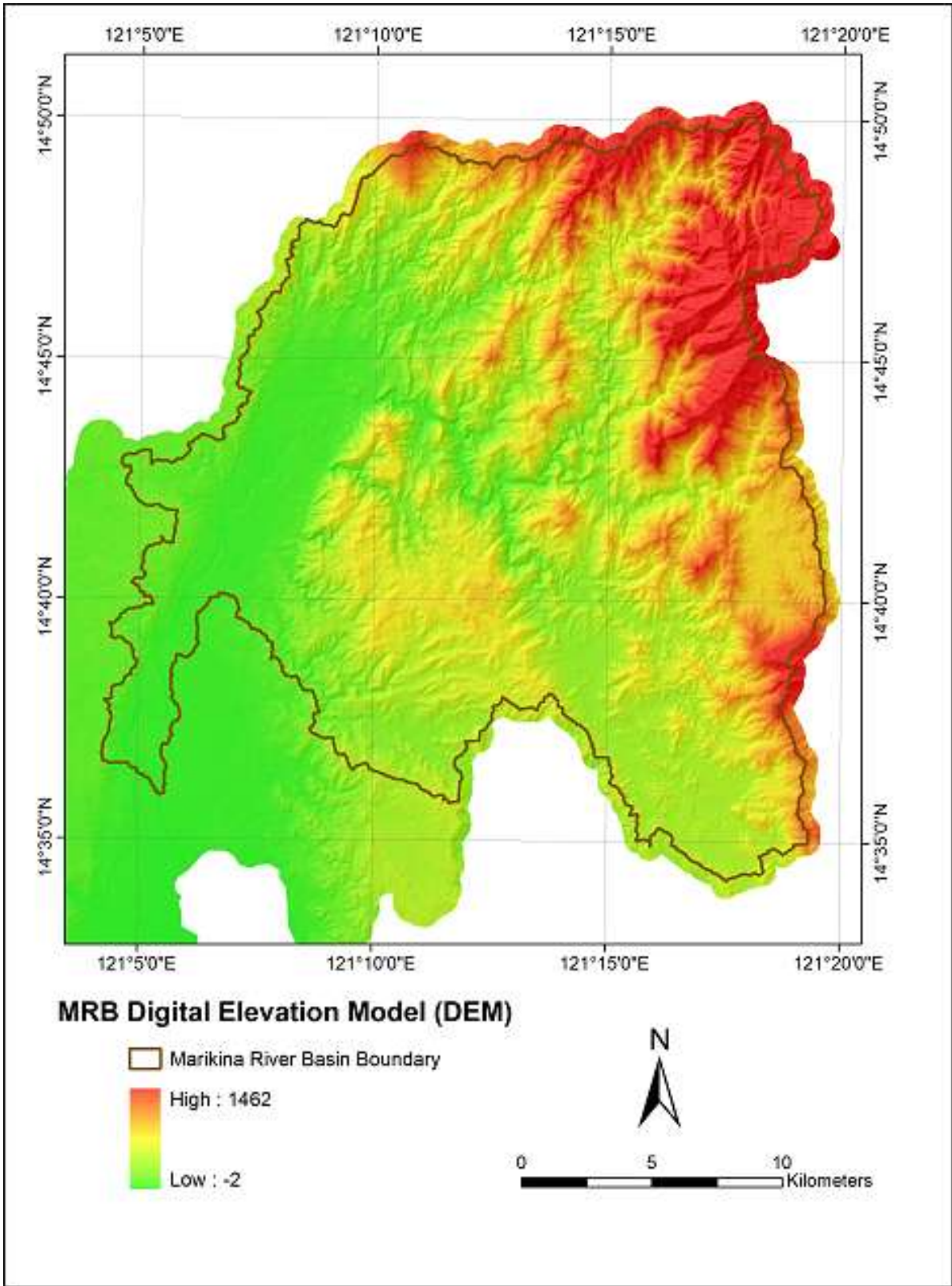
Figure 67. The MRB DEM generated using contour lines of MMEIRS, 1:50,000 NAMRIA and adjusted ASTER GDEM elevation datasets.

Chapter Summary and Conclusions

In this chapter, the collection, processing and analysis of topographic and hydrographic datasets were presented and discussed. Through conduct of field surveys and processing of outputs, the project was able to generate river bed surface elevation grids that were integrated into a 1-m resolution LIDAR DEM. This updated LIDAR DEM was used as primary source of topographic information for HEC RAS model development (river profile, cross-sections, river width) of Marikina River, San Juan River and Pasig River. It was also used as input DEM for HEC HMS model development of San Juan River Basin (watershed delineation, slope estimation, river width and river profile).

The project was also able to generate a 10-m resolution DEM of the MRB for hydrological model development. This DEM was produced using multi-source approach with data coming from MMEIRS, NAMRIA and ASTER GDEM.

Chapter 4. Land-cover Information Generation from Satellite Images for Flood Model Development

Overview

Land-cover information is necessary in flood model development. The hydrologic component of a flood model requires land-cover information as a way to estimate the effects of vegetation and other land-cover classes in transforming rainfall into runoff through such processes as interception, evaporation and infiltration. On the other hand, the hydraulic component of a flood model also requires land-cover information as a way to estimate river bed and flood plain surface roughness – a parameter that dictates how fast water will flow and where it will flow during a flood event.

In this chapter, land-cover information is generated though the analysis of satellite images. Two land-cover maps were generated: a 10-m resolution land-cover map that covers the Marikina River Basin, San Juan River Basin and floodplains of Pasig River based on ALOS AVNIR-2 satellite images; and a 0.5-m resolution land-cover map of San Juan River Basin based on a Worldview-2 satellite image.

Land-cover mapping using ALOS AVNIR-2 Satellite Images

Image Pre-processing

Two scenes of Level 1B ALOS AVNIR-2 satellite images acquired on 02 February 2010 and covering the project areas (Figure 68) were obtained from SMTFCCMS-Project 4. Each scene contains 4 bands representing the blue, green, red and near infrared and were already in UTM 51 WGS 1984 projection. Each scene was subjected to three pre-processing procedures using ENVI 4.8 software: radiometric calibration, atmospheric correction, and geometric correction.

Radiometric calibration was done by converting the digital numbers (DN) in each band to top-of-atmosphere (TOA) spectral radiance (L_λ), where $L_\lambda = DN_\lambda * Gain_\lambda + Offset_\lambda$. The gain and offset values for each band were obtained from Bouvet et al. [46]. The TOA radiance values were then converted to TOA reflectance for each band (R_λ) using the equation $R_\lambda = \dfrac{\pi L_\lambda}{E_\lambda \cos\theta}$ where E_λ is the TOA solar irradiance for each band, and θ is the solar zenith angle during the time of image acquisition [46]. The solar zenith angles are 39.29^0 for the upper scene and 38.94^0 for the lower scene. Atmospheric correction using dark-object subtraction was then applied to the TOA reflectance image.

Geometric correction is also a standard image pre-processing procedure to correct for geometric distortions as well as to put the image into a proper reference system such that

other spatial data can be overlaid. Since preliminary geo-referencing have been done by the image supplier, it was necessary to check the consistencies of the image-based coordinates of pixels within the overlapping regions of the two scenes. This was done to see if the two scenes are correctly co-registered in their preliminary coordinate system/map projection. Random checks consisting of about 30 pixels common to both scenes showed no differences in their UTM 51 WGS 1984 X and Y coordinates which indicated that the two scenes were correctly co-registered.

After checking the co-registration of the two scenes, mosaicking was done. Initial assessment of the mosaicked image showed that vector data such as the MMEIRS 2004 does not overlay well. To geometrically correct it, image-to-image geo-referencing was made. In this task, rectified ALOS AVNIR-2 satellite images from NAMRIA were used as based images. Initially these rectified images were planned to be used for land-cover mapping. However, the images that were provided were of different dates (one image was acquired on 02 February 2010 while the other one was acquired on 17 September 2009). Also, the rectified images were not radiometrically calibrated and radiometric calibration can no longer be done because of the rectification made.)

The results of the image-to-image geo-referencing using a first order polynomial equation (Table 12) showed an acceptable total RMSE of 0.297 of a pixel which is equivalent to 2.97 m. The rule-of-thumb suggest that a geo-referenced image is geometrically accurate and acceptable for use in subsequent processes if the total RMSE of the geo-referencing process is less than half a pixel (or 5 meters).
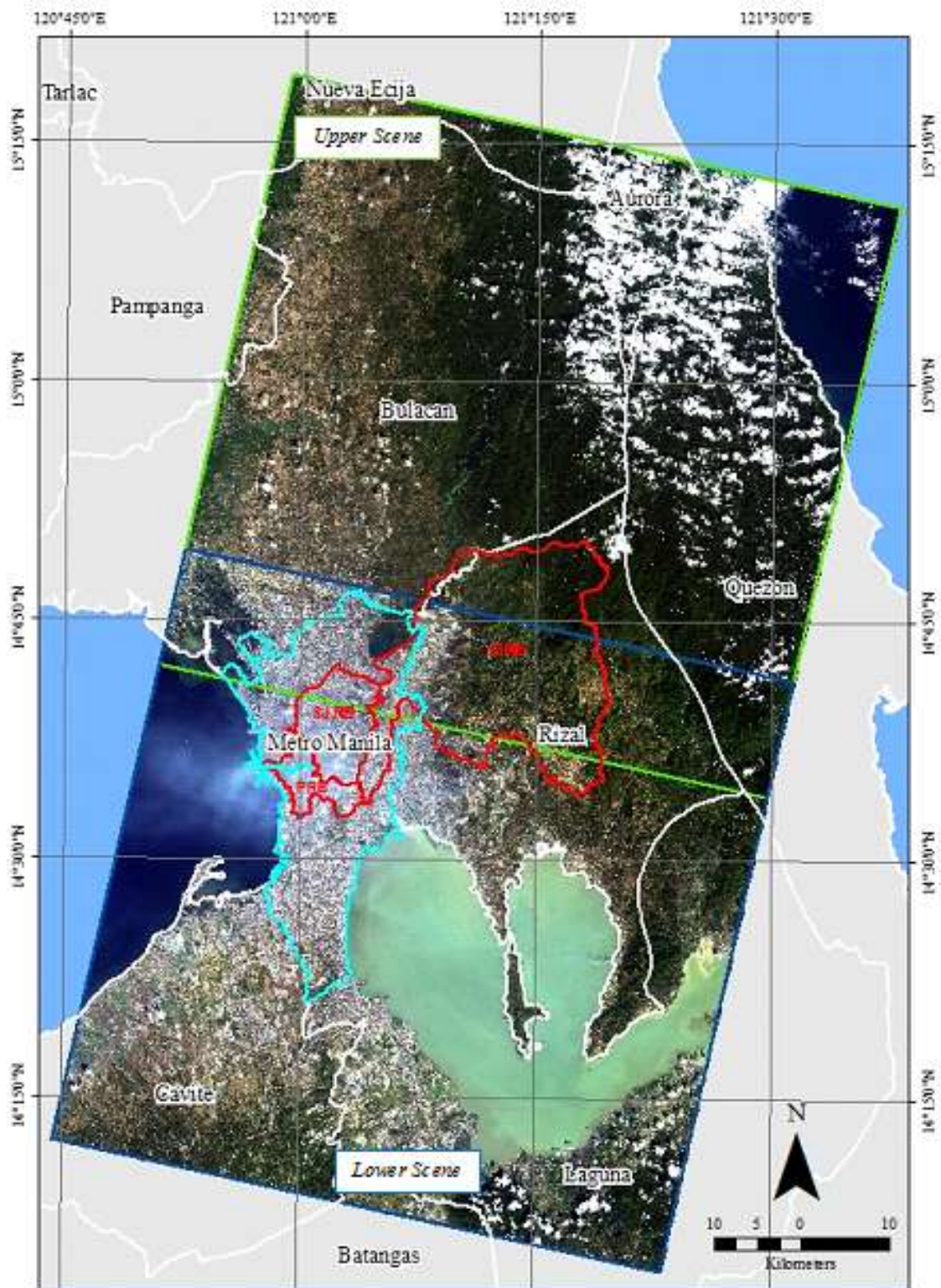
Figure 68. The two scenes of raw ALOS AVNIR-2 satellite images covering the Marikina River Basin, San Juan River Basin and floodplains of Pasig River.

Table 12. Summary of control points used in image-to-image geo-referencing of the mosaicked ALOS AVNIR-2 image, including the RMS errors.*

GCP	Base X	Base Y	Warp X	Warp Y	Predict X	Predict Y	Error X	Error Y	RMS
1	352.00	11866.00	354.00	11860.00	353.8846	11860.1023	-0.1154	0.1023	0.1542
2	352.00	11866.00	354.00	11860.00	353.8846	11860.1020	-0.1154	0.1023	0.1542
3	4557.00	12744.00	4560.00	12739.00	4559.6717	12739.2039	-0.3283	0.2039	0.3864
4	7191.00	11607.00	7194.00	11602.00	7194.1024	11602.3037	0.1024	0.3037	0.3205
5	2454.00	7980.00	2456.00	7973.00	2456.0865	7972.9397	0.0865	-0.0603	0.1054
6	2546.00	10885.00	2548.00	10879.00	2548.2339	10879.1221	0.2339	0.1221	0.2639
7	2448.00	3696.00	2450.00	3687.00	2449.8925	3687.2220	-0.1075	0.2220	0.2467
8	1707.00	9271.00	1709.00	9264.00	1709.0045	9264.2777	0.0045	0.2777	0.2777
9	7283.00	1032.00	7286.00	1024.00	7285.8070	1024.1172	-0.1930	0.1172	0.2258
10	2742.00	438.00	2744.00	428.00	2743.8094	428.0398	-0.1906	0.0398	0.1947
11	3067.00	2189.00	3069.00	2180.00	3068.9549	2179.8551	-0.0451	-0.1449	0.1517
12	7193.00	10356.00	7196.00	10351.00	7196.0655	10350.9228	0.0655	-0.0772	0.1013
13	7865.00	2969.00	7868.00	2962.00	7867.9851	2961.9176	-0.0149	-0.0824	0.0838
14	5031.00	9745.00	5034.00	9739.00	5033.6452	9739.2392	-0.3548	0.2392	0.4279
15	6337.00	13689.00	6340.00	13685.00	6340.0164	13684.8099	0.0164	-0.1901	0.1908
16	6761.00	8854.00	6764.00	8848.00	6763.9392	8848.3578	-0.0608	0.3578	0.3629
17	3863.00	7382.00	3865.00	7375.00	3865.3323	7375.0915	0.3323	0.0915	0.3447
18	8695.00	5520.00	8698.00	5514.00	8698.2212	5513.9222	0.2212	-0.0778	0.2345
19	6794.00	4102.00	6797.00	4095.00	6796.7978	4094.8792	-0.2022	-0.1208	0.2355
20	5528.00	11280.00	5531.00	11275.00	5530.7916	11274.8730	-0.2084	-0.1270	0.2441
21	3885.00	3728.00	3887.00	3720.00	3887.1890	3719.7399	0.1890	-0.2601	0.3215
22	3252.00	9811.00	3254.00	9805.00	3254.3171	9804.8554	0.3171	-0.1446	0.3485
23	2353.00	12743.00	2355.00	12738.00	2355.2829	12737.8299	0.2829	-0.1701	0.3301
24	1732.00	6117.00	1734.00	6109.00	1733.8600	6108.9747	-0.1400	-0.0253	0.1423
25	5627.00	7745.00	5630.00	7739.00	5629.6864	7738.7035	-0.3136	-0.2965	0.4316
26	824.00	10565.00	826.00	10559.00	825.9039	10558.6269	-0.0961	-0.3731	0.3853
27	4211.00	6233.00	4213.00	6226.00	4213.3545	6225.7688	0.3545	-0.2312	0.4232
28	6549.00	6112.00	6552.00	6105.00	6551.8118	6105.4338	-0.1882	0.4338	0.4728
29	4968.00	885.00	4970.00	876.00	4970.3063	876.1262	0.3063	0.1262	0.3313
30	7944.00	8821.00	7947.00	8816.00	7947.1617	8815.6416	0.1617	-0.3584	0.3932
								TOTAL RMS ERROR	0.29684

The base image is a rectified, mosaicked ALOS AVNIR image from NAMRIA. The X and Y coordinates are pixel coordinates, with each pixel equal to 10 m x 10 m.

Inclusion of Band Ratios, NDVI and DEM

After the pre-processing procedures, band ratios (2/4, 3/4) and NDVI bands were then derived from the mosaicked and geo-referenced image. These derivative bands were then added to the mosaicked image through layer-stacking.

In addition to the band ratios and NDVI, an ASTER DEM covering the mosaicked image was also included as another additional band. Prior to layer-staking, it was first resampled to 10-m resolution and with elevation values normalized to a range of 0 to 1 so that it will be compatible with the data range of the image bands. Incorporation of a digital elevation model (DEM) and a normalized differenced vegetation index (NDVI) image as additional data sources has also been found to increase classification accuracy as these

datasets account for the rugged topography so as to eliminate the presence or absence of certain classes in some elevation zones, and reduce the impact of shadows and to enhance the separability among various vegetation classes [**47,48**].

In the next section, the layerstacked image consisting of ALOS AVNIR-2 bands, NDVI, Band Ratios and ASTER DEM is referred to as "layerstacked image".

Land-cover Classification

Manual digitizing aided by visual interpretation, supervised classification using Maximum Likelihood and K-means clustering were utilized to derive a land-cover classification map from the layerstacked image. The overall process is depicted in Figure 69. The land-cover classification process is further depicted in Figure 70.
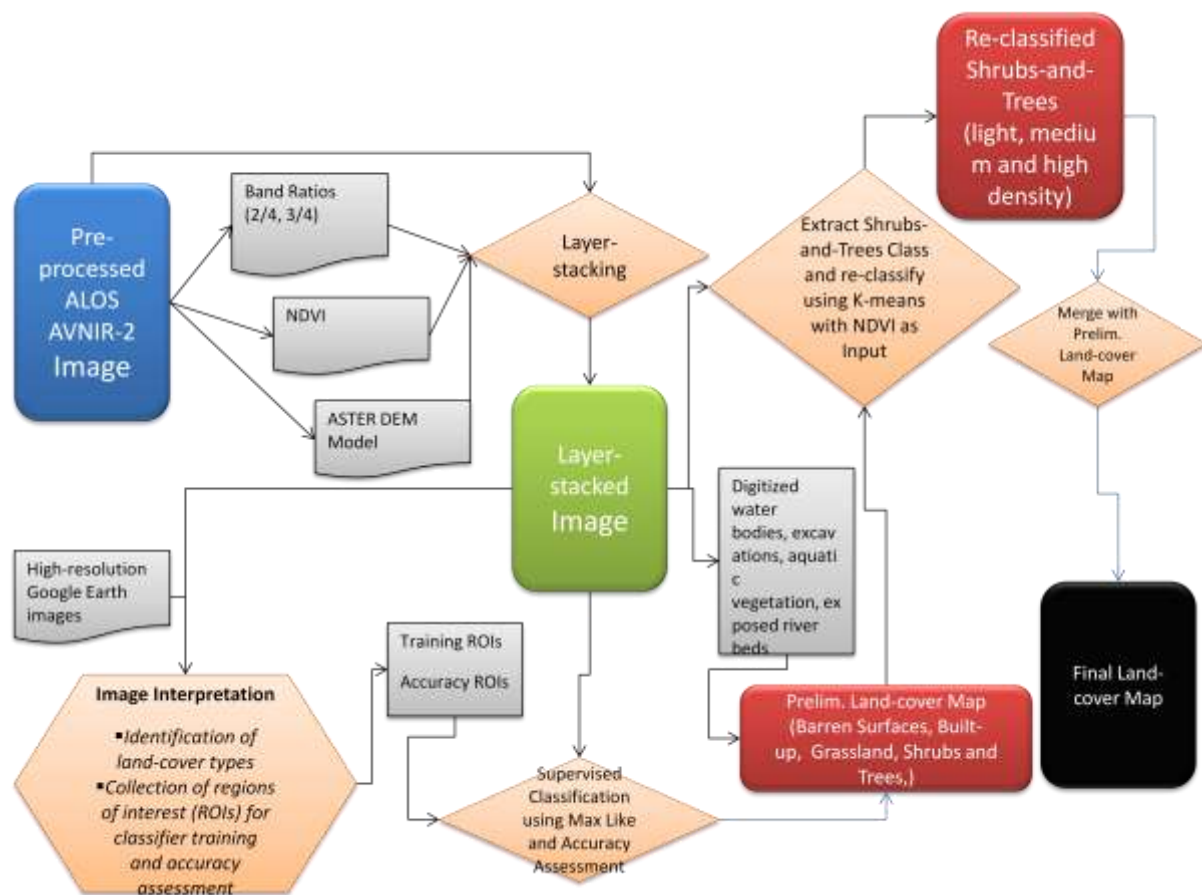
Figure 69. Diagram showing the flow of pre-processing and land-cover classification using the ALOS AVNIR-2 image.
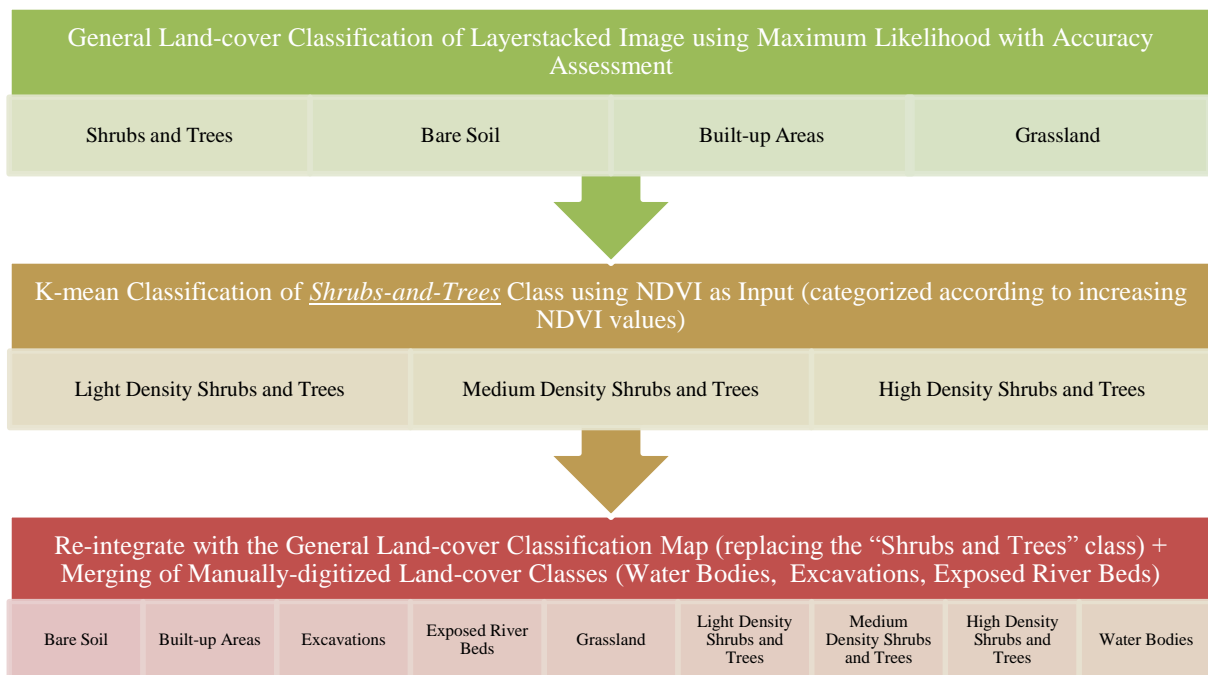
Figure 70. The land-cover classification process.

Using high resolution images dated 05 February 2010 that are available in Google Earth, 8 land-cover classes were identified in the layerstacked image. The classes include bare soil, built-up areas, exposed river beds, excavations, shrubs and trees (dense vegetation), grasslands, and water bodies. Water bodies (which include lakes, rivers, sea), exposed river beds and excavations were manually digitized to limit the classification to 4 classes (bare soil, built-up areas, grassland and shrubs and trees). Low classification accuracies were obtained during preliminary supervised classifications when all the indentified classes were included. High misclassifications were found for exposed river beds and excavations classes because of the similarity of the spectral reflectance of these classes to built-up areas. Another purpose of manually digitizing water bodies is for rivers and streams be accurately depicted in the resulting land-cover map.

For the Maximum Likelihood classification, a training set of pixels/regions of interests (ROIs) were selected for bare soil, built-up areas, grassland, and shrubs and trees in order to derive the classification parameters (class means and covariance matrices). The number of pixels for each class is listed in Table 13. Another set of randomly selected pixels for each class (but different from the training set) were selected for accuracy assessment. A total of 250 pixels were selected for each class based on the formula of Fitzpatrick-Lins [49] in determining the minimum number of pixels for classification accuracy assessment given that the desired accuracy is at least 85% at 95% confidence level, and with an allowable margin of error of 5%. After defining the training and accuracy assessment sets, Maximum Likelihood classification was then applied to six combinations of the ALOS AVNIR-2 bands, NDVI, Band Ratios and ASTER GDEM (Table 14). The best classification result among the six was chosen for further processing based on their average Producer's and User's Accuracy, kappa coefficient, and overall classification accuracy. The Producer's Accuracy is an

indication of how much of the actual land-cover classes have been correctly classified and depicted in the classification map. On the other hand, the User's Accuracy indicates how much of the pixels classified as belonging to a particular land-cover class is actually that class (e.g., are all pixels classified as "Grassland" actually "Grassland"?). The result which has the highest values of these four statistics was the one chosen.

Table 13. Number of pixels per class for the training set of the Maximum Likelihood classification.

Class Name	Number of Pixels
Bare Soil	13,902
Built-up Areas	16,918
Grassland	7,189
Shrubs and Trees	14,164

Table 14. List of combinations of the ALOS AVNIR-2 bands, NDVI, Band Ratios and ASTER GDEM for Maximum Likelihood Classification.

Combination No.	Included Data Layers
1	All ALOS AVNIR-2 Bands (1-4)
2	All ALOS AVNIR-2 Bands (1-4) + ASTER GDEM
3	All ALOS AVNIR-2 Bands (1-4) + Band Ratios
4	All ALOS AVNIR-2 Bands (1-4) + NDVI
5	All ALOS AVNIR-2 Bands (1-4) + NDVI + Band Ratios
6	All ALOS AVNIR-2 Bands (1-4) + NDVI + Band Ratios + ASTER GDEM

Prior to land-cover classification, clouds and cloud-shadows were removed from the mosaicked image by manual digitizing. These pixels were labeled as "No Data" in the final land-cover map.

After the Maximum Likelihood classification, all the pixels classified as "Shrubs and Trees" in the best classification result were further subdivided into high density shrubs and trees, medium density shrubs and trees, and low density shrubs and trees. This further classification of the "Shrubs and Trees" class was necessary to have a detailed land-cover map. Using only the "Shrubs and Trees" class will lead to difficulty later on in assigning the land-cover related model parameters (e.g., Manning's roughness coefficient, Curve Number) because of unavailability of look-up table of roughness value for this particular class. The reclassification was done using K-means with the NDVI band as input. The K-means classifier groups the NDVI values into 3 classes that will correspond to low, medium and high NDVI values. It is assumed that high density shrubs and trees will have high NDVI values while the low density shrubs and trees will have low NDVI values. After this, the land-cover map was finalized by integrating the re-classified shrubs and trees class, and the land-cover classes that were digitized earlier.

Land-cover Classification Results

Figure 71 shows the results of the Maximum Likelihood classification of the six combinations of data bands of the layerstacked image. Manually-digitized classes as well as clouds and cloud shadows were excluded in the classification and are not shown in the results. The accuracy of the six classification results are summarized in Table 15.
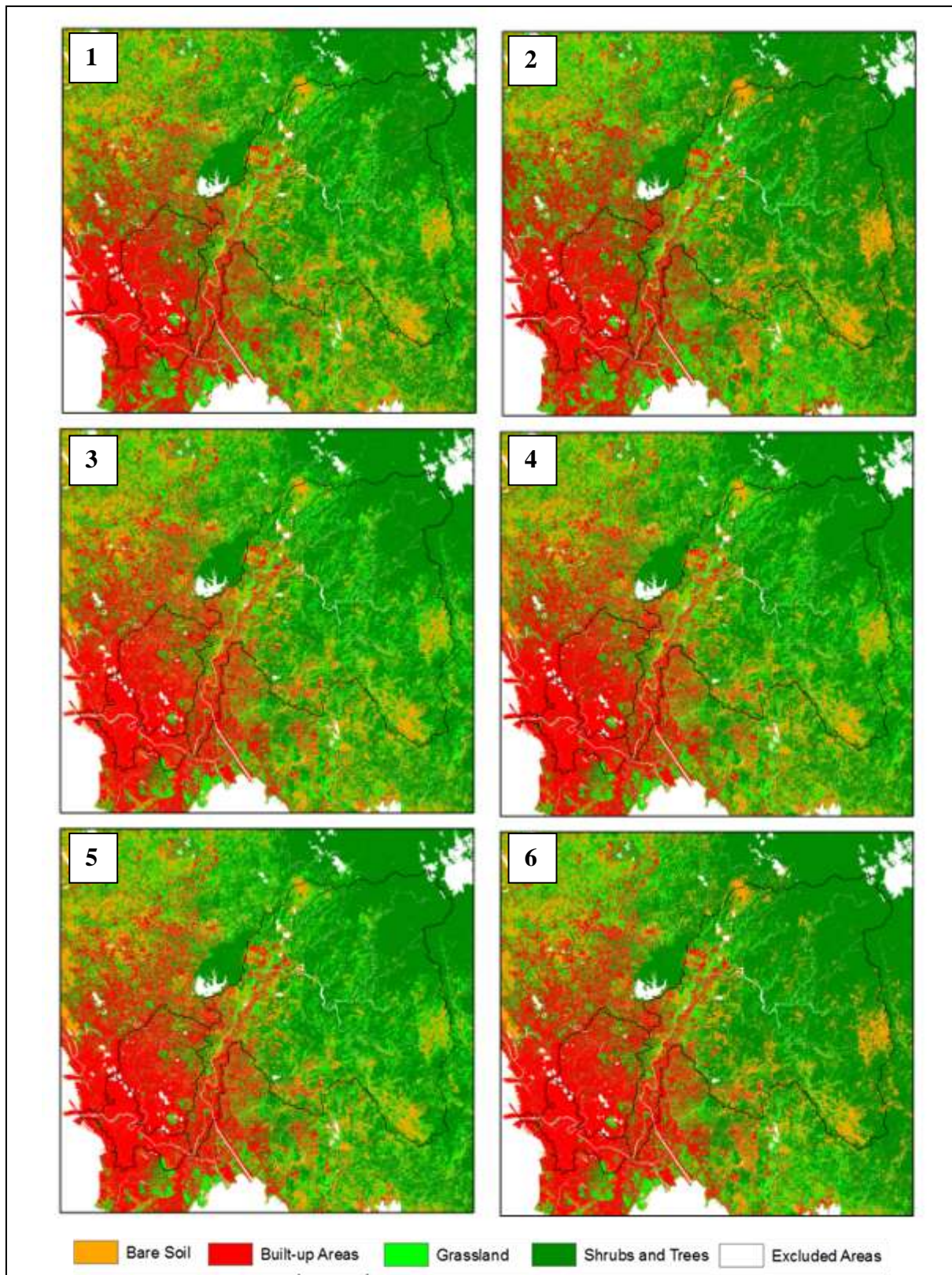
Figure 71. Results of Maximum Likelihood classification of six combinations of the ALOS AVNIR-2 bands, NDVI, *Band* Ratios and ASTER GDEM.

Table 15. Accuracy of the Maximum Likelihood Classification of the layerstacked image.

Combination Number	Overall Classification Accuracy (%)	Kappa Coefficient	Average Producer's Accuracy (%)	Average User's Accuracy (%)
1	91.1	0.8813	91.1	91.4
2	**92.4**	**0.8987**	**92.4**	**92.5**
3	91.9	0.8920	91.9	92.1
4	90.7	0.8760	90.7	91.0
5	91.5	0.8867	91.5	91.8
6	92.0	0.8933	92.0	92.3

According to Table 15, the Maximum Likelihood classification of combination 2 which consist of All ALOS AVNIR-2 Bands (1-4) + ASTER GDEM gave the best result. It has an overall classification accuracy of 92.4%. The average Producer's Accuracy (for the four land-cover classes) is 92.4% while the average User's Accuracy is 92.5%. The confusion or error matrix of this classification is shown in Table 16.

Table 16. Confusion or error matrix of the Maximum Likelihood Classification of combination 2 (best result) which consist of All ALOS AVNIR-2 Bands (1-4) + ASTER GDEM).

	Land-cover Class	Ground Truth Pixels					User's Accuracy
		Bare Soil	Built-up Areas	Grassland	Shrubs and Trees	Total	
Classified Pixels	Bare Soil	215	12	3	2	232	92.7%
	Built-up Areas	25	236	2	0	263	89.7%
	Grassland	6	2	228	3	239	95.4%
	Shrubs and Trees	4	0	17	245	266	92.1%
	Total	250	250	250	250	1,000	
Producer's Accuracy		86.0%	94.4%	91.2%	98.0%		

Using the combination #2 classification result, the "Shrubs and Trees" clustering into low, medium and high density shrubs and trees was made using NDVI. The histogram of clustered NDVI values is shown in Figure 72

The final land-cover map was then obtained by integrating the re-classified shrubs and trees class, and the land-cover classes that were digitized earlier (water bodies, exposed river beds and excavations). This map is shown in Figure 73.
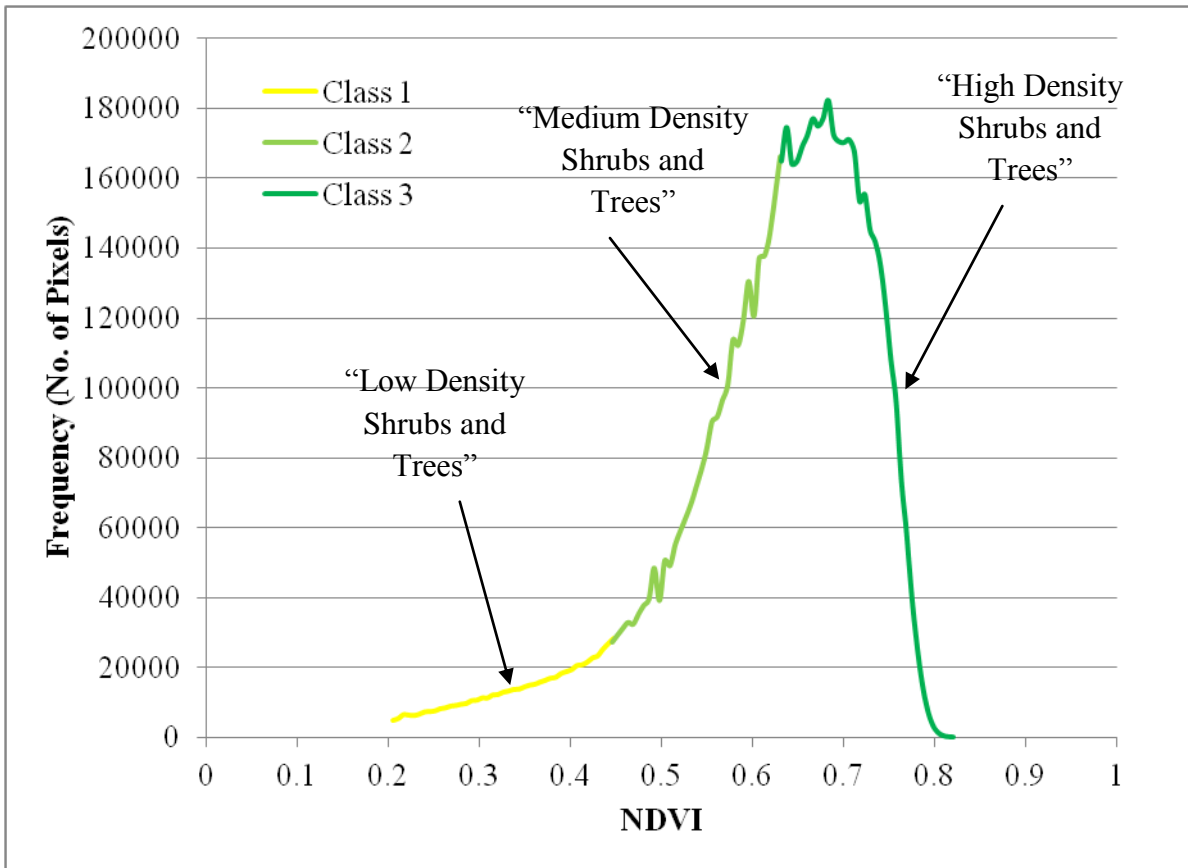
Figure 72. Histogram of clustered NDVI values of pixels classified as "Shrubs and Trees". The "Shrubs and Trees" class was initially classified through Maximum Likelihood classification of combination #2.
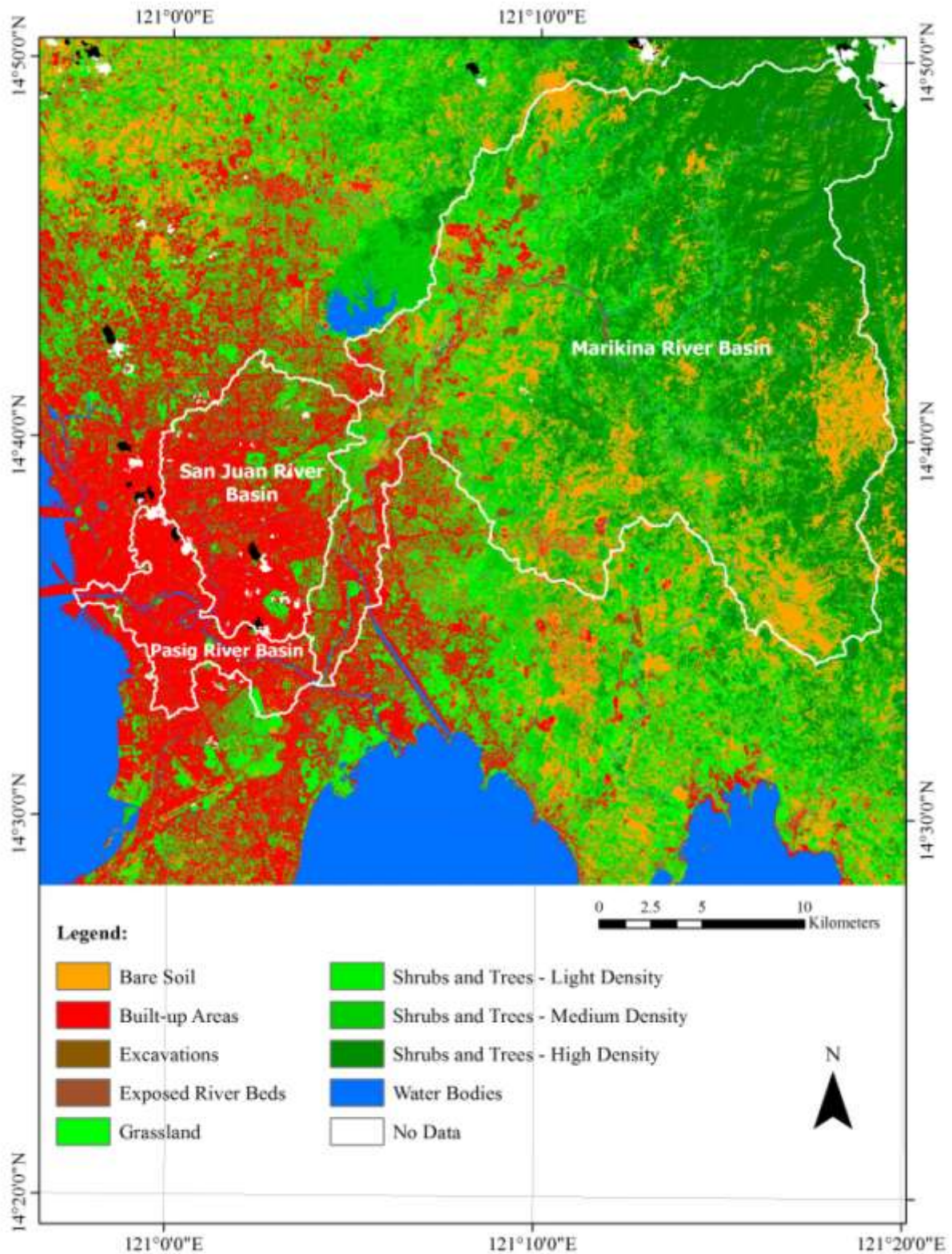
Figure 73. The final land-cover map covering the Marikina River Basin, San Juan River Basin and floodplains of Pasig River derived through manual digitizing aided by visual interpretation, supervised classification using Maximum Likelihood and K-means clustering of a layer-stacked image consisting of ALOS AVNIR-2 bands, NDVI and ASTER GDEM.

High resolution land-cover mapping in the San Juan River Basin using Worldview-2 Satellite Image

Image Description

A high resolution land-cover map of San Juan River Basin was generated through the use of Worldview-2 (WV2) satellite data acquired on 05 February 2010. WV2 is a commercial high resolution satellite that provides a 2-m resolution multi-spectral image through its 8 spectral sensors in the visible to near-infrared range. Each sensor is narrowly focused on a particular range of the electromagnetic spectrum that is sensitive to a particular feature on the ground, or a property of the atmosphere [50]. It also provides a 0.5-m resolution panchromatic band image that can be used to enhance the spatial detail of the multispectral image through a pansharpening process. Some WV2 characteristics are shown in Table 17.

The WV2 data used in this project was purchased from a local Digital Globe distributor, and it was delivered in GeoTIFF format and orthorectification-ready with map projection set to UTM 51 WGS 84.

Table 17. WV2 image bands and characteristics.

Band Name	Spectral Range (nm)	Spatial Resolution
Coastal Blue	400 – 450	2 m.
Blue	450 – 510	
Green	510 – 580	
Yellow	585 – 625	
Red	630 – 690	
Red-Edge	705 – 745	
NIR1	770 – 895	
NIR2	860 – 900	
Panchromatic	450 – 800	0.5 m.

The WV2 image covers the main Marikina River and its flood plains, a portion of Pasig River and its floodplain and majority of the San Juan River Basin.

Figure 74. The high resolution WV2 satellite image displayed in true color (RGB = Band 5, Band 3, Band 2). Inset: a close-up view in a portion of the image.

Image Processing

The WV2 multispectral and panchromatic images were separately subjected to both radiometric calibration and orthorectification without ground control points. Radiometric calibration, which consisted of converting the raw pixel values (in digital numbers with 11-bit range) into spectral radiance (in units of (uW)/(cm^2*nm*sr)), was done using the built-in tools of ENVI 4.8. The procedure utilized the image metadata that includes date and time of image acquisition and the sun altitude/elevation.

Orthorectification was then employed after radiometric calibration in order to correct, or at least lessen the distortions or errors due to terrain relief and sensor tilt which occur when the image was captured. Essentially, orthorectification transforms the central perspective of a satellite-derived image to an orthogonal view of the ground, which removes the effects of sensor tilt and terrain relief. Scale is constant throughout the orthoimage, regardless of elevation, thus providing accurate measurements of distance and direction. Each pixel in the orthoimage represents a true ground location and all geometric, terrain, and sensor distortions have been removed to within a specified accuracy [51]. In ENVI 4.8, the WV2 images were orthorectified separately without the use of ground control points. The orthorectification utilized the 1-m LIDAR DEM (as elevation source) together with Rational Polynomial Coefficients (RPCs) contained in the image metadata in order to correct for the distortions.

The orthorectified multispectral and panchromatic images were then fused using the Gram-Schmidt Spectral Sharpening (GSS) algorithm to create a 0.5-m resolution multispectral image. GSS is one of the most popular pan-sharpening algorithms that are used to sharpen multispectral data using high spatial resolution panchromatic data. An underlying assumption of the algorithms is that one can accurately estimate what the panchromatic data would look like using lower spatial resolution multispectral data [51]. The GSS algorithm was implemented in ENVI 4.8 together with the multi-spectral response function of WV2 as additional information in order to estimate what the panchromatic data look like based on multi-spectral data.

The pan-sharpened WV2 image was then subjected to georeferencing to enhance its geometric accuracy. Fourteen (14) ground control points gathered through differential GPS technique were utilized for this purpose. The total RMS error of the georeferencing process was found to be 0.24 m which is within the rule-of-thumb of 0.25 m (or half a pixel). The distribution of the GCPs used in the georeferencing is shown in Figure 75.
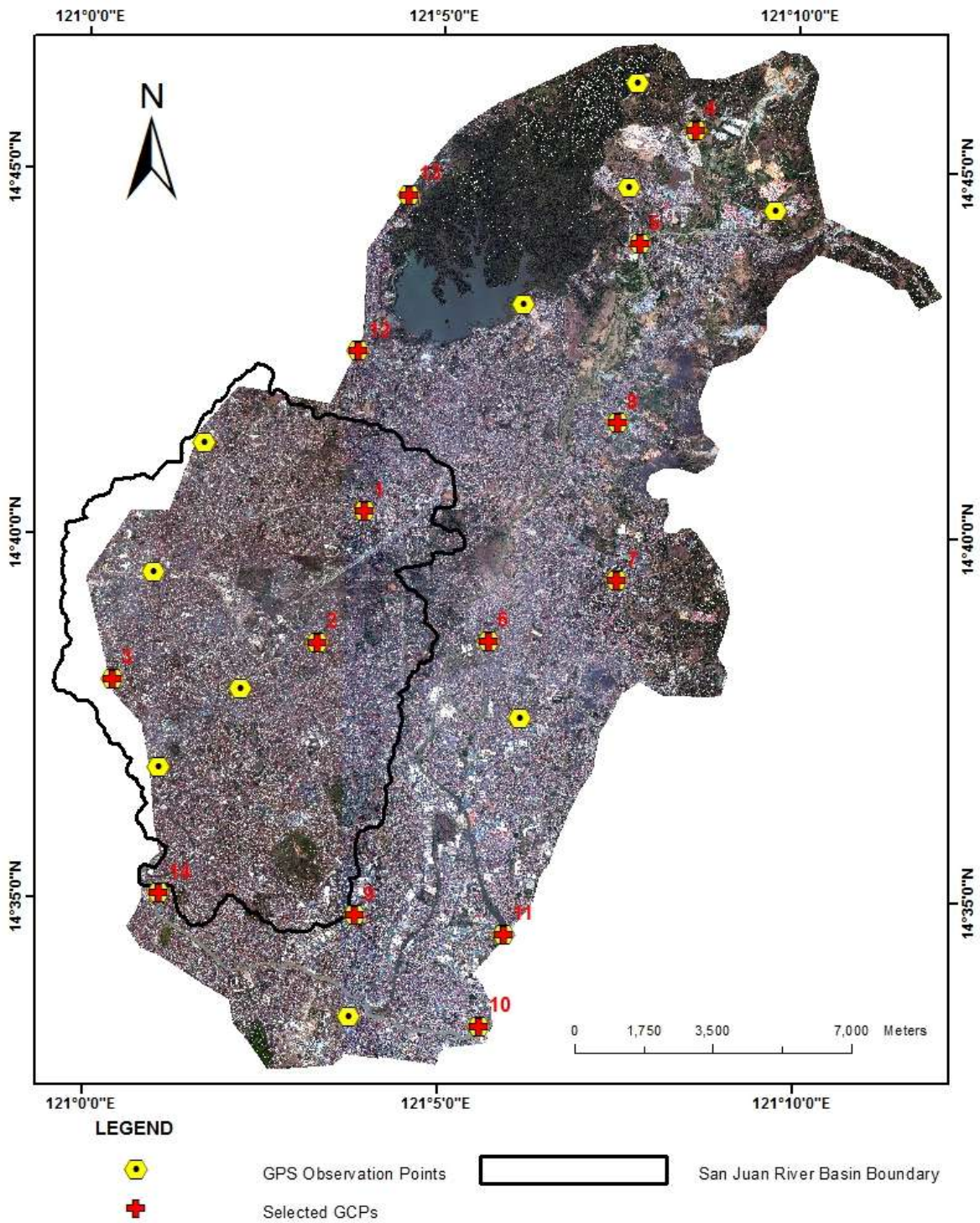
Figure 75. Snapshot of the pansharpened WV2 image overlaid with GCPs. GCPs with red markers (cross) were the ones used in georeferencing.

Table 18. Results of georeferencing the pansharpened WV2 image.

GCP	GCPs		WorldView-2				Residual		RMS Error
	Map X	Map Y	Image X	Image Y	Predict X	Predict Y	Error X	Error Y	
1	286463.720	1613311.170	3705.500	43016.000	3705.310	43015.940	-0.190	-0.060	0.200
2	292796.580	1630946.280	16370.250	7751.750	16370.430	7752.010	0.180	0.260	0.310
3	291514.070	1626996.500	13805.250	15652.000	13804.930	15651.990	-0.320	-0.010	0.320
4	295187.250	1612248.250	21155.250	45124.750	21155.380	45125.030	0.130	0.280	0.300
5	300053.330	1632576.880	30891.250	4462.500	30891.400	4462.680	0.150	0.180	0.230
6	298636.120	1629700.380	28055.500	10220.750	28055.290	10220.560	-0.210	-0.190	0.290
7	285305.030	1618723.260	1385.000	32204.250	1385.170	32204.150	0.170	-0.100	0.190
8	290483.680	1619629.490	11745.000	30380.000	11745.060	30380.060	0.060	0.060	0.080
9	298092.560	1625185.820	26967.500	19250.000	26967.450	19249.980	-0.050	-0.020	0.060
10	294821.590	1619669.530	20423.500	30289.000	20423.380	30288.840	-0.120	-0.160	0.200
11	294555.960	1609928.420	19893.000	49764.000	19892.830	49763.890	-0.170	-0.110	0.200
12	291417.270	1612740.770	13614.000	44146.750	13614.200	44147.000	0.200	0.250	0.320
13	298065.000	1621198.670	26912.000	27223.000	26912.140	27222.810	0.140	-0.190	0.240
14	291669.040	1622952.240	14115.750	23735.500	14115.810	23735.330	0.060	-0.170	0.180
								TOTAL RMS ERROR	*0.237417*

Land-cover Mapping and Results

The derivation of land-cover map from the processed WV2 image was done through visual interpretation and manual digitizing using ArcGIS. Land-cover descriptions and interpretation keys used in the digitizing are shown in Table 12. As can be seen in Figure 75, some portions of San Juan River Basin are not covered by the image. To complete the land-cover map, high resolution images from Google Earth (also WV2 acquired on the same date, 05 February 2010) were saved and co-registered with the WV2 image and used in the land-cover mapping.

The land-cover map is shown in Figure 76.

Table 19. Land-cover descriptions and interpretation keys used deriving high resolution land-cover map of San Juan River Basin from a WV2 image. (Descriptions are referenced from [52] and [53].)

Sample Imagette (RGB = 5-3-2)	Name	Description
	Barren Areas/Bare Soil	Primarily non-vegetated areas. Areas like bare sands and bare rock are included.
	Built-up Areas	Land covered by buildings and other man-made structures.
	Grasslands	Lands with herbaceous types of cover (grass). Trees and shrubs is less than 10%.
	Shrubs (Small Trees)	Lands with woody vegetation less than 2m tall and with shrub canopy cover.
	Trees/Forest (Dense Vegetation)	Determined by the presence of trees and absence of predominant land uses.
	Water Bodies	Artificial or natural water bodies. Flowing or standing water. The land cover consists of water bodies like rivers, man-made lakes, dams and creeks.
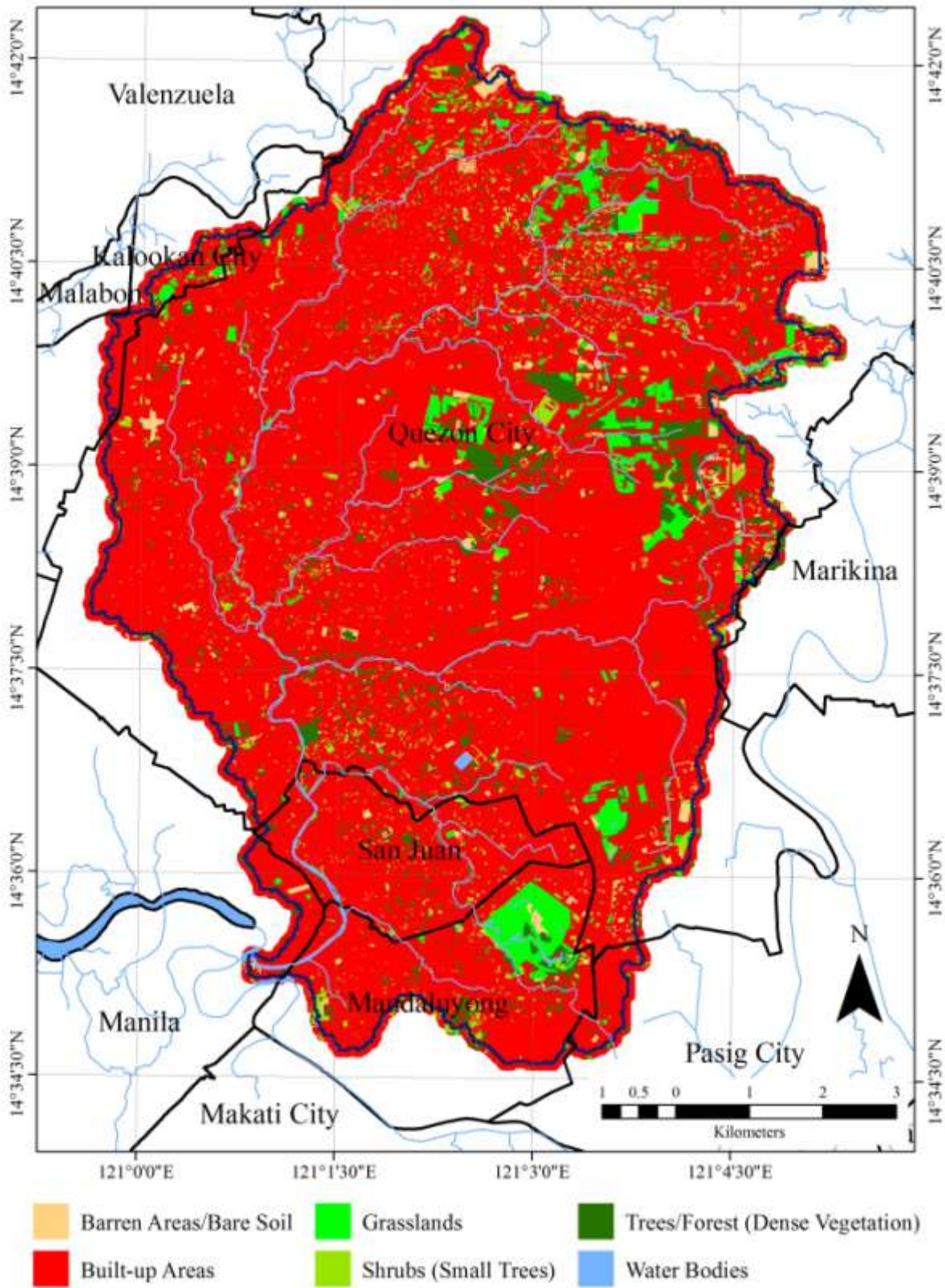
Figure 76. The high resolution land-cover map of San Juan River Basin derived from WV2 image.

Chapter Summary and Conclusions

This chapter has presented the generation of land-cover maps though the analysis of medium resolution and high resolution satellite images. Two land-cover maps were generated: a 10-m resolution land-cover map that covers the Marikina River Basin, San Juan River Basin and floodplains of Pasig River based on ALOS AVNIR-2 satellite images; and a 0.5-m resolution land-cover map of San Juan River Basin based on Worldview-2 satellite image. These maps were utilized in estimating the land-cover related parameters of the flood models.

Chapter 5. Development, Calibration and Validation of the Marikina River Flood Model Using Combined HEC HMS and HEC RAS

Overview

This chapter presents the development of the flood model of Marikina River that will be utilized for water level forecasting, reconstruction of actual flood events, and for simulation of flooding due to hypothetical and extreme rainfall events. The flood model was developed according to the theoretical framework presented and discussed earlier in Chapter 1 and shown again in Figure 77. It consists of HEC HMS and HEC RAS to simulate upstream watershed hydrology and river and floodplain hydraulics, respectively. The updated LIDAR DEM and land-cover maps derived previously were utilized in building the geometry of the model and for estimation of its land-cover parameters. The model was subjected to calibration and validation using hydrological data (discharge, water level and rainfall) and flood inundation information collected during actual flood events to increase its accuracy in predicting discharge and water levels, and in predicting flooded areas, respectively.
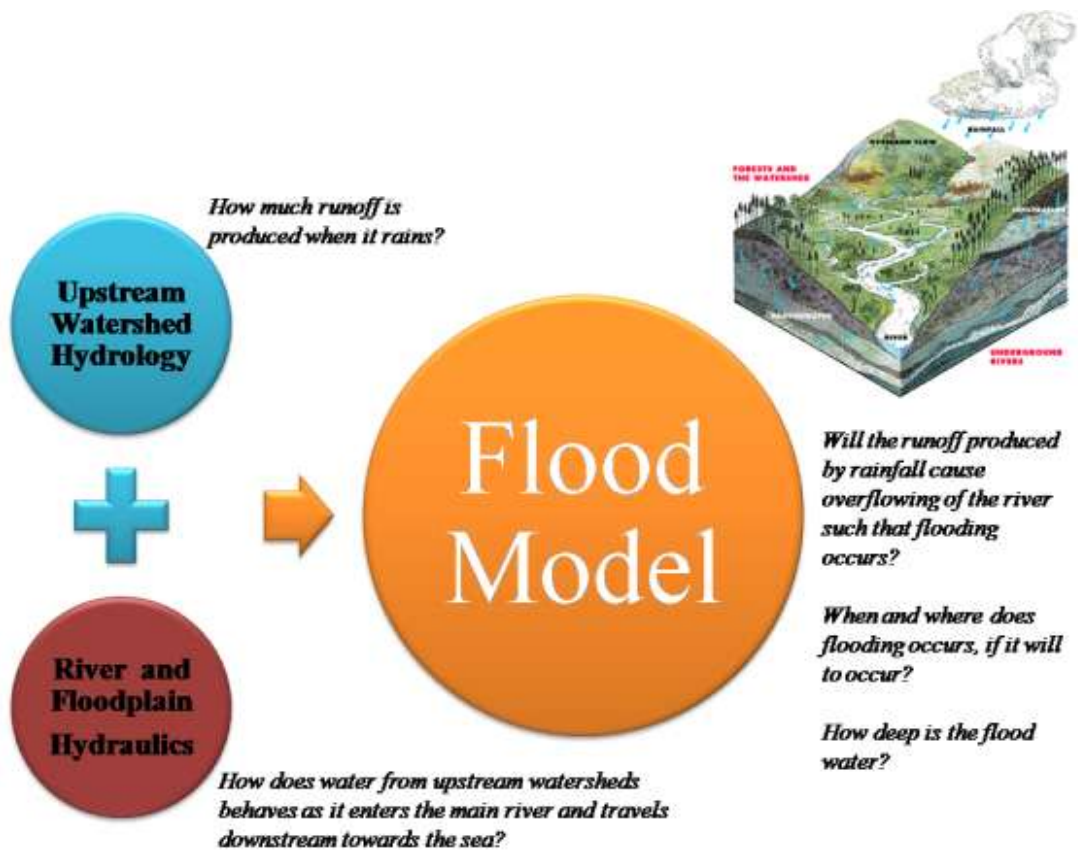
Figure 77. The flood model development framework.

The Model Domains

In this study, two model domains were defined: one for the hydrologic model, and another one for the hydraulic model. The hydrologic model domain is the Marikina River Basin with a total area of 523.183 km^2. It covers a majority of Rizal Province, specifically the municipalities of Rodriguez, San Mateo and Tanay, and the city of Antipolo.

The hydraulic model domain, with a total area of 77.300 km^2, represents the floodplain where water from the upstream watersheds enters through it at several locations until the main outlet is reached. The hydraulic model domain is the portion of Marikina River Basin where flood depth and hazard maps will be generated. The main outlet is at the Rosario JS water level station in Manggahan, Pasig City.
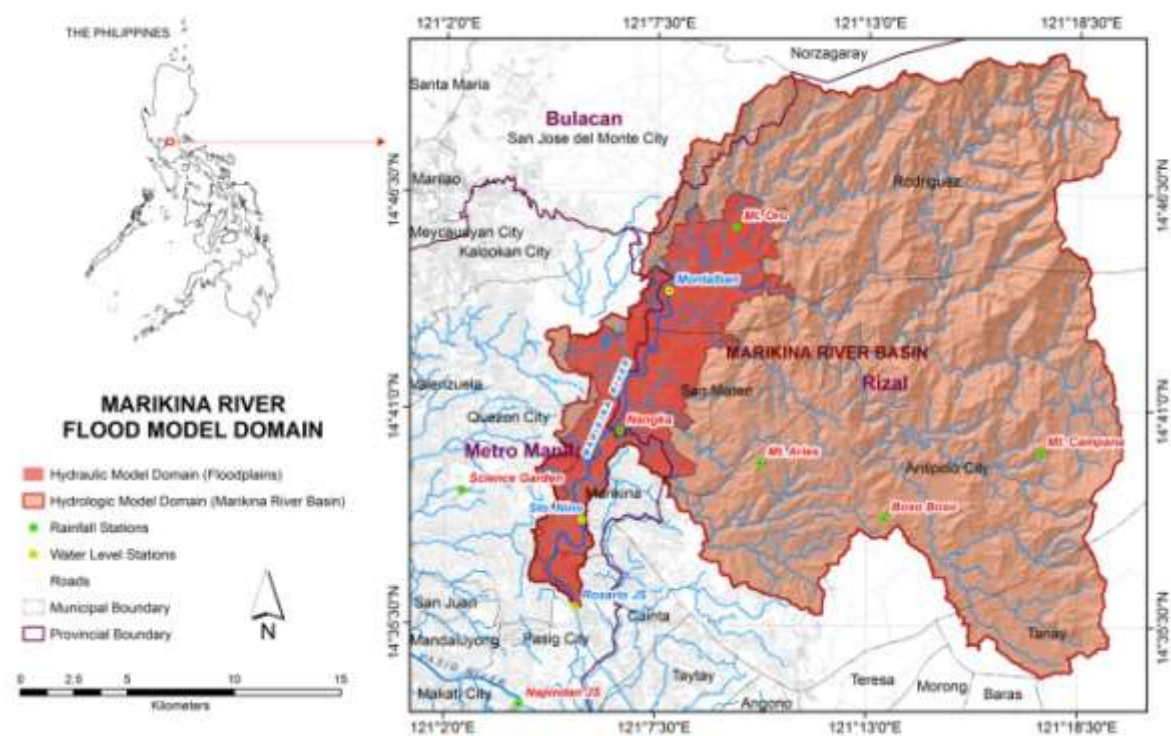
Figure 78. The hydrologic and hydraulic model domains.

HEC HMS Hydrologic Model Development

HEC HMS Model Components

The hydrologic model was developed using HEC HMS Version 3.5 and has four components to simulate the basic hydrologic processes of runoff generation from rainfall, its transformation and combination with baseflow, and its routing towards the outlet. These four components are (1) an infiltration loss model, (2) a direct runoff model, (3) a baseflow model, and (3) a channel routing model (Table 20).

The infiltration loss model based on the SCS-CN method computes for the volume of rainfall that falls on the watershed and addresses questions on how much of rainfall infiltrates on the surface and when does it run off (USACE, 2000). The direct runoff model using the

Clark Unit Hydrograph method describes two critical processes in the transformation of excess precipitation to runoff which are 1) translation or movement of the excess from its origin throughout the drainage to the watershed outlet; and 2) attenuation or reduction of the magnitude of the discharge as the excess is stored throughout the watershed. The baseflow model based on the Exponential Recession model is used to explain the drainage from natural storage of the watershed. The channel routing model, using the Muskingum-Cunge method, simulates the flow of runoff in the channels towards the main outlet. Mathematical equations of these models can be found in HEC HMS Technical Reference Manual [**54**].

Table 20. Models selected to constitute the four components of the hydrologic model.

Component	Model Name
Infiltration loss	US Soil Conservation Service – Curve Number (US SCS-CN)
Direct runoff	Clark Unit Hydrograph
Baseflow	Exponential Recession Model
Channel routing	Muskingum-Cunge Standard

Although several models of each component exist, the models presented in Table 20 were carefully selected based on the following reasons:

1. All the models selected are already well-established, well documented and readily available for use;
2. The HEC-HMS computer program combines the four models into a single system and allow seamless preparation of parameters and model simulations;
3. All the inputs required by the models, for the specification of the flow domain, for the specification of the boundary and initial conditions and for the specification of the parameter values can be provided within the time and cost constraint of the study. This is possible because of the use of GIS software in model preparation; and
4. The models are not complicated and can be implemented under a minimum amount of information that is known about the model domain. The parameters of the models can be automatically estimated or optimized using available hydrologic data.

HEC HMS Model Development

The development of the HEC HMS model primarily involved the physical representation of watershed and streams within MRB into hydrologic elements namely watersheds, reaches, and junctions interconnected in a network to simulate rainfall-runoff processes. With a lumped-parameter approach, direct runoff is computed using the SCS-CN model for each watershed and routed and translated toward each watershed's outlet using the Clark Unit Hydrograph model. The computed direct runoff and baseflow hydrographs for each watershed are then routed through channels (or "reaches") towards the main outlet of the MRB using the Muskingum-Cunge method.

Modeling in HEC-HMS relies in three specific components: a basin model, a meteorological model, and a set of control specifications. The basin model is the physical

representation of watersheds (termed as "sub-basin" in HEC HMS) and river systems into hydrological elements, each one configured with its proper method for the simulation of hydrologic processes. A meteorological model consists of a time series data of rainfall used for the simulation. The set of control specifications determines the simulation time step and period/duration.

HEC-HMS's preprocessor, HEC-GeoHMS (version 1.1), was used to prepare the basin model. HEC-GeoHMS is an extension of ArcView GIS software that allows users to visualize spatial information, document watershed characteristics, perform spatial analysis, delineate watershed boundaries, and construct inputs to HEC HMS [55].

The followings datasets were used in model preparation using HEC GeoHMS: (i.) 10-m MRB DEM generated using contour lines of MMEIRS, 1:50,000 NAMRIA and adjusted ASTER GDEM elevation datasets, (ii.) rivers and stream networks, (iv.) MRB land cover map derived from ALOS AVNIR-2, (v.) Soil Map (published by the Bureau of Soils and Water Management of the Department of Agriculture, BSWM-DA), and (vi.) river widths derived from field surveys and from the processed 0.5-m resolution WV2 image.

The 10-m MRB DEM together with the rivers and stream network were used to delineate the watershed boundaries ("sub-basin") and to generate the reach elements of the model. This was done using watershed delineation algorithms of HEC Geo-HMS. The result is shown in Figure 79. The basin model consisted of 153 watersheds ("sub-basins"), 89 reaches, and 89 junctions (including the main outlet). The delineated watersheds range from 0.020 to 11.708 km^2 in area, and with an average area of 3.425 km^2.
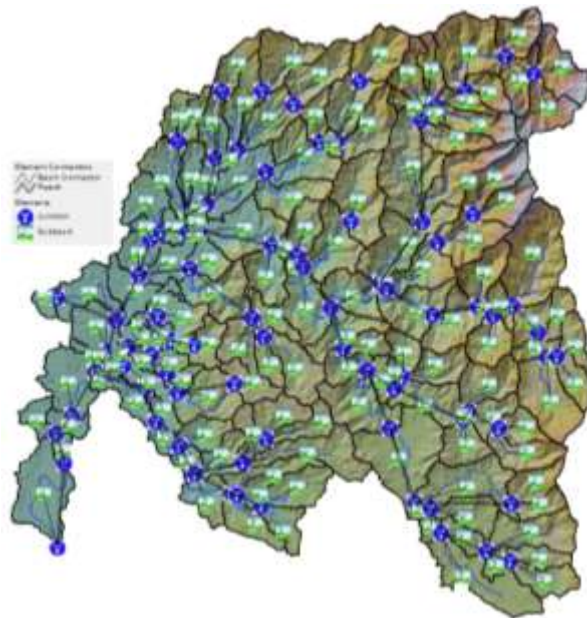
Figure 79. The MRB basin model showing the delineated watersheds/sub-basins, reaches and junctions.

HEC HMS Model Parameterization

Table 21 shows the list of parameters for the four components of the MRB hydrologic model.

Table 21. List of hydrologic model parameters.

Component	Model Name	Parameters	Source of Initial Estimates/Method of Estimating Initial Values (prior to calibration)
Infiltration loss	US SCS-CN	Curve Number (CN)	Look-up table of CN values of land-cover classes under different hydrologic soil groups (HSG)
		Initial Abstraction, mm. (Ia)	$I_a = 0.2S$ Where S = (25400/CN) - 254
Direct runoff	Clark Unit Hydrograph	Time of Concentration, in hours (T_c)	Computed using TR55 method [53]
		Storage coefficient, in hours (R)	$R = T_c$
Baseflow	Exponential Recession Model	Initial baseflow (Q_0)	Estimated for each watershed by ratio-and-proportion based on initial discharge at the outlet, the total basin area, and the area of each watershed.
		Recession Constant (k)	Initially set to 1
		Baseflow threshold (ratio-to-peak flow)	Initially set to 0.05
Channel routing	Muskingum-Cunge Standard	Reach length	Estimated based on river data
		Reach slope	Estimated based on DEM
		Channel roughness (Manning's n)	Initially set to 0.04
		Channel Shape	Rectangular
		Side Slope (xH:1V)	x=1
		Bottom width	Estimated based field survey data and from the processed 0.5-m resolution WV2 image

The soil and land-cover maps of MRB were used to compute for the Curve Number (*CN*) parameter of the SCS-CN infiltration loss component. The *CN* parameter is dependent on land-cover, hydrologic soil group based on the soil texture, and antecedent moisture condition. In the MRB, there are four kinds soil textures namely loam, silt loam, clay, and clay loam (Figure 80). The hydrologic soil grouping (including description) for different soil textures in MRB is shown in Table 22. In the MRB, the major soil texture is clay which constitute 81.03% of the total area. In terms of soil group, more than 90% of MRB have group D soils which indicate high runoff potential.
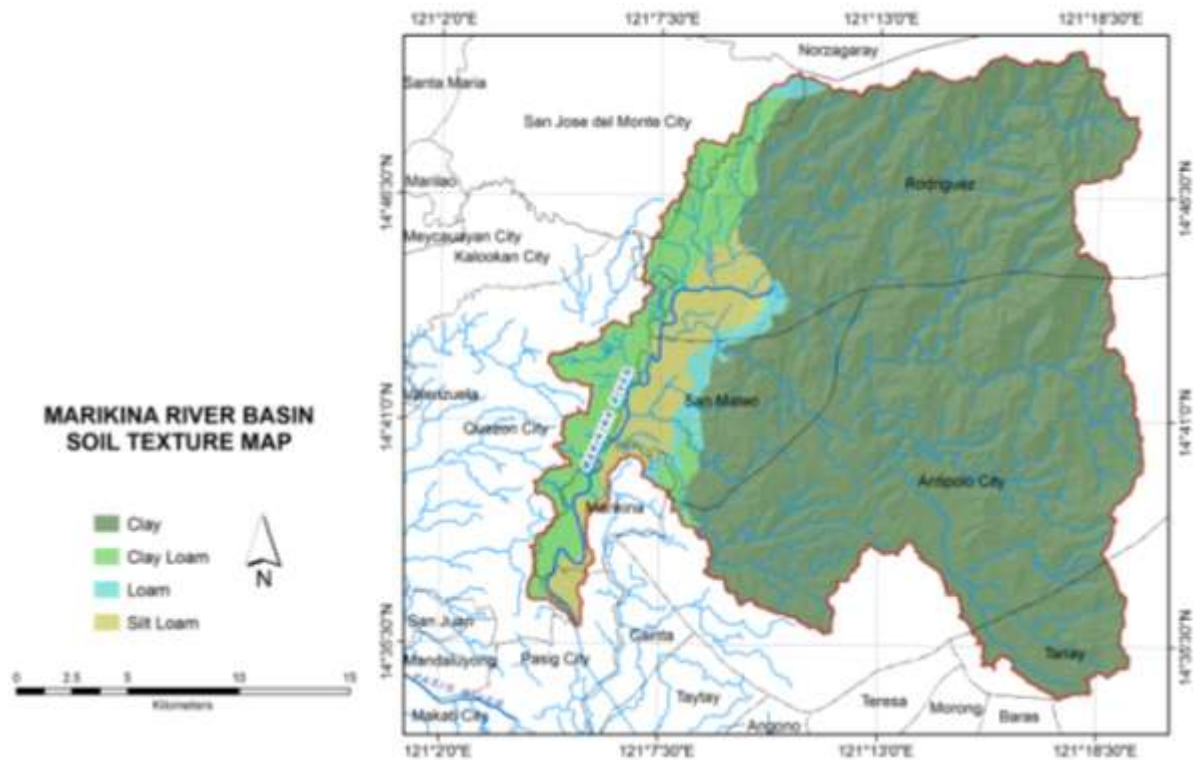
Figure 80. Soil textures in the Marikina River Basin. (Source: DA-BSWM)

Soil Texture	Area within MRB by Soil Texture, in km^2	Hydrologic Soil Group	Soil Group Description	Area within MRB by Group, in km^2
Loam	10.562 (2.02%)	B	Soils having moderate infiltration rates when thoroughly wetted and consisting of moderately deep to deep, moderately well to well drained soils with moderately fine to moderately coarse textures. These soils have moderate rate of water transmission. (Moderate runoff potential)	44.489 (8.50%)
Silt loam	33.926 (6.49%)			
Clay	423.952 (81.03%)	D	Soils having very slow infiltration rates when thoroughly wetted and consisting chiefly of clay soils with a high swelling potential, soils with a permanent high water table, soils with a claypan or clay layer at or near the surface, and shallow soils over nearly impervious material. (High runoff potential)	478.694 (91.50%)
Clay loam	54.743 (10.46%)			

A combination of a hydrologic soil group and land-cover class is a hydrologic soil-cover complex; and to indicate their specific runoff potential, curve numbers are assigned to such complexes. For example, a watershed having a higher *CN* (e.g., *CN* = 100) means it has higher runoff potential while a watershed having a lower *CN* (e.g., CN = 35) has a lower runoff potential. This would indicate that the higher the *CN*, the higher the runoff potential.

In assigning a curve number to a hydrologic soil-cover complex, it is necessary to consider first the antecedent moisture condition (AMC) of the watershed (Table 23). AMC is the total rainfall in the five-day period preceding a storm or rainfall event under consideration for the description). Chow, et al. [57] provided a set of formulas for the computation of CN under different AMC's, given that the CN for AMCII is known:

$$CN(I) = \frac{4.2CN(II)}{10 - 0.058CN(II)}$$

$$CN(III) = \frac{23CN(II)}{10 + 0.13CN(II)}$$

In the above equations, *CN(I)*, *CN(II)*, and *CN(III)* refer to *CN* values under antecedent moisture conditions I, II, and III, respectively. AMCI is basically a "dry" condition, while AMCII connotes a "normal" moisture condition of the watershed. AMCIII refers to a "wet" condition of the watershed. In this study, *CN(II)* values were initially used and later transformed to either CN(I) or CN(III) based on the AMC of watershed according to actual model simulation periods.

Table 23. Classification of antecedent moisture conditions (AMC) for the runoff curve number method. (Source: [57])

AMC Group	Total 5-day antecedent rainfall
I	Less than 1.4 inches (<35.56 mm.)
II	1.4 to 2.1 (35.56 to 53.34 mm)
III	Over 2.1 (> 53.34 mm)

Table 24 shows the *CN(II)* values of different combinations of land cover and hydrologic soil group. The *CN(II)* values were adapted from US Natural Resources Conservation Service [53]. As the land-cover classes of NRCS are different from those of the MRB land-cover map (Figure 81), it was necessary to re-classify first the land-cover classes to that of the NRCS (i.e., the NRCS class nearest to a particular MRB land-cover map class is used). Some of the watersheds have more than one land-cover class and soil type/soil group. An area-weighted averaging approach was used to assign a *CN(II)* value to each watershed. The area-weighted *CN(II)* map is shown in Figure 82. It should be noted that the MRB land-cover map initially have "No Data" for pixels contaminated by cloud and cloud shadows. The actual land-cover of "No Data" pixels were obtained through image interpretation of high resolution satellite images available in Google Earth, and the map was updated accordingly.

Table 24. NCRS conversion and CN look-up table of land-cover classes under different hydrologic soil groups (HSG).

Class Based on Land-cover Classification	Land-cover Area within MRB, in km^2	Equivalent or closest NRCS Land-cover Class (in terms of surface characteristics)	CN(II)			
			HSG A	HSG B	HSG C	HSG D
Bare Soil	113.584 (21.71%)	Fallow – Bare Soil	77	86	91	94
Built-up Areas	27.706 (5.30%)	Urban and residential districts [CN for A, B, C and D are average of commercial & business (85% impervious), industrial (72% impervious) and residential (65% impervious with 1/8 acre or less floor area) districts]	82	88	92	93
Exposed River Bed	1.964 (0.38%)	Gravel	76	85	89	91
Excavations	0.962 (0.18%)	Graded Areas	77	86	91	94
Grasslands	47.895 (9.15%)	Pasture, Grassland or range (Fair, 50-75% cover)	49	69	79	84
Vegetation – High Density Trees and Shrubs (assumed to be mixed with Grass)	180.438 (34.49%))	Wood-grass combination (>75% combination)	32	58	72	79
Vegetation – Medium Density Trees and Shrubs ((assumed to be mixed with Grass))	126.410 (24.16%)	Wood-grass combination (50-75% combination)	43	65	76	82
Vegetation – Low Density Trees and Shrubs ((assumed to be mixed with Grass)	18.540 (3.54%)	Wood-grass combination (<50% combination)	57	73	82	86
Water Bodies (Lakes, Rivers)	5.684 (1.09%)	Water	98	98	98	98
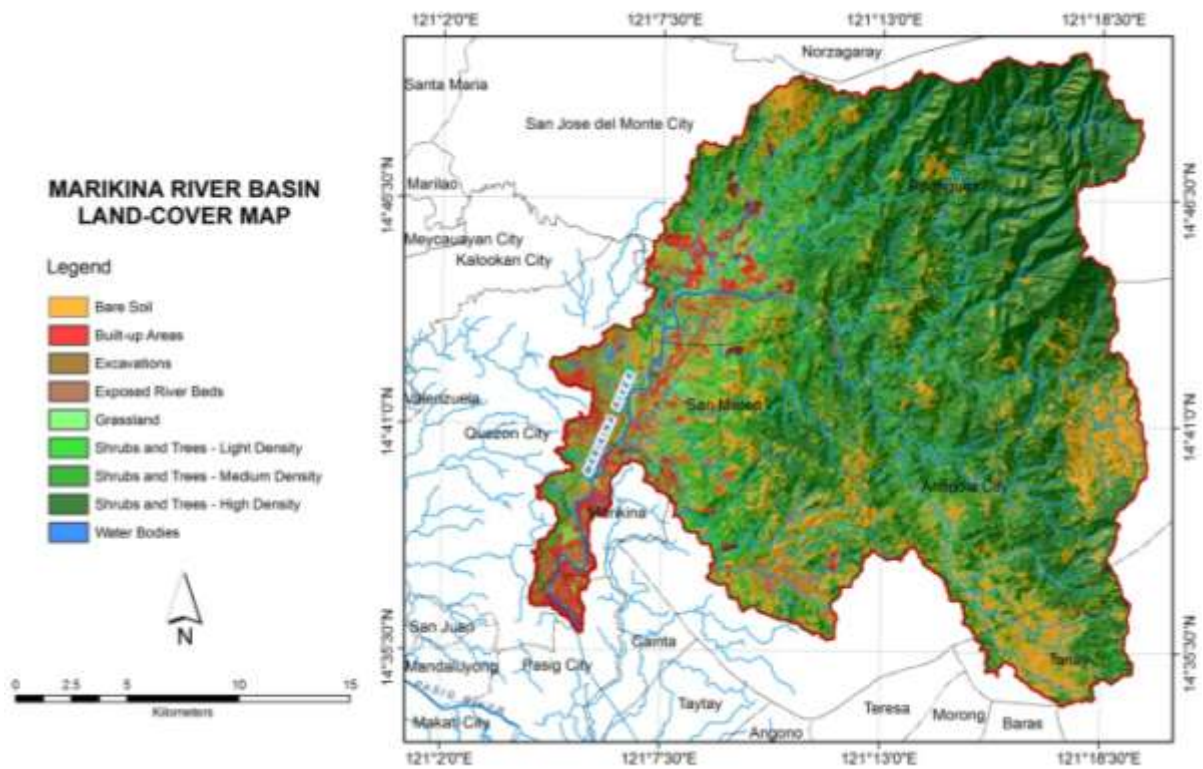
Figure 81. Land-cover map of Marikina River Basin based on 2010 ALOS AVNIR-2 satellite image.
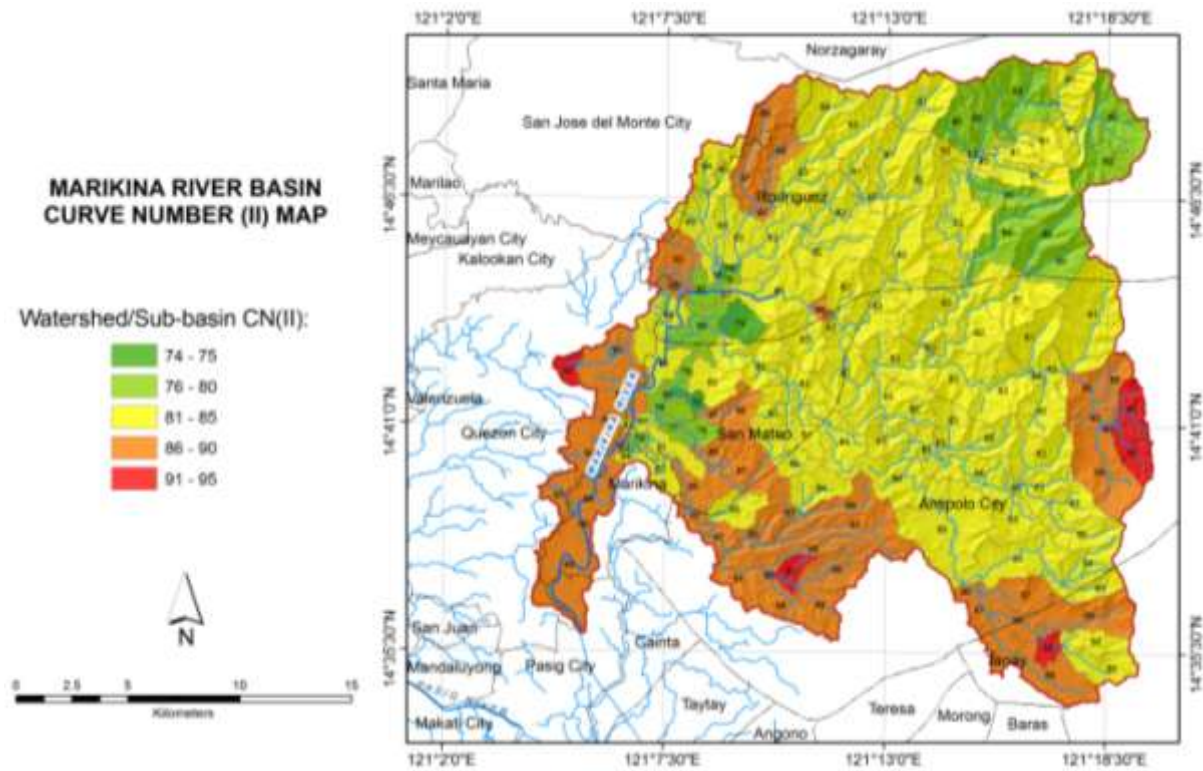
Figure 82. Map showing the area-weighted *CN(II)* for each watershed/sub-basin of MRB (indicated by numbers)

For the Clark Unit Hydrograph model, the two parameters (T_c and R) were estimated for each sub-basin/watershed by implementing the TR55 method [53] in HEC GeoHMS. The time of concentration is the sum of individual travel times for three flow regimes that occurs in a watershed – sheet flow, shallow concentrated flow, and channel flow. Travel times were estimated by providing HEC GeoHMS the following information: 2-year 24 hour rainfall amount, slopes, surface roughness (based on land-cover), bed roughness coefficient (0.04), and flow distance of precipitation excess on the land's surface for the three flow regimes. Watershed and reach slopes and flow distances were estimated using HEC-GeoHMS. The 2-year, 24-hour rainfall amount of 155 mm was obtained from the Rainfall-Intensity Duration Frequency (RIDF) generated by DOST PAGASA for Science Garden Station based on 41 years of data [58].

For the exponential recession model, the recession constant (k) and the baseflow threshold (ratio-to-peak flow) were initially set for each watershed with values of 1 and 0.05, respectively. On the other hand, initial baseflow (Q_0) was estimated for each watershed by ratio-and-proportion based on initial discharge at the several water level monitoring stations (e.g., MONTALBAN, STO. NINO, and ROSARIO JS) along Marikina River at the start of simulation, the drainage area at the monitoring stations($A_{Drainage}$), and the area of each watershed above the station (A_i): $Q_{0,i} = \dfrac{A_i \cdot Q_{Monitoring\ Station}}{A_{Drainage\ Area\ at\ Monitoring\ Station}}$. It is assumed that if the initial flow at a monitoring station along Marikina River is known, then initial flow for each watershed above this station is directly proportional to its area. To compute Q_0, it is necessary to group the 153 watersheds based on whether they are (i) upstream of MONTALBAN, (ii) upstream of STO. NINO but downstream of MONTALBAN, or (iii.) upstream of ROSARIO JS but downstream of both MONTALBAN and STO. NINO stations. The grouping of the watersheds is shown in Figure 83.
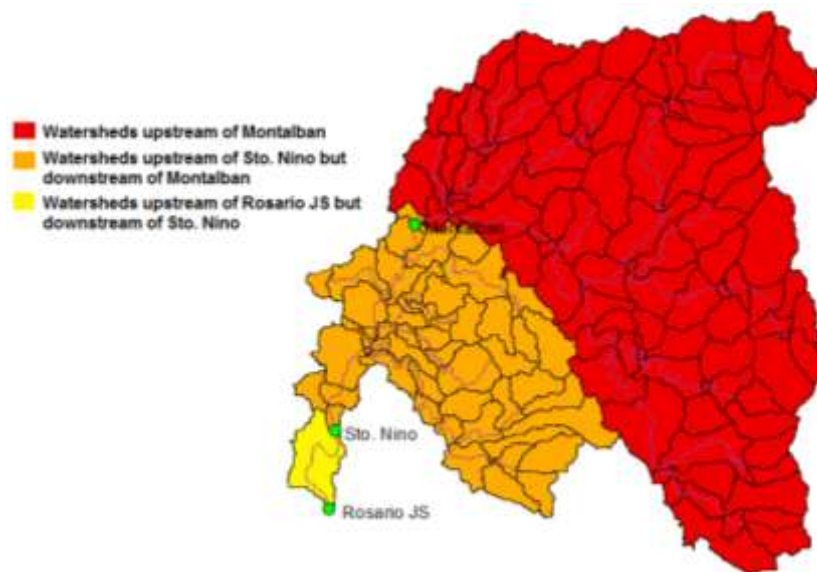
Figure 83. Grouping of watersheds according to whether they are upstream or downstream of monitoring stations.

Using this grouping, it is assumed that discharge at MONTALBAN is the sum of all Q_0 of watersheds upstream of the station. Similarly, discharge at STO. NINO is the addition of the discharge at MONTALBAN and the sum of discharge of watersheds upstream of STO. NINO but downstream of MONTALBAN. Finally, discharge at ROSARIO JS is the addition of discharge at STO. NINO and sum of discharge of watershed upstream of ROSARIO JS but downstream of STO. NINO. Using these relationships, Q_0 for each watershed is computed using the following equations:

Let :

$Q_{MONTALBAN}$ = known discharge at Montalban

$Q_{STO.NINO}$ = known discharge at Sto. Nino

$Q_{ROSARIOJS}$ = known discharge at Rosario JS

$A_{MONTALBAN}$ = total area of watersheds upstream of Montalban

$A_{STO.NINO}$ = total area of watersheds upstream of Sto. Nino but downstream of Montalban

$A_{ROSARIOJS}$ = total area of watersheds upstream of Rosario JS but downstream of Sto. Nino

Assuming that $Q_{ROSARIOJS} > Q_{STO.NINO} > Q_{MONTALBAN}$, then:

For watersheds upstream of Montalban:

$$Q_{watershed-upstream-Montalban} = \frac{A_{watershed} \cdot Q_{MONTALBAN}}{A_{MONTALBAN}}$$

For watersheds upstream of Sto. Nino but downstream of Montalban:

$$Q_{watershed-upstream-Sto.Nino} = \frac{A_{watershed} \cdot (Q_{STO.NINO} - Q_{MONTALBAN})}{A_{STO.NINO}}$$

For watersheds upstream of Sto. Nino but downstream of Montalban:

$$Q_{watershed-upstream-RosarioJS} = \frac{A_{watershed} \cdot (Q_{ROSARIOJS} - Q_{STO.NINO})}{A_{ROSARIOJS}}$$

If $Q_{STO.NINO} < Q_{MONTALBAN}$, $Q_{watershed-upstream-Sto.Nino} = 0$

If $Q_{ROSARIOJS} < Q_{STO.NINO}$, $Q_{watershed-upstream-RosarioJS} = 0$

As there is no actual data to properly estimate initial flow in all the 153 watersheds, the above equations are used to provide a fast and simple way of estimating initial flows to simulation.

The next sets of parameters that were estimated were the Muskingum-Cunge routing parameters for each river reach/stream segment. The parameters are the channel side slope (m/m), channel bottom width, and Manning's channel roughness coefficient. The channel was assumed to be rectangular in shape (side slope = 1). Bottom widths used were those derived from field surveys and from the processed 0.5-m resolution WV2 image. For the river roughness coefficient parameter, a value of 0.04 was initially used for all the reach elements. The values of this parameter were later improved through calibration with measured data.

HEC HMS Final Model Setup

The estimated parameters were then integrated into the basin model file and imported into HEC HMS for final model setup. In HEC-HMS, components such as a meteorological

model, time series data of rainfall and outflow/discharge at EFCOS water level measurement stations (MONTALBAN, STO. NINO and ROSARIO JS; see Figure 78 for their locations), and set of control specifications indicating the simulation periods were constructed.

The meteorological model was set to utilize rainfall data from five stations namely MT. ORO, MT. ARIES, BOSO-BOSO, NANGKA, and MT. CAMPANA (see Figure 78 for their locations). During simulation, rainfall received by each watershed is computed through inverse distance squared method, as shown in Figure 84. In case there is missing data in one of the stations, this station is not used in the simulation and rainfall is computed based on stations that have available data.

$$p_{node}(t) = w_A p_A(t) + w_C p_C(t) + w_D p_D(t) + w_E p_E(t)$$

$$w_C = \frac{\dfrac{1}{d_C^2}}{\dfrac{1}{d_C^2} + \dfrac{1}{d_D^2} + \dfrac{1}{d_E^2} + \dfrac{1}{d_A^2}}$$

P_{node} = rainfall at the watershed
w = weights (computed using inverse distance squared method)
A, B, C, D, E = rainfall stations
d = distance of the watershed from the rainfall station
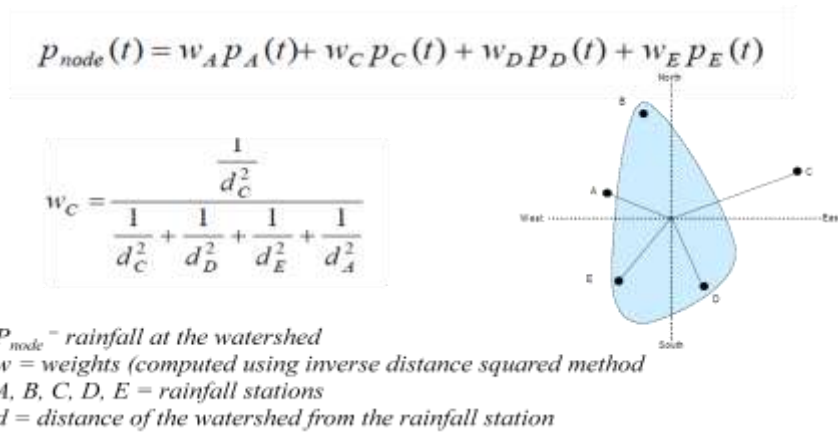
Figure 84. Illustration of the inverse-distance squared method of calculating rainfall received at a watershed based on rainfall data from several stations.

Figure 85 shows the interface of the MRB HEC HMS model.
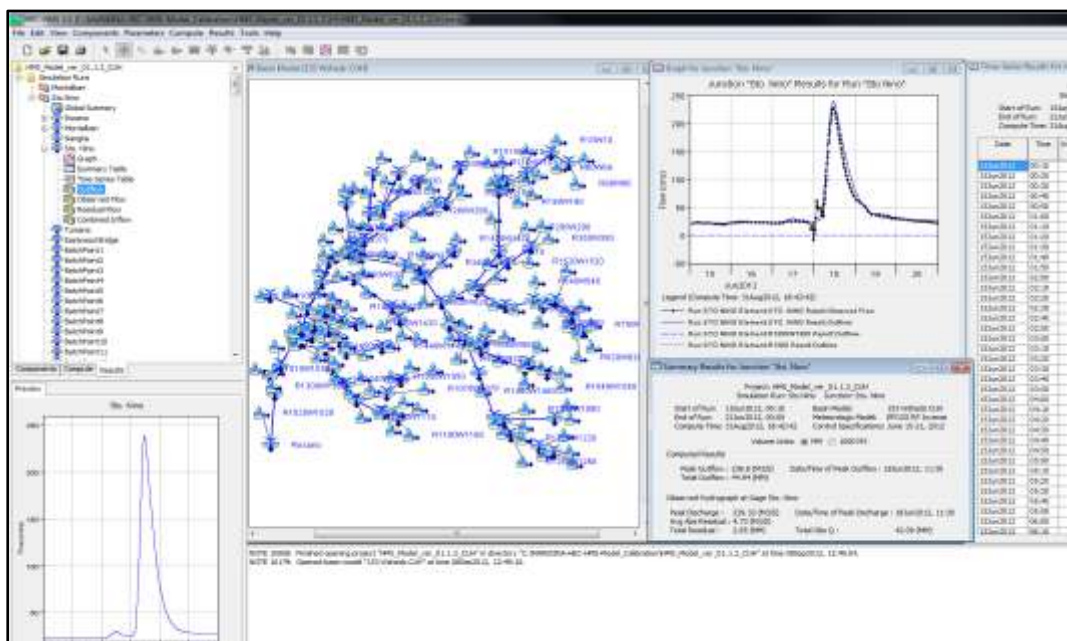
Figure 85. Interface of the MRB HEC HMS model.

Calibration and validation data

Rainfall recorded by MT. ORO, MT. ARIES, BOSO-BOSO, NANGKA, and MT. CAMPANA, and discharge data at MONTALBAN, STO. NINO and ROSARIO JS stations for three events (Table 25) were utilized to calibrate and validate the HEC HMS model. Data was recorded by EFCOS-MMDA, and downloaded from the Predict server (http://repo.pscigrid.gov.ph/predict) maintained by the ASTI-DOST. This data is shown in Figure 86 and Figure 87. Data from ROSARIO JS station (the main outlet) was not used in model calibration as it was found that flow of water at this station is sometimes affected by flow from Laguna Lake through the Manggahan floodway.

The discharge data used is actually based on recorded water level data that was transformed into discharge using a HEC RAS model of the main river. During the conduct of this project, water level and velocity sensors were installed for long term measurement of water level and velocity at Sto. Nino station during heavy rainfall events, which could be used to compute for discharge together with cross-section data. Unfortunately, velocity data after the deployment were unusable because of several missing values especially during the time when water level began to rise. The missing values were actually due to incapability of the velocity sensor to measure data as it was already buried in sediments. As an alternative, we constructed a HEC RAS model of the main Marikina River and fed it with actual water level measurements to derive time series of discharge at the two stations (MONTALBAN, STO. NINO) using unsteady flow simulation. The HEC RAS model is reported in [**59**], and has satisfactory performance, with Nash-Sutcliffe Model Efficiency of 0.88 based on comparison of simulated water level with measured water level in Tumana Bridge. The model has average error of -0.16 m which indicates that the simulated water level is approx. 16 cm higher than the actual level (error = actual − simulated WL). Using the results of the HEC RAS simulation, rating curves were then generated for MONTALBAN, STO. NINO and ROSARIO JS (Figure 88). These rating curves were utilized to transform the HEC HMS simulated discharge into water levels for forecasting purposes.

Table 25. Rainfall events with corresponding discharge data used in calibration and validation of the HEC HMS model.

Dataset	Period	Antecedent Moisture Condition / Total Rainfall Recorded 5-days prior (average of included rainfall stations)	Source of Data
Calibration	06/15/2012 00:10 - 06/21/2012 00:00	AMC III / 83.6 mm (all 5 stations)	EFCOS MMDA / ASTI Predict Server
Validation	08/3/2012 00:00 - 08/10/2012 16:00 ("Habagat 2012")	AMC III / 97.75 mm (4 stations only; Mt. Campana excluded due to absence of data)	EFCOS MMDA / ASTI Predict Server
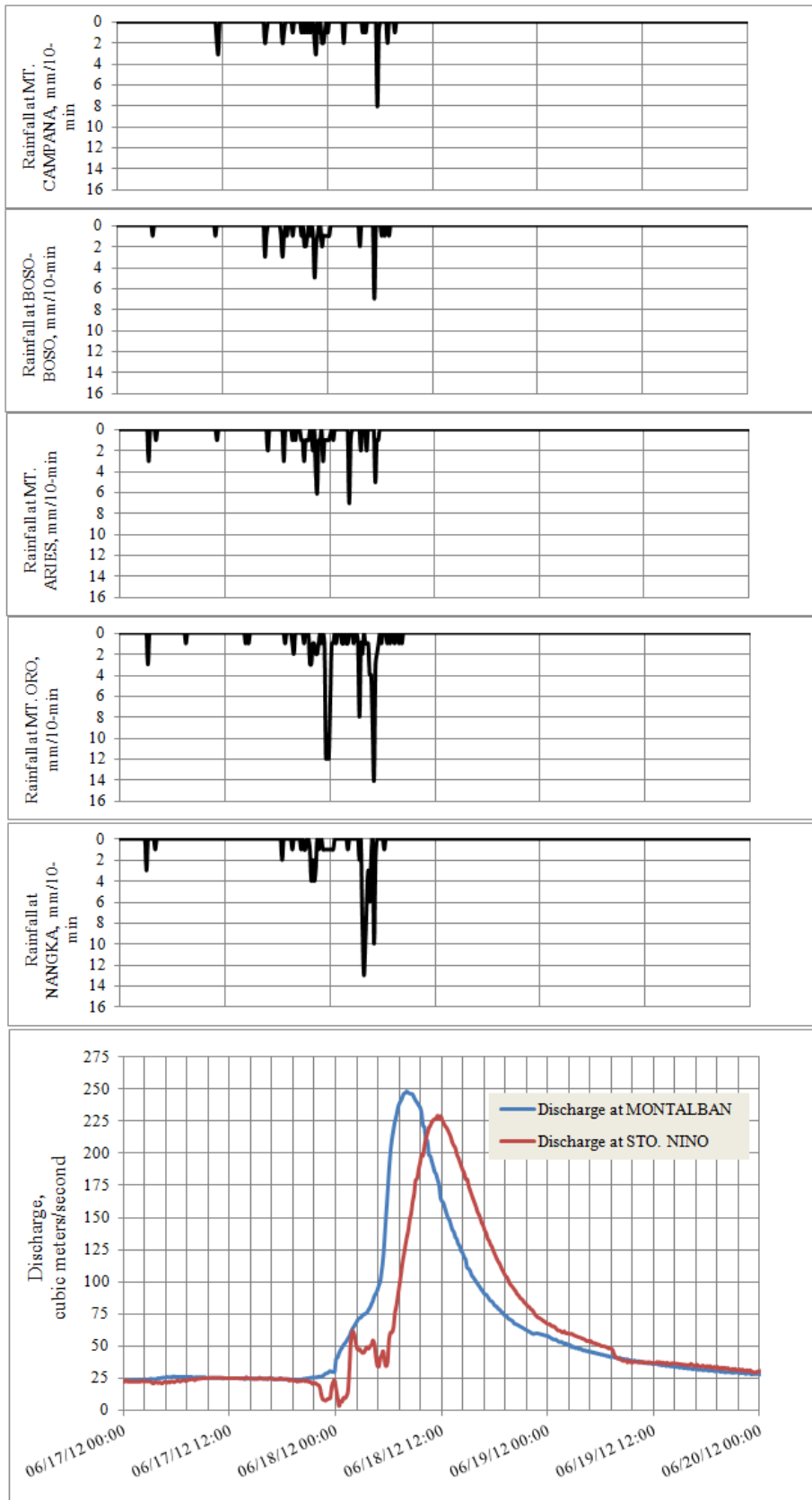
Figure 86. The June 2012 calibration data showing rainfall hyetographs of the five rainfall stations, and discharge hydrographs at monitoring stations.
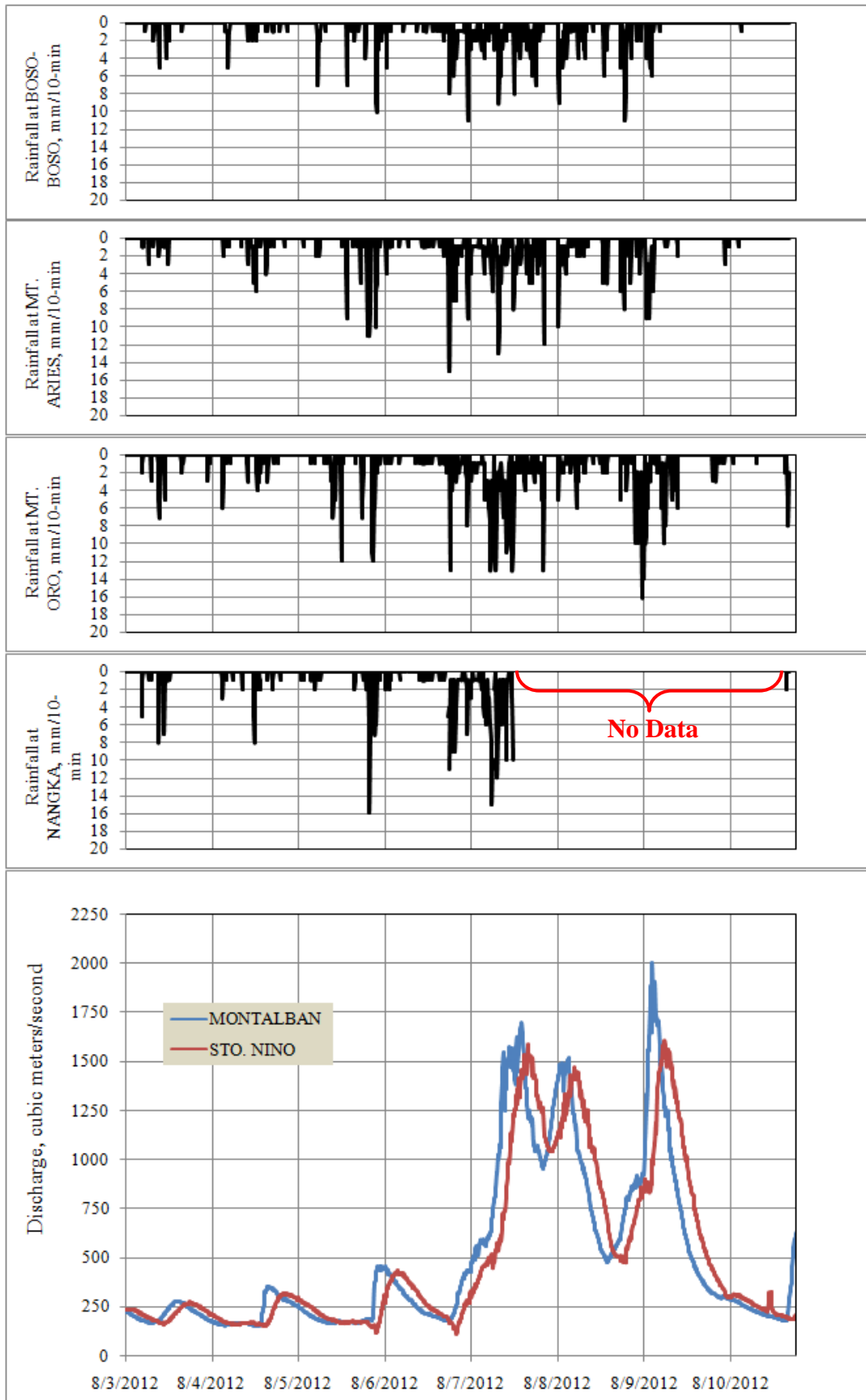
Figure 87. The August 2012 validation data showing rainfall hyetographs of the four rainfall stations, and discharge hydrographs at monitoring stations.
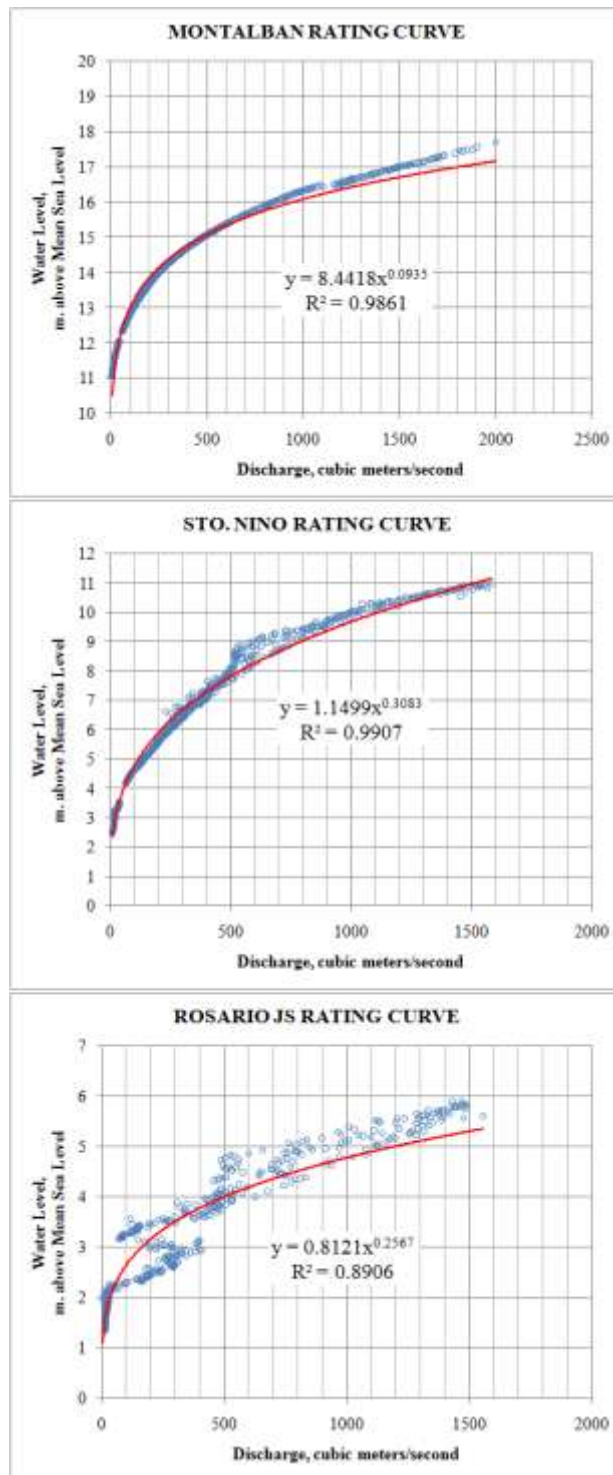
Figure 88. Rating curves for MONTALBAN, STO. NINO and ROSARIO JS derived from the results of running a HEC RAS model of the main Marikina River with actual water level measurements as inputs.

Model calibration and validation

Model calibration is defined here as the process of estimating model parameters by comparing model predictions (output) with observed data for the same conditions while

model validation involves running a model using input parameters measured or determined during the calibration process [60].

The HEC-HMS model was calibrated using the June 2012 rainfall events recorded by the five rainfall stations, and the 10-minute discharge hydrographs at MONTALBAN and STO. NINO. Records of 5-day accumulated rainfall depths before the simulation showed average of total rainfall recorded at the five stations to be greater than 53.34 mm, indicating AMCIII. Hence, the AMC II *CN* values that were initially set for all watersheds were transformed to AMC III *CN* using Chow et al.'s formula [57], and the values of I_a were updated accordingly.

The model calibration made use of the available automatic calibration utility in HEC-HMS. This procedure was done to fine tune the runoff depth parameters (*CN* and I_a) of SCS-CN model, the time-related parameters Clark Unit Hydrograph model, the initially assumed values of the parameters of the Exponential Recession baseflow model, and the channel roughness parameter of the Muskingum Cunge model. The procedure iteratively adjusts the initial values of these parameters until the model simulated hydrographs acceptably match the reference discharge hydrographs at the two stations. The parameter adjustments were done sequentially into four batches. The first batch of parameters that were simultaneously adjusted were the *CN* and I_a. The next batch were the T_c and *R*. The third batch were the *k* and the baseflow threshold (ratio-to-peak flow). The fourth batch included the channel roughness coefficients (*n*).

At each iteration during each batch of parameter calibrations, the peak-weighted root mean square error (PWRMSE) served as the objective function to minimize. For every change in parameter value during an iteration, the PWRMSE is computed and is compared with the PWRMSE of the previous iteration. Parameters of the model were adjusted iteratively until the PWRMSE is minimized. PWRMSE is implicitly a measure of the comparison of the magnitudes of the peaks, volumes, and times of peak of the simulated and measured hydrographs [54]. To aid in parameter value adjustment, the Univariate Gradient searching algorithm was used to minimize the PWRSME by identifying the most reasonable parameter values that will yield the best fit of computed to the reference hydrograph [54]. A total of 3000 iterations were set for each batch of parameter adjustment. When the iterations for the first batch has finished, the optimized parameters were then obtained and replaced the parameter values that were initially set. After this, the next batch of parameters were adjusted in the same manner. This procedure is repeated until all the batches of parameters have been adjusted to have optimal values.

As there were two calibration stations, parameters of reaches and watersheds upstream of Montalban (see Figure 83) were first subjected to the cycle of calibration procedure. Once all the four batches of parameters have been adjusted for these specific watersheds and reaches, the model was updated with the adjusted values. Then, the parameters of reaches and watersheds downstream of Sto. Nino (but downstream of Montalban) were next subjected to the cycle of calibration procedure. The logic behind this is based upon the fact that flow at Montalban station is a function of hydrologic processes in

watersheds and reaches that are upstream of the station. Once the parameters of these watersheds and reaches have been adjusted, keeping them constant during the calibration of the parameters of watersheds downstream of the Montalban station is essential so that it would be faster to adjust the parameters of the remaining watersheds and reaches. This would indicate that differences of the simulated with the observed hydrographs at Sto. Nino station are caused only by non-optimal parameter values of watersheds and reaches that are downstream of Montalban Station.

The model was then validated using independent datasets of rainfall and discharge hydrographs of the *Habagat* 2012 (August 8-10) event. During these event, the hydrologic condition of the MRB is AMC III which makes is suitable for validation purposes since the model was calibrated under AMC III condition.

Model performance evaluation

Three measures of accuracy were used to evaluate the performance of the HEC HMS model before and after calibration, as well as during validation based on the guidelines presented by Moriasi et al [60]: the Nash-Sutcliffe Coefficient of Model Efficiency(E), percent bias (*PBIAS*), and RMSE-observations standard deviation ratio (*RSR*). Each statistic is computed through comparison of reference hydrograph with the simulated hydrographs according to the following equations [60]:

$$E = 1 - \left[\frac{\sum_{i=1}^{M}(m_{obs,i} - m_{sim,i})^2}{\sum_{i=1}^{M}(m_{obs,i} - m_{mean})^2} \right]$$

$$PBIAS = 100 \times \left[\frac{\sum_{i=1}^{M}(m_{obs,i} - m_{sim,i})}{\sum_{i=1}^{M}(m_{obs,i})} \right]$$

$$RSR = \frac{\sqrt{\sum_{i=1}^{M}(m_{obs,i} - m_{sim,i})^2}}{\sqrt{\sum_{i=1}^{M}(m_{obs,i} - m_{mean})^2}}$$

In the above equations, m_{obs} and m_{sim} refer to the observed and simulated discharge values, respectively, while m_{mean} refers to the averaged observed values and M refers to the number of computed hydrograph ordinates.

E is a normalized, dimensionless statistic that determine the relative magnitude of the residual variance ("noise") compared to the measured data variance and indicates how well the plot of observed versus simulated data fits the 1:1 line. E ranges between -∞ and 1 (1 included) with E=1 being the optimal value. Values between 0.0 and 1 are generally viewed as acceptable levels of performance while values less than or equal to 0 indicates that the mean observed value is a better predictor than the simulated value, which indicates unacceptable model performance.

PBIAS measures the average tendency of the simulated data to be larger or smaller than their observed counterparts. This statistic has the ability to clearly indicate poor model performance: optimal value is 0, with low magnitude values indicating accurate model simulation; positive values indicate model underestimation bias, and negative values indicate model overestimation.

The *RSR* statistic standardizes the RMSE using the observations standard deviation. It incorporates the benefits of error index statistics and includes a scaling/normalization factor. *RSR* varies from the optimal value of 0, which indicates zero RMSE or residual variation and therefore perfect model simulation, to a large positive value. The lower *RSR*, the lower the RMSE, and the better the model simulation performance.

The above statistics were used to systematically quantify the HEC HMS model performance as very good, good, satisfactory, or unsatisfactory using the guidelines of Moriasi et al [60] as summarized in . The model has satisfactory model performance if all of the following is true: $E > 0.50$, $RSR < 0.70$, and *PBIAS* within ± 15 to $\pm 25\%$. In instances when each statistic has different ratings (e.g, very good in terms of E, good in terms of PBIAS, but satisfactory in terms of RSR, then the lowest rating (satisfactory) will define the overall model performance.

Table 26. HEC HMS performance ratings based on three model performance evaluation statistics. (Source: [60])

Performance Rating	Statistics		
	E	*PBIAS*	*RSR*
Very good	$0.75 < E \leq 1.00$	$PBIAS < \pm 10$	$0.00 < RSR \leq 0.50$
Good	$0.65 < E \leq 0.75$	$\pm 10 \leq PBIAS < \pm 15$	$0.50 < RSR \leq 0.60$
Satisfactory	$0.50 < E \leq 0.65$	$\pm 15 \leq PBIAS < \pm 25$	$0.60 < RSR \leq 0.70$
Unsatisfactory	$E \leq 0.50$	$PBIAS \geq \pm 25$	$RSR > 0.70$

HEC HMS Model Development: Discussion of Results

Calibration Results

Figure 89 shows the hydrographs simulated by the model before and after its calibration. The model performance evaluation statistics are listed in Table 27. At the MONTALBAN station, the un-calibrated model performance was found to be already "very good". However, looking at the comparison between the simulated and observed hydrographs, there are differences in terms of peak flows and the overall shape of the hydrographs. After calibration, the performance statistics improved although it still appears that there are portions of the observed hydrograph that the model seems to underestimate. This is confirmed by the positive *PBIAS* of 4.79% that clearly indicates the calibrated model is biased towards underestimation of flow in MONTALBAN station.

At the STO. NINO station, the un-calibrated model generally overestimates flow by 20.63% with relatively large *RSR*. The computed *E* is only 0.76. After calibration, the model's performance in simulating flow at the station improved considerably from satisfactory to a very good performance. The improvement is very visible in Figure 89, with a significant change in peak flow and timing. Although the calibration result is very good, the model is biased towards overestimation by 4.12%.
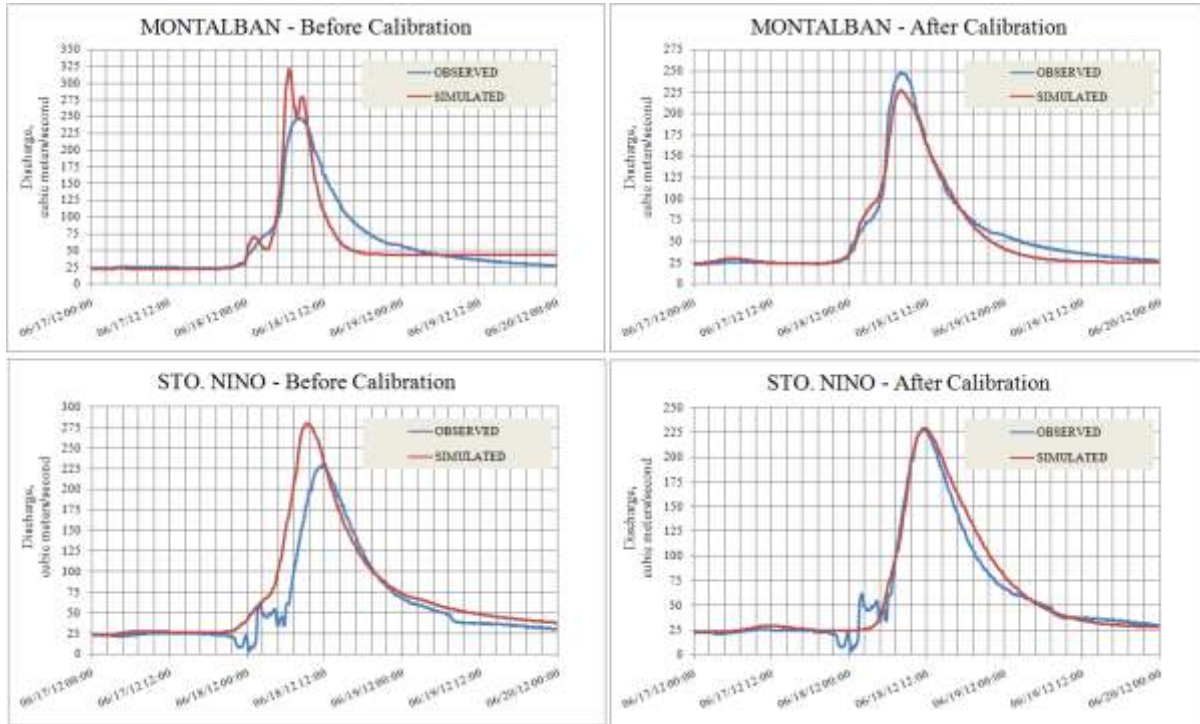
Figure 89. Graphs showing observed and simulated hydrographs before and after HEC HMS model calibration.

Table 27. HEC HMS model performance before and after calibration.

Station / Statistics / Rating	Before Calibration	After Calibration
MONTALBAN		
E	0.83	0.98
PBIAS	-3.62%	4.79%
RSR	0.42	0.15
Rating	Very good	Very good
STO. NINO		
E	0.76	0.97
PBIAS	-20.63	-4.12
RSR	0.49	0.17
Rating	Satisfactory	Very Good

Table 28. Comparison of observed and the calibrated HEC HMS model simulated hydrograph for the calibration period.

Station / Parameter	Observed	Simulated	Difference
MONTALBAN			
Peak flow, m^3/s	247.9	226.8	21.1
Time of Peak	6/18/2012 8:00 AM	6/18/2012 8:00 AM	No difference (model is on time)
Total flow, x 10^9 m^3	18,722.56	17,834.07	888.49 (underestimation)
STO. NINO			
Peak flow, m^3/s	229.3	228.9	0.4
Time of Peak	6/18/2012 11:40 AM	6/18/2012 11:40 AM	No difference (model is on time)
Total flow, x 10^9 m^3	18,739.50	19,544.72	-805.22 (overestimation)

In Table 28, observed hydrograph characteristics are compared with hydrograph simulated by the calibrated model. It appears that the calibrated model is relatively accurate in predicting peak flows. The difference between the observed and simulated peak flows are 21.1 m^3/s in MONTALBAN, and 0.4 m^3/s in STO. NINO, with both indicating underestimation. The time of peaks predicted by the calibrated model were accurate, with no difference between observed and simulated time of peaks. In terms of total flow, there was underestimation in MONTALBAN but overestimation in STO. NINO. This result confirms the positive *PBIAS* in MONTALBAN and the negative *PBIAS* in STO. NINO station. While the information presented in Table 28 indicated more than satisfactory model performance, further evaluation through examination of validation results is necessary.

Validation Results

Figure 90 shows the result of the HEC HMS model validation using the August 2012 dataset. The model performance statistics are summarized in Table 29 while the comparison between observed and simulated hydrograph characteristics are listed in Table 30.

The validation results generally shows a satisfactory to very good performance of the calibrated HEC HMS model. Very good performance was obtained for the MONTALBAN station, with *E*=0.88 and very low values of *PBIAS* and *RSR*. Looking at the graph, the model was able to capture the first major peak with a slight overestimation of peak flow by 79.9 m^3/s. The difference in time of peak is 40 minutes, with the simulated peak being ahead of the observed peak. However, the model failed to accurately capture the second major peak although it was able to predict in time the third major peak with some underestimation.

In the case of STO. NINO station, the model's performance is only satisfactory due to the failure of the model to match the observed hydrograph. It can be noticed that the model

overestimated flow (including peak flows) at this station. The model simulated peak flow is 559.8 m^3 more than the observed peak flow, and it was ahead by 1 hour and 40 minutes.

Table 29. Performance of the HEC HMS model for the validation period.

Station / Statistics / Rating	August 2012 Validation
MONTALBAN	
E	0.88
PBIAS	-0.26%
RSR	0.35
Rating	Very Good
STO. NINO	
E	0.71
PBIAS	-25.38%
RSR	0.54
Rating	Satisfactory (*PBIAS* exceeding 25% by 0.38% is considered negligible)
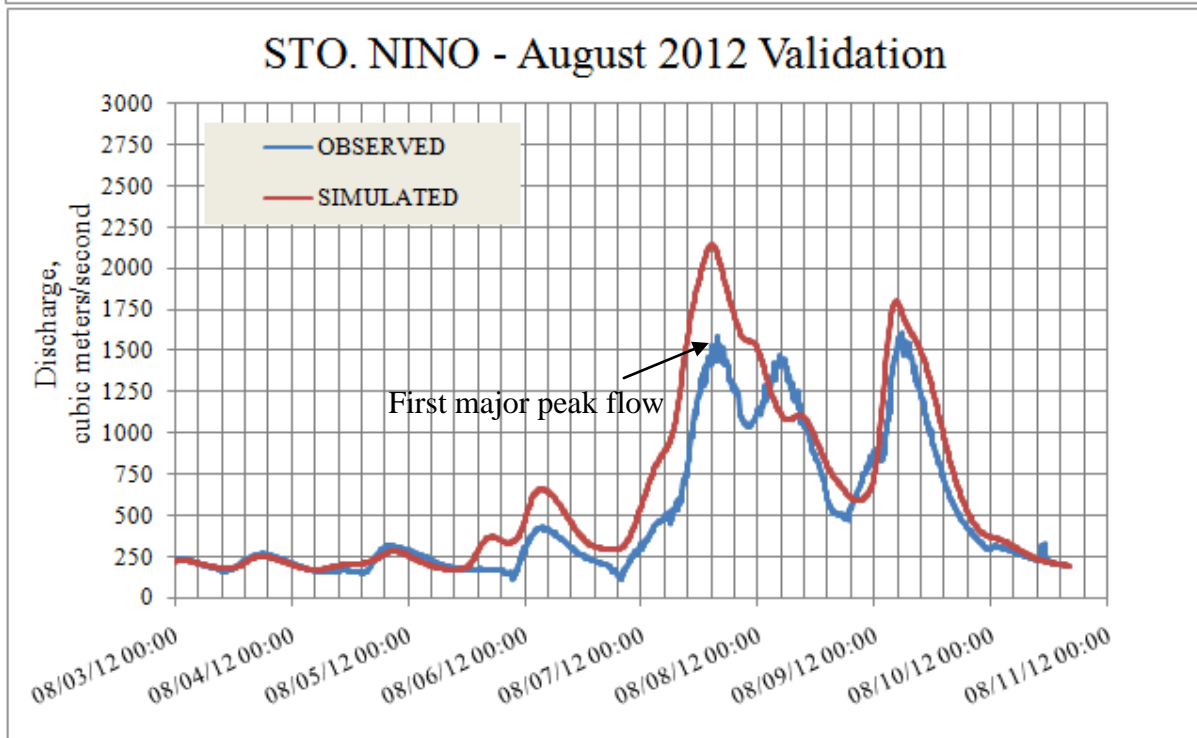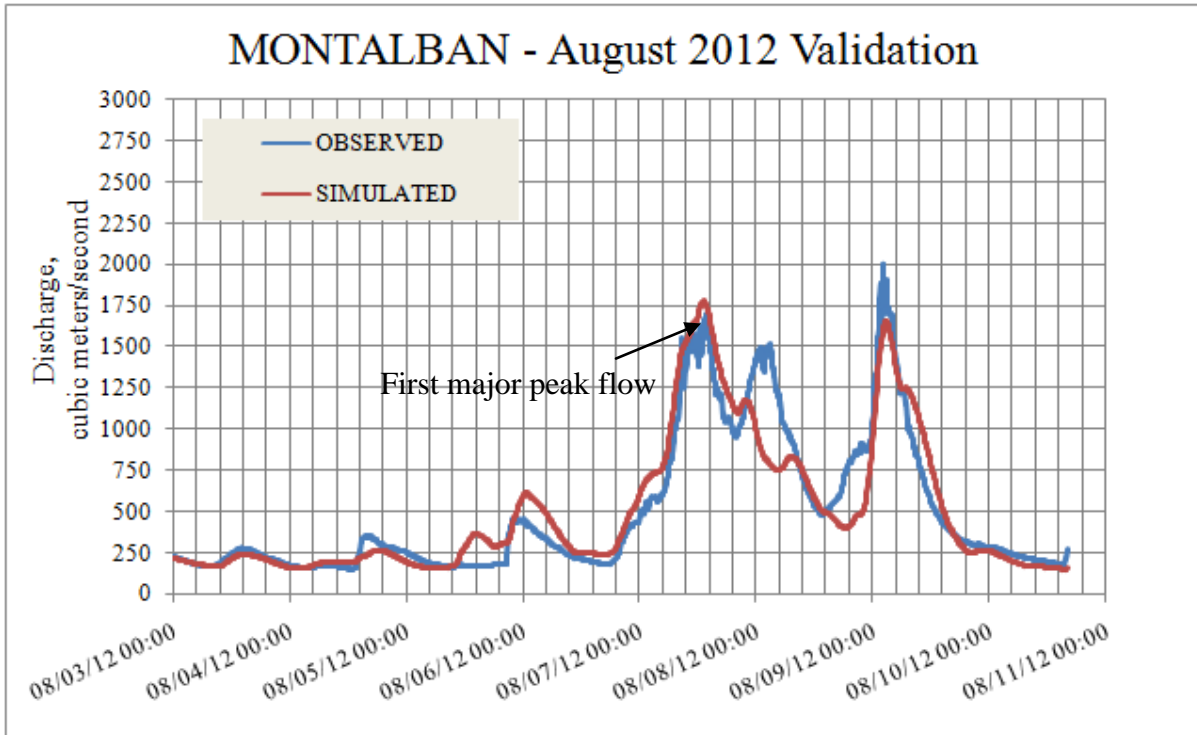
Figure 90. Graphs showing the result of the HEC HMS model validation using the August 2012 validation data.

Table 30. Comparison of observed and the calibrated HEC HMS model simulated hydrograph for the August 2012 validation period.

Station / Parameter	Observed	Simulated	Difference
MONTALBAN			
1st Major Peak flow, m^3/s	1,696.6	1,776.5	-79.9 (overestimation)
Time of 1st Major Peak Flow	8/7/2012 1:50 PM	8/7/2012 1:10 PM	40 minutes (model is ahead)
Total flow, x 10^9 m^3	366,293.36	367,239.13	-945.77 (overestimation)
STO. NINO			
1st Major Peak flow, m^3/s	1,585.2	2,145.0	-559.8 (overestimation)
Time of 1st Major Peak Flow	8/7/2012 3:40 PM	8/7/2012 2:30 PM	1 hour and 10 minutes (model is ahead)
Total flow, x 10^9 m^3	366,302.63	459,295.71	-92,993.08 (overestimation)

The overestimation of flows at STO. NINO station might be due to incapability of the model to incorporate bank overflows. It can be recalled that the validation period had a major flooding event in Marikina River [**4**]. Looking back at Figure 87 where the observed hydrographs of MONTALBAN and STO. NINO are overlaid, it can be noticed that discharge at MONTALBAN is far greater than the discharge at STO. NINO. But considering that STO. NINO is at the downstream, it can be initially thought that discharge at STO. NINO should be greater than the discharge at MONTALBAN. But this was not true. In fact, there was a decrease in discharge from MONTALBAN prior to its arrival in STO. NINO station. This may be due to occurrence of flow diversions or impoundments, specifically bank overflows, just before STO. NINO. As the HEC HMS model did not incorporate flow diversions/impoundments which could mimic bank overflows, the simulated hydrograph at STO. NINO station will be greater than the hydrograph simulated at MONTALBAN. With this, it can be inferred that at STO. NINO and at locations further downstream (e.g., Rosario JS), discrepancy between actual and simulated data may be due to this failure of the model to incorporate bank overflows. Nevertheless, the calibrated HEC HMS model may be used for discharge estimation as necessary inputs of hydraulic models since the model's performance is satisfactory based on evaluation statistics.

Using the Calibrated HEC HMS as a Water Level Forecasting System

The discharge hydrographs simulated by the calibrated HEC HMS model at MONTALBAN and STO. NINO stations can be converted into time series of water level through the use of rating curves shown previously in Figure 88. Noting that the overestimation of discharge in the STO. NINO station will also lead to overestimation of

water levels, the computed water levels were subtracted by 1 meter. This value was selected as it was found that the computed water levels are approximately 1 meter higher than the observed water levels. The results are shown in Figure 91 while performance statistics are listed in Table 31.

The results of the comparison of the simulated water levels with observed data indicates that the use of the calibrated HEC HMS model to simulate discharge and converting this discharge into water levels using rating curves provides a fast and relatively accurate way of forecasting water levels at MONTALBAN and STO. NINO stations. The average water level errors are relatively low, while the RMS errors indicate sub-meter accuracy of the predicted water levels. With this, forecasting water levels during rainfall events in MRB can be one of the applications of the calibrated HEC HMS model, in addition to providing discharge data necessary for running the HEC RAS model to generate flood depth and hazard maps.

Table 31. Performance and accuracy of the HEC HMS model in simulating water levels for the August 2012 period through conversion of simulated discharge by the use of rating curves.

Station / Statistics / Rating	
MONTALBAN	
Average Error, m.	-0.09
RMS Error, m.	0.45
E	0.89
PBIAS	1.37%
RSR	0.34
Rating	Very Good
STO. NINO	
Average Error, m.	-0.33
RMS Error, m.	0.64
E	0.92
PBIAS	-5.09%
RSR	0.29
Rating	Very Good
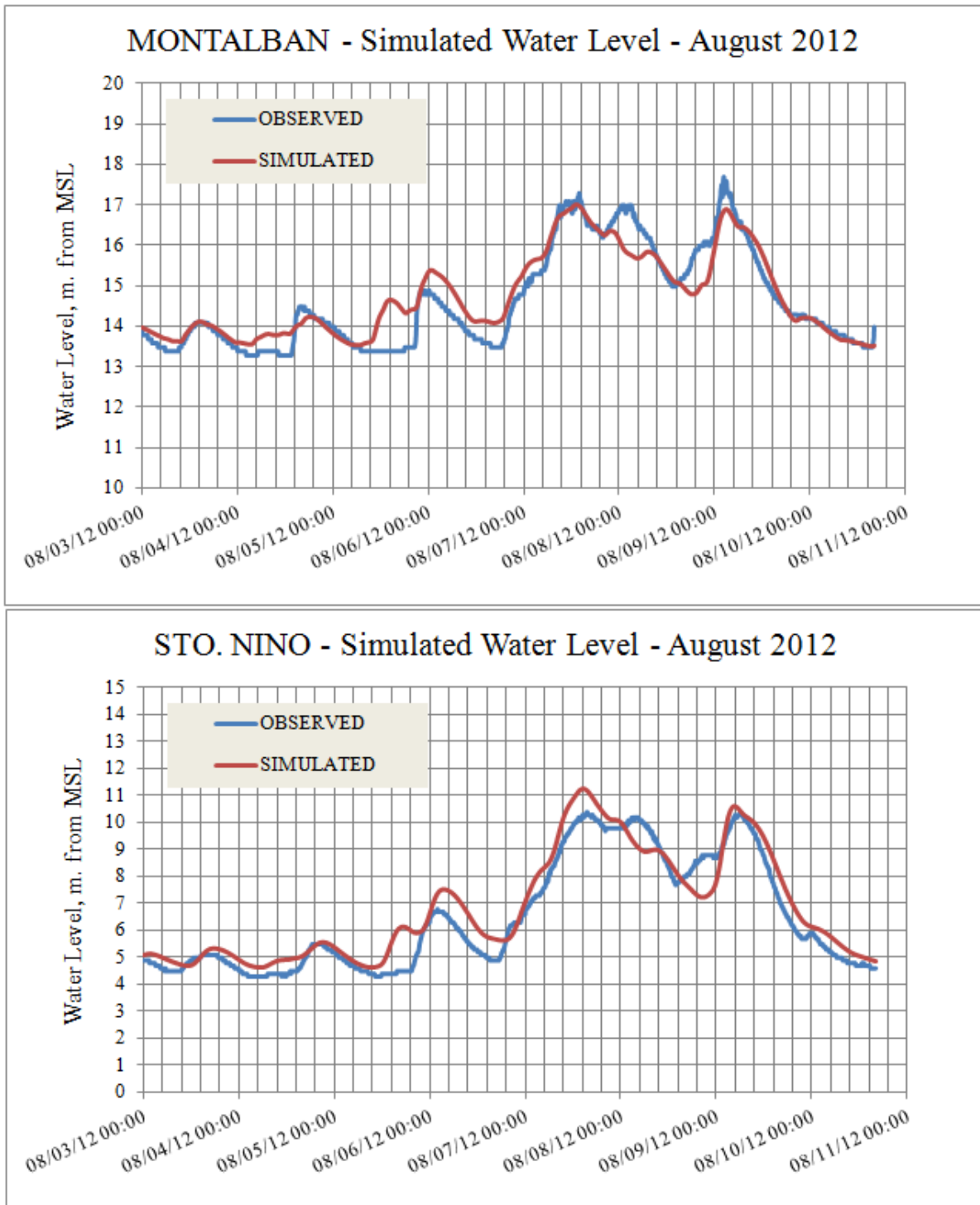
Figure 91. Graphs showing the observed and HEC HMS-simulated water levels derived from conversion of discharge using rating curves.

HEC RAS Hydraulic Model Development

Model preparation and parameterization

The HEC RAS model of Marikina River and tributaries (see Figure 78 for the domain) was developed by first constructing a geometric representation of the rivers and their flood plains. This includes cross-sections, river banks and centerline, and the flood plain boundaries (i.e. the domain). The high resolution 1-m LIDAR DEM integrated with river bed data was used as the primary source of the cross-section data. River banks and centerlines were digitized from the high resolution WV-2 image. All the model pre-processing was done in ArcView GIS 3.2 using HEC GeoRAS extension. HEC GeoRAS is the pre-processor of HEC RAS, and it basically prepares the model's geometric data. It is also used to assign basic model parameters. This geometric data is then imported in HEC RAS for further model setup.

A total of 1,273 cross-section lines (average interval of 66 m), 29 river reaches (total length of 83.835 km), 58 river bank lines, and 14 junctions (Figure 92). Some of the cross-sections were extended beyond the model domain just to make sure all of the domain is covered. During post-processing, the model results (e.g., flood depth and hazard maps) were clipped accordingly. The resulting geometric representation, as imported in HEC RAS version 4.1, is shown in Figure 93.

Flow resistance coefficients, also called Manning's roughness coefficients n, were assigned to the cross-section segments (or the portion between cross-section points) using land-cover information from the ALOS AVNIR-2 land-cover map. A look-up table based on the HEC RAS Hydraulic Reference Manual [22] was used to transform the land-cover classes to Manning's n land-cover classes (Table 32).

Table 32. Look-up table of Manning's *n* surface roughness (Source: [22]).

Land-cover class based on the ALOS AVNIR-2 land-cover map	Equivalent or nearest Manning's *n* class	Manning's *n*
Bare Soil	Bare soil	0.030
Built-up Areas	Concrete	0.019
Exposed River Bed	Bare soil	0.030
Excavations	Excavated or dredged channel - no vegetation	0.028
Grasslands	Pasture, no brush	0.038
Vegetation – High Density Trees and Shrubs (assumed to be mixed with Grass)	Heavy stand of timber	0.103
Vegetation – Medium Density Trees and Shrubs (assumed to be mixed with Grass))	Medium to dense brush and trees	0.100
Vegetation – Low Density Trees and Shrubs ((assumed to be mixed with Grass)	Light brush and trees	0.058
Water Bodies (Lakes, Rivers)	Natural channel, clean, winding, some pools and shoals	0.040
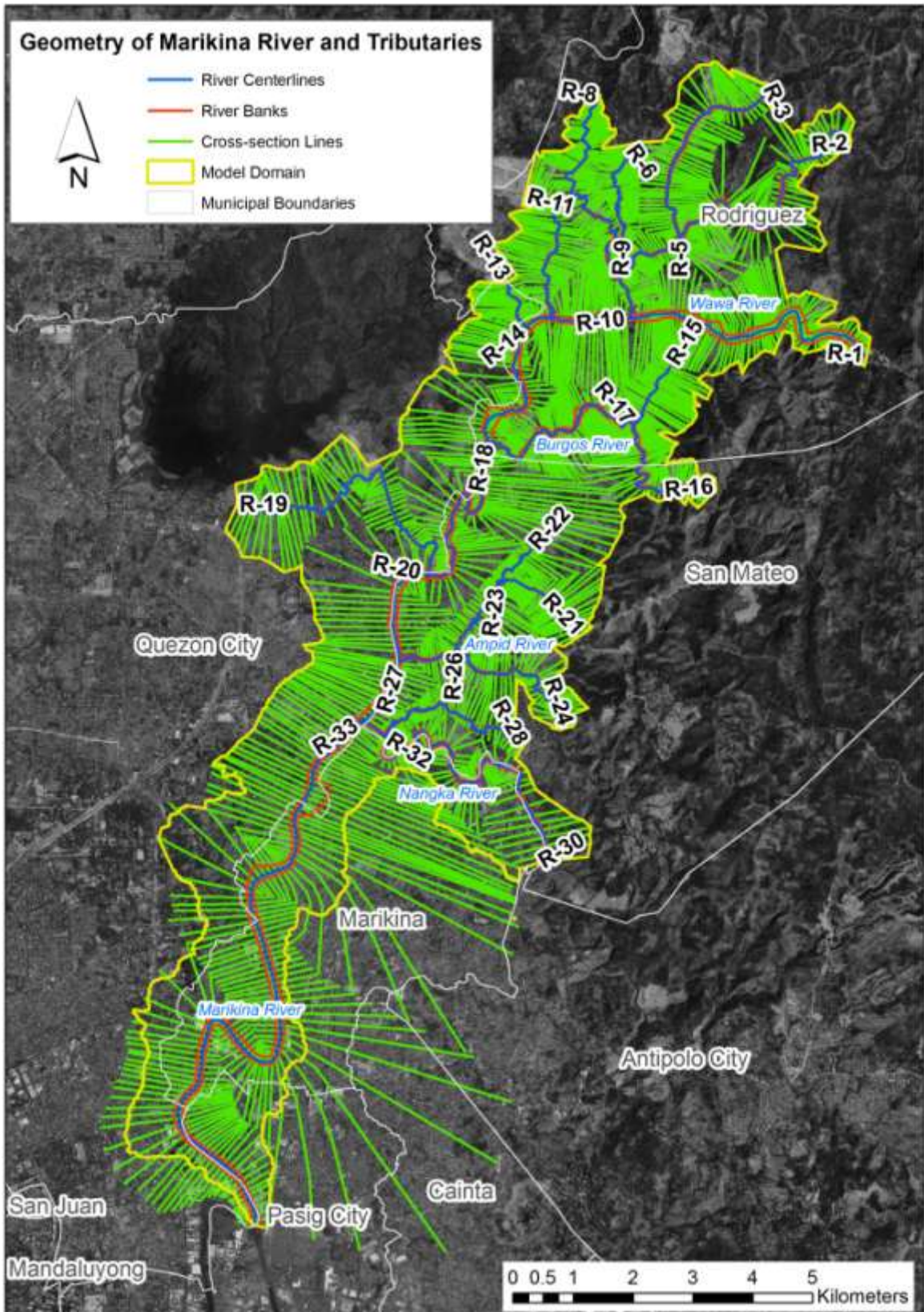
Figure 92. Geometric representation of Marikina River and its tributaries within the hydraulic model domain. The upstream-most portion of each reach is labeled (e.g., R-33).
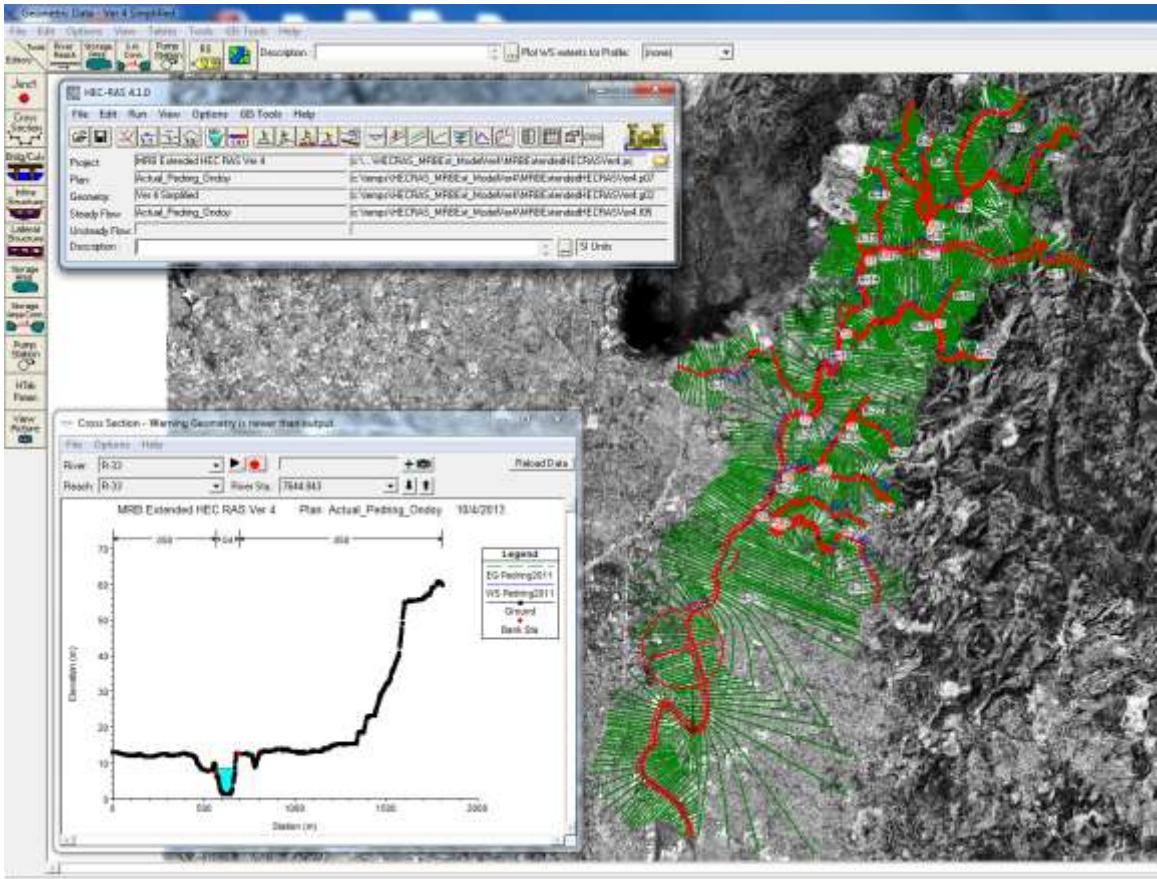
Figure 93. The resulting geometric data of the Marikina River and tributaries as imported in HEC RAS.
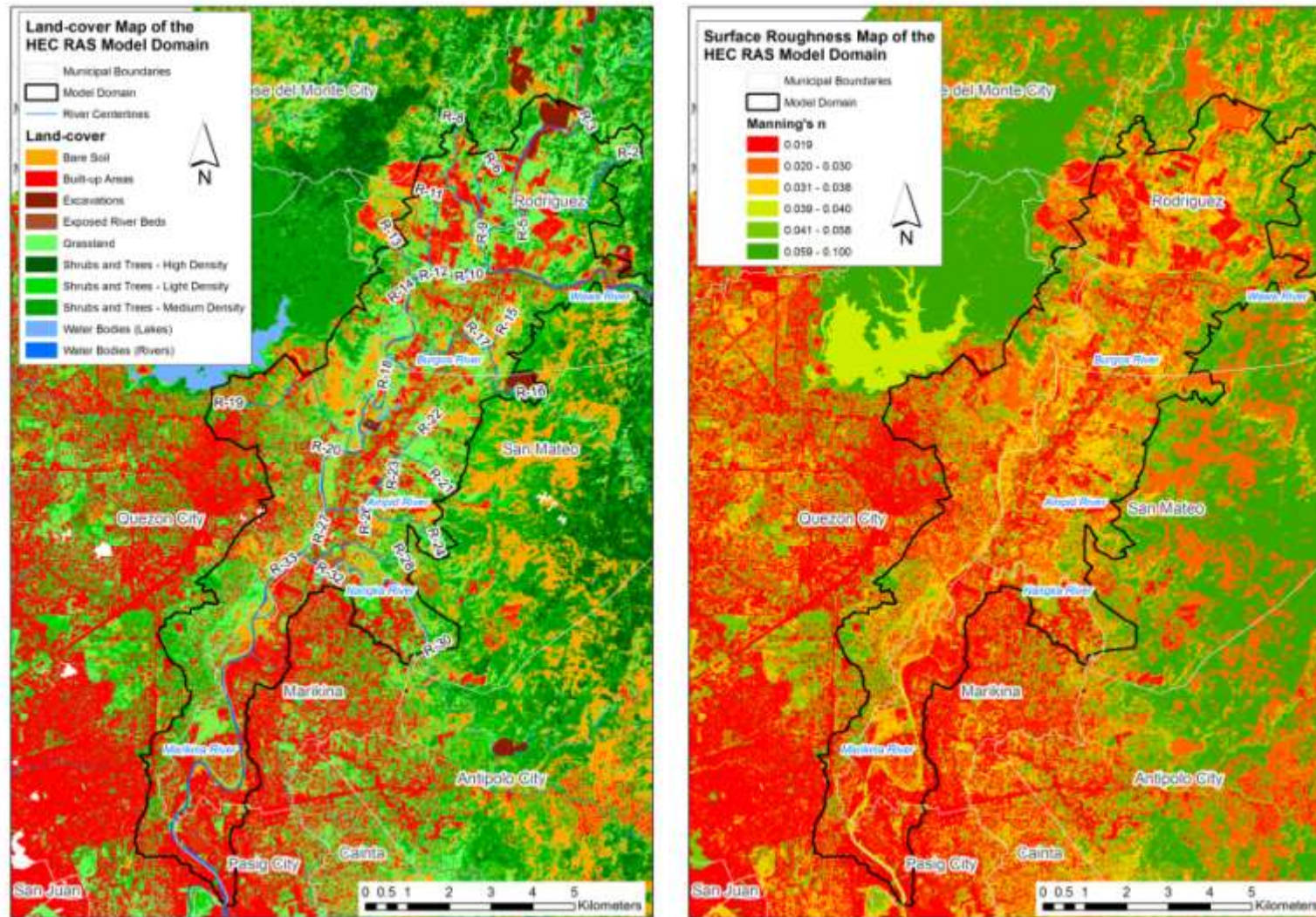
Figure 94. Land-cover and surface roughness (Manning's *n*) maps of the HEC RAS model domain.

Model Boundary Condition Locations

As a hydraulic model, the HEC RAS model cannot run on its own to provide the required information (flood depths). In a simulation run, it requires information on how much water is entering at specific locations as well as water level conditions at the downstream-most portion (e.g., outlet) of the model domain. This required information are called boundary conditions that needs to be set in order to reflect (i) the volume of water that the river receives (or inflow) from upstream watersheds, and (ii) the elevation of the water surface at the outlet.

For the HEC RAS model of Marikina River and tributaries, there were 30 boundary condition (BC) locations (Figure 95) consisting of 1 open BC (at the outlet), 15 inflow BCs (at the upstream of the tributaries), and 14 internal flow BCs (at the junctions). Each BC location corresponds to an element of the HEC HMS model which will provide the needed information on flow rates and water surface elevation (Table 33).
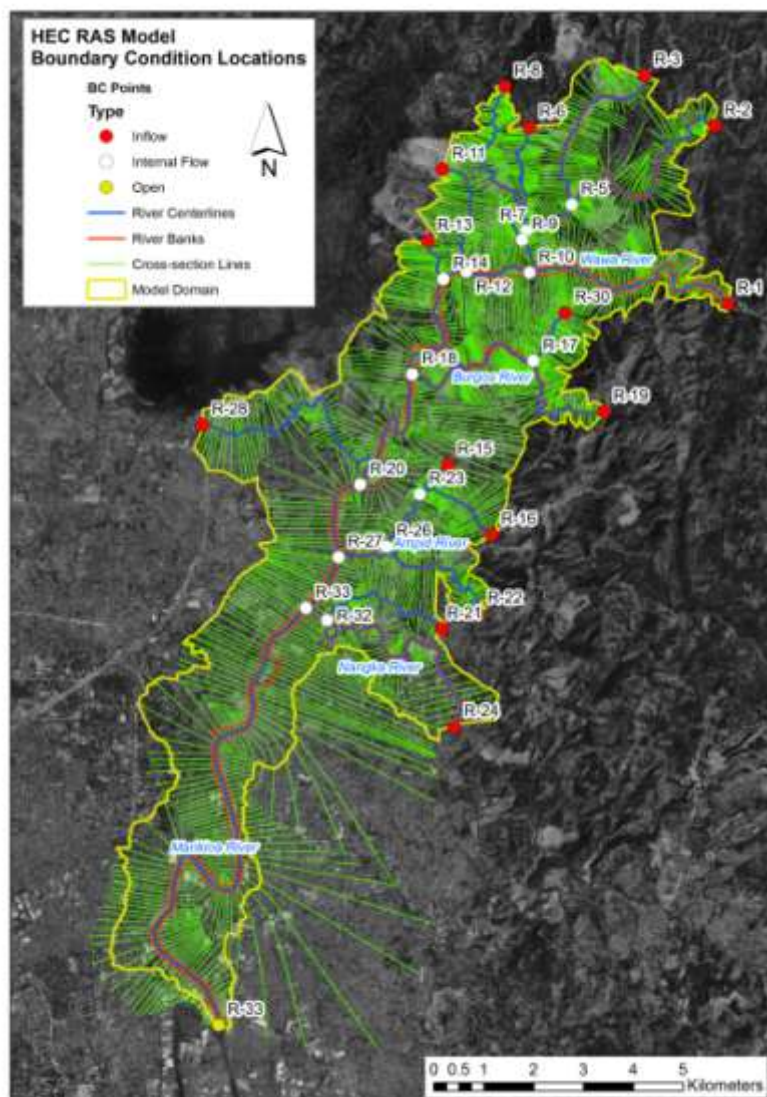
Figure 95. Map showing the HEC RAS model boundary condition locations.

Table 33. Boundary Condition (BC) points in the HEC RAS model and their corresponding HEC HMS model elements.

HEC RAS Model Element		Corresponding HEC HMS Model Element	Type of BC
Reach Name	Cross-section Name (where the BC is assigned)		
R-1	4860.071	JR 1320	Inflow
R-10	1320.757	JR 430	Internal flow
R-11	2794.43	R 370 W 370	Inflow
R-12	441.904	JR 1280	Internal flow
R-13	964.856	R 1280 W 1280	Inflow
R-14	2444.695	MONTALBAN	Internal flow
R-15	1309.435	R 500 W 500	Inflow
R-16	3106.857	JR 510	Inflow
R-17	3529.422	JR 520	Internal flow
R-18	3572.773	JR 530	Internal flow
R-19	5869.432	BATCH PT 9 + R 570 W 570	Inflow
R-2	4899.811	JR 300	Inflow
R-20	1829.185	JR 680	Internal flow
R-21	1968.467	BATCH PT 8	Inflow
R-22	994.788	R 640 W 640	Inflow
R-23	1705.603	BATCH PT 7	Internal flow
R-24	3417.992	BATCH PT 3	Inflow
R-26	1277.531	JR 780	Internal flow
R-27	1227.713	JR 1380	Internal flow
R-28	3507.934	BATCH PT 13	Inflow
R-3	3805.757	JR 280	Inflow
R-30	6030.957	BATCH PT 1	Inflow
R-32	475.603	NANGKA	Internal flow
R-33 (upstream)	11974.42	NANGKA @ MARIKINA	Internal flow
R-5	1284.32	JR 360	Internal flow
R-6	2927.012	R 330 W 330	Inflow
R-7	198.33	JR 390	Internal flow
R-8	4734.293	JR 240	Inflow
R-9	709.79	JR 400	Internal flow
R-33 (downstream)	27.459	ROSARIO JS	Open

HEC RAS Model Application for Flood Depth Estimation and Hazard Mapping

Figure 96 shows the interface of the HEC RAS model.
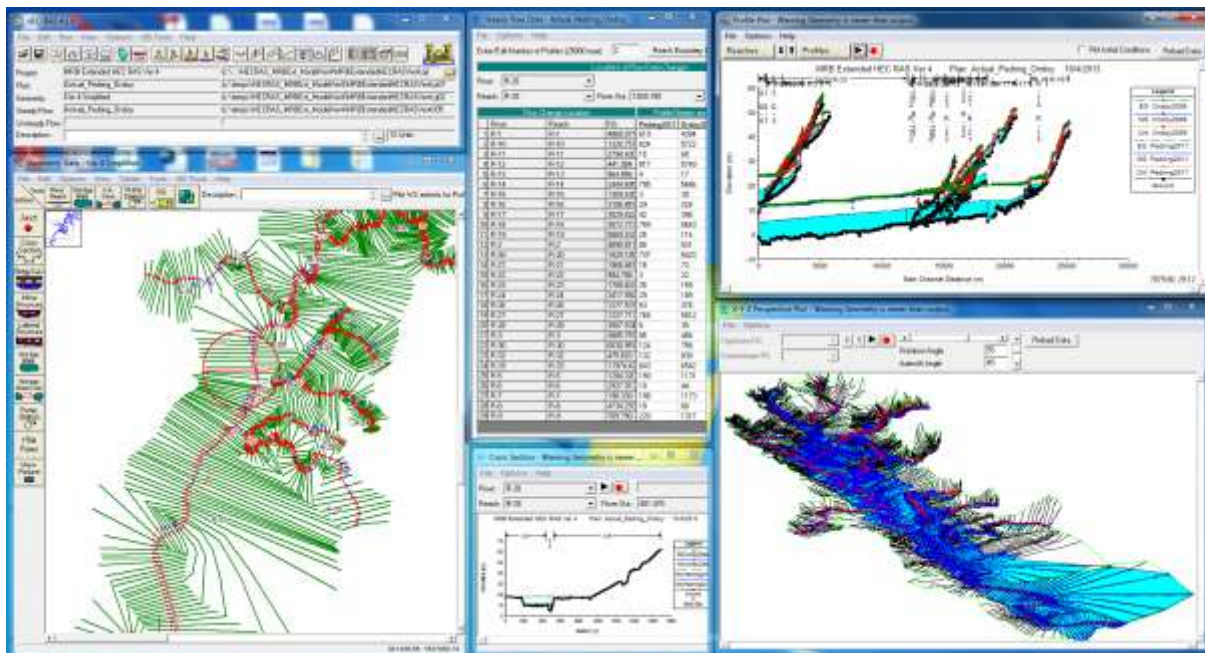
Figure 96. Interface of the HEC RAS model of Marikina River and tributaries.

To use the model for flood depth estimation during rainfall events, the steady flow simulation module of HEC RAS was used. This module can do one-dimensional water profile calculations for steady gradually varied flow. Water surface profiles are computed from one cross section to the next by solving the Energy equation (shown in Figure 97). Under steady flow, the following were specified using the result of the HEC HMS simulation: (1) flow or discharge at the inflow and internal flow boundary condition points, and (2) stage at the downstream boundary (outlet). The steady flow model proceeds to calculate stages throughout the interior points, while keeping the discharge constant [61].

$$Z_2 + Y_2 + \frac{a_2 V_2^2}{2g} = Z_1 + Y_1 + \frac{a_1 V_1^2}{2g} + h_e$$

Where: Z_1, Z_2 = elevation of the main channel inverts

Y_1, Y_2 = depth of water at cross sections

V_1, V_2 = average velocities (total discharge/ total flow area)

a_1, a_2 = velocity weighting coefficients

g = gravitational acceleration

h_e = energy head loss

Figure 97. The Energy equation (Source: [22]).

The steady flow calculation implemented in HEC RAS is based on the assumptions that flow is steady, flow is gradually varied, flow is one dimensional (i.e., velocity components in directions other than the direction of flow are not accounted for), and river channels have "small" slopes(e.g., < 1:10) [22]. According to the HEC RAS Technical Reference Manual, flow is assumed to be steady because time-dependent terms are not included in the energy equation. Flow is assumed to be gradually varied because the energy equation is based on the premise that at hydrostatic pressure distribution exists at each cross-section. Flow is assumed to be one-dimensional because the Energy equation is based on the premise that the total energy head is the same for all points in a cross-section.

For generating flood depth and hazard maps for an extreme rainfall event, the maximum flow rate at inflow and internal flow BC locations were obtained from discharge hydrographs simulated by the calibrated HEC HMS model and used as input for HEC RAS steady flow estimation. At the open BC (outlet, ROSARIO JS station), the maximum water level during the simulation period was obtained by using the rating curve for the station. This was done to comply with the assumptions of the model. With this information set as boundary conditions, HEC RAS will be able to compute the maximum water surface profiles in all the cross-sections within the model domain for a particular event.

The water surface profiles computed by the HEC RAS model can be converted into flood depth maps through GIS post-processing using HEC GeoRAS, an extension of ArcGIS. The procedures include generating a Triangulated Irregular Network (TIN) of water surface elevation based on the computed water surface profiles at the cross-sections, converting the TIN to into a water surface elevation (WSE) grid, and then overlaying the WSE grid into the 1-m LIDAR DEM to estimate the flood depths (i.e., subtracting the WSE grid by the DEM grid). Once the flood depths are obtained, flood hazard maps can then be generated by classifying the depths into hazard levels (e.g., low: less than 0.5 m depth; medium: greater than or equal to 0.5 m but less than 1.5 m.; high: greater than or equal to 1.5 m).

Testing the HEC HMS-HEC RAS Flood Model in Simulating Actual Flood Events

Flood inundation during the *September 2009 Ondoy Flood Event* and the *August 2012 Habagat Flood Event*, were reconstructed through the use of the combined HEC HMS-HEC RAS flood model. To verify the accuracy of the flood inundation maps for the two events, they were compared with observed flood inundation derived from the analysis of synthetic aperture radar (SAR) images captured by the RADARSAT-2 and ALOS PALSAR sensors during the time of flooding.

SAR Images of Flood Events

Information on the actual or observed extent of flooding were derived from ALOS PALSAR and RADARSAT-2 images that were acquired during the September 2009 and August 2012 flooding events in Marikina River. Basic information about these images are listed in Table 34. The use of SAR images as source of flood extent information has been demonstrated to be a useful tool for validating numerical inundation models [24].

Table 34. SAR images of flooding events in Marikina River and tributaries.

Image No.	Sensor	Polarization	Date and Time of Acquisition
1	ALOS PALSAR	HH / HV	26 Sep 2009, 1435 UTC in ascending mode (26 Sep 2009, 10:35 PM Local Time)
2	RADARSAT-2	HH	28 Sep 2009, 2144 UTC in descending mode (29 Sep 2009, 5:44 AM Local Time)
3	RADARSAT-2	HH	10 Aug 2012, 1019 UTC (10 Aug 2012, 6:19 PM Local Time)

The images were processed using the Next ESA Tool Box (NEST) version 4C-1.1 in order to generate a radiometrically calibrated, ortho-rectified back scattering (sigma nought, σ_0) image in linear scale and projected in UTM 51 WGS 1984. The order of the steps employed are: (1) radiometric calibration to convert the DN values (amplitude) to radar backscatter or sigma nought (σ_0); (2) de-speckling using the Enhanced/Refined Lee filter; and (3) terrain correction using rigorous SAR simulation where a 3-arcsecond SRTM DEM was utilized. The equations used in each step and other details are available in the NEST documentation available at http://nest.array.ca/web/nest/documentation. Each processed image was then co-registered to the ALOS AVNIR-2 dataset using at least 6 ground control points common to both images. The average and total RMSE during the co-registration of each image is less than 0.5 pixel. All the processed and co-registered images have spatial resolutions of 10 meters.

Each image was then subjected to unsupervised classification using K-means clustering to map flooded/inundated areas. Flooded or inundated areas are usually represented by very low back-scattering values making them appear dark in the images. The K-means clustering was run for 1000 iterations with 20 classes. Image interpretation was then applied to re-classify the K-means result into flooded and non-flooded. The accuracies of the flooded/non-flooded classification maps were then assessed by comparing it with an independent set of validation ROIs. The validation ROIs were collected through image interpretation prior to the K-means clustering. Post-processing of the classification map was then conducted to further classify the "flooded" areas according to their nature of flooding: if they were bank overflows (i.e. connected to a river), or if they were caused by accumulation of rainfall and/or due to overflow of banks from previous days (prior to image acquisition). This post-processing procedure is necessary so that it will be feasible to use it for comparison with flood extents simulated by the HEC RAS model. In this case, only those flooded areas that are connected to a river or stream are the one used to validate the HEC RAS result. Areas flooded due to accumulation of rainfall and/or due to overflow of banks from previous days were excluded and not used for comparison because the hydraulic processes involved are not represented by the HEC RAS model.
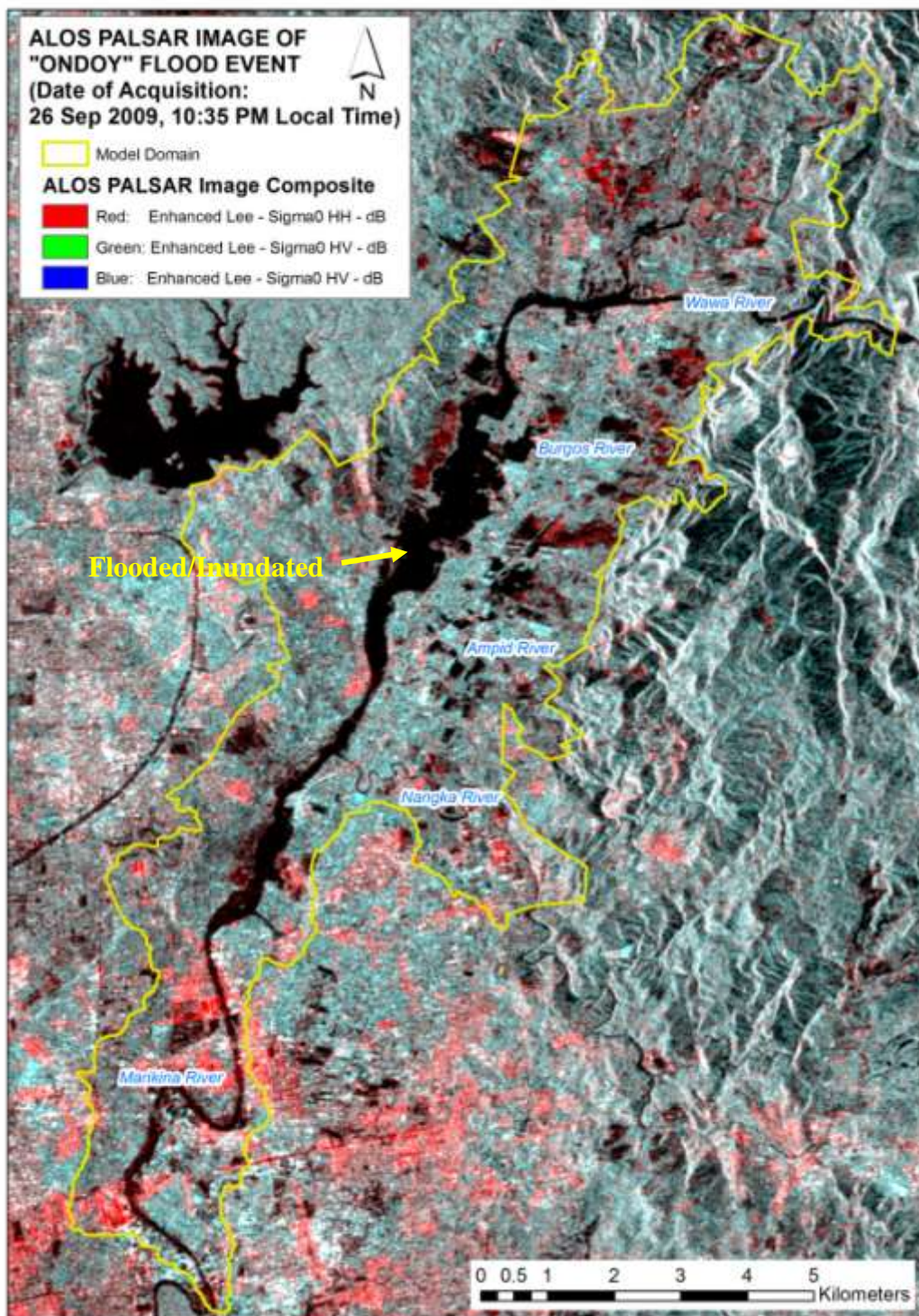
Figure 98. Radiometrically-calibrated and terrain-corrected ALOS PALSAR image composite of the *Ondoy* flood event (26 September 2009, 10:35 PM). (Image © JAXA, 2009)
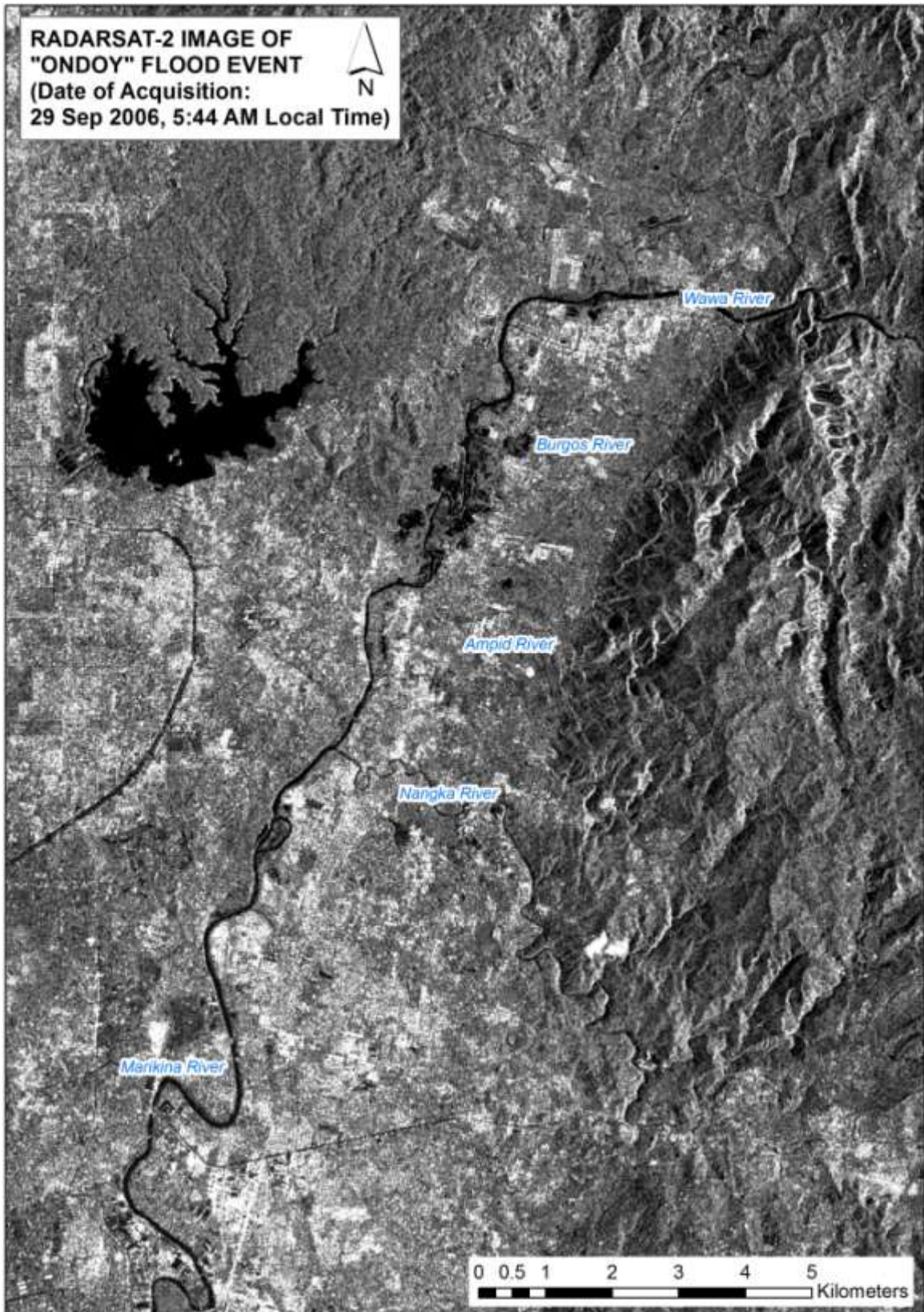
Figure 99. Radiometrically-calibrated and terrain-corrected RADARSAT-2 image of the *Ondoy* flood event (29 September 2009, 5:44 AM). (Image Data and Products © MacDonald, Dettwiler and Associates Ltd., 2009)

139
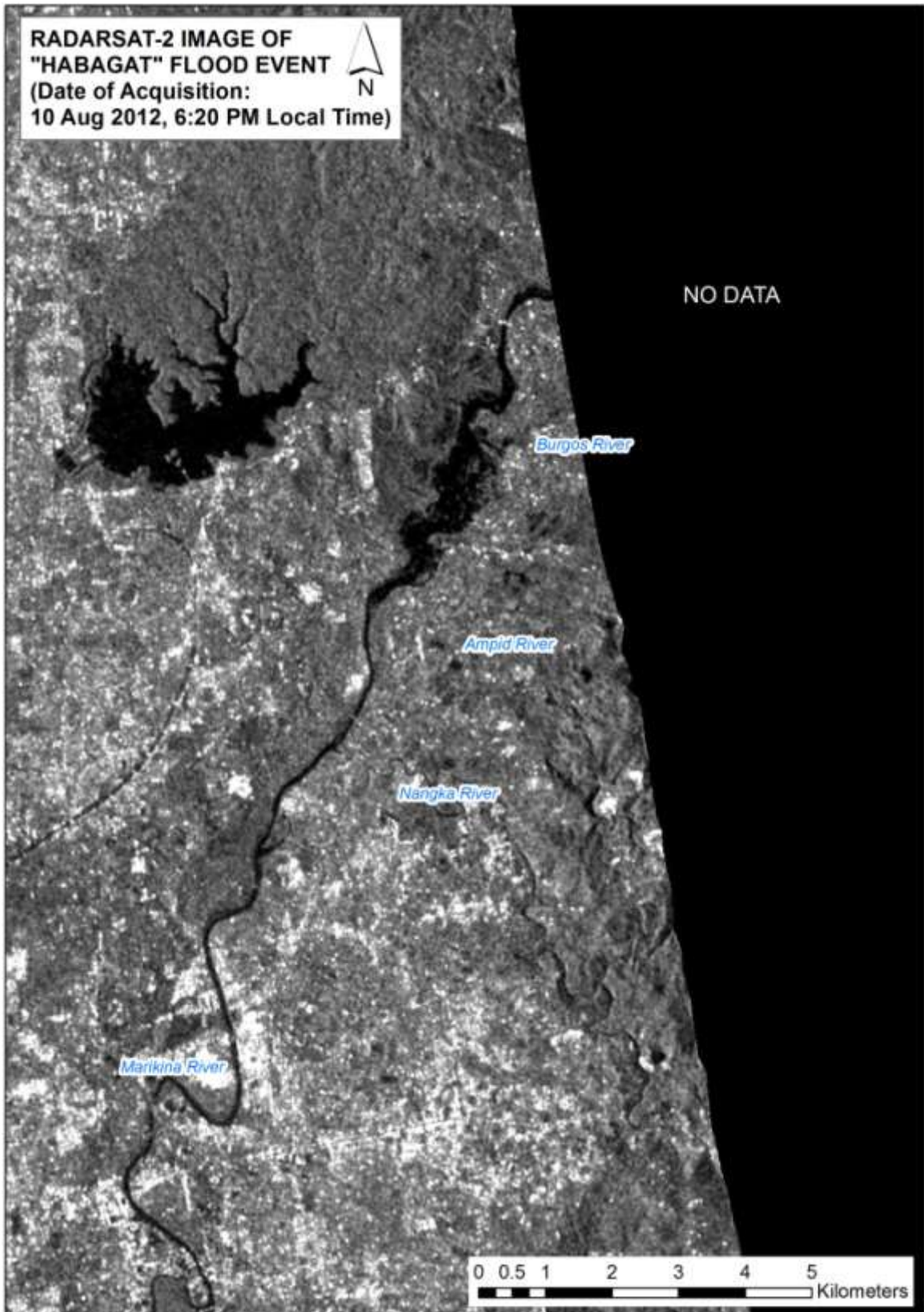
Figure 100. Radiometrically-calibrated and terrain-corrected RADARSAT-2 image of the *Habagat* flood event (10 August 2012, 6:20 PM). (Image Data and Products © MacDonald, Dettwiler and Associates Ltd., 2012)

Simulation of Flood Extents

Time series of rainfall data corresponding to actual flood events were collected and fed into HEC HMS model. The HEC HMS model was used to simulate hydrographs (Figure 100) at the inflow and internal flow BCs and water surface elevation at the open BC (ROSARIO JS). Then, the computed flow and water level at the BC points <u>corresponding or nearest</u> to the date and time of acquisition of the SAR images were extracted from the hydrographs and used as input to HEC RAS for steady flow simulation of water surface profiles. For the September 2009 events, 10-minute rainfall data recorded at the rooftop of Melchor Hall, College of Engineering, University of the Philippines, Diliman, Quezon City was used. Rainfall data from PAGASA-Science Garden was also available however the time resolution is coarse (at 3-hour interval). For the August 2012 event, flow and water level data was just extracted from the earlier HEC HMS simulation.

The HEC-RAS-simulated flood inundation maps were then derived through HEC GeoRAS post-processing in ArcGIS. For validation purposes, the resolution of the LIDAR DEM used in generating the flood extents were degraded to 10-m to be compatible with the food extent maps derived from SAR images.
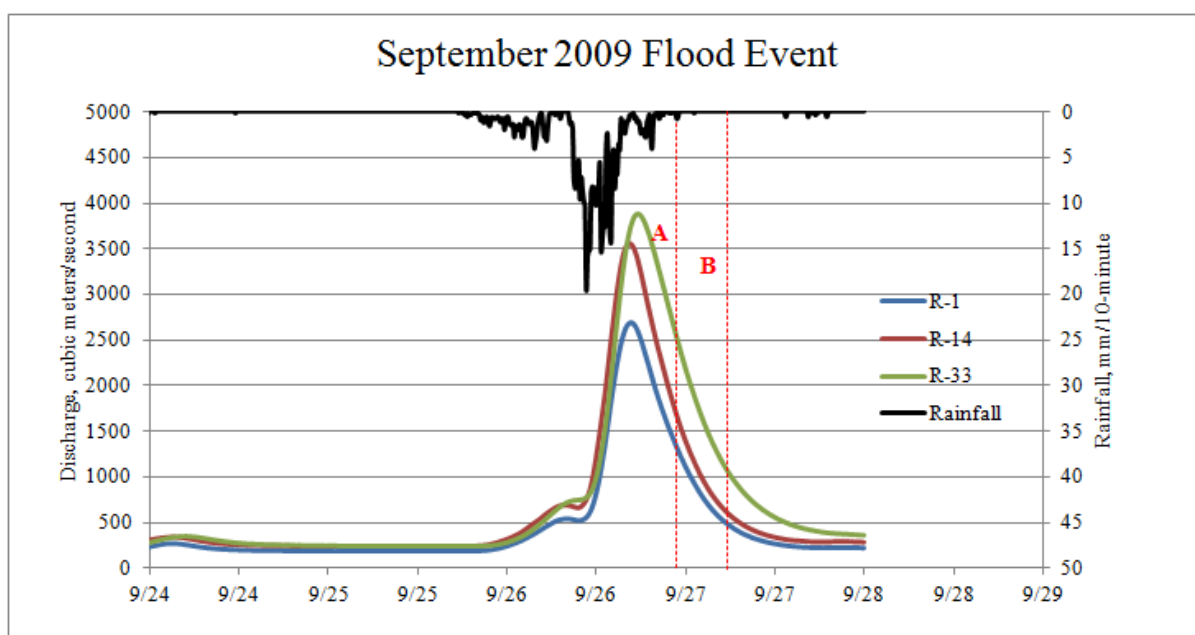
Figure 101. Example discharge hydrographs simulated by the calibrated HEC HMC model for the September 2009 flood event at R-1, R-14 and R-33. (Lines A and B indicate the date and time where data is extracted for HEC RAS flood simulation).

Comparison of Observed-*vs.*-Simulated Flood Extents

The accuracy of the HEC-RAS-simulated flood inundation extents were assessed by comparing it with flood inundation extents derived from the SAR images through union analysis of the GIS shapefiles. From this, the following information was obtained:

- Flooded areas that were correctly predicted by the model (F_{CP}) – areas that are common in both the observed and simulated flood extent data;

- Flooded areas that were over predicted by the model (F_{OP}) – areas that are not flooded in the observed data but predicted by the model as flooded; and
- Flooded areas that were under predicted by the model (F_{UP}) – areas that are flooded in the observed data but not predicted as flooded by the model.

By getting the area (in m^2) of F_{CP}, F_{OP}, and F_{UP}, three measures of accuracy (listed in Table 35) were computed.

Table 35. Measures of accuracy for the model simulated flood extents.

Measures of Accuracy (in %)	Formulation
Simulated Flood Extent Accuracy	$\dfrac{F_{CP}}{F_{CP} + F_{OP}} x100$
Error of Commission	$\dfrac{F_{OP}}{F_{CP} + F_{OP}} x100$
Error of Omission	$\dfrac{F_{UP}}{F_{CP} + F_{UP}} x100$

Results and Discussion

The accuracy of observed flood extent maps derived from the SAR images are summarized in Table 36.

Table 36. Classification accuracy of the observed flood extents derived from SAR images.

Image Source	Overall Classification Accuracy (%)	Producer's Accuracy (%)		User's Accuracy (%)	
		Flooded	Non-Flooded	Flooded	Non-Flooded
ALOS PALSAR (26Sep2009)	98.48 (778/790)	96.96 (383/395)	100 (395/395)	100 (383/383)	97.05 (395/407))
RADARSAT-2 (29Sep2009)	98.84 (939/950)	98.53% (468/475)	99.16 (471/475)	99.15 (468/472)	98.54 (471/478)
RADARSAT-2 (10Aug2012)	99.82% (545/546)	99.63% (272/273)	100 (273/273)	100 (272/272)	99.64 (273/274)

Shown in Figure 102, Figure 103 and Figure 104 are the observed flood extent derived from the analysis of ALOS PALSAR and RADARSAT-2 images and its comparison with model simulated flood extents. The accuracy of the flood extents are summarized in Table 37.
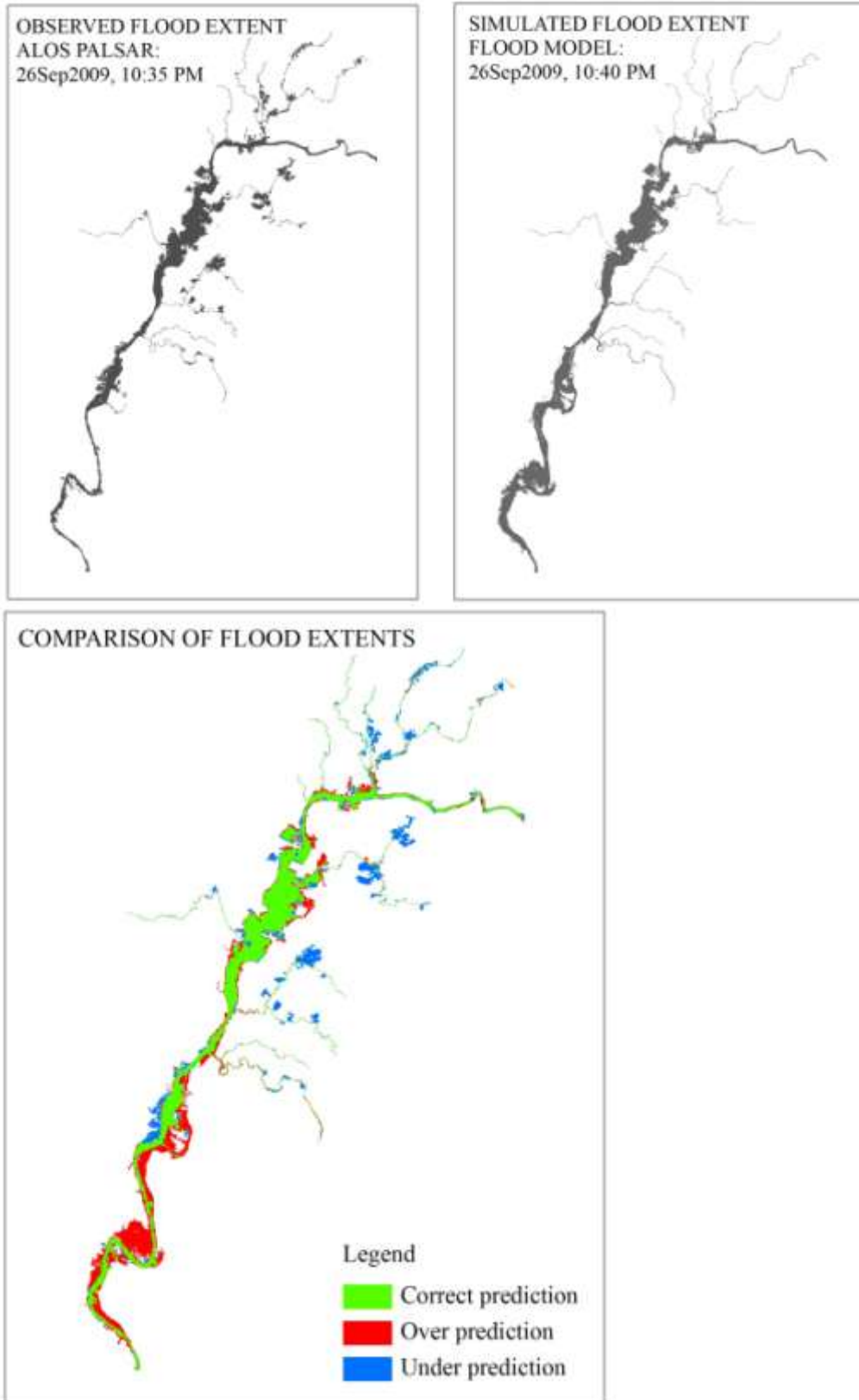
Figure 102. Comparison between observed and model-simulated flood extent for the 26Sep2009 *Ondoy* event.
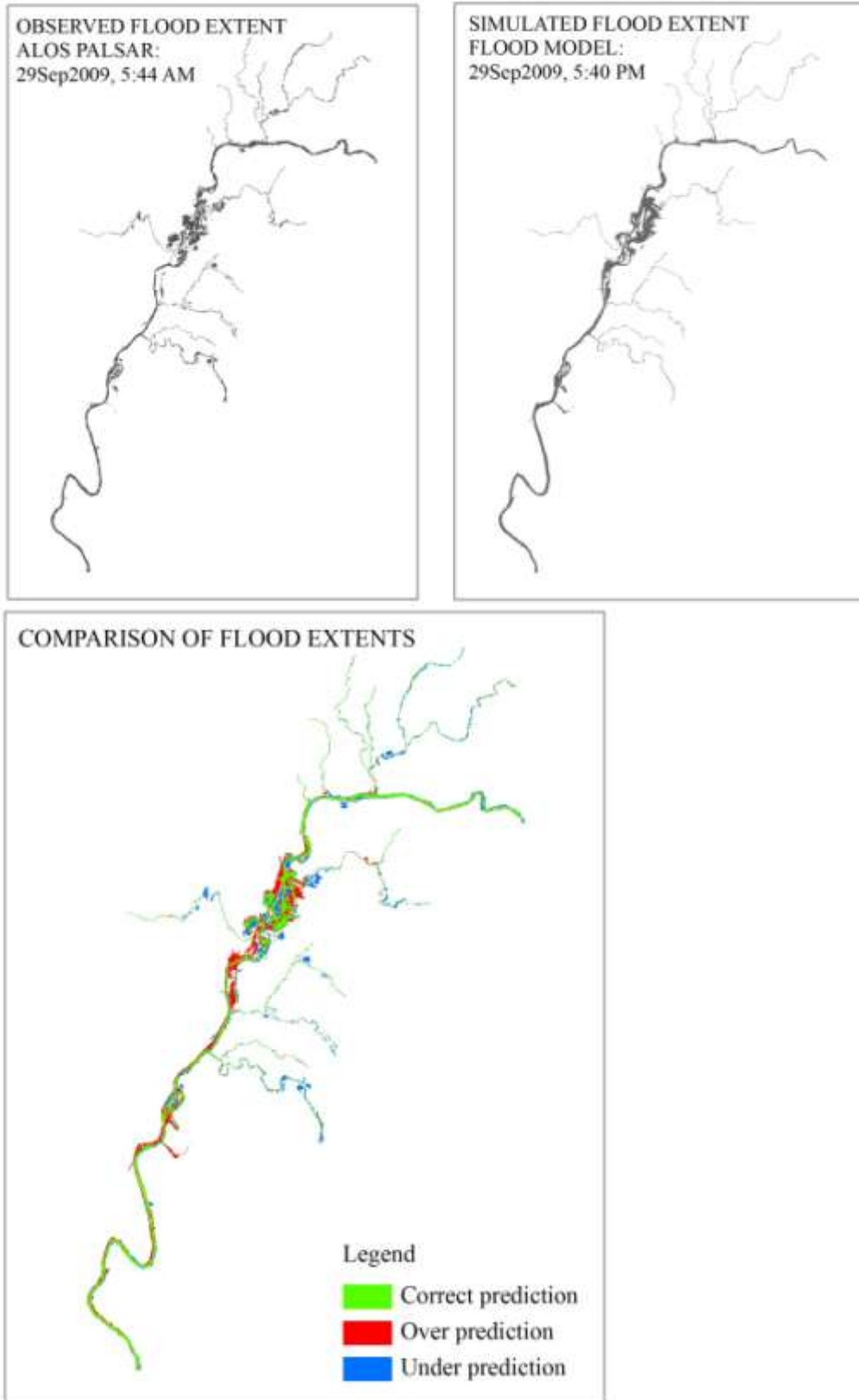
Figure 103. Comparison between observed and model-simulated flood extent for the 29Sep2009 *Ondoy* event.
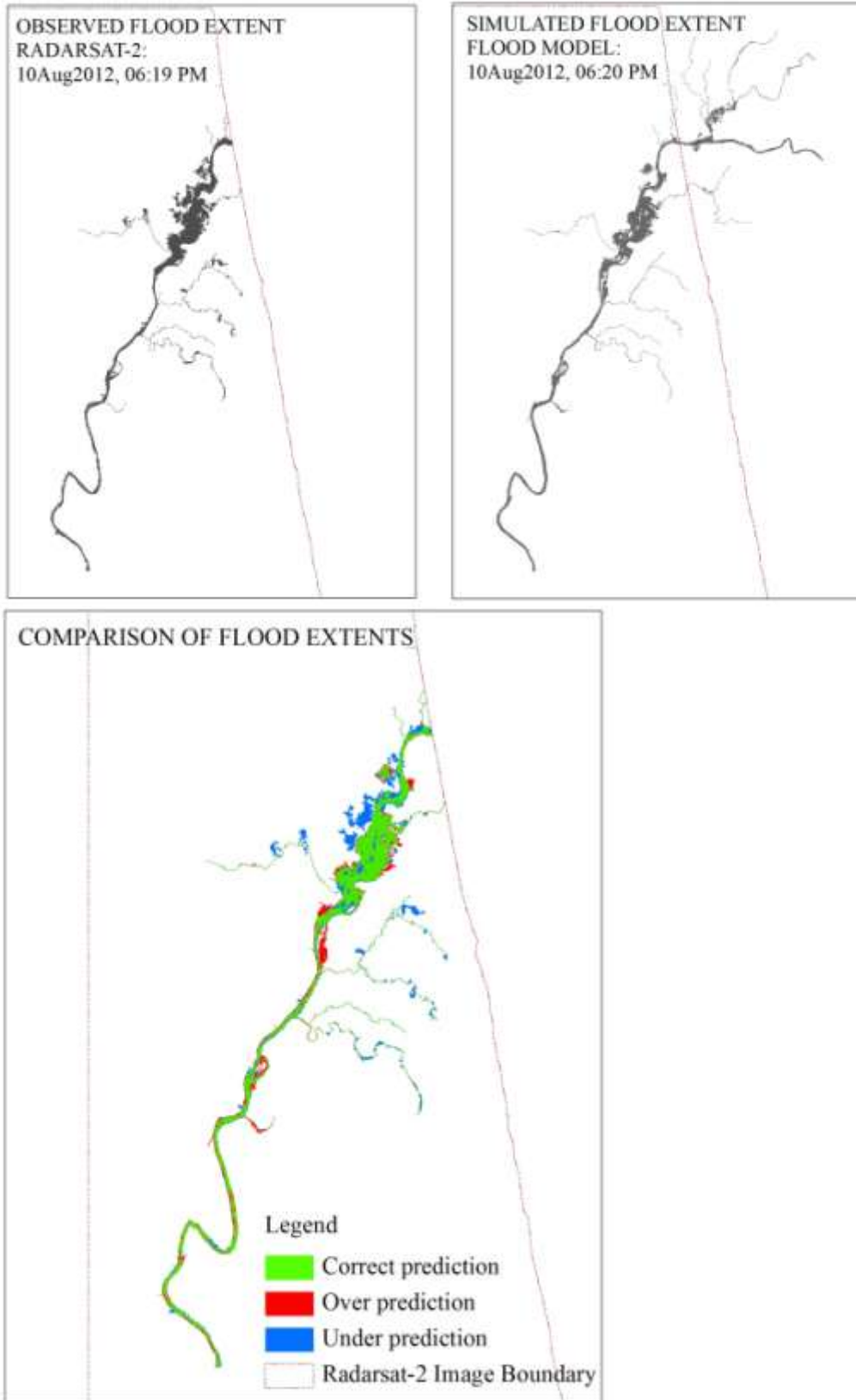
Figure 104. Comparison between observed and model-simulated flood extent for the 10Aug2012 *Habagat* event. Note that accuracy assessment was only done for the portion covered by the SAR image.

Table 37. Summary of accuracy of the simulated flood extents for three flood events.

| Flood Areas and Measures of Accuracy	Flood Event		
	26Sep2009	29Sep2009	10Aug2012
Total Area of Observed Flooding based on SAR Image ($F_{CP} + F_{UP}$)	8,752,400	4,799,000	5,021,563
Total Area of Flooding as Simulated by the Model ($F_{CP} + F_{OP}$)	9,819,700	4,829,500	4,444,494
Total Area of Correct Predictions (F_{CP}), m^2	6,313,400	3,183,400	3,528,234
Total Area of Over Predictions (F_{CP}), m^2	3,506,300	1,646,100	916,260
Total Area of Under Prediction (F_{UP}), m^2	2,439,000	1,615,600	1,493,329
Simulated Flood Extent Accuracy, %	64	66	79
Error of Commission, %	36	34	21
Error of Omission, %	28	34	30

The flood extents shown in the previous figures are considered as flood extents due to overflowing of banks. Results of the comparison with flood extents derived from SAR images shows a simulated flood extent accuracy ranging from 64-79%. The model simulated flood extents were found to have commission errors ranging from 21-36%, and omission errors ranging from 28-30%.

It can be noticed that the model's errors of commission is quite high – the model seemed to have over predicted flooding in some areas around the Marikina River and its tributaries. This is partly due to overestimation of flow by the model. Aside from this, the high commission errors may have also been contributed by the failure to completely map flood inundation extents due to bank overflows in the SAR images. It is highly possible that there were flooded areas that were undetected in the SAR images due to presence of built-ups which may have contaminated the backscattering signals of flooded areas. Another major reason is that the SAR images appeared to have low sensitivity in depicting areas with low levels of flooding. As low levels of flooding were undetected, this will not be portrayed in the final "observed" flood extent map. On the other hand, the HEC RAS simulated flood extent portrays flooding with depths ranging from 0.01 m to more than 1.5 meters. Because the simulated flood extent includes both low and high levels of flooding, comparing it with flood extents derived from the SAR images will result to high commission errors because low levels of flooding are absent in the observed flood extent map. Another reason for the high commission error is related to how the simulated flood extents were generated. In generating simulated flood extents based on water profiles computed by HEC RAS, the DEM used is

"bare earth" and the presence of structures were not considered – this may have increased the flooded areas.

The difference in river and flood plain geometries may be another reason for high commission errors as well as high omission errors. The geometry of the rivers was based on field surveys conducted in 2011-2012, and this was assumed to be the same geometry when the *September 2009 Ondoy* flooding events were simulated. Sedimentation and erosion in the river due to flooding events prior to 2011 and 2012 may have increase the bed elevation (and hence decreased the depth of the rivers) in some portions while decreasing the bed elevations in other areas. In areas where sedimentation occurred, it could be expected that for the *Ondoy* flood event, the model will produce higher water surface elevations that may have increased the simulated flood extent leading to commission errors. In areas where bed elevations had decreased, it could be expected that the model will simulate a lesser extent of flooding in those portions leading to omission errors.

Although the measures of accuracy indicate relatively good model performance in predicting flood extents, further validation is necessary through conduct of in-situ measurements of depth and extent during flooding events.

Chapter Summary and Conclusions

This chapter presented the development of the flood model of Marikina River consisting of HEC HMS and HEC RAS. Based on the results of independent validations using observed data at MONTALBAN and STO. NINO stations, it was shown that the HEC HMS model has more than satisfactory performance in simulating discharge due to rainfall events. Its coefficient of model efficiency E ranges from 0.77 to 0.88. On the other hand, the results of the comparison of the simulated water levels with observed data indicates that the use of the calibrated HEC HMS model to simulate discharge and converting this discharge into water levels using rating curves provides a fast and relatively accurate way of forecasting water levels at MONTALBAN and STO. NINO stations. The average water level errors are relatively low, while the RMS errors indicate sub-meter accuracy of the predicted water levels. The HEC HMS model was also found to simulated peak flows ahead of the observed peaks flows by 40 minutes to 1 hours and 10 minutes.

For flood inundation mapping, the combined HEC HMS-HEC RAS models can predict flood extent during rainfall with accuracy ranging from 64-79%, which is relatively good and comparable to results of other studies (e.g., [24]).

With these results, the flood model can be utilized for water level forecasting, reconstruction of actual flood events, and for simulation of flooding due to hypothetical and extreme rainfall events.

Chapter 6. Reconstruction and Analysis of Recent Flood Events in Marikina River Using Combined HEC HMS-HEC RAS Modeling

Overview

In this chapter, the calibrated and validated flood model was utilized to reconstruct and analyze actual flood events in Marikina River. The reconstruction involves generation of discharge hydrographs necessary to analyze peak flows and time of peaks at different locations along Marikina River which are important information for preparedness and evacuation. The generation of maximum flood depth maps – which show all areas that have been flooded due to bank overflows during the flood events - is also part of the flood reconstruction. From the flood depth maps, hazard maps were then generated.

The *September 2009 Ondoy* Flood Event

Figure 105 shows the time series of hydrographs simulated by the calibrated HEC HMS model at different locations along Marikina River: Wawa, Montalban, Nangka, Tumana, Sto. Nino and Rosario JS. The simulation period was from 10:00 AM September 14, 2009 to 12:00 AM September 28, 2009. This was done to account for the effects of rainfall prior to the *Ondoy* event.

Based on rainfall data recorded at UP Diliman, continuous and heavy rainfall event started to occur around 5:20 PM of September 25, 2009. Peak rainfall rate was at 19.4 mm/10-minute which is equivalent to 116.4 mm/hour, and this occurred on 10:40 AM of September 26. During this time, the total accumulated rainfall was at 190.4 mm, with average intensity of 2.7 mm/10-minute or 16.12 mm/hour. The event lasted for 29 hours and 40 minutes, with the last burst of rainfall ending at around 11:00 PM of September 26. The total accumulated rainfall during this period is 480.8 mm.
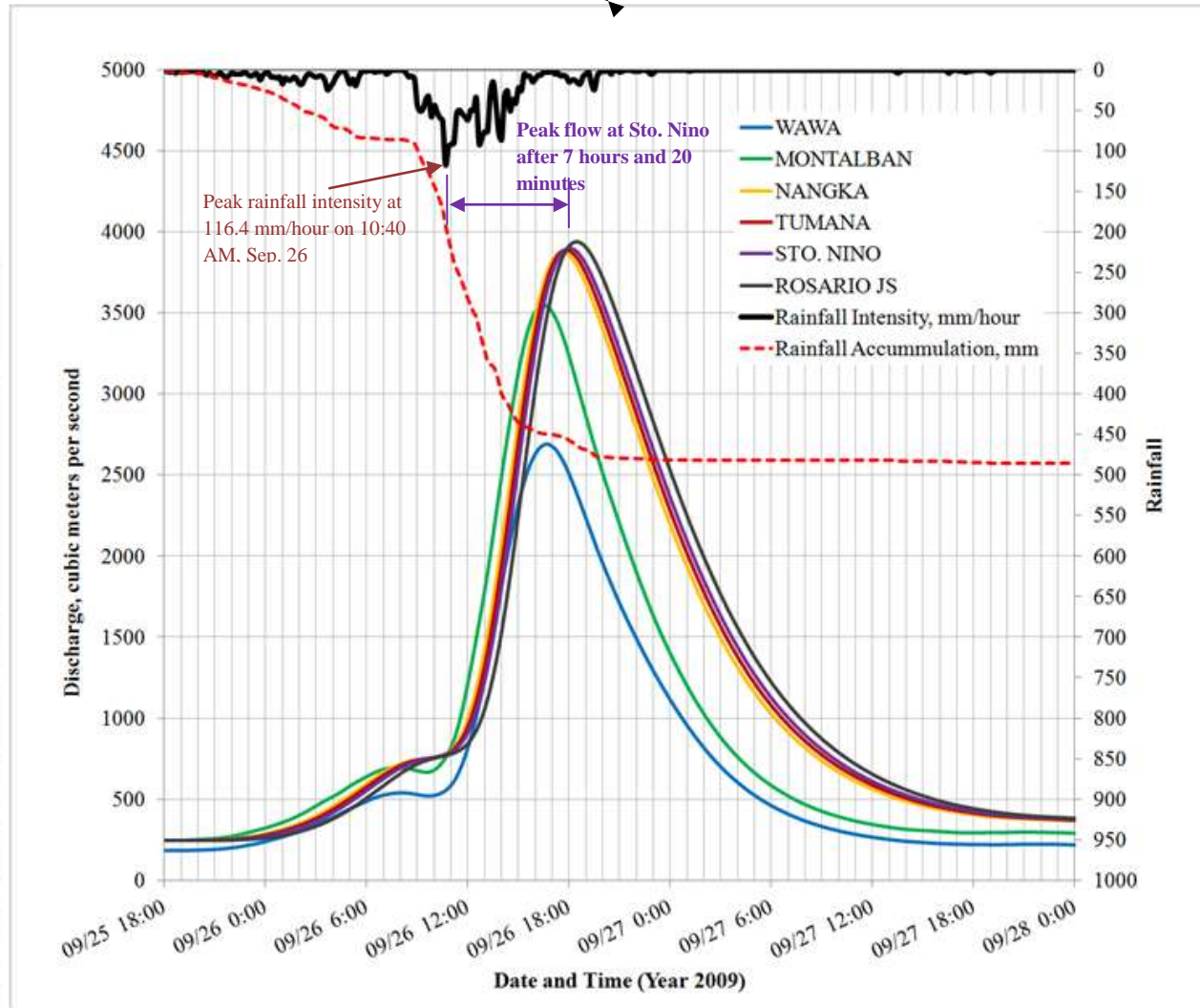
Figure 105. Hydrographs of the *September 2009 Ondoy* Flood Event simulated by the calibrated HEC HMS model at six locations along Marikina River.

Analysis of Simulated Hydrographs: peak rainfall, peak flows

Table 38 shows how much time it took for the flows at the six locations to reach their peaks after the rainfall intensity peaked at 116.4 mm/hour and when the accumulated rainfall depth was already 190.4 mm.

At Wawa, a peak flow of 2,694.6 m^3/s was reached in 6 hour. In Montalban, it only takes 5 hours and 50 minutes to achieve a peak flow of 3,549 m^3/s. In Nangka, peak flow of 3,877.4 m3/s was reached after 7 hours. Ten minutes after this, peak flow reached to 3,891.2 m^3/s in Tumana.

In Sto. Nino, peak flow was attained 7 hours and 20 minutes after peak of rainfall intensity. After this, it took another 30 minutes for flows to peak at Rosario JS.

It can be noticed that peak flow was earlier in Montalban than in Wawa by 10 minutes. This is due to additional contribution of watersheds upstream of the station other than those watersheds upstream of Wawa.

Between stations, the time difference between peak flows is very minimal. For example, the difference in times of peak between Montalban and Sto. Nino is only 1 hour and 30 minutes. Using Montalban station as a basis for evacuation preparation is therefore not a good option during this kind of extreme rainfall events. When peak flow has been reached at Montalban station, there is so little time for evacuation in areas near the Sto. Nino station.

Table 38. Peak flows at different locations along Marikina River during the *Ondoy* flood event as simulated by the calibrated HEC HMS model.

Location	Peak Flow, m^3/s	Time of Peak	No. of Hours after the peak of rainfall intensity at 10:40 AM of September 26
Wawa	2,694.6	26SEP2009, 16:40	6:00
Montalban	3,549.0	26SEP2009, 16:30	5:50
Nangka	3,877.4	26SEP2009, 17:40	7:00
Tumana	3,891.2	26SEP2009, 17:50	7:10
Sto. Nino	3,900.9	26SEP2009, 18:00	7:20
Rosario JS	3,940.3	26SEP2009, 18:30	7:50

The results of this simple analysis show potential of the calibrated HEC HMS model as an early warning system during extreme flood events. Should an extreme rainfall event with intensity similar to that of the *Ondoy* event occurred again, the information presented in Table 38 would imply that there is a lag time of at least 5 to 7 hours before the effect of the extreme rainfall event is felt downstream. This number of hours can be utilized to prepare for evacuation provided that the peak intensity is known together with the accumulated rainfall.

Simulated Changes in Water Levels for Early Flood Warning during an *Ondoy* like event

In terms of changes in water levels, the HEC HMS model (together with rating curves) was able to simulate how water level will increase at the start of the extreme rainfall event like *Ondoy* (Sep. 25, 5:20 PM). In Montalban, water level was simulated to increase by 4.02 meters in 11 hours and 10 minutes after the start of rainfall. In Sto. Nino, the increase in water level is very large, reaching 8.44 meters in 12 hours and 40 minutes. In both stations, the increase in water levels is gradual before the time of peak of rainfall intensity. After the rainfall peak, the increase in water levels was found to be relatively rapid.
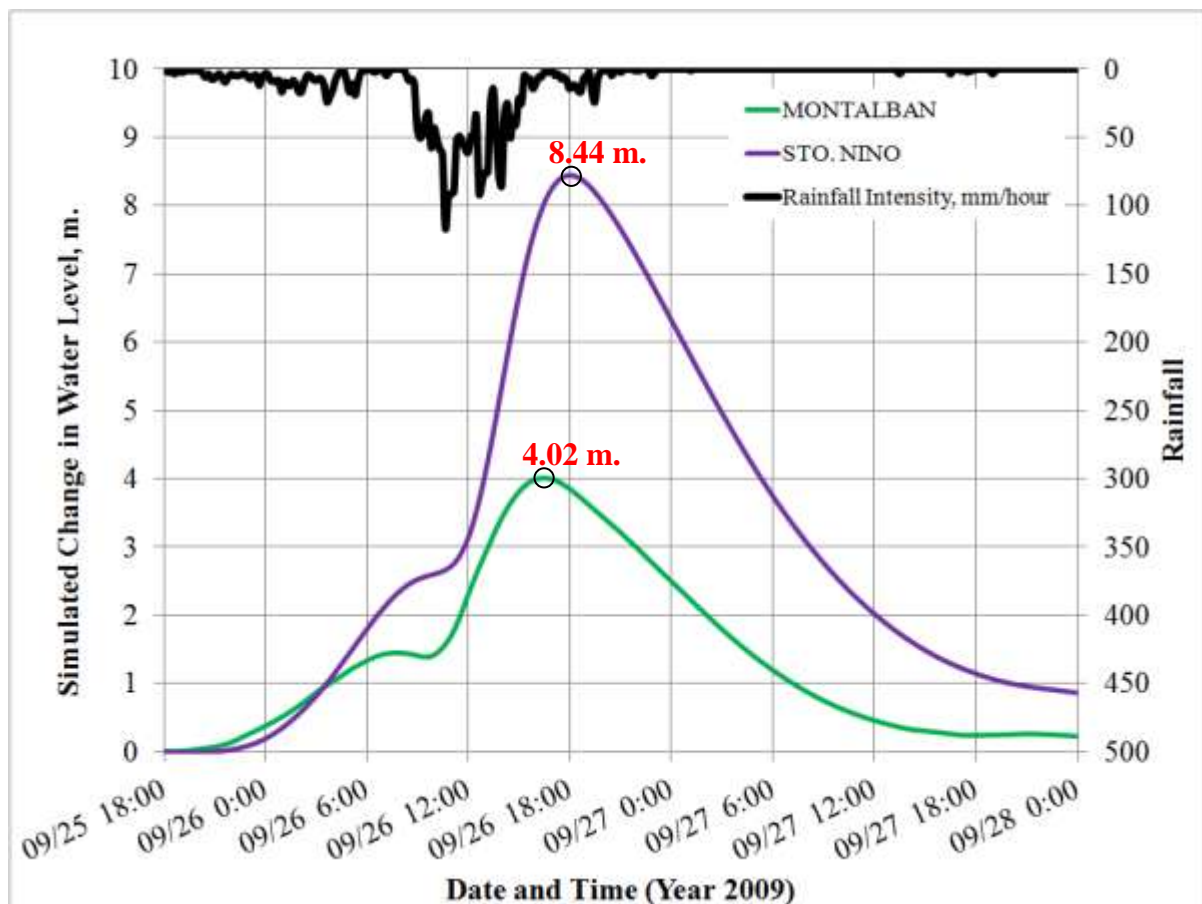
Figure 106. HEC HMS model simulated increase in water levels at Montalban and Sto. Nino Stations from the start of the *Ondoy* extreme rainfall event.

The simulated changes in water levels could also be used determine how much time it will take to reach levels of flood warnings along Marikina River. According to the Project NOAH website (noah.dost.gov.ph), the Marikina City Council (http://syncsysph.com/councilmarikinagovph/data/riverlevel.html) uses its own system in warning its residents. When the water level of the Marikina River reaches 15 meters, residents living in low-lying areas beside the river are warned of impending danger. At 16 meters, residents are asked to prepare to evacuate. When the level of the Marikina River reaches 17 meters, people are asked to evacuate. Those that do not follow these instructions

are forced to leave when the water level reaches 18 meters. All warning levels of the Marikina City Council are based on measurements and reports from the Sto. Nino station. The datum of the water levels mentioned is based on a datum used by the DPWH which is approximately 10.60 meters above the Mean Sea Level according to the 1999 EFCOS Feasibility study.

Using the simulated changes in water level at Sto. Nino station, issuance of flood warnings can be made feasible by getting the current water level at Sto. Nino and then adding to it the simulated changes in water level. As an example, let the water level at Sto. Nino be at 12 meters during the start of an *Ondoy*-like rainfall event. By adding the simulated change in water level, it can be computed that from the start of rainfall, water level will reach a "warning" level (15 m) in 1 hour, "evacuation preparation" (16 m) in 2 hours and 20 minutes, "voluntary evacuation" (17 m) in 3 hours, and "forced evacuation" (18 m) in 3 hours and 50 minutes. This is illustrated in Figure 107. The time interval between warning and forced evacuation is only 2 hours and 50 minutes which is may be limited for complete evacuation during an *Ondoy*-like event. The simulated result is also helpful in estimating the time it needs for water levels to recede below the warning level which can be used as indicator for safe return of those that has been evacuated.
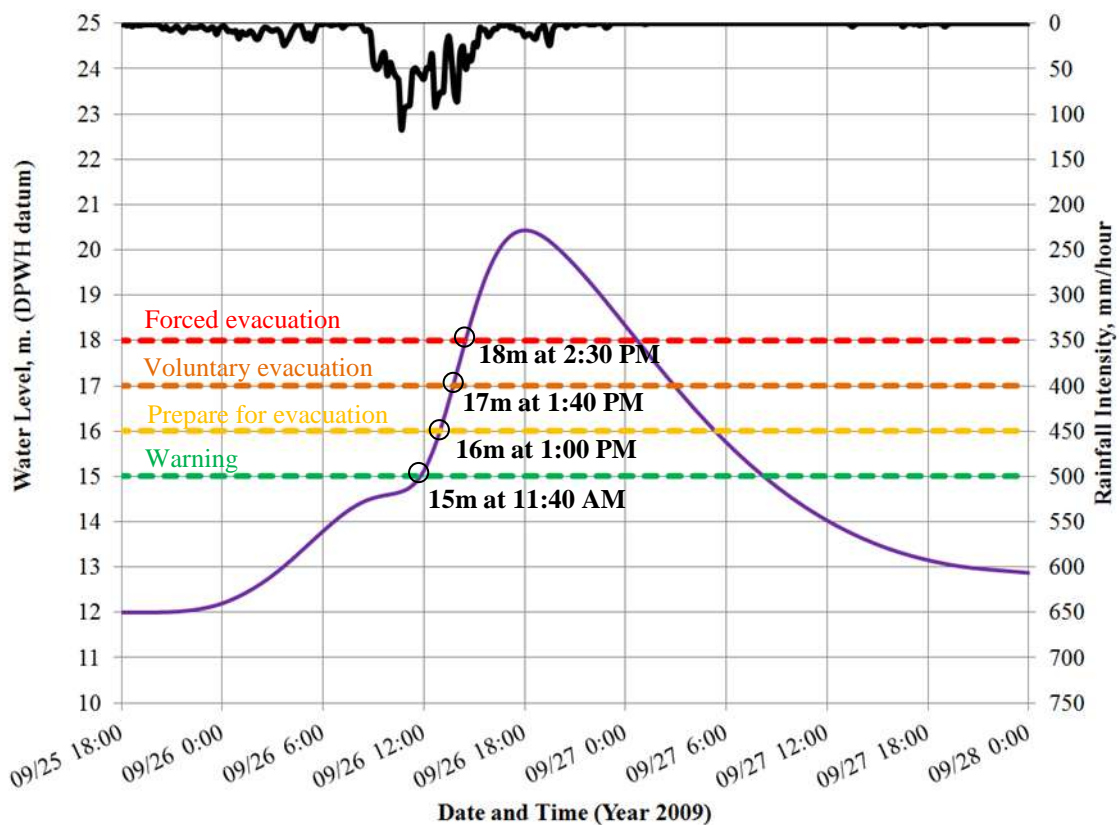

Figure 107. Illustration of using the HEC-HMS simulated change in water levels at Sto. Nino station for early issuance of flood warning. In this example, it was assumed that the starting water level is at 12 meters.

Mapping Maximum Flood Depths and Flood Hazards of Recent Flood Events

Another major purpose of the combined HEC HMS – HEC RAS flood model is for generation of maximum flood depth maps and flood hazard maps for actual flood events. These flood events are the September 2009 Typhoon *Ondoy*, the September 2011 Typhoon *Pedring*, and the August 2012 *Habagat* (Table 39). The simulated hydrographs at specific locations along Marikina River are shown in Figure 105 (for *Ondoy*), Figure 108 (for *Pedring*), and Figure 109 (for *Habagat 2012*). The summary of peak flows simulated by the model are listed in Table 40. It can be noticed that the *Ondoy* 2009 event is approximately more than twice in magnitude of the *Habagat* 2012 flood event based on peak flows.

Peak flows at the boundary condition locations and peak water level at the outlet (Rosario JS) were extracted from the simulated hydrographs to generate maximum flood depth map using HEC RAS. The maximum flood depth map shows all areas that have been flooded during the duration of the flood event. To create flood hazard maps, the flood depths are categorized into low: less than 0.5 m depth; medium: greater than or equal to 0.5 m but less than or equal to 1.5 m.; high: greater than to 1.5 m. The flood depth and hazard maps are shown in Figure 110 to Figure 115. The summary of maximum flood depths and total flooded areas are shown in Table 41. It should be noted that the flood depth and hazards shown are due to bank overflows. Flooding due to water accumulation due to clogged drainage or natural ponding were not simulated as HEC RAS does not have the capability to simulate this kinds of processes.

Table 39. List of actual flood events simulated using combined HEC HMS-HEC RAS to generate maximum flood depth and flood hazard maps.

| Flood Event	Duration of Rainfall Event	Peak Rainfall Intensity	Total accumulated rainfall	Rainfall Stations Used in HEC HMS simulation
September 2009 Typhoon *Ondoy*	5:20 PM September 25 to 11:00 PM September 26, 2009 (29 hours and 40 minutes	116.4 mm/hour (10:40 AM, September 26)	480 mm	Melchor Hall, College of Engineering, UP Diliman
September 2011 Typhoon *Pedring*	12:00 AM September 26 to 12:00 AM September 28, 2011 (3 days)	90 mm/hour at MT. ORO (1:00 PM, September 27)	217 mm at MT. ORO	MT. ORO, MT. ARIES, BOSO-BOSO, NANGKA
August 2012 *Habagat*	12:00 AM August 5 to 12:00 AM August 13, 2012 (8 days)	96 mm/hour at MT. ORO	999 mm at MT. ORO	MT. ORO, MT. ARIES, BOSO-BOSO, NANGKA
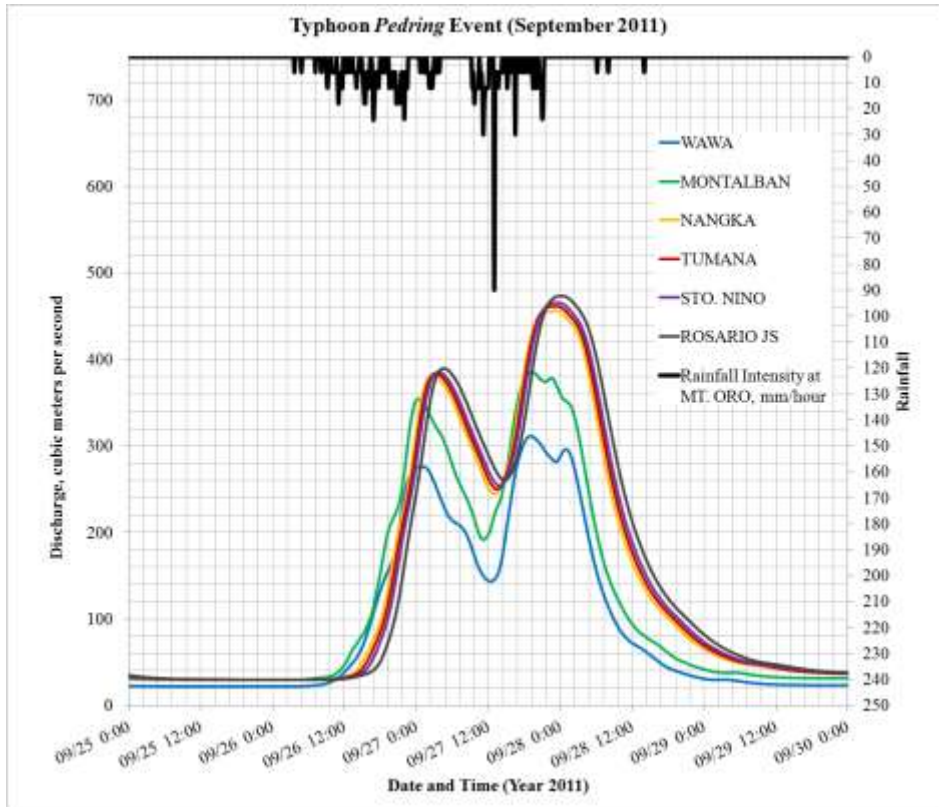
Figure 108. Hydrographs of the *September 2011 Pedring* Flood Event simulated by the calibrated HEC HMS model at six locations along Marikina River.
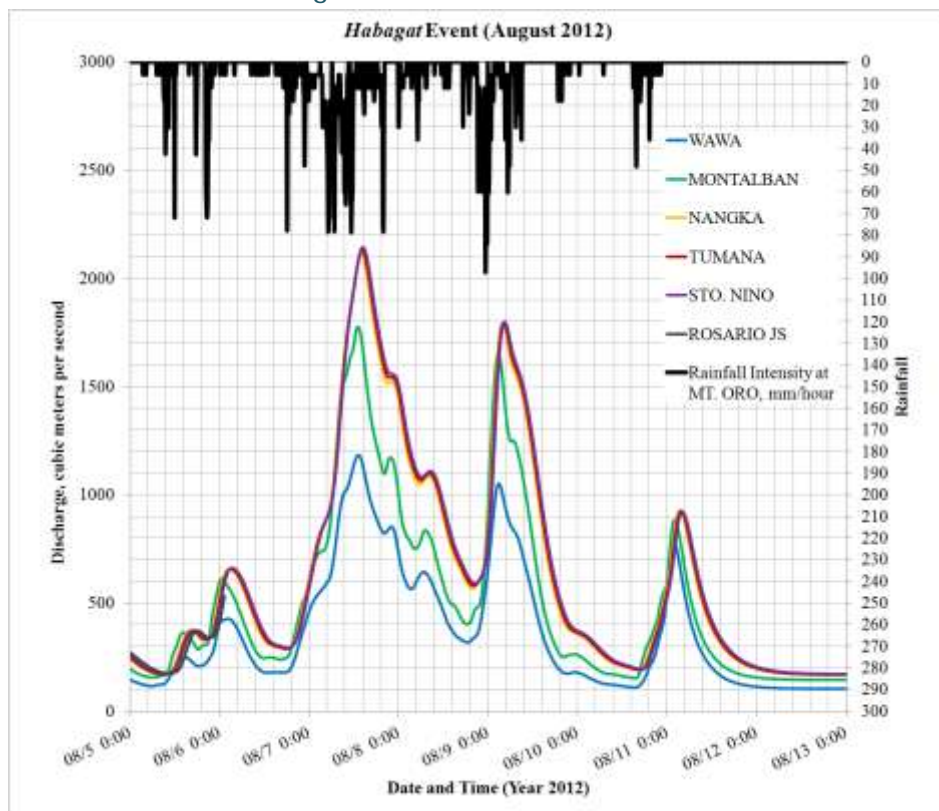

Figure 109. Hydrographs of the *August 2012 Habagat* Flood Event simulated by the calibrated HEC HMS model at six locations along Marikina River.

Table 40. Summary of peak flows at six locations along Marikina River for the three actual flood events.

Location	Simulated Peak Flows, m³/s		
	September 2009 *Ondoy*	September 2011 *Pedring*	August 2012 *Habagat*
Wawa	2,694.6	311.9	1,182.2
Montalban	3,549.0	385.7	1,776.5
Nangka	3,877.4	456.3	2,111.3
Tumana	3,891.2	461.6	2,130.2
Sto. Nino	3,900.9	465.8	2,145.0
Rosario JS	3,940.3	473.3	2,170.9

Table 41. Summary of maximum flood depths and total flooded areas for the three actual flood events.

Flood Event	Maximum Flood Depth, m.	Total Flooded Areas, km²		
		Low Hazard (< 0.5 m depth)	Medium Hazard ($0.5 \leq$ depth $\leq$ 1.5 m)	High Hazard (depth > 1.5 m)
September 2009 *Ondoy*	17.16	2.842	5.116	18.428
September 2011 *Pedring*	11.12	1.345	2.028	3.233
August 2012 *Habagat*	14.13	1.346	2.862	9.272
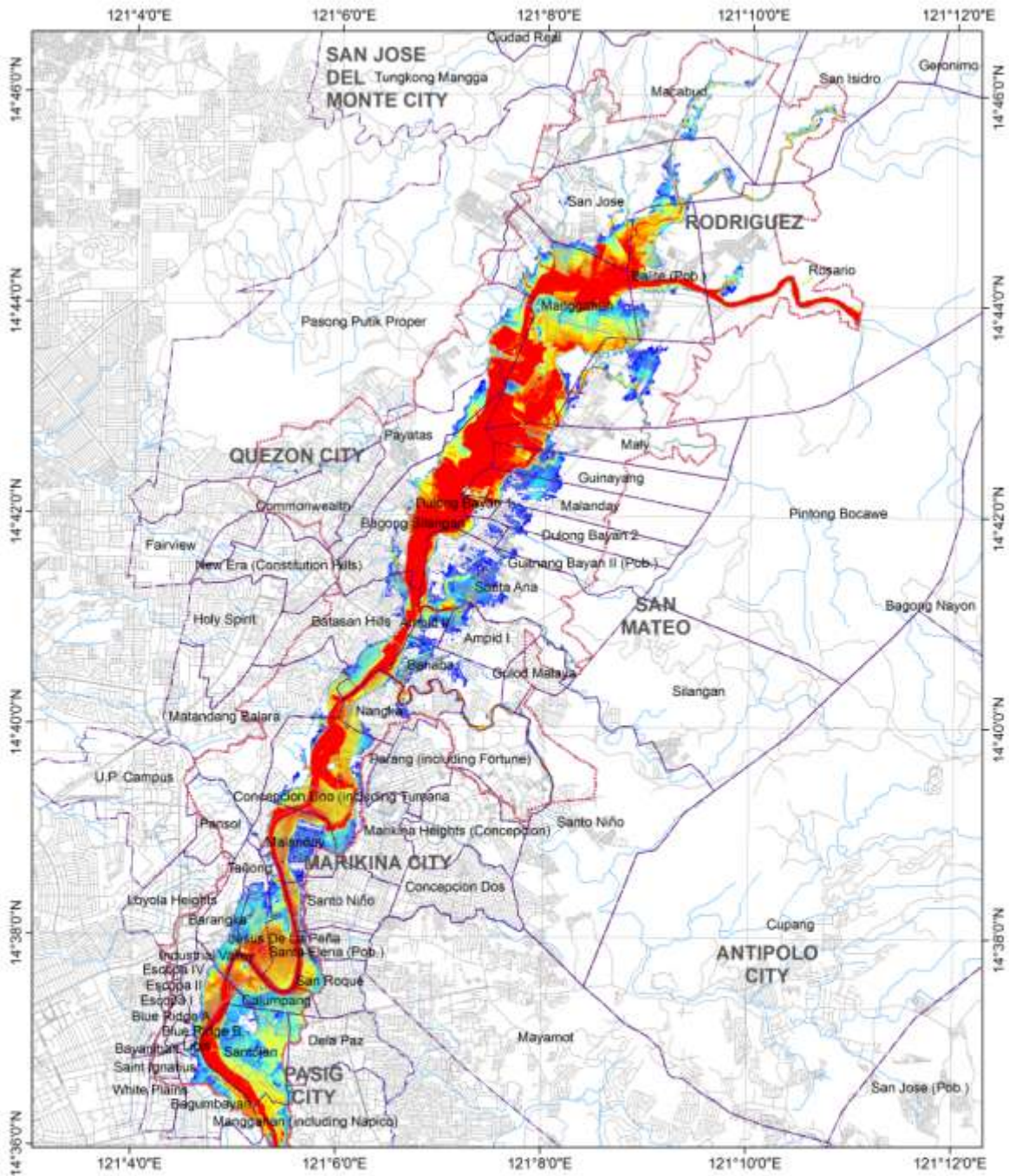
MARIKINA RIVER TYPHOON "ONDOY" FLOOD DEPTH MAP

Model Simulated Maximum Flood Depth and Extent due to Bank Overflows during Typhoon Ondoy, September 2009

Flood Depth, in m.

0.01 - 0.25	0.76 - 1.00	1.51 - 1.75
0.26 - 0.50	1.01 - 1.25	1.76 - 2.00
0.51 - 0.75	1.26 - 1.50	2.01 - 2.50

2.51 - 3.00	4.01 - 4.50
3.01 - 3.50	4.51 - 5.00
3.51 - 4.00	>5.01

Model Domain   Barangay Boundaries   — Roads

Figure 110. Model simulated maximum flood depth map for the September 2009 *Ondoy* event.

156
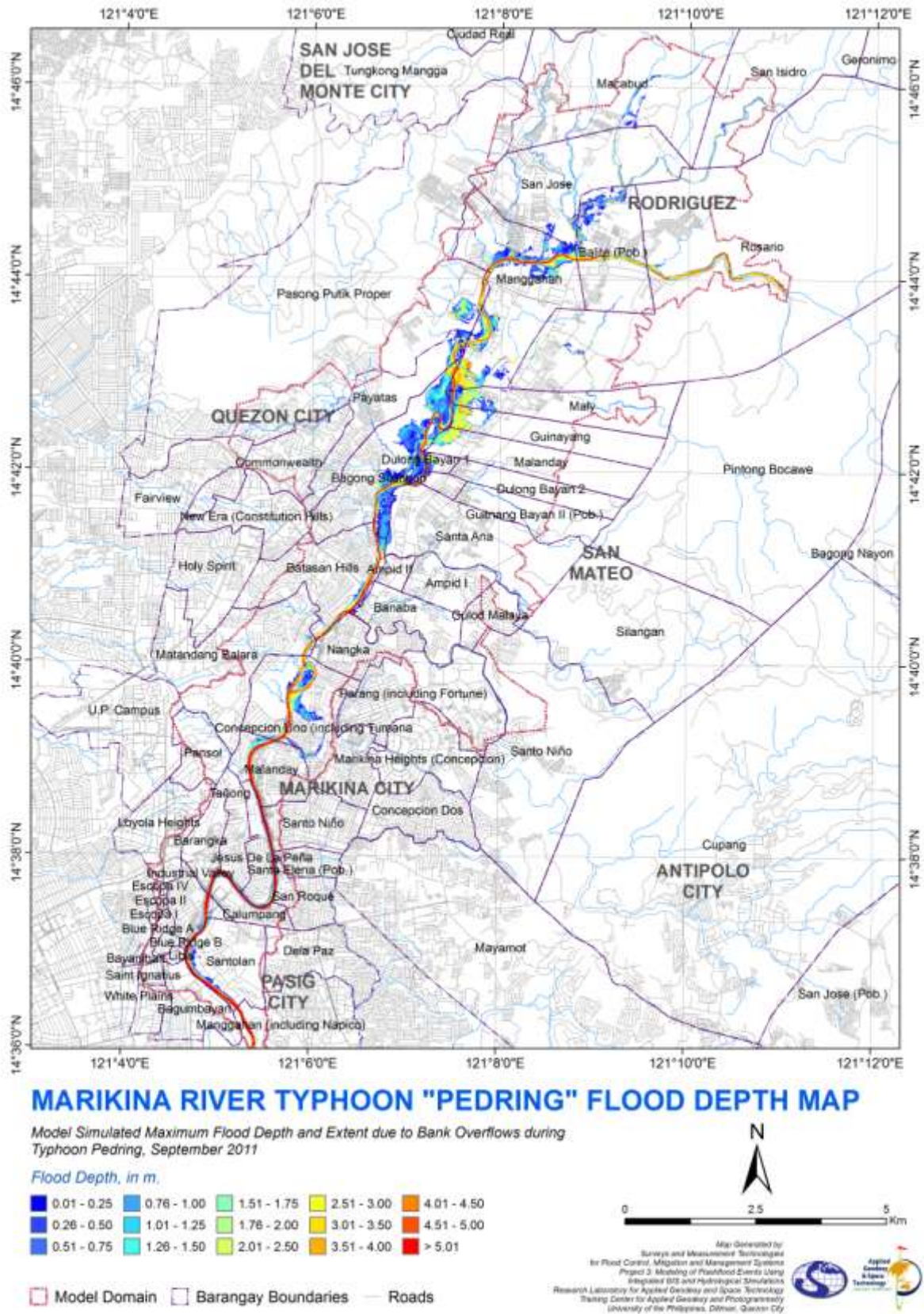
Figure 111. Model simulated maximum flood depth map for the September 2011 *Pedring* event.

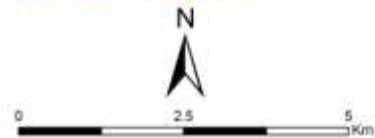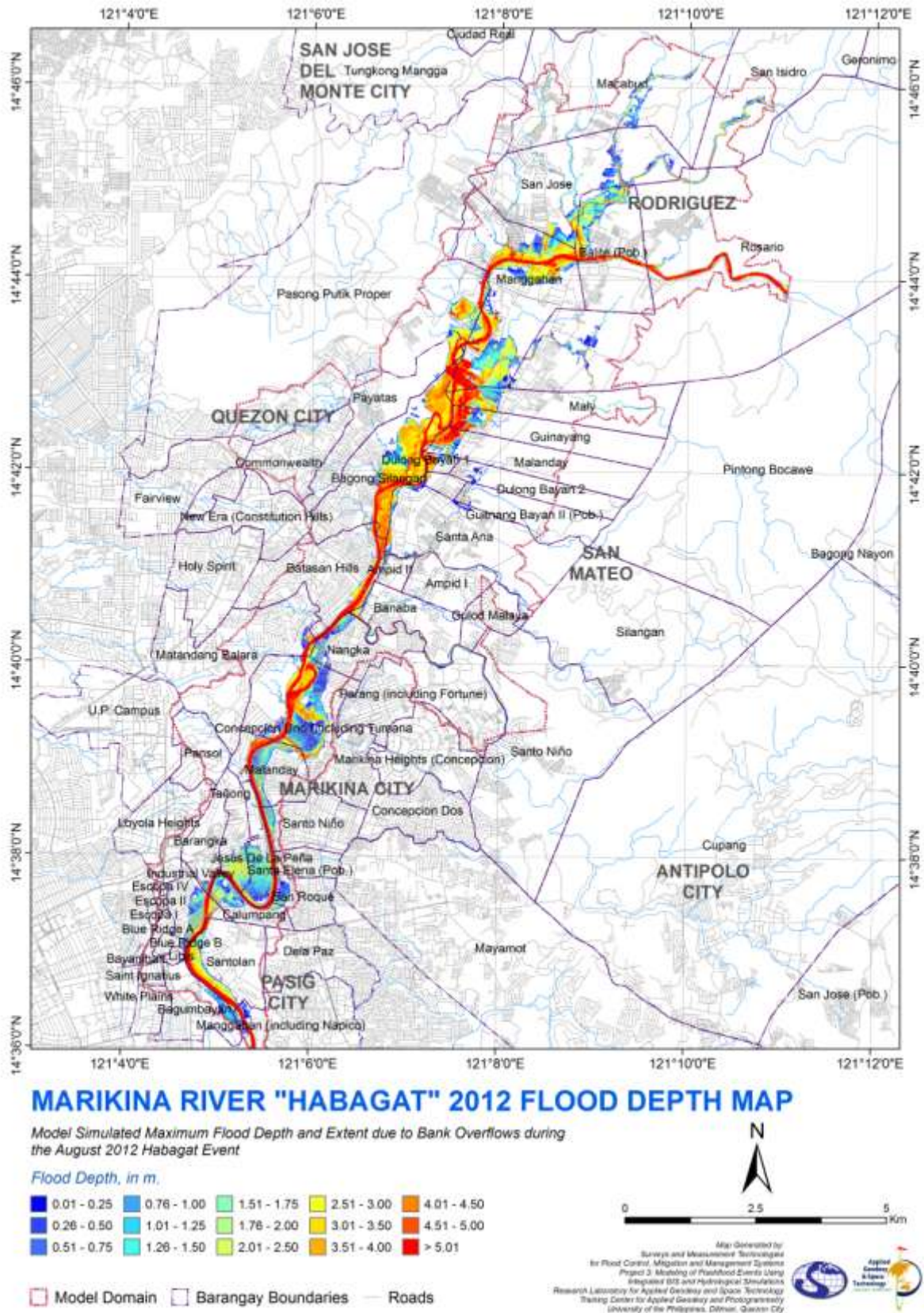Figure 112. Model simulated maximum flood depth map for the August 2012 *Habagat* event.
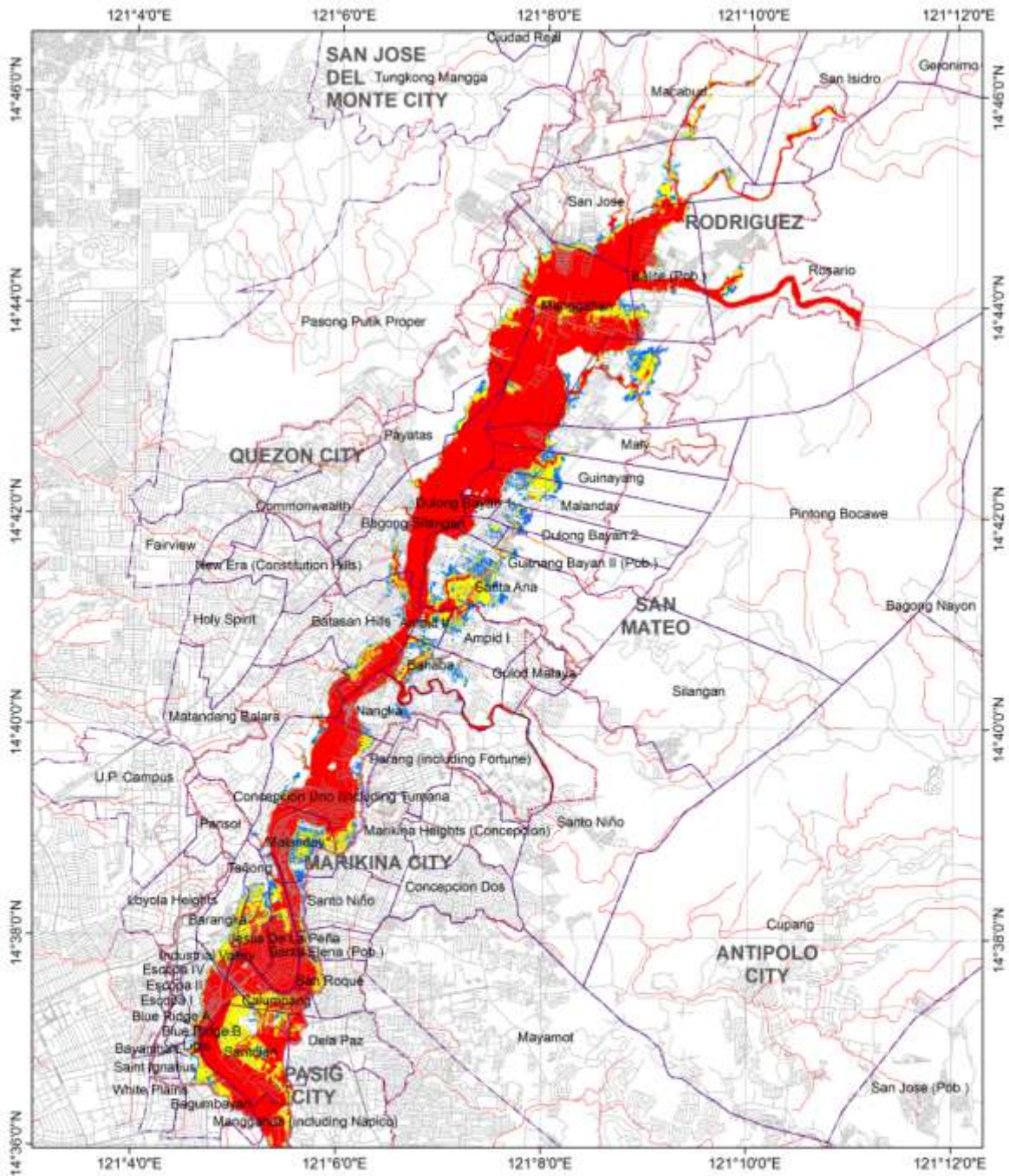
MARIKINA RIVER TYPHOON "ONDOY" FLOOD HAZARD MAP

Model Simulated Flood Hazard due to Bank Overflows during Typhoon Ondoy, September 2009

Hazard Type:

Low   Medium   High

Explanation:
Low hazard: Flood depth is less than 0.5 m.
Medium hazard: Flood depth is from 0.5 to 1.5 m.
High hazard: Flood depth is greater than 1.5 m.

Model Domain   Barangay Boundaries   Roads

Figure 113. Flood hazard map for the September 2009 *Ondoy* event.

159

MARIKINA RIVER TYPHOON "PEDRING" FLOOD HAZARD MAP

Model Simulated Flood Hazard due to Bank Overflows during
Typhoon Pedring, September 2011

Hazard Type:

Low   Medium   High

Explanation:
Low hazard: Flood depth is less than 0.5 m.
Medium hazard: Flood depth is from 0.5 to 1.5 m.
High hazard: Flood depth is greater than 1.5 m.

Model Domain   Barangay Boundaries   Roads

Figure 114. Flood hazard map for the September 2011 *Pedring* event.

Figure 115. Flood hazard map for the August 2012 *Habagat* event.

Chapter Summary and Conclusion

In this chapter, discharge hydrographs and maps of depths and hazards were generated for the *Ondoy* 2009, *Pedring* 2012 and *Habagat* 2012 flood events through the use of the calibrated and validated HEC HMS and HEC RAS models. The flood depth and flood hazard maps show the magnitude and extent of flooding due to bank overflows. Should similar flood events occur again in the future, the flood hazard maps would provide important information for preparation, evacuation, and damage estimation.

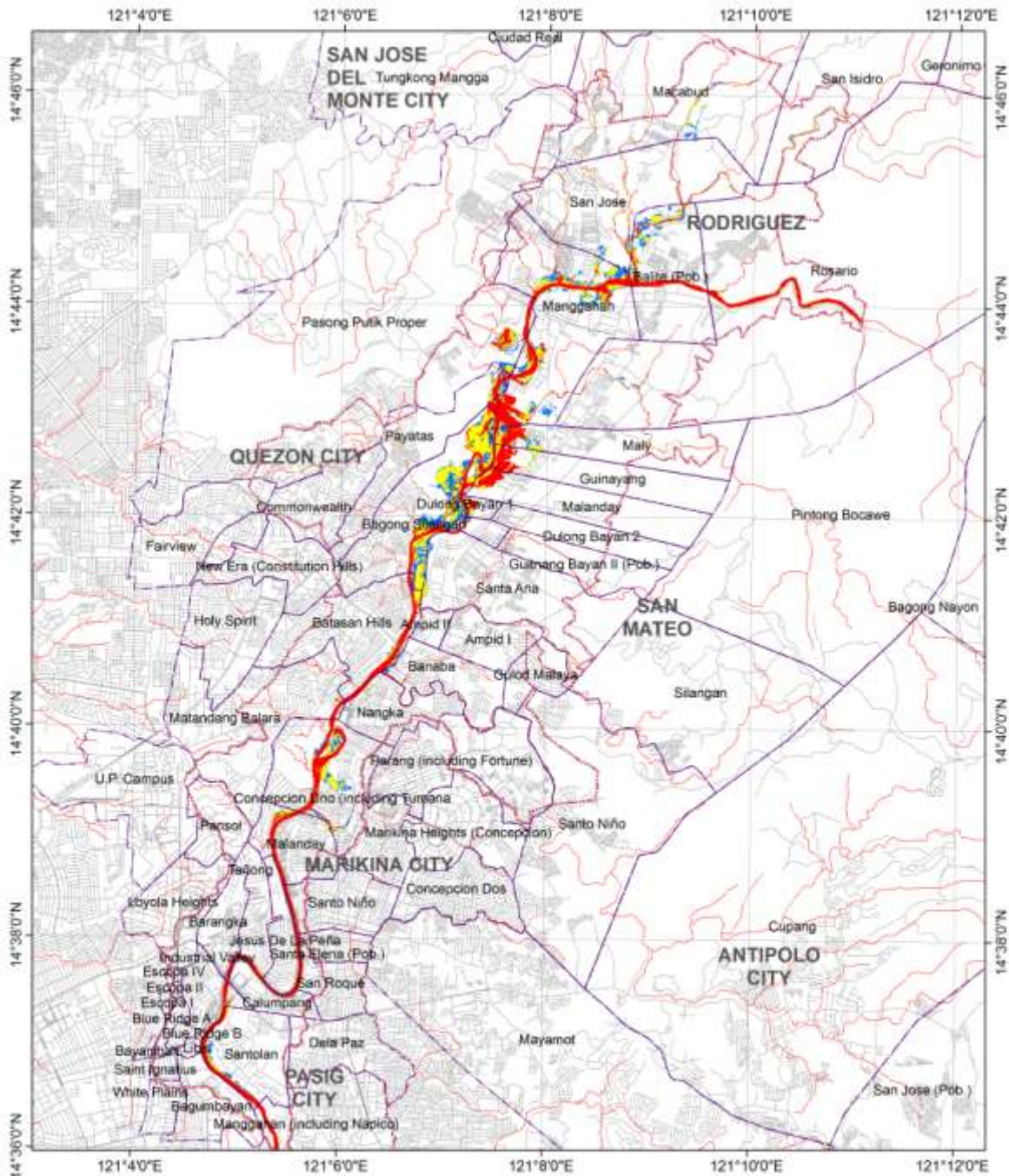One of the important findings presented in this chapter is the results of the simple analysis on the potential of the calibrated HEC HMS model as an early warning system during extreme flood events. It was shown that should an extreme rainfall event with intensity similar to that of the *Ondoy* event occurred again, there is a lag time of at least 5 to 7 hours before the effect of the extreme rainfall event is felt downstream areas such as Wawa, Montalban, Nangka, Tumana, Sto. Nino and Rosario JS. This number of hours can be utilized to prepare for evacuation provided that the peak intensity is known together with the accumulated rainfall.

Chapter 7. Modeling and Mapping Flood Hazards Due to Hypothetical, Extreme Rainfall Events in Marikina River

In this chapter, the methodology employed in the previous chapter to simulate hydrographs and to generate flood depth and flood hazard maps of actual flood events using the combined HEC HMS and HEC RAS models are utilized to model and map flood hazards due to hypothetical, extreme rainfall events in Marikina River.

The hypothetical, extreme rainfall events were derived by utilizing Rainfall-Intensity Duration Frequency (RIDF) data of the Science Garden rainfall station. The RIDF data was based on 41 years of data provided by the Hydrometeorological Data Applications Section of the Hydro-Meteorology Division of the Philippine Atmospheric, Geophysical and Astronomical Administration (PAGASA). The RIDF data is summarized in Table 42 and plotted in Figure 116.The first two columns (5-minute and 15-minute data) are originally 10-minute and 20-minute data, respectively. The values were revised for compatibility with HEC-HMS. Essentially, the RIDF data provides information on how much rainfall is being accumulated within 24 hours for each event. The lower the return period years, the more frequent and less intense the rainfall event is.

The 24-hour rainfall events derived from the RIDF data and entered in HEC HMS are shown in Figure 117. In deriving the time series of rainfall events, it is possible to place the peak intensity in the first few hours of the event, at the middle, or at the later hours. In this study, the peak intensity was placed at the middle to mimic the rainfall events in Marikina River Basin. The example of this the September 2009 *Ondoy* rainfall (shown previously in Figure 105) where the peak intensity is at approximately at the middle.

Table 42. RIDF data for PAGASA Science Garden Station.

Return Period	Rainfall Depth by Duration, mm.							
	5	15	1	2	3	6	12	24
(yrs)	mins	mins	hr	hrs	hrs	hrs	hrs	hrs
2	9.6	21.5	48.7	70.1	84.2	113.1	131.5	155.0
5	14.0	31.6	75.2	108.1	131.9	183.1	213.1	242.3
10	16.9	38.3	92.8	133.3	163.5	229.5	267.1	300.1
20	19.7	44.7	109.7	157.4	193.8	273.9	318.9	355.5
25	20.6	46.7	115.0	165.0	203.5	288.0	335.3	373.1
50	23.3	53.0	131.5	188.6	233.1	331.5	386.0	427.2
100	26.1	59.3	147.8	212.0	262.5	374.6	436.2	481.0
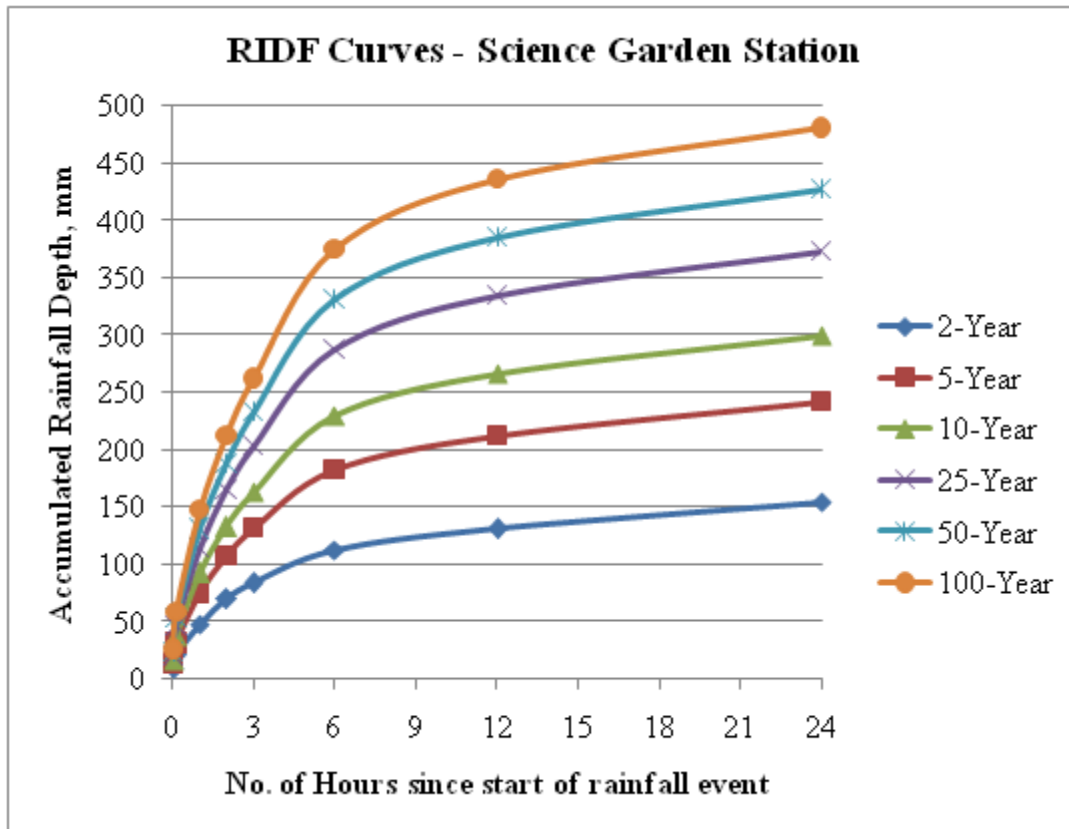
Figure 116. Science Garden Station RIDF curves.
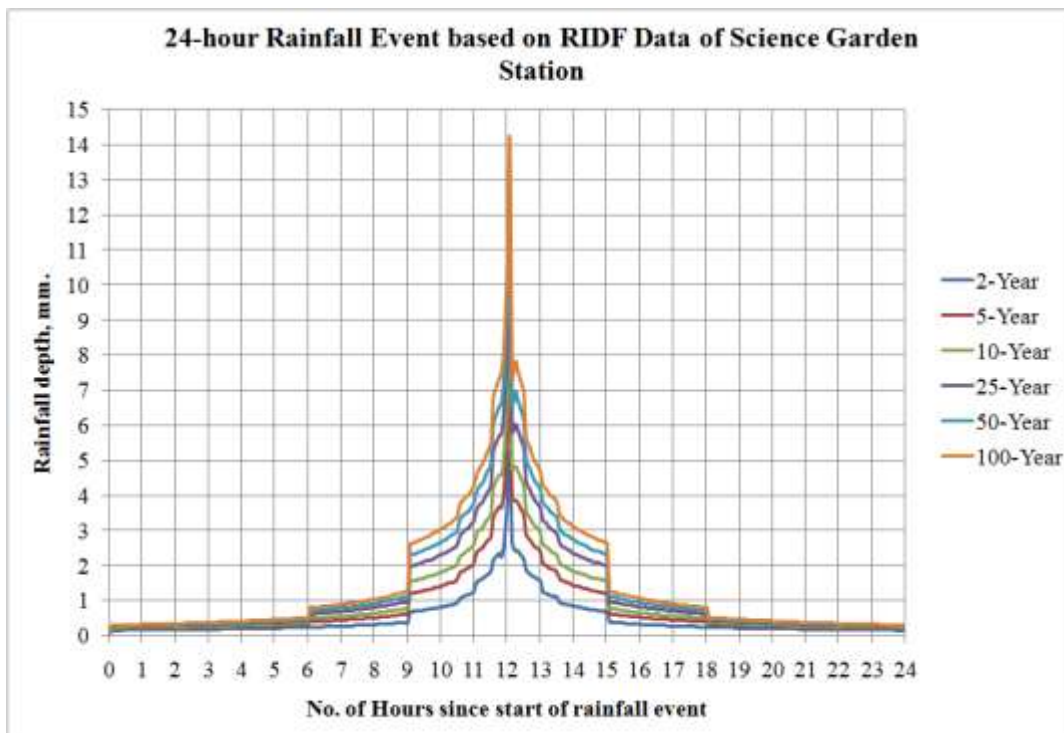
Figure 117. 24-hour duration rainfall events derived from Science Garden RIDF data.

Simulated Flood Maps due to Hypothetical, Extreme Rainfall Events

The flood depth and flood hazard maps of Marikina River according to the rainfall return periods are shown in Figure 142 to Figure 150.

The maps indicate increase in flood affected areas as the return period increases. The areas most affected in all type of events are in the upstream portion of the domain, specifically the barangays of San Mateo, Rizal (e.g., Maiy, Guinayang, Malanday, Dulong Bayan, Gitnang Bayan) and portions of barangays of Quezon City (e.g., Bagong Silangan).

In the downstream where Marikina and Pasig Cities are located, flooding due to 2-year rainfall is found to be not significant. But for rainfall events with return period greater than 2 years, the hazard due to flooding is found to be significant, especially in Nangka, Tumana, Concepcion Uno, Malanday, Sto. Nino, Jesus dela Pena, Santa Elena, Industrial Valley, and Calumpang. All these barangays have medium to high flood hazard levels.

Figure 118. Simulated flood depth map of Marikina River Basin for a 2-year rainfall event.
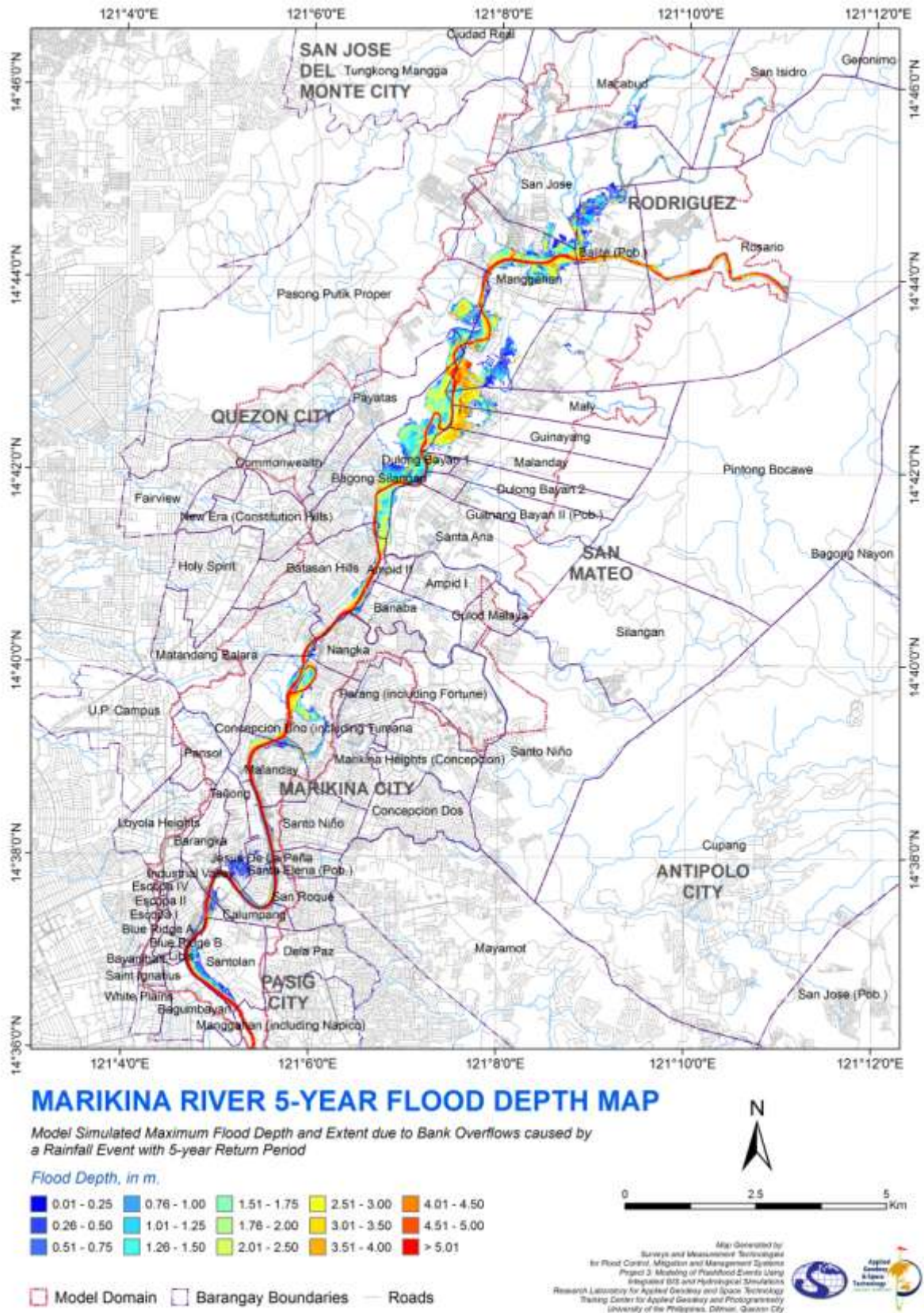
Figure 119. Simulated flood depth map of Marikina River Basin for a 5-year rainfall event.
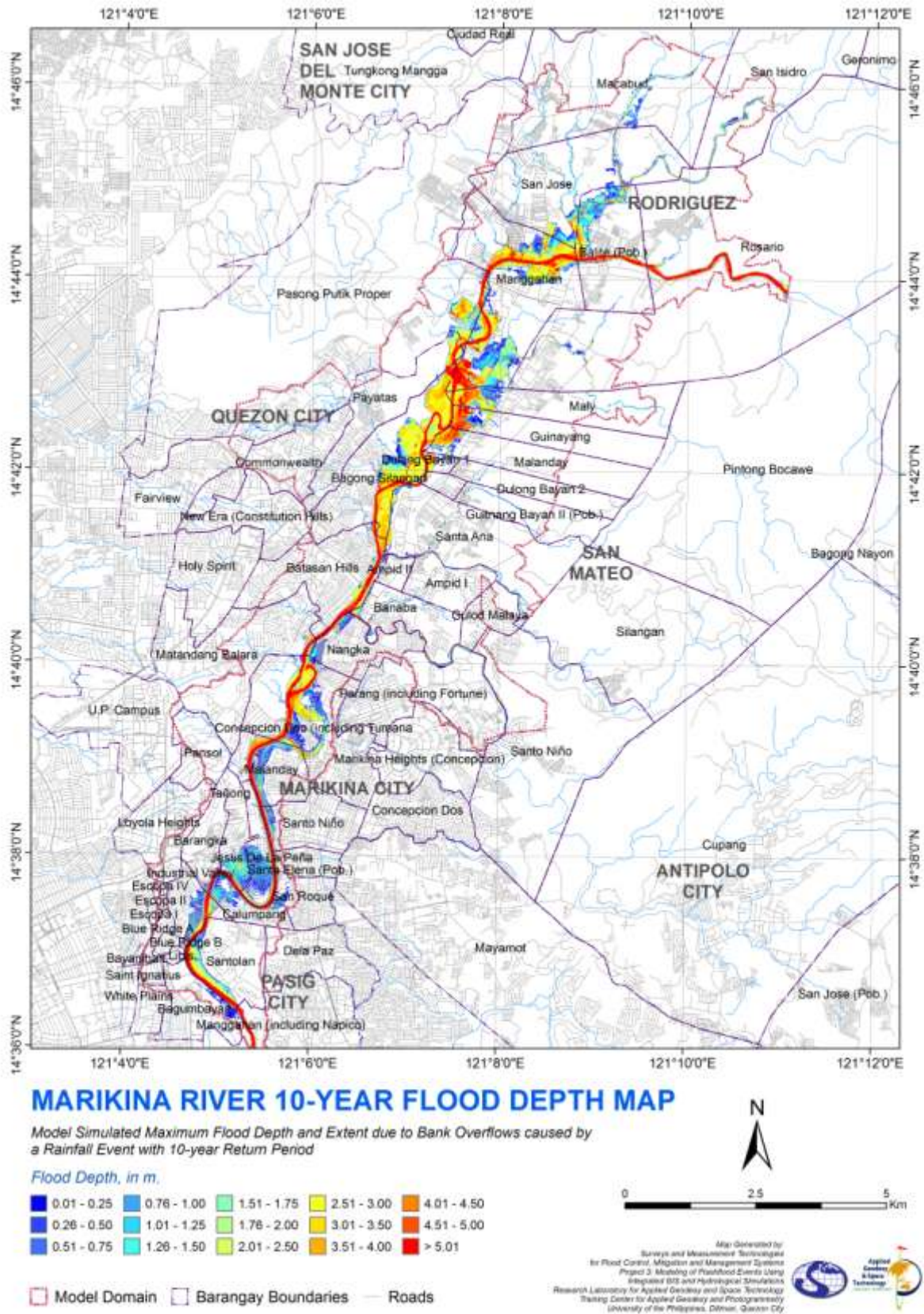
Figure 120. Simulated flood depth map of Marikina River Basin for a 10-year rainfall event.
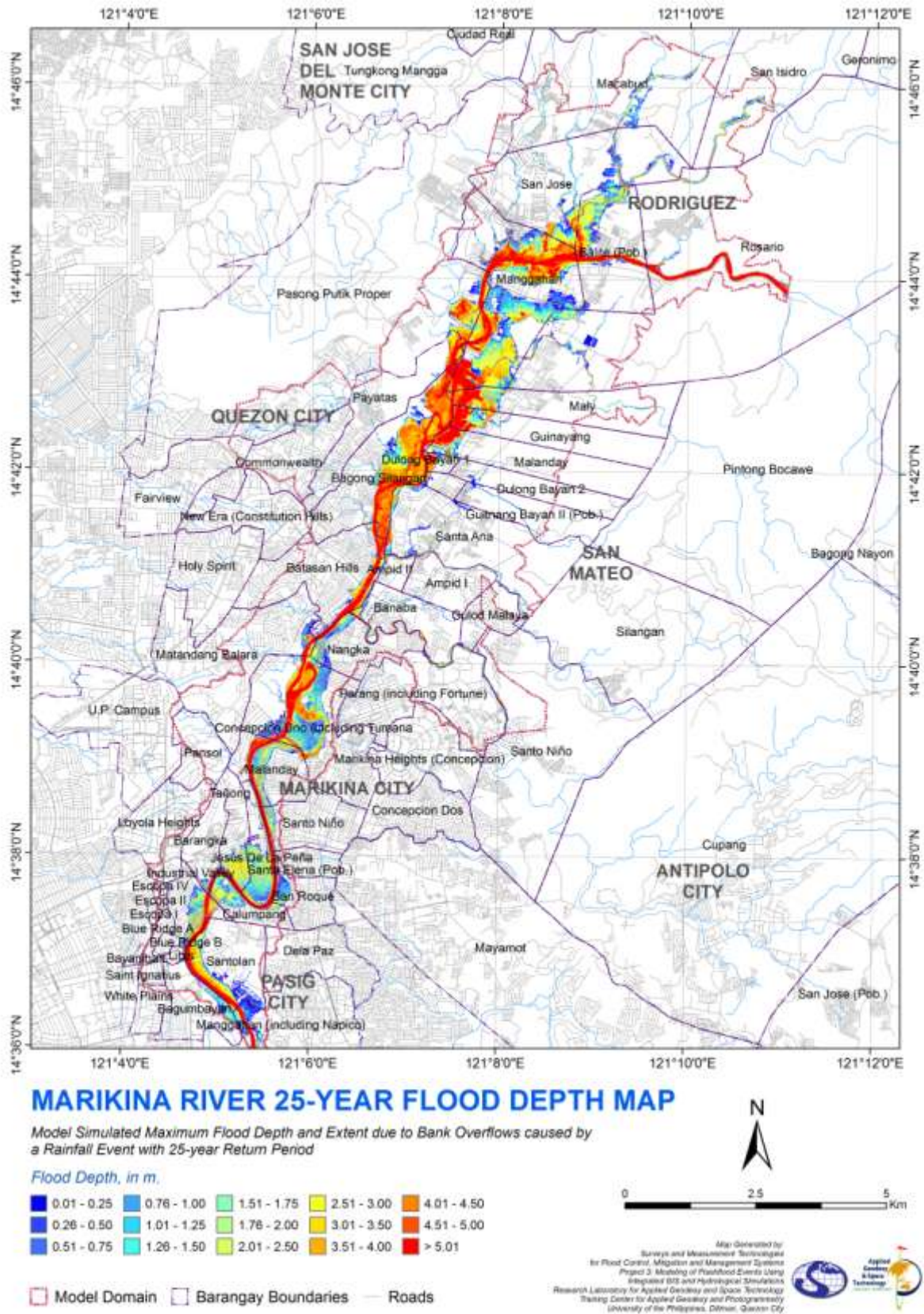
Figure 121. Simulated flood depth map of Marikina River Basin for a 25-year rainfall event.
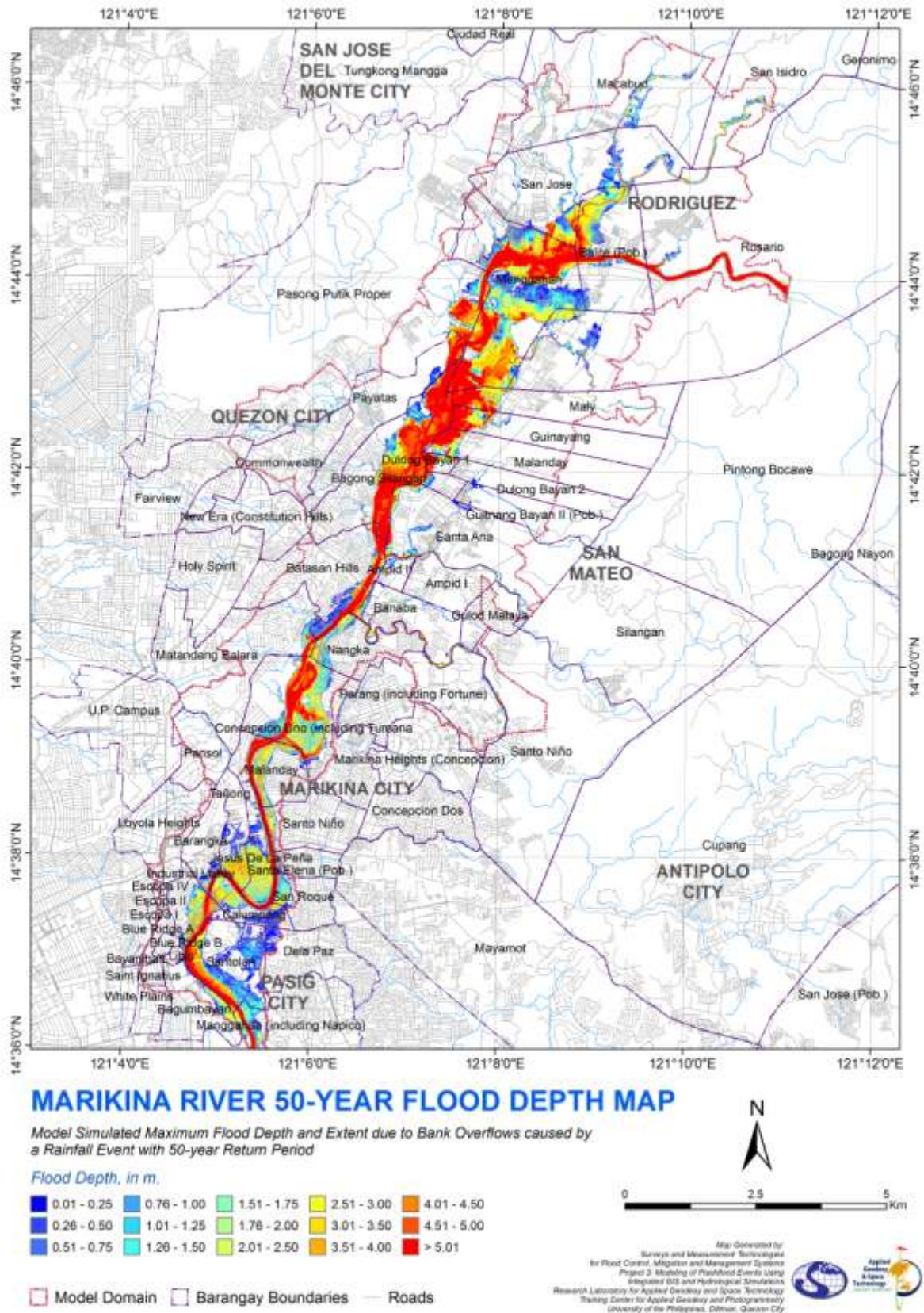
Figure 122. Simulated flood depth map of Marikina River Basin for a 50-year rainfall event.
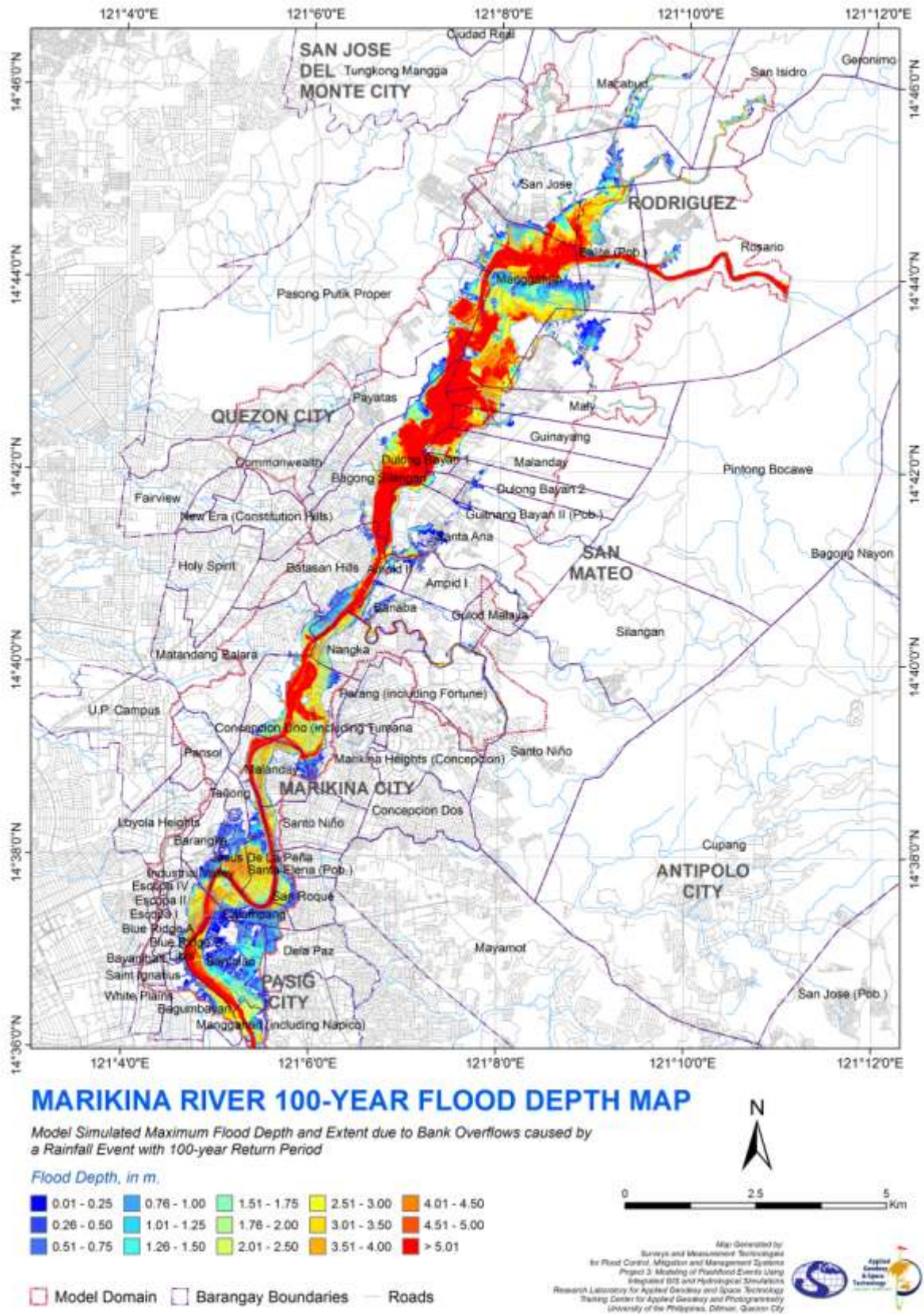
Figure 123. Simulated flood depth map of Marikina River Basin for a 100-year rainfall event.

MARIKINA RIVER 2-YEAR FLOOD HAZARD MAP

Model Simulated Flood Hazard due to Bank Overflows caused by a Rainfall Event with 2-year Return Period

Hazard Type:

Low   Medium   High

Explanation:
Low hazard: Flood depth is less than 0.5 m.
Medium hazard: Flood depth is from 0.5 to 1.5 m.
High hazard: Flood depth is greater than 1.5 m.

Model Domain   Barangay Boundaries   — Roads

Figure 124. Simulated flood hazard map of Marikina River Basin for a 2-year rainfall event.

MARIKINA RIVER 5-YEAR FLOOD HAZARD MAP

Model Simulated Flood Hazard due to Bank Overflows caused by a Rainfall Event with 5-year Return Period

Hazard Type:

Low   Medium   High

Explanation:
Low hazard: Flood depth is less than 0.5 m.
Medium hazard: Flood depth is from 0.5 to 1.5 m.
High hazard: Flood depth is greater than 1.5 m.

Model Domain   Barangay Boundaries   — Roads

Figure 125. Simulated flood hazard map of Marikina River Basin for a 5-year rainfall event.

MARIKINA RIVER 10-YEAR FLOOD HAZARD MAP

Model Simulated Flood Hazard due to Bank Overflows caused by a Rainfall Event with 10-year Return Period

Hazard Type:

Low | Medium | High

Explanation:
Low hazard: Flood depth is less than 0.5 m.
Medium hazard: Flood depth is from 0.5 to 1.5 m.
High hazard: Flood depth is greater than 1.5 m.

Model Domain | Barangay Boundaries | — Roads

Figure 126. Simulated flood hazard map of Marikina River Basin for a 10-year rainfall event.

MARIKINA RIVER 50-YEAR FLOOD HAZARD MAP

Model Simulated Flood Hazard due to Bank Overflows caused by
a Rainfall Event with 50-year Return Period

Hazard Type:

Low Medium High

Explanation:
Low hazard: Flood depth is less than 0.5 m.
Medium hazard: Flood depth is from 0.5 to 1.5 m.
High hazard: Flood depth is greater than 1.5 m.

Model Domain Barangay Boundaries — Roads

Figure 127. Simulated flood hazard map of Marikina River Basin for a 50-year rainfall event.

175

MARIKINA RIVER 100-YEAR FLOOD HAZARD MAP

Model Simulated Flood Hazard due to Bank Overflows caused by
a Rainfall Event with 100-year Return Period

Hazard Type:

| Low | Medium | High |

Explanation:
Low hazard: Flood depth is less than 0.5 m.
Medium hazard: Flood depth is from 0.5 to 1.5 m.
High hazard: Flood depth is greater than 1.5 m.

Model Domain   Barangay Boundaries   — Roads

Figure 128. Simulated flood hazard map of Marikina River Basin for a 100-year rainfall event.

Chapter 8. Applying the Combined HEC HMS-HEC RAS Modeling Approach in Modeling Flood Events in San Juan River Basin

The methodology that has been developed for hydrologic modeling of Marikina River Basin and for hydraulic modeling of the Marikina River and its floodplains to generate flood depth and hazard maps was applied to the San Juan River Basin to test its repeatability and applicability. The framework for the application of the combined HEC HMS-HEC RAS to San Juan River Basin is shown in Figure 129.
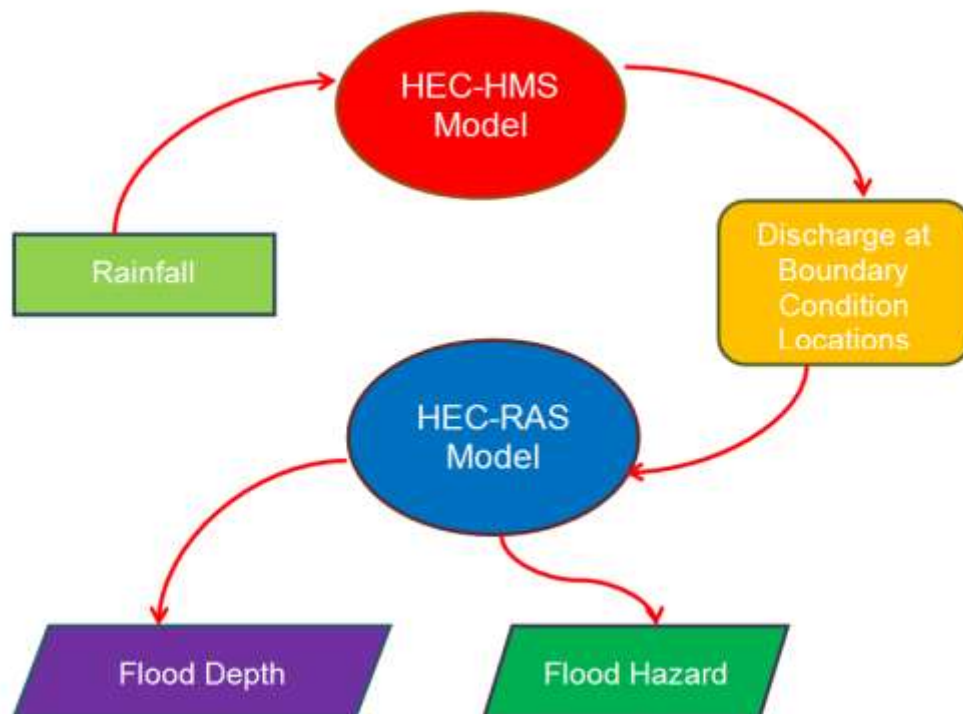
Figure 129. Framework for application of combined HEC HMS-HEC RAS for flood depth and hazard mapping in San Juan River Basin.

Introduction

The San Juan River Basin has a drainage area of approximately 90.08 km^2. The basin covers major portions of Quezon City and a minor portion of Caloocan City in the upstream, and the whole of San Juan City and portions of Manila City and Mandaluyong City in the downstream (Figure 130). Based on the 2010 land-cover map of the basin derived from high resolution WV-2 image, the basin is highly urbanized, with built-up areas comprising 84.64% of the basin's total area (Figure 131).
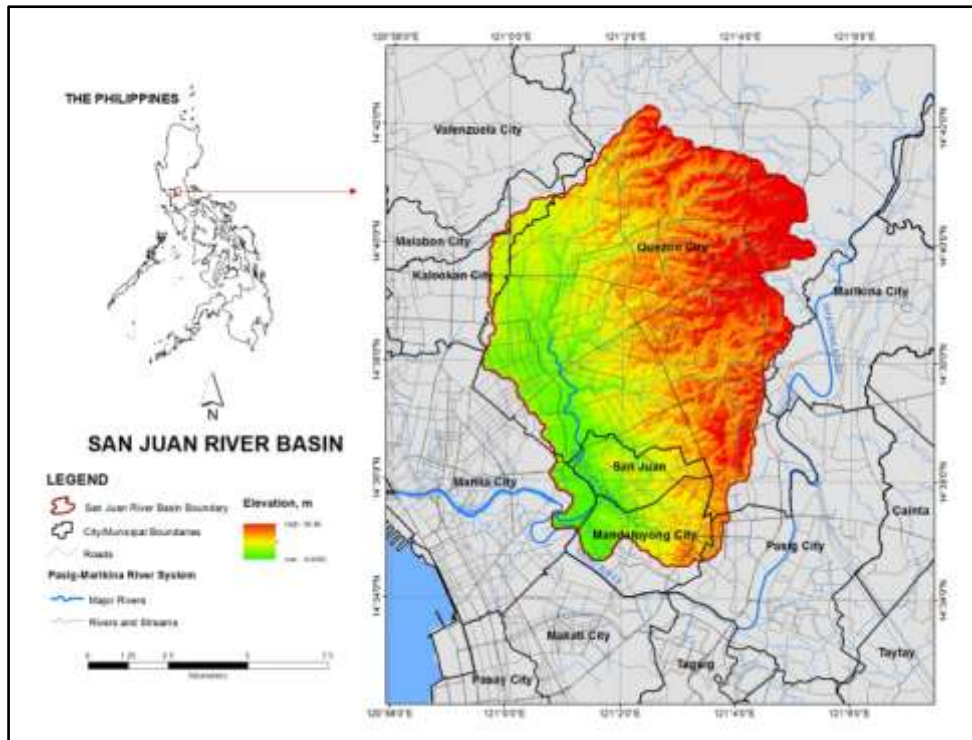
Figure 130. The San Juan River Basin.

Land-cover	Area, in sq. km.	Percent of Total Area
Barren Areas/Bare Soil	1.64	1.82
Built-up Areas	76.24	84.64
Grasslands	3.90	4.33
Shrubs (Small Trees)	2.84	3.15
Trees/Forest (Dense Vegetation)	4.66	5.17
Water Bodies	0.80	0.89
Total	90.08	100.00
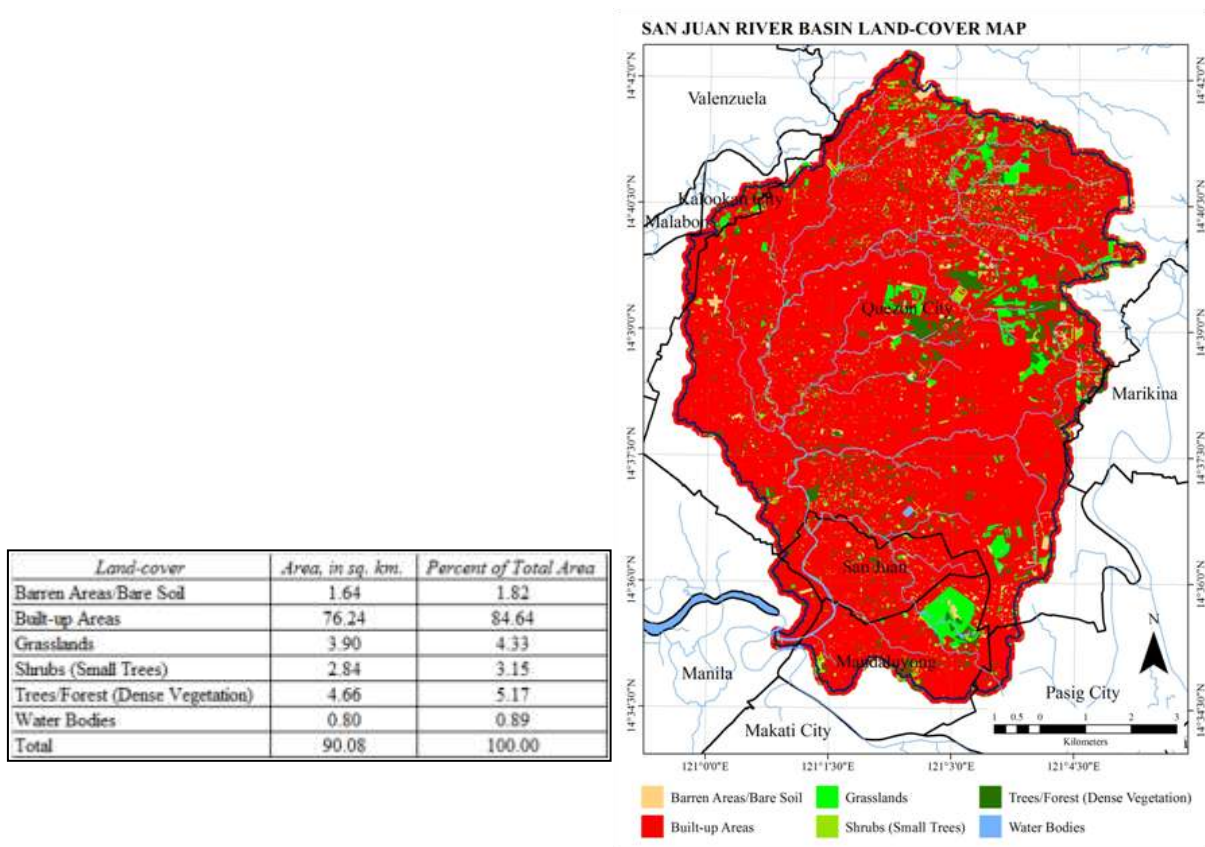
Figure 131. Land-cover map and statistics of San Juan River Basin.

178

The basin is drained by a number of tributaries that includes Culiat Creek, Pasong Tamo River, Dario River, Talayan River, San Francisco River, Mariblo Creek, Kamias Creek and Diliman Creek. All these tributaries connect to San Juan River that drains into Pasig River.

San Juan River Basin HEC HMS Model Development

Figure 132 shows the interface of the HEC HMS model of San Juan River Basin. The model consisted of the 4 model components that was used for the Marikina River Basin (SCS-CN, Clark Unit Hydrograph, Exponential Recession, and Muskingum-Cunge).

The development of the models utilized the updated LIDAR DEM, land-cover map derived from the WV-2 image, BSWM soil map, and rainfall data from rainfall stations installed by EFCOS, PAGASA and ASTI within and near San Juan River Basin (Figure 133). The calibration and validation of the model utilized discharge data of the *August 2012 Habagat* event estimated from water level data recorded by stations installed along San Juan and San Francisco Rivers (Figure 134). A HEC RAS model of the main portion of these two rivers were initially developed to derive the equivalent discharge hydrographs from time series of water level data through unsteady flow simulation.

The HEC HMS model has 154 subbasins (with area ranging from 0.010 to 2.12 km^2), 128 reaches, and 129 junctions (including the main outlet located at the junction of San Juan River with Pasig River).
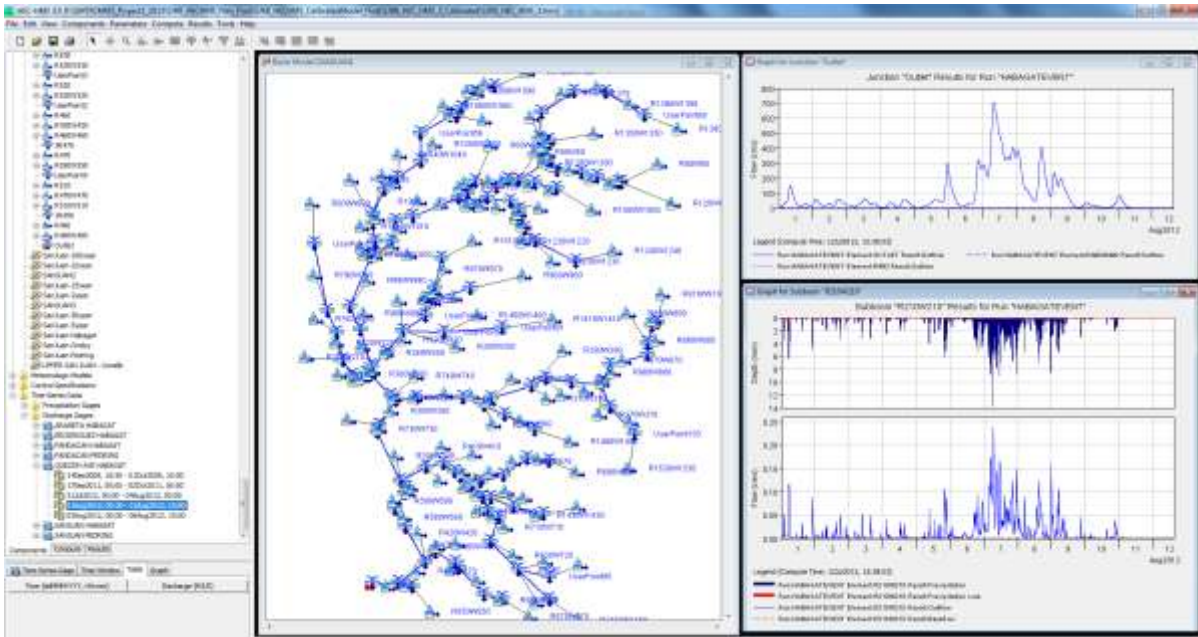
Figure 132. Interface of the HEC HMS model of the San Juan River Basin.
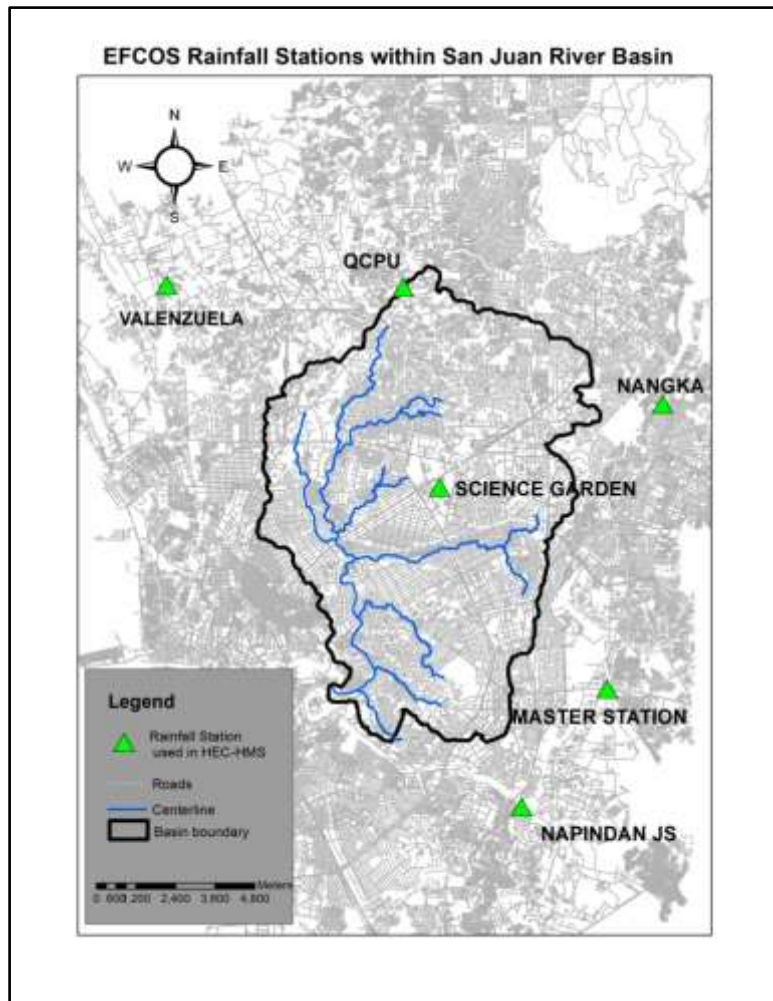
Figure 133. Map of rainfall stations used in San Juan River Basin HEC HMS model development, calibration, validation and simulation of actual and hypothetical flood events.
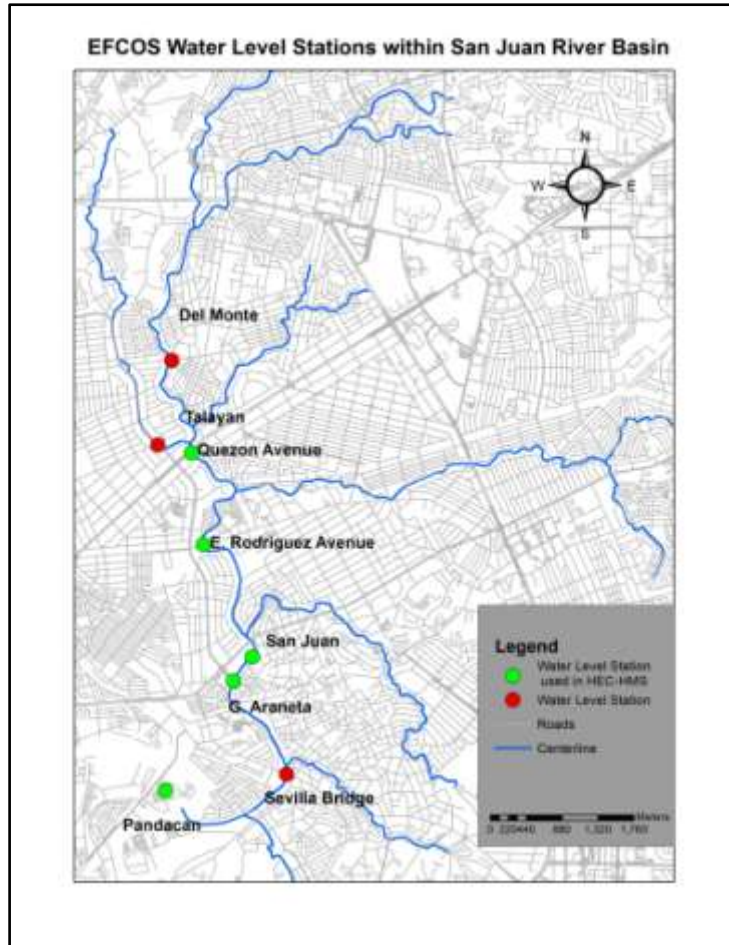
Figure 134. Water level stations used in HEC HMS model calibration and validation.

HEC HMS Calibration and Validation

As the outlet of San Juan River Basin is affected by tidal fluctuations, discharge data at this location cannot be used to calibrate the model because of presence of backflows. For the model calibration, a subset containing the upstream portion of the San Juan River Basin was created instead (Figure 135). This portion has its outlet corresponding to E. Rodriguez Station. Based on time series of water level data, this station is least affected by tidal fluctuations compared to other stations downstream (San Juan, G. Araneta, Sevilla and Pandacan).

Discharge data estimated from time series of water level recorded at this station (August 3-6, 2012) was then used to optimize the parameters. Because of the tidal effects, it was difficult to calibrate the parameters of sub-basins and reach elements downstream of E. Rodriguez Station.

The calibration results is shown in Figure 136. The calibrated model was validated using the same rainfall event but the validation station was at Quezon Avenue (Figure 137). The summary of model performance is shown in Table 43.
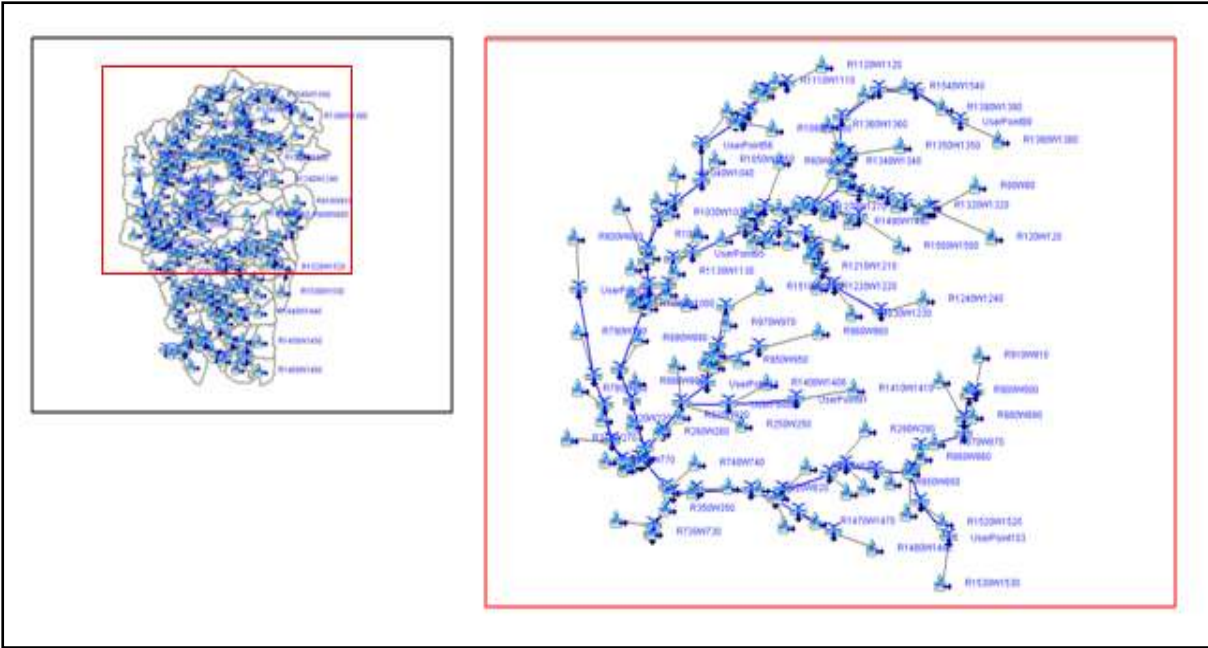
Figure 135. A subset of the HEC HMS model that was calibrated using discharge data at the E. Rodriguez station.
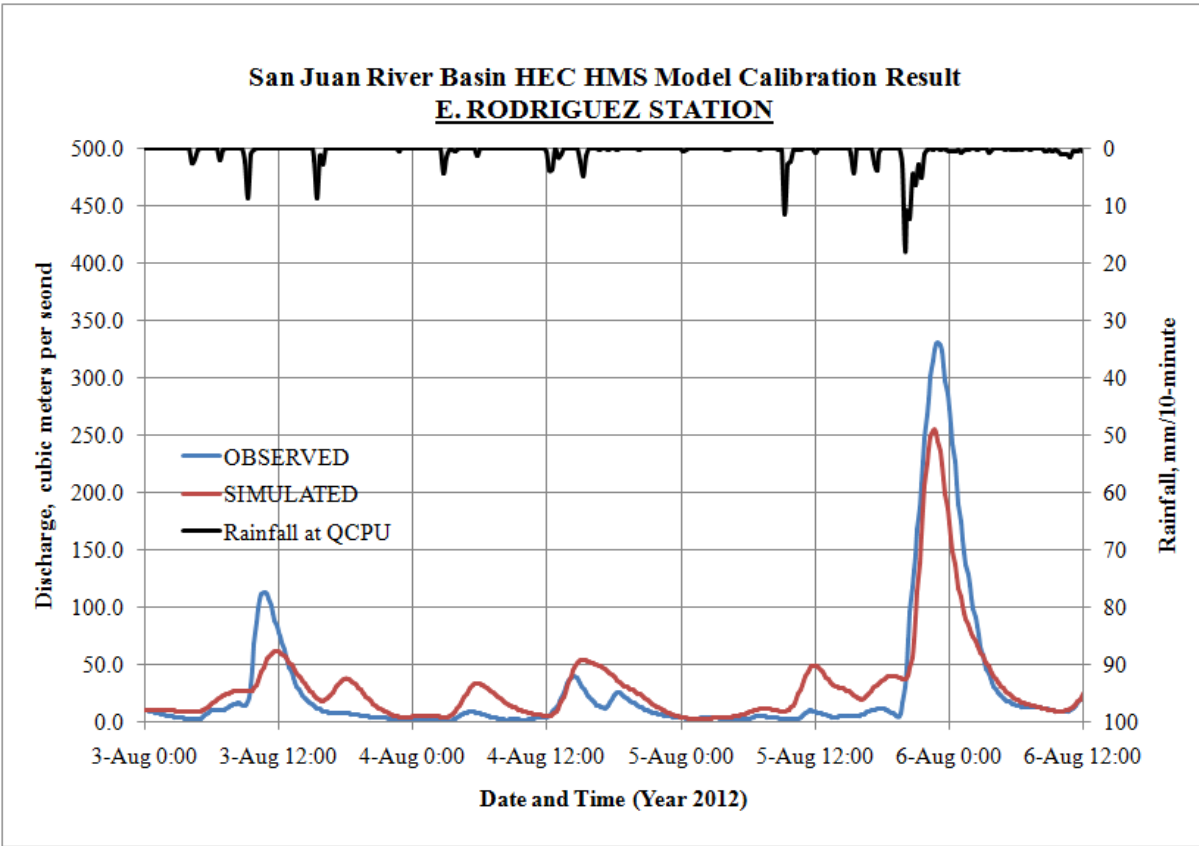
Figure 136. Results of HEC HMS model calibration at the E. Rodriguez Station.
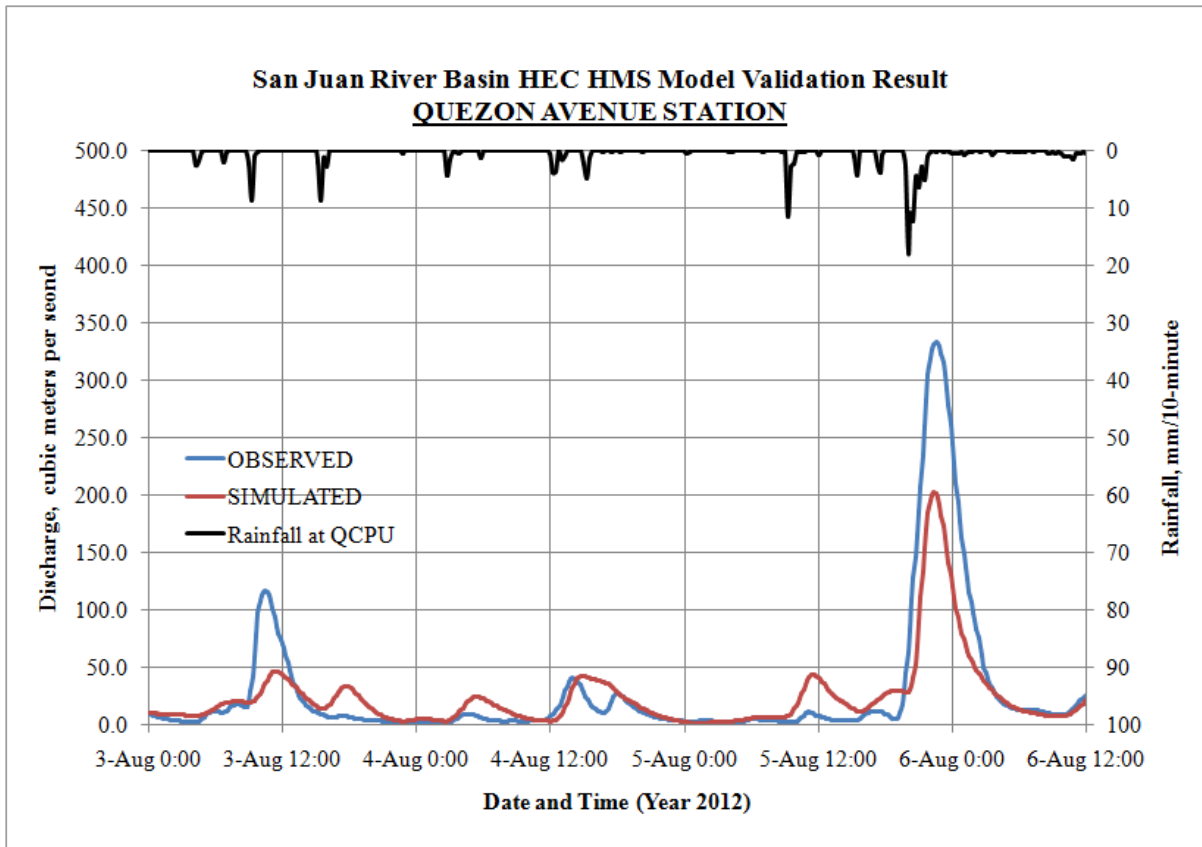
Figure 137. Results of HEC HMS model validation at the Quezon Avenue Station.

Table 43. HEC HMS model performance during calibration and validation,

Performance Statistic	E. Rodriguez Station (Calibration)	Quezon Avenue (Validation)
NSE	0.71	0.83
RSR	0.53	0.41
PBIAS	14.82	-12.65
Model Performance	"Good"	

Based on the performance statistics, the HEC HMS model has good performance, at least for the August 2012 *Habagat* event. At the E. Rodriguez Station, it appears that <u>in general</u> the model is biased towards underestimation as indicated by the positive PBIAS of 14.82%. At Quezon Avenue Station, the model is biased towards under overestimation (negative PBIAS of 12.65%), although it appears that model simulated peak flows are lower than the observed peak flows.

Although the model's performance is acceptable based on performance statistics, further calibration and validation is needed.

San Juan River Basin HEC RAS Model Development

The geometric data of the HEC RAS model for San Juan River Basin is shown in Figure 138. The model domain has a total area of 49.75 km^2. The rivers included in the model domain are shown in Figure 139. The model domain does not cover the whole river basin because river geometry data are only available for the rivers included in the domain.

The model consisted of 513 cross-sections, 21 reaches and 22 junctions (including the outlet). The Manning's n of the cross-sections were derived from the high-resolution land-cover map through the use of look-up table (similar to the one used in developing the Marikina River HEC RAS model, Table 32).

The HEC RAS model interface is shown in Figure 140.

The model boundary condition points (total of 21) corresponding to elements of HEC HMS model are shown in Figure 141 and described in Table 44.
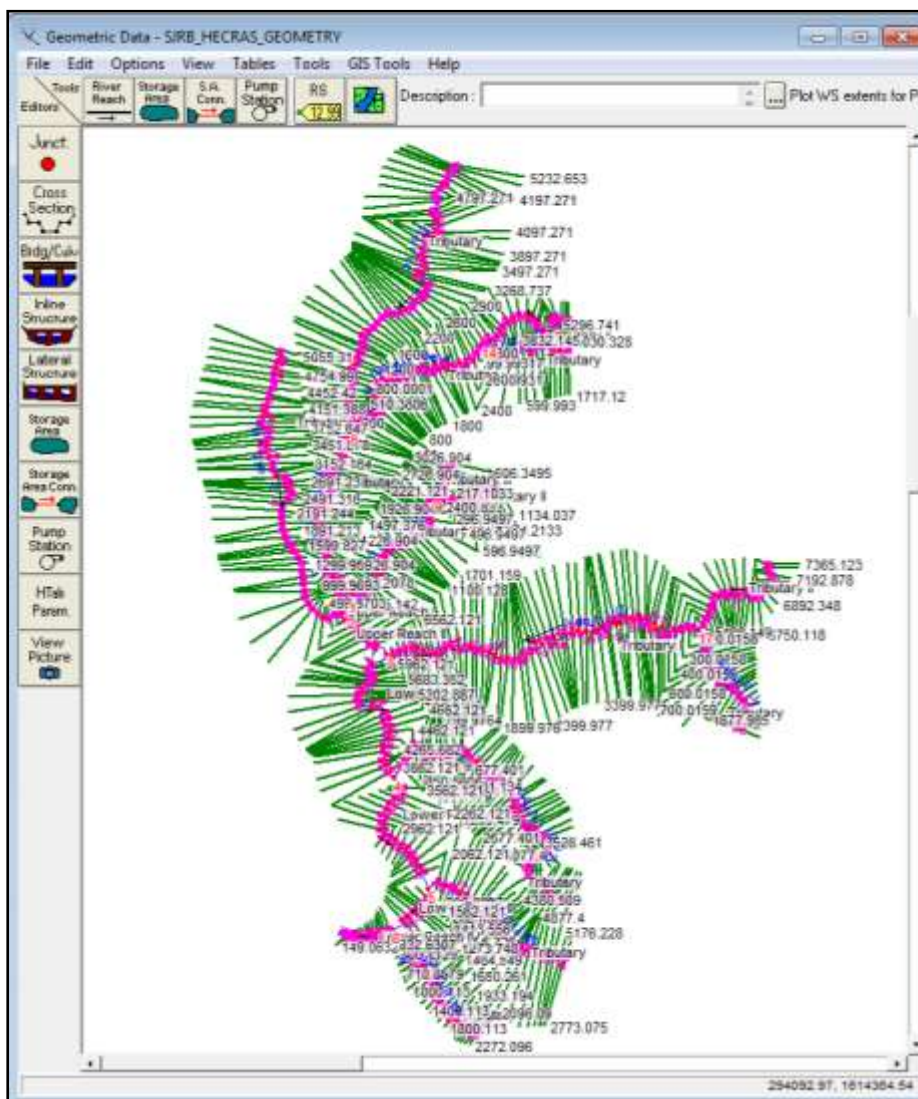
Figure 138. Geometric data of the San Juan River Basin HEC RAS Model.
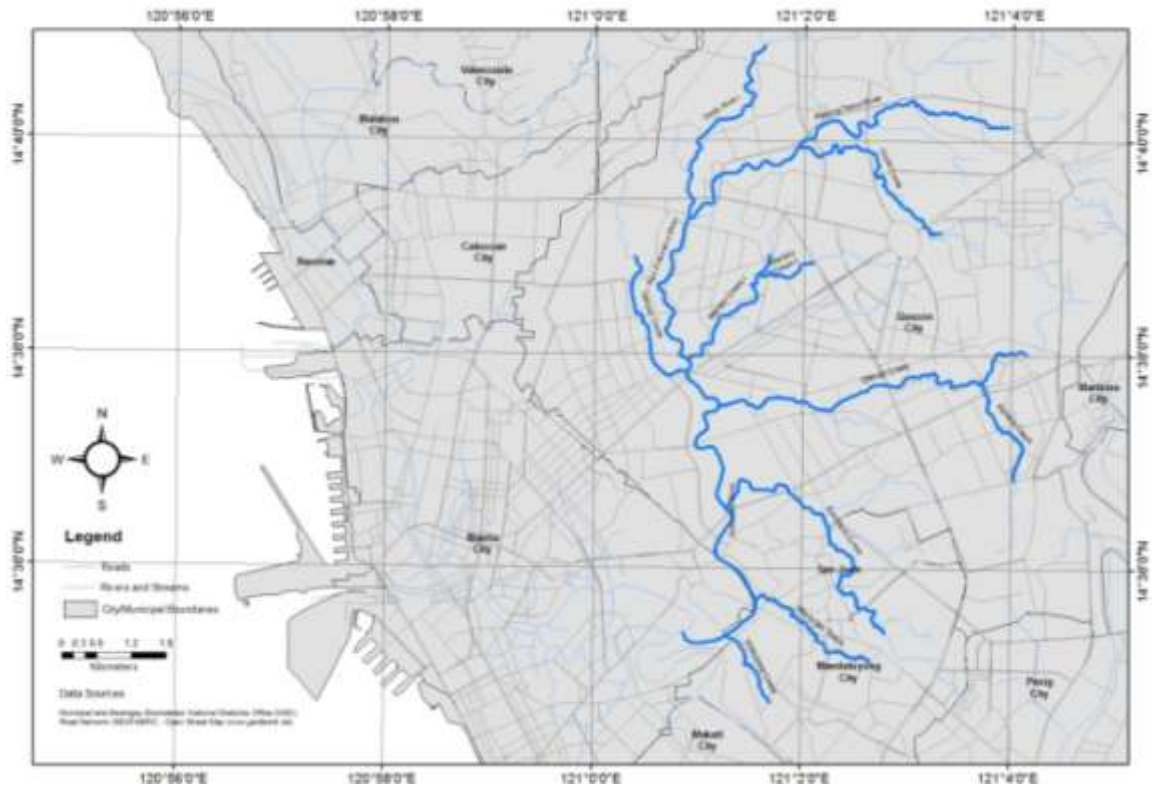
Figure 139. Rivers included in the HEC RAS model domain.
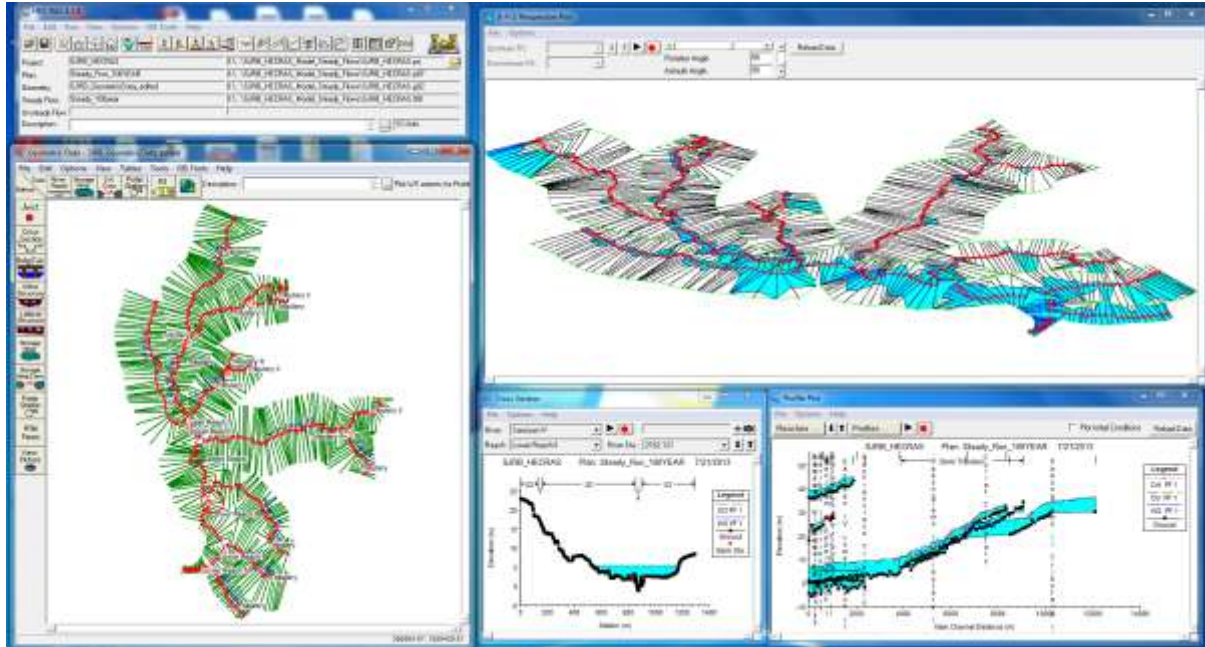
Figure 140. The interface of the HEC RAS model of San Juan River Basin.
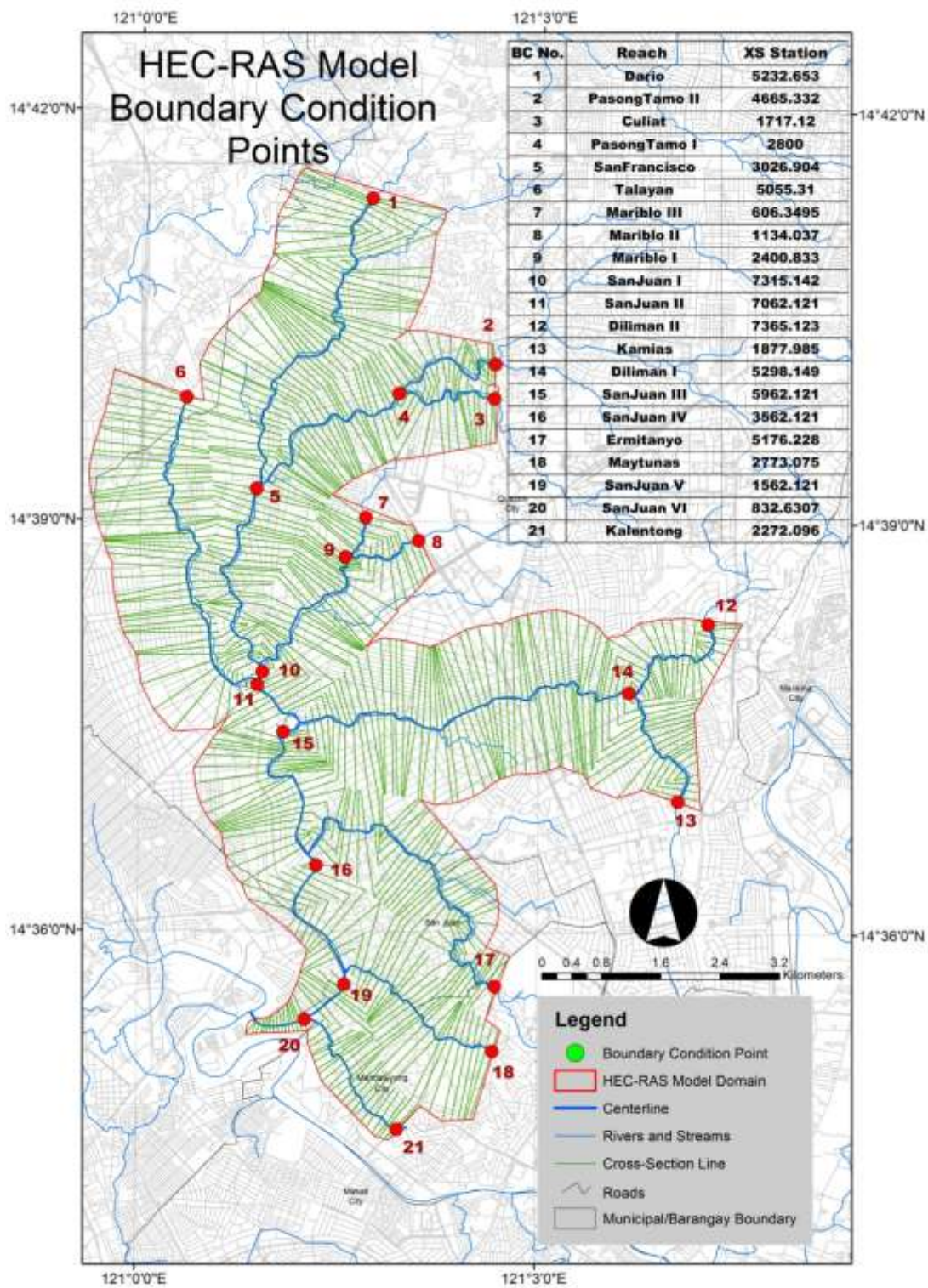
Figure 141. Map showing the HEC RAS model boundary condition points.

Table 44. Description of HEC RAS model boundary condition points.

BC Point No.	Locality	HEC-RAS Model Element No.	Corresponding HEC HMS Model Element No.
1	Near Mindanao Ave and boundary of Brgy. Ugong and Brgy. San Bartolome	XS 5232.65 (Reach Dario)	USERPOINT 61
2	Junction near the Bridge of Visayas Ave corner Congressional Ave extension, Quezon City	XS 4665.33 (Reach Pasong Tamo II)	JR 1270
3	Bridge along Visayas Ave near road 7, Quezon City	XS 1717.12 (Reach Culiat)	USERPOINT 68
4	Along Congressional Avenue near Brgy. Bahay Toro, Quezon City	XS 2800.00 (Reach Pasong Tamo I)	JR 1150
5	Balintawak, Near EDSA corner Congressional Avenue	XS 3026.90 (Reach San Francisco)	USERPOINT 50
6	At Brgy. 143 near the boundary of Brgy. 142., Quezon City	XS 5055.31 (Reach Talayan)	USERPOINT 30
7	At Brgy. Bungad, near the boudary of Brgy. San Antonio, Quezon City	XS 606.3495 (Reach Mariblo III)	USERPOINT 101
8	Along EDSA, near TriNoma, Quezon City	XS 1134.04 (Reach Mariblo II)	USERPOINT 46
9	Along East River Side St. Del Monde Avenue, Quezon City	XS 2400.83 (Reach Mariblo I)	JR 930
10	Quezon Avenue corner Colonel Moran Street	XS 7315.14 (Reach San Juan I)	JR 280
11	Bridge along Quezon Avenue near G. Araneta Avenue	XS 7062.12 (Reach San Juan II)	JR 740
12	Bridge along Rosa Alvero Loyola Heights. Quezon City	XS 7365.12 (Reach Diliman II)	USERPOINT 39
13	Near Kalantiaw Street corner Rajah Matanda, Brgy. Masagana,Quezon City	XS 1877.99 (Reach Kamias)	USERPOINT 103
14	Located near Quirino 2-C, Anonas, Quezon City	XS 5298.15 (Reach Diliman I)	JR 850
15	Along San Juan River beside Montgomery Road	XS 5962.12 (Reach San Juan III)	JR 350
16	San Juan near San Juan EFCOS Station	XS 3562.12 (Reach San Juan IV)	USERPOINT 11
17	Near Wack-Wack Area, near May Street	XS 5176.23 (Reach Ermitanyo)	JR 720
18	Corner Nuevo de Febrero and Correction Road, Addition Hills, Mandaluyong City	XS 2773.08 (Reach Maytunas)	USERPOINT 7
19	Located at Sevilla Bridge, P.Sanchez Street, Kalentong, Mandaluyong City	XS 1562.12 (Reach San Juan V)	JR 470
20	Located near Brgy.620, Makisig Street along Bagumbayan, Mandaluyong City	XS 832.63 (Reach San Juan VI)	JR 490
21	Beside Francisco St along New Panaderos near Brgy.895, Kalentong, Mandaluyong City	XS 2272.10 (Reach Kalentong)	USERPOINT5

Flood Simulations

The steady flow module of HEC-RAS was used to determine water surface profiles for flood inundation mapping. The input flow data consists of maximum discharge values computed by the HEC-HMS model at each BC point. Flooding due to rainfall events brought by the September 2009 *Ondoy*, the September 2011 *Pedring*, and the August 2012 *Habagat*, were simulated using the combined HEC HMS-HEC RAS. The simulated peak flows for these events at the HEC RAS BC points are shown in Table 45.

Flooding due to hypothetical, extreme rainfall scenarios with different return periods were also simulated. Similar to the case of Marikina River, Rainfall-Intensity Duration Frequency (RIDF) data of the Science Garden rainfall station was used for the simulations in HEC-HMS to produce the outflow hydrographs. The simulated peak flows for these events at the BC points which were entered into HEC RAS are shown in Table 46. The water profiles computed by HEC RAS were then post-processed in GIS and overlaid in the 1-m LIDAR DEM to generate flood depth maps and flood hazard maps (shown in Figure 142 to Figure 160). It should be noted that the flood depth and hazards shown are due to bank overflows. Flooding due to water accumulation due to clogged drainage or due to natural ponding were not simulated as HEC RAS does not have the capability to simulate these kind of processes. Also, the map only shows flood information on area within the model domain. Areas outside the domain were not included in the simulations.

Table 45. Peak flows simulated by the HEC HMS model for the actual flood events.

REACH	HEC-RAS XS	HEC-HMS ELEMENT	PEAK FLOWS (m3/s)		
			ONDOY	PEDRING	HABAGAT 2012
Culiat	1717.12	USERPOINT 68	71.589	21.004	41.244
Dario	5232.65	USERPOINT 61	27.357	12.592	20.52
Diliman I	5298.15	JR 850	127.65	33.163	52.091
Diliman II	7365.12	USERPOINT 39	42.562	11.617	19.565
Ermitanyo	5176.23	JR 720	64.03	12.934	23.626
Kalentong	2272.10	USERPOINT5	21.971	4.6198	7.7438
Kamias	1877.99	USERPOINT 103	20.2	4.5457	8.3782
Mariblo I	2400.83	JR 930	65.918	17.331	40.231
Mariblo II	1134.04	USERPOINT 46	31.026	7.4604	17.819
Mariblo III	606.3495	USERPOINT 101	17.85	4.803	11.364
Maytunas	2773.08	USERPOINT 7	21.619	4.7912	7.0754
PasongTamo I	2800.00	JR 1150	326.23	117.51	208.69
PasongTamo II	4665.33	JR 1270	217.84	82.896	142.05
SanFrancisco	3026.90	USERPOINT 50	508.92	187.3	344.68
SanJuan I	7315.14	JR 280	696.93	232.84	451.79
SanJuan II	7062.12	JR 740	803.85	260.75	520.51
SanJuan III	5962.12	JR 350	1058.6	322.63	622.21
SanJuan IV	3562.12	USERPOINT 11	1307.2	373.8	698.45
SanJuan V	XS 1562.12	JR 470	1380.9	385.84	708.84
SanJuan VI	XS 832.63	JR 490	1402.1	388.95	709.28
Talayan	XS 5055.31	USERPOINT 30	33.709	8.7152	23.465

Table 46. Peak flows simulated by the HEC HMS model at the HEC RAS BC points for the hypothetical, extreme rainfall events.

REACH	HEC-RAS XS STATION	HEC-HMS ELEMENT	PEAK FLOWS (m3/s)					
			2-YEAR	5-YEAR	10-YEAR	25-YEAR	50-YEAR	100-YEAR
Culiat	1717.12	USERPOINT 68	25.162	42.322	53.744	68.168	78.853	89.433
Dario	5232.65	USERPOINT 61	12.163	19.352	24.128	30.136	34.599	39.022
Diliman I	5298.15	JR 850	53.897	86.469	108.25	135.75	156.21	176.46
Diliman II	7365.12	USERPOINT 39	17.231	28.022	35.161	44.128	50.824	57.428
Ermitanyo	5176.23	JR 720	26.646	43.882	55.395	69.92	80.702	91.369
Kalentong	2272.10	USERPOINT5	10.1	15.838	19.654	24.468	28.048	31.597
Kamias	1877.99	USERPOINT 103	9.4266	14.749	18.283	22.736	26.046	29.324
Mariblo I	2400.83	JR 930	24.783	41.57	52.688	66.639	76.962	87.163
Mariblo II	1134.04	USERPOINT 46	11.621	20.006	25.54	32.468	37.579	42.624
Mariblo III	606.3495	USERPOINT 101	6.6685	11.074	13.974	17.605	20.29	22.945
Maytunas	2773.08	USERPOINT 7	10.552	16.415	20.312	25.226	28.879	32.499
PasongTamo I	2800.00	JR 1150	124.78	205.13	258.61	325.83	375.72	425.33
PasongTamo II	4665.33	JR 1270	87.978	143.2	179.74	225.75	259.8	293.71
SanFrancisco	3026.90	USERPOINT 50	200.89	327.27	411.4	517.45	596.29	674.46
SanJuan I	7315.14	JR 280	265.04	434.26	546.94	689.27	794.72	899.31
SanJuan II	7062.12	JR 740	309.21	504.82	635.15	799.52	921.53	1042.5
SanJuan III	5962.12	JR 350	405.8	662.18	832.81	1048.4	1208.5	1367.4
SanJuan IV	3562.12	USERPOINT 11	484.14	794.44	1001.5	1263.6	1458.8	1652.7
SanJuan V	1562.12	JR 470	498.82	821.56	1037.3	1310.9	1515.3	1717.2
SanJuan VI	832.63	JR 490	502.43	828.3	1046.2	1322.4	1527.9	1732.3
Talayan	5055.31	USERPOINT 30	15.762	24.682	30.589	38.023	43.545	49.013
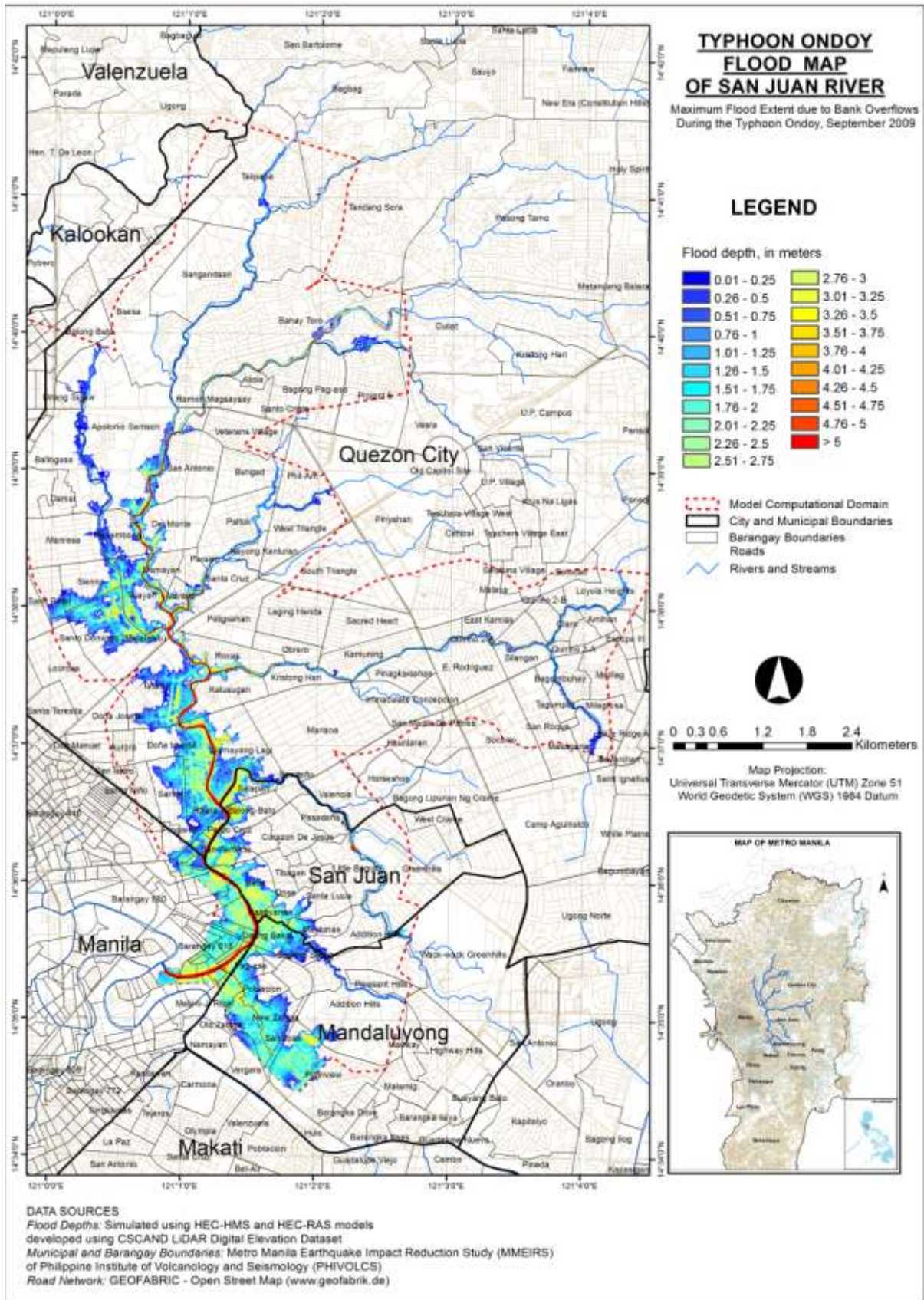
Figure 142. Model simulated maximum flood depth map in San Juan River Basin due to bank overflows during the September 2009 *Ondoy* event.
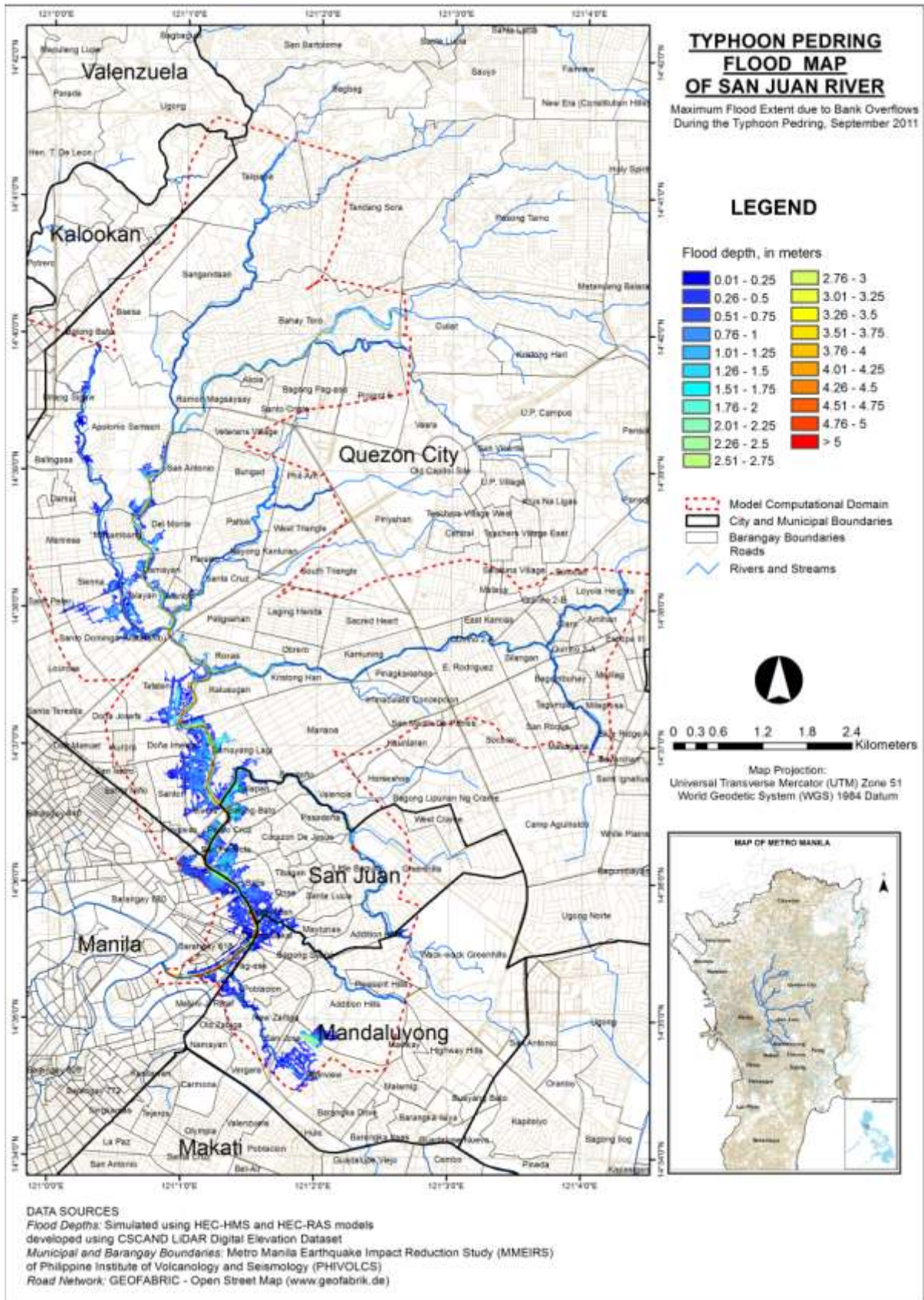
Figure 143. Model simulated maximum flood depth map in San Juan River Basin due to bank overflows during the September 2011 *Pedring* event.
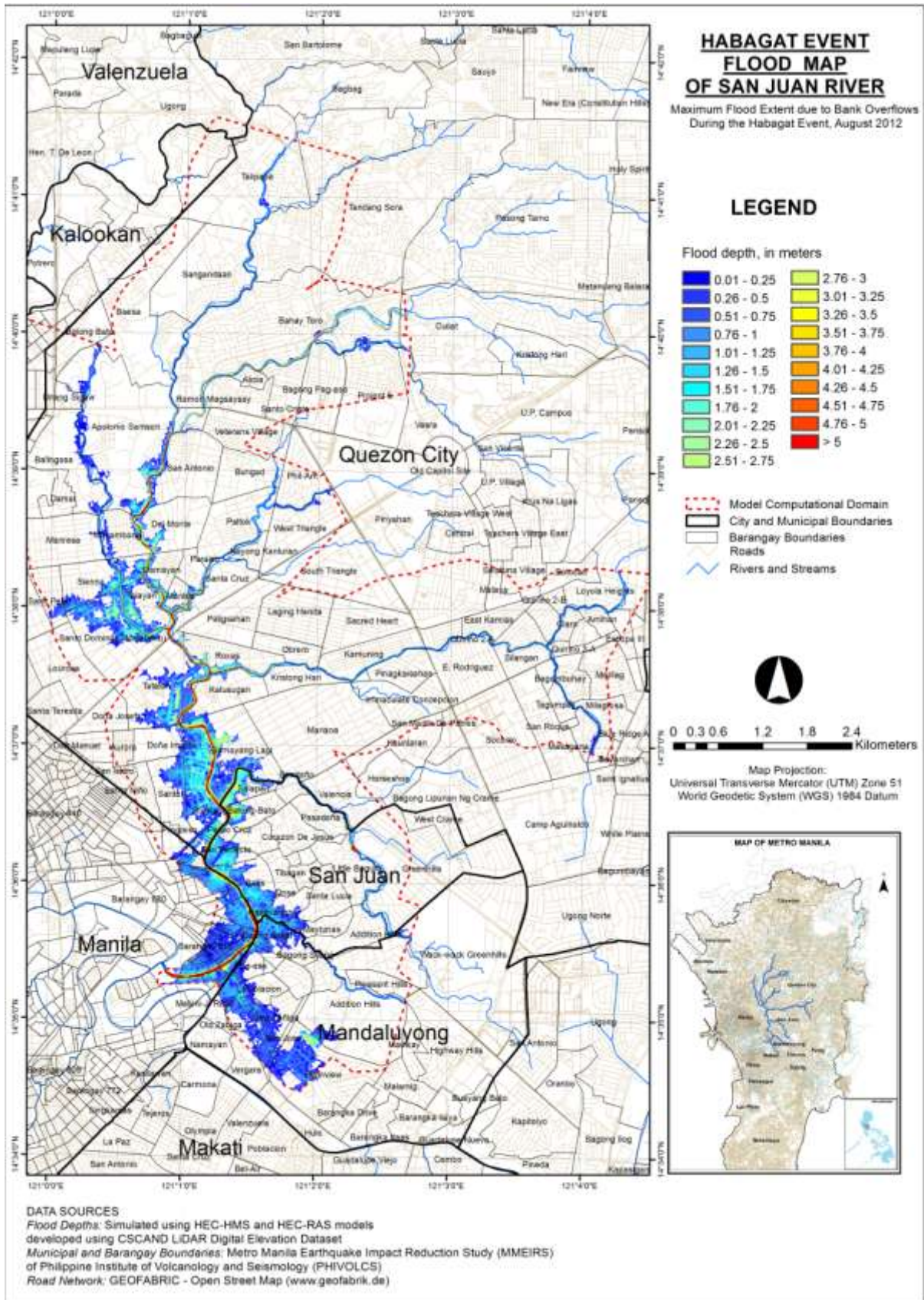
Figure 144. Model simulated maximum flood depth map in San Juan River Basin due to bank overflows during August 2012 *Habagat* event.
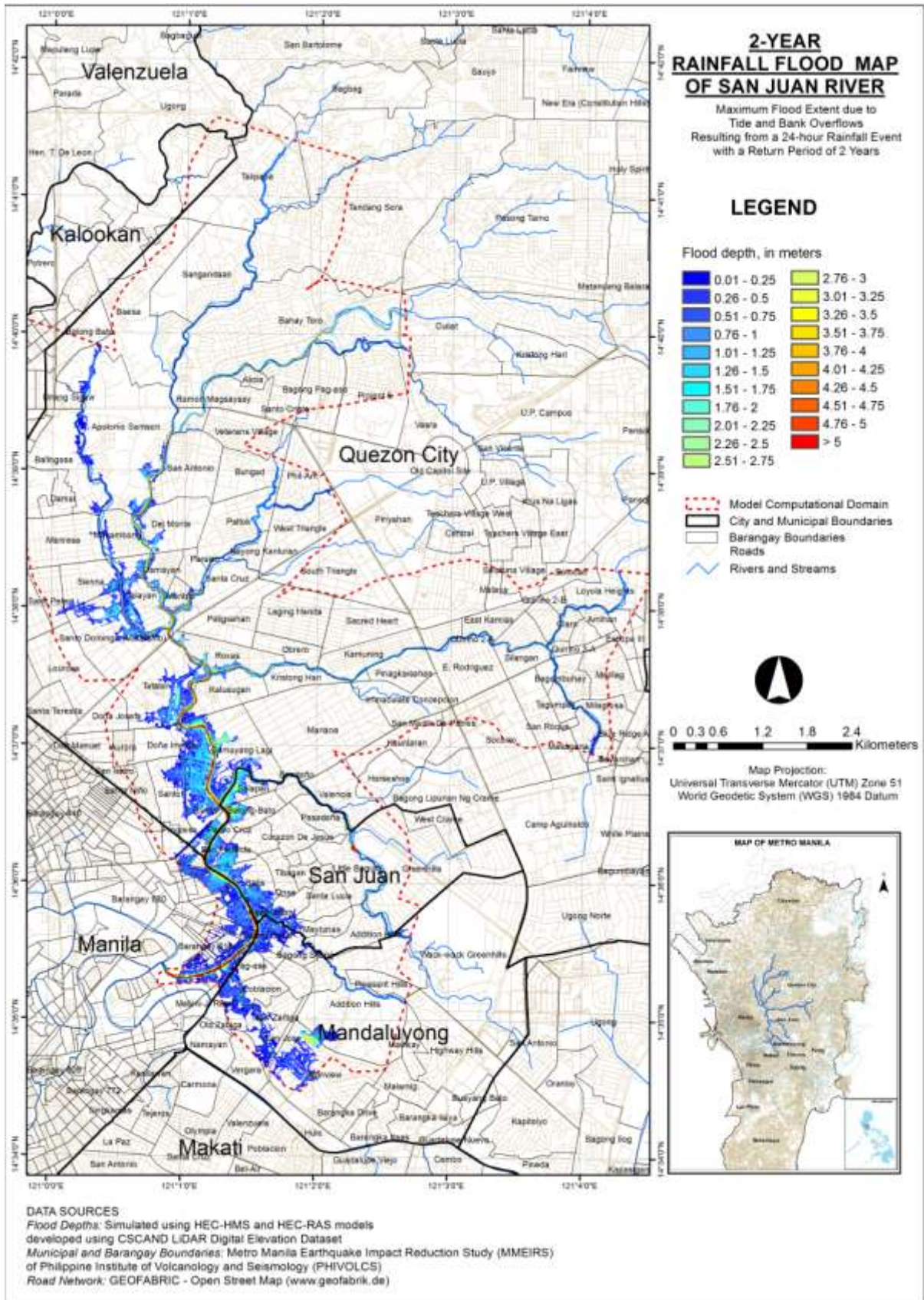
Figure 145. Model simulated maximum flood depth map in San Juan River Basin due to bank overflows caused by rainfall event with 2-year return period.
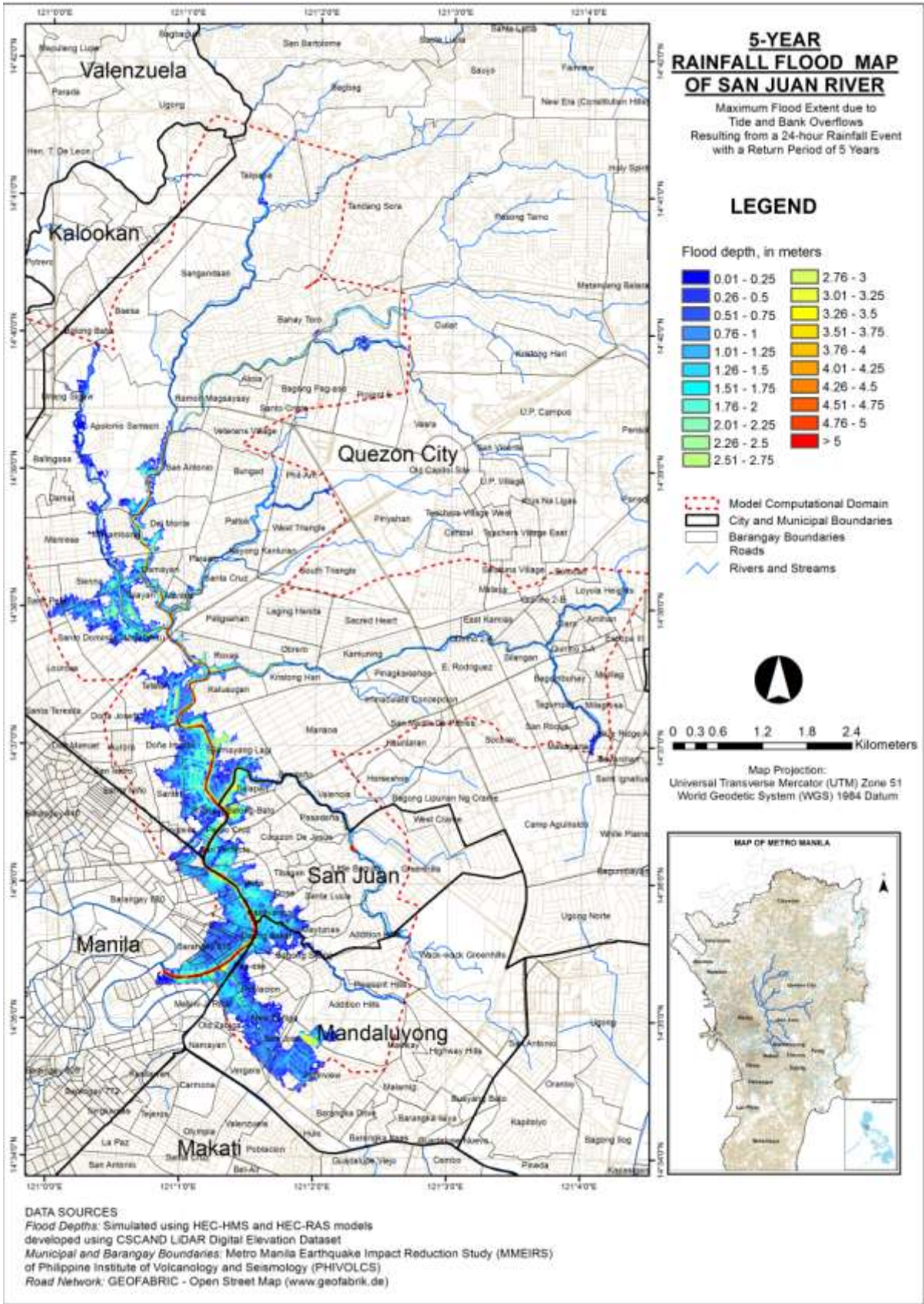
Figure 146. Model simulated maximum flood depth map in San Juan River Basin due to bank overflows caused by rainfall event with 5-year return period.
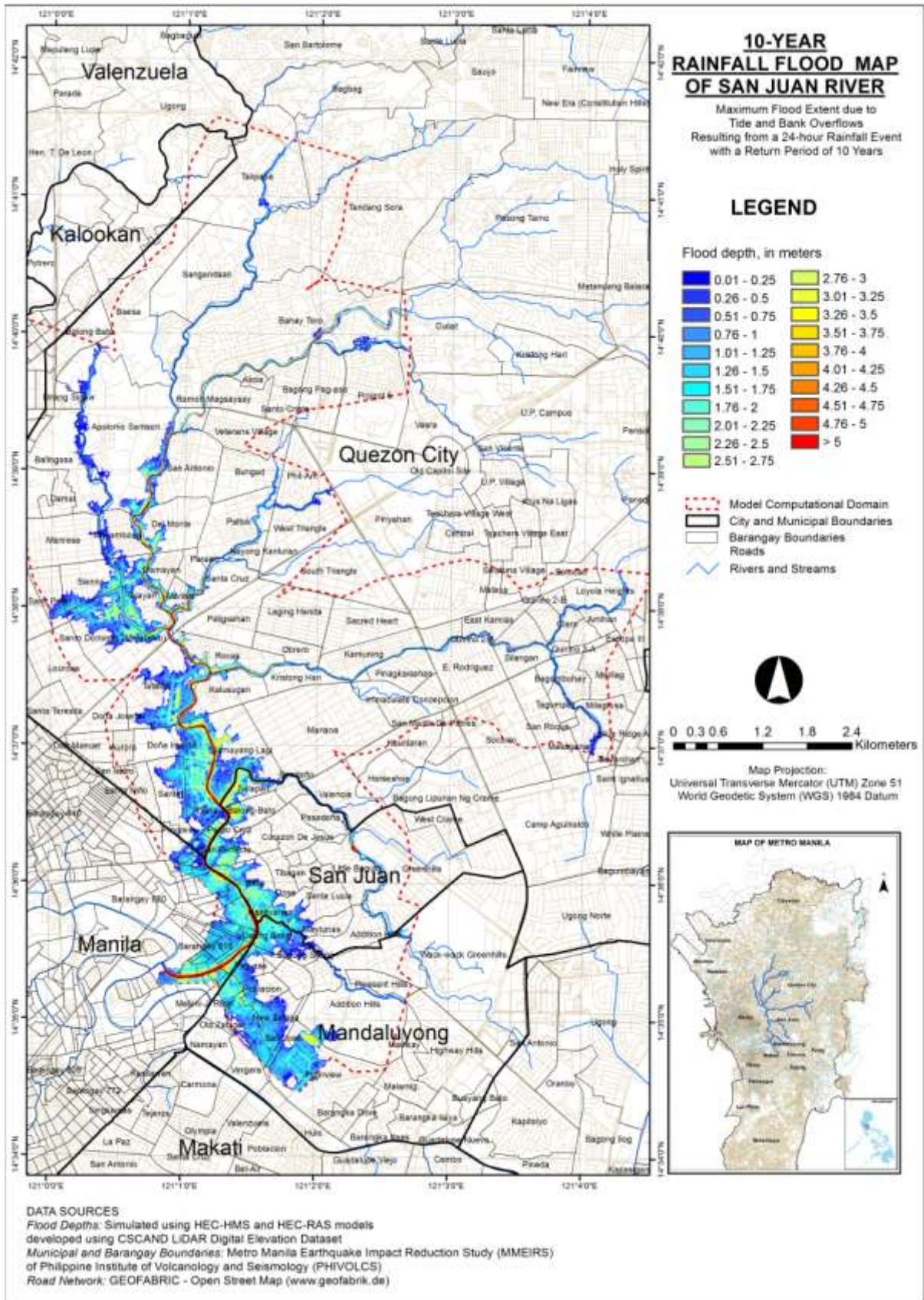
Figure 147. Model simulated maximum flood depth map in San Juan River Basin due to bank overflows caused by rainfall event with 10-year return period.
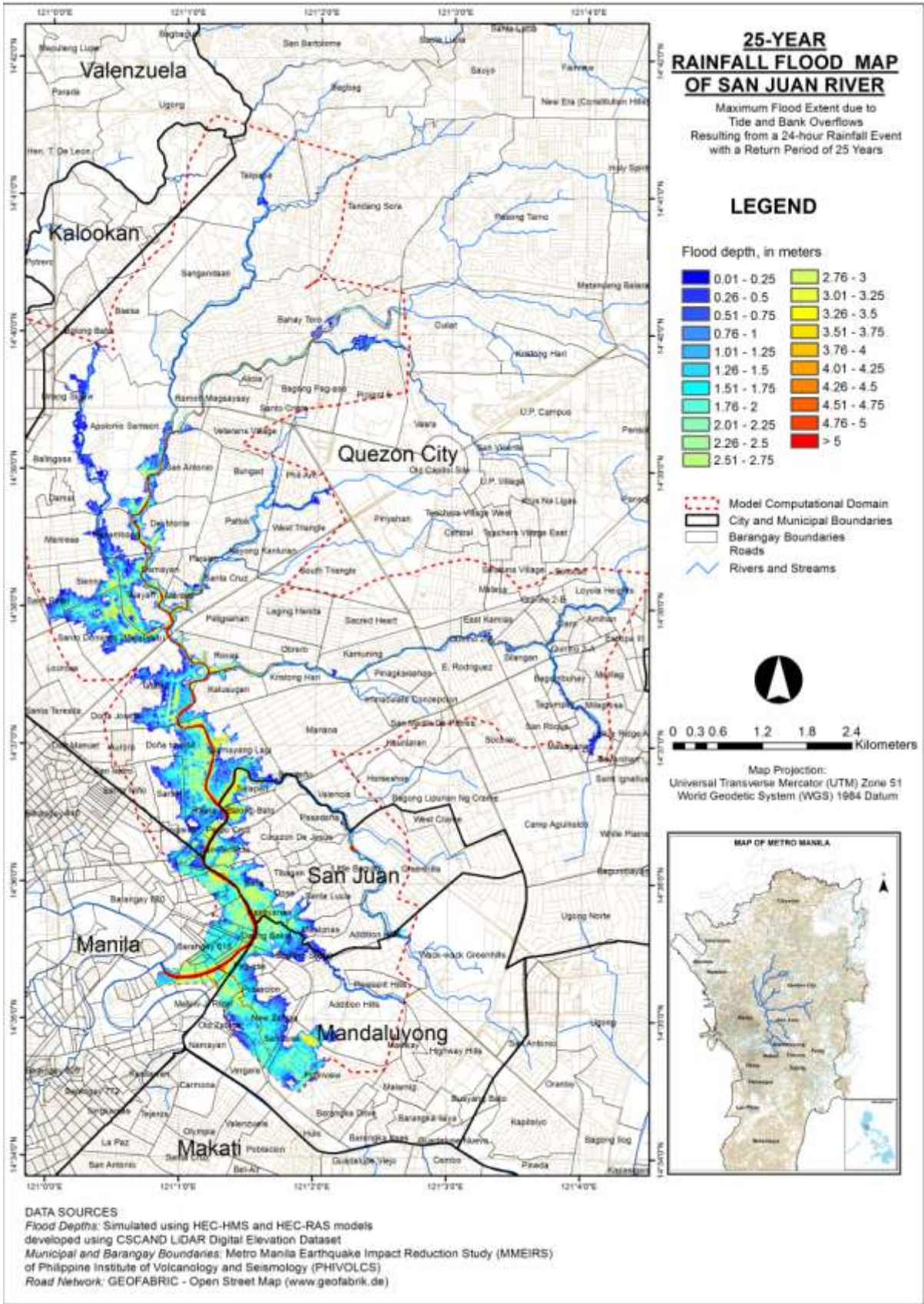
Figure 148. Model simulated maximum flood depth map in San Juan River Basin due to bank overflows caused by rainfall event with 25-year return period.

196
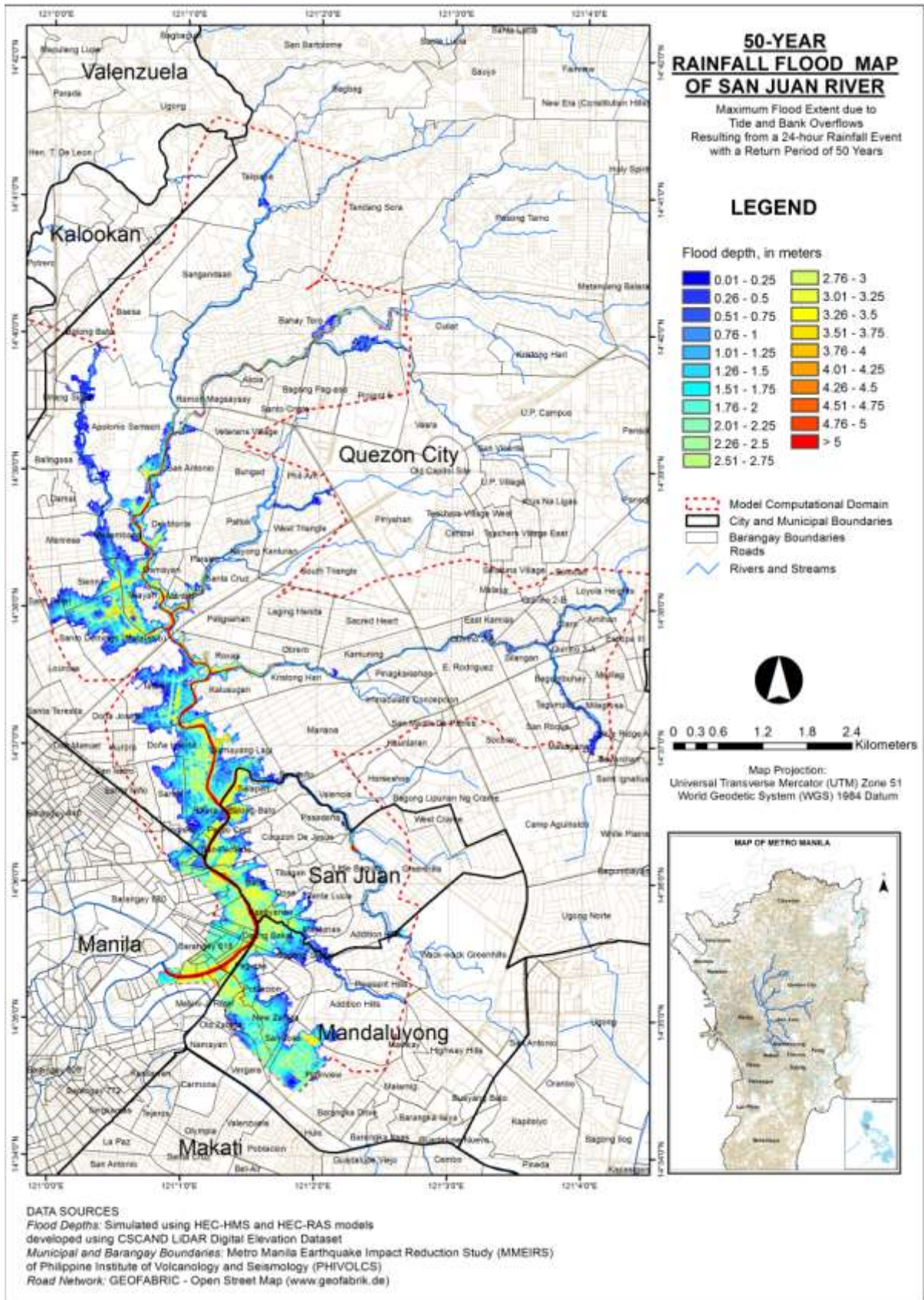
Figure 149. Model simulated maximum flood depth map in San Juan River Basin due to bank overflows caused by rainfall event with 50-year return period.
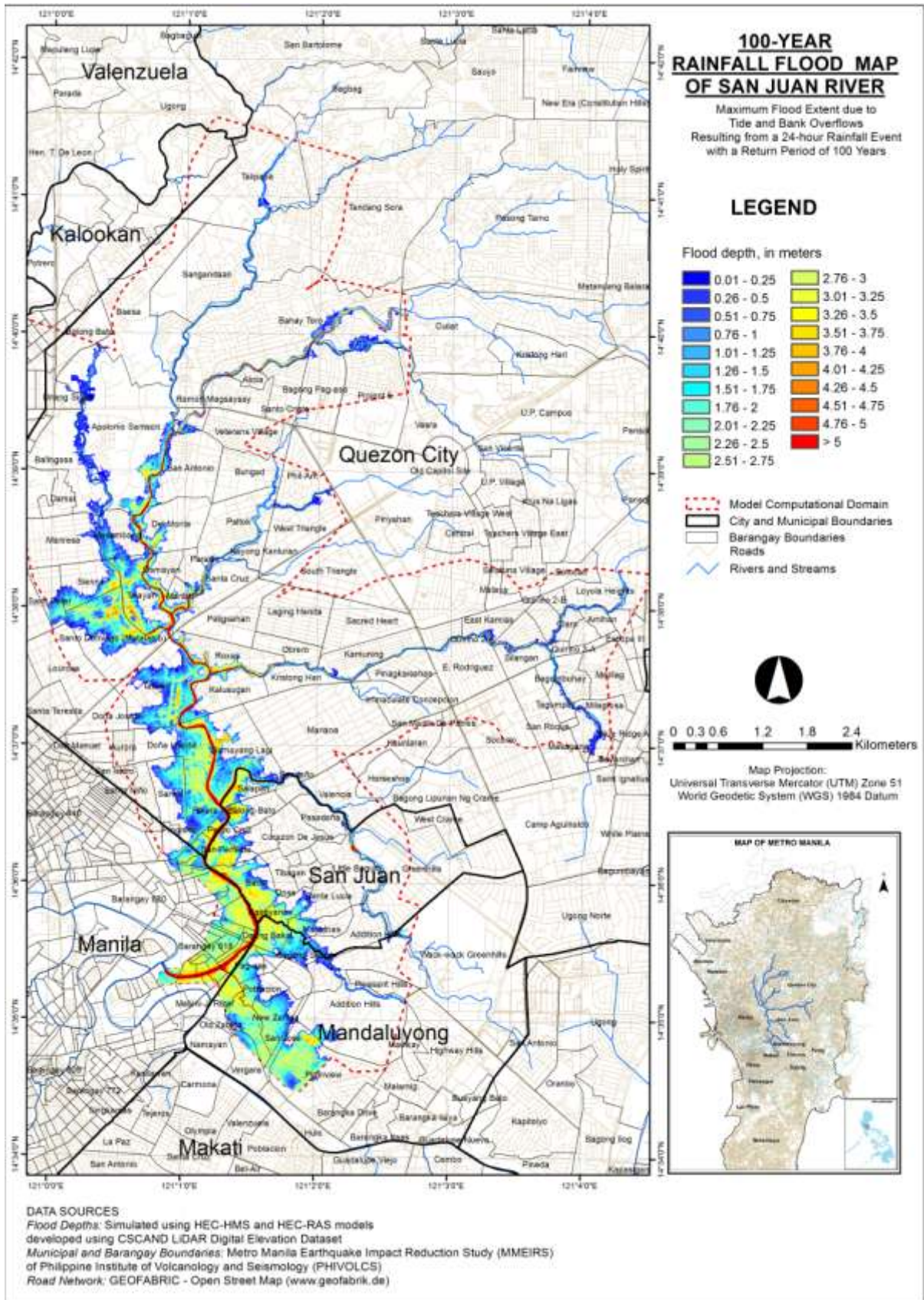
Figure 150. Model simulated maximum flood depth map in San Juan River Basin due to bank overflows caused by rainfall event with 100-year return period.
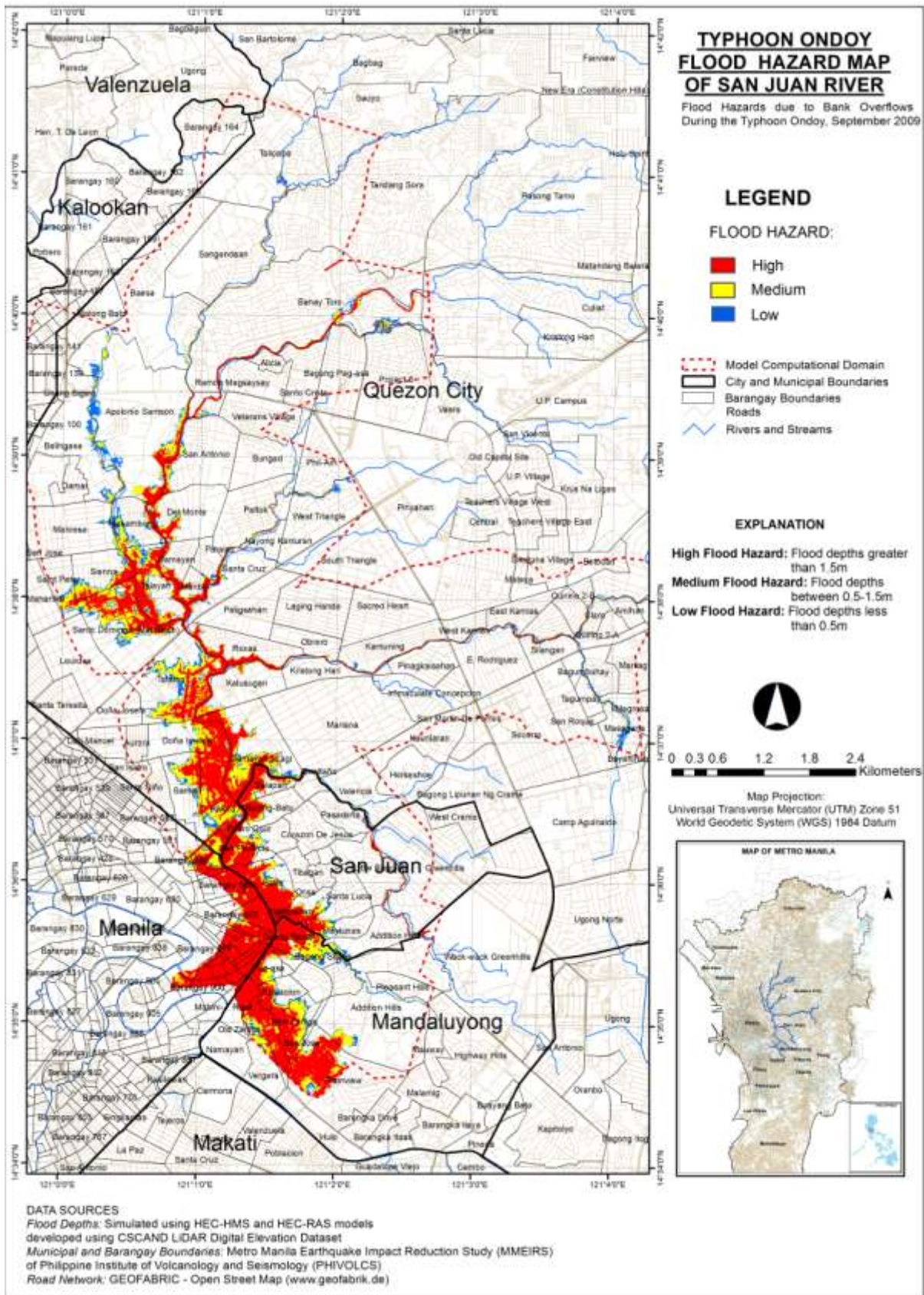
Figure 151. Simulated flood hazard map of San Juan River Basin for the September 2009 *Ondoy* event.
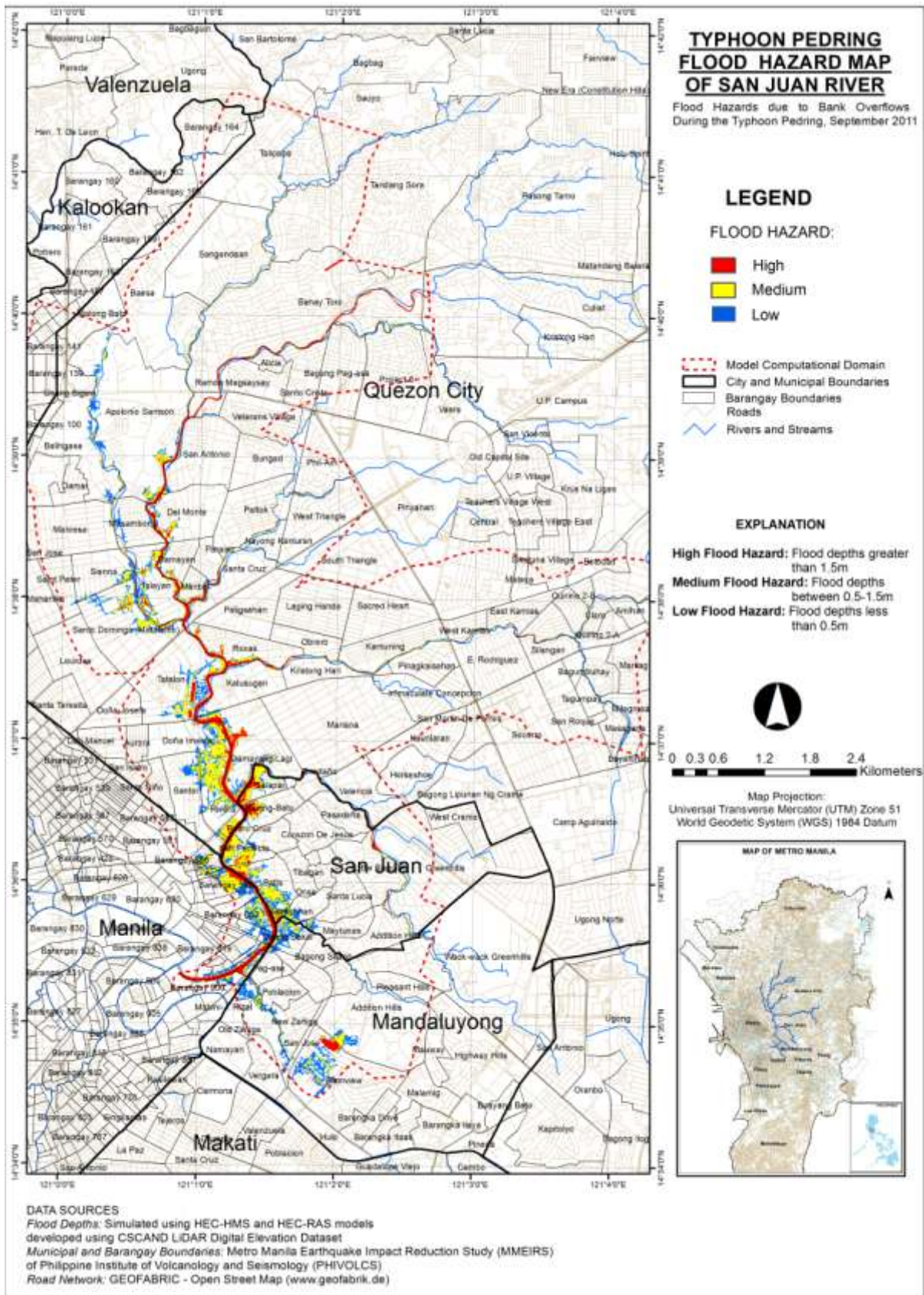
Figure 152. Simulated flood hazard map of San Juan River Basin for the September 2011 *Pedring* event.
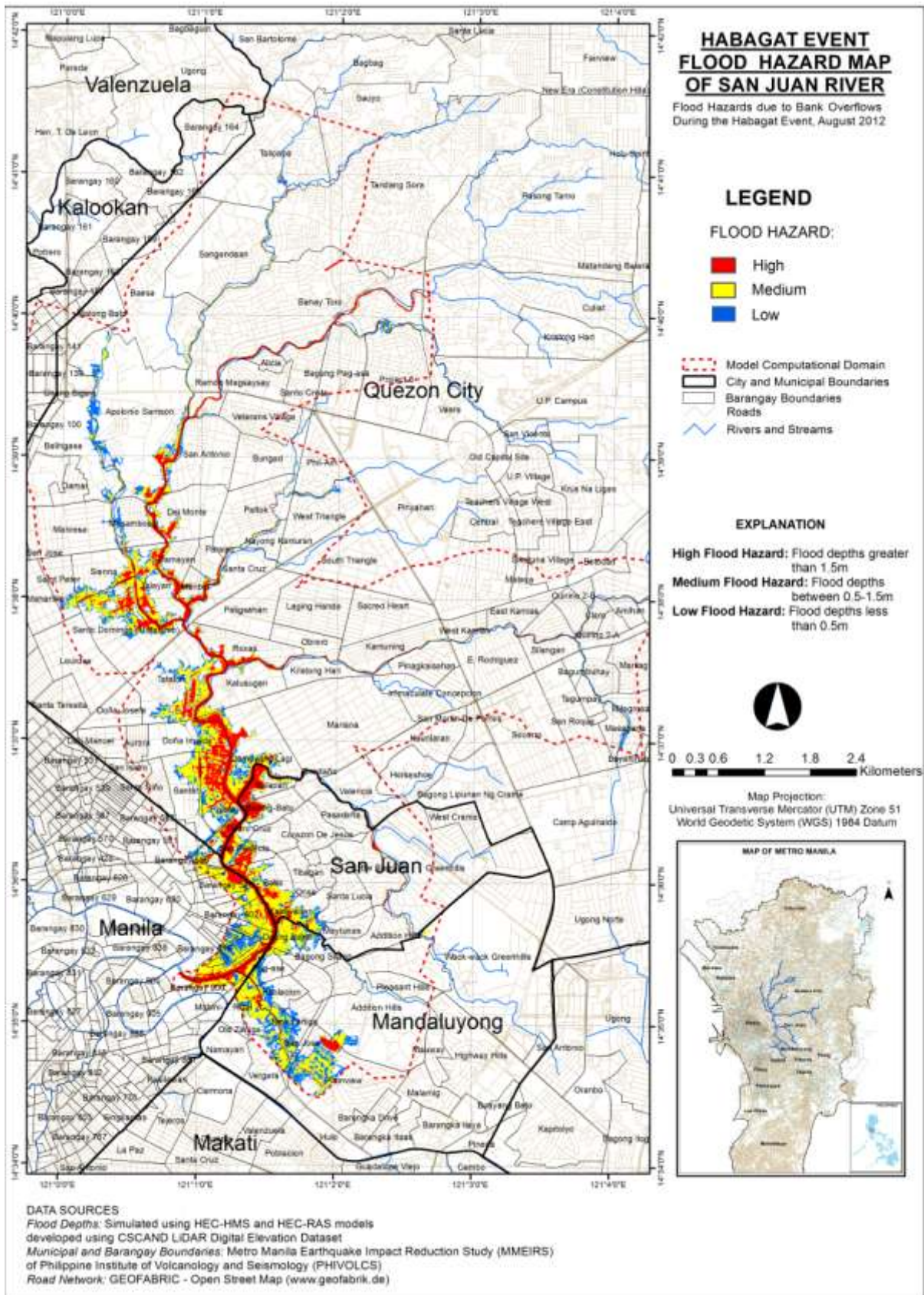
Figure 153. Simulated flood hazard map of San Juan River Basin for the August 2012 *Habagat* event.
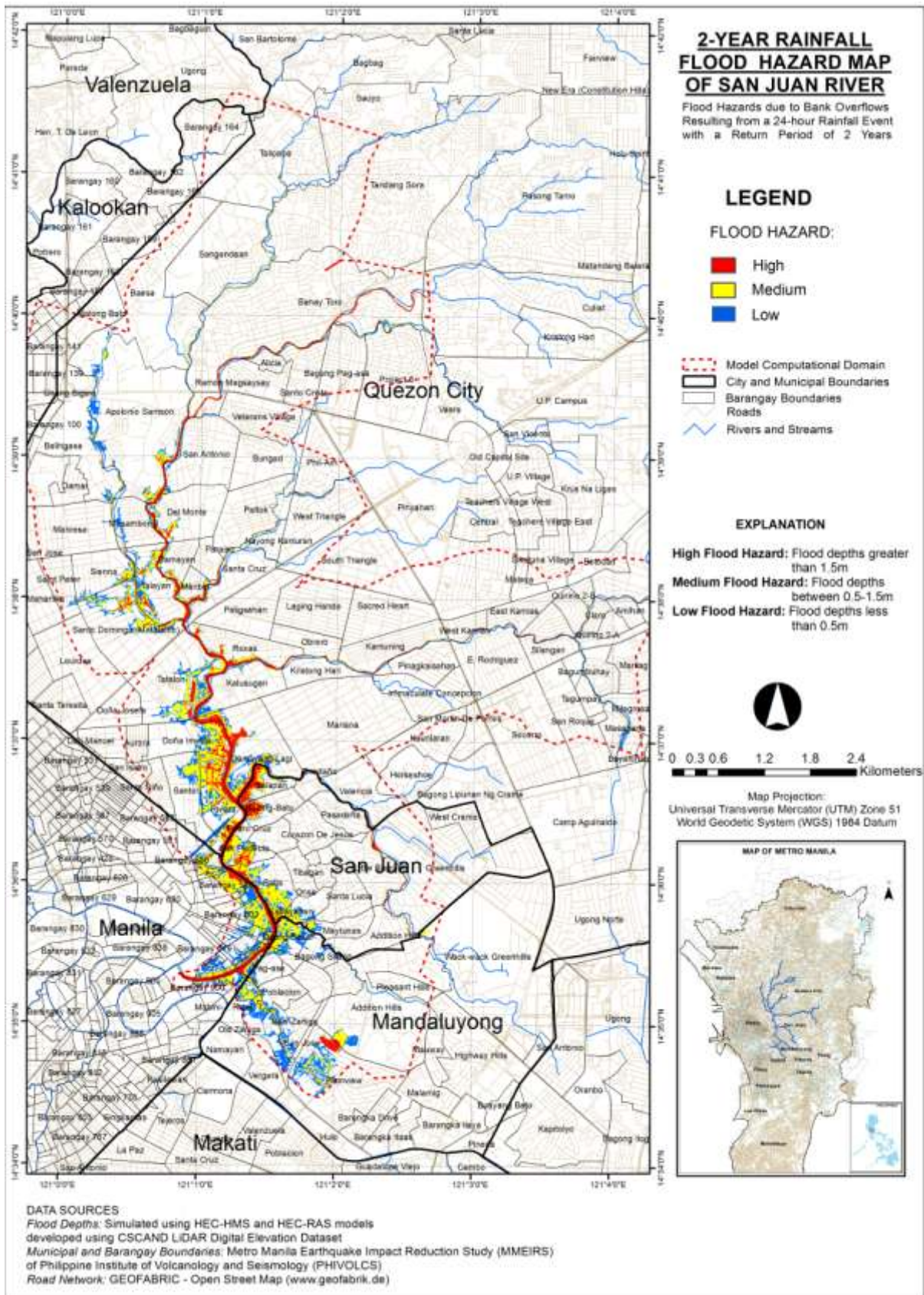
Figure 154. Simulated flood hazard map of San Juan River Basin for a 2-year rainfall event.
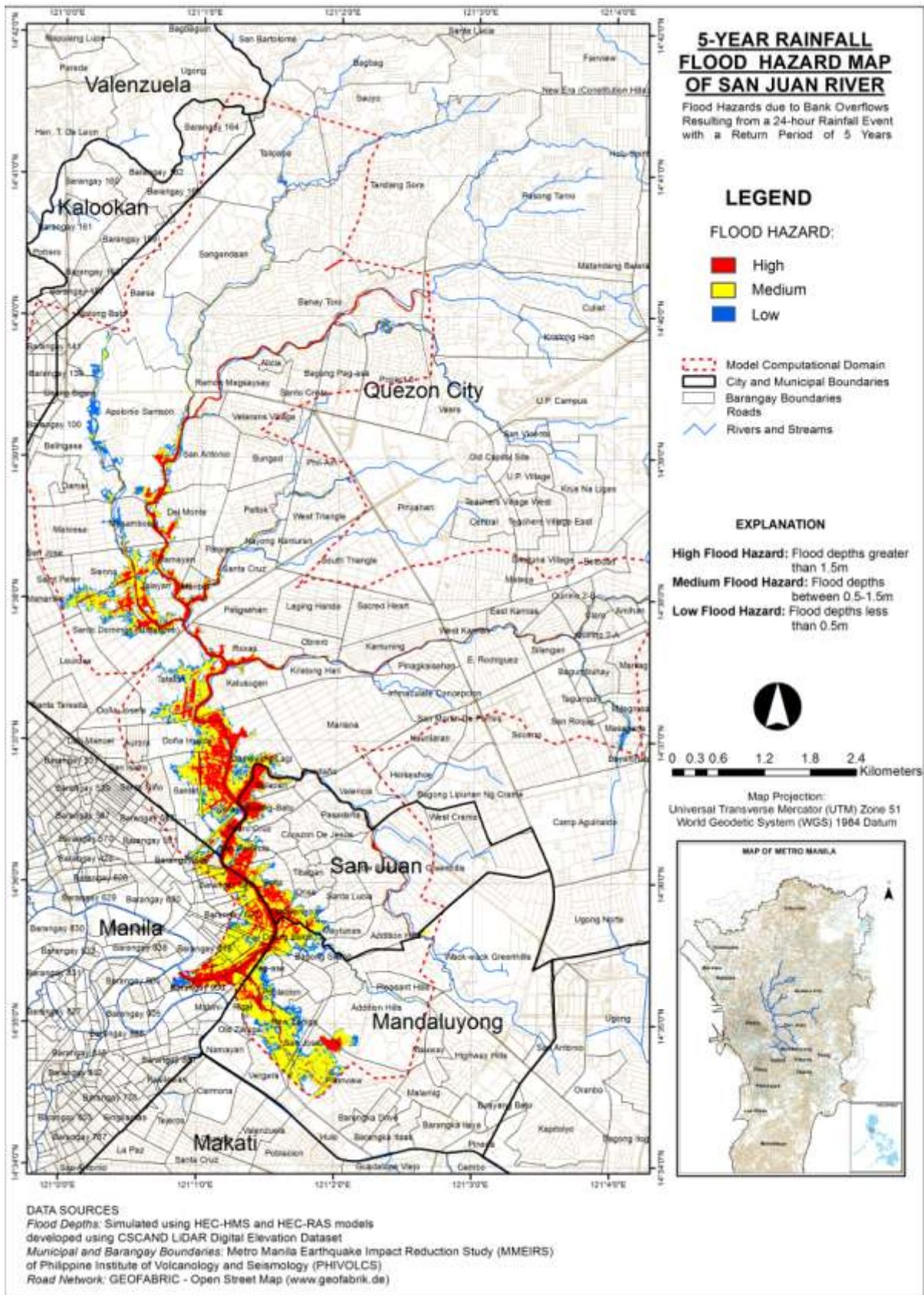
Figure 155. Simulated flood hazard map of San Juan River Basin for a 5-year rainfall event.
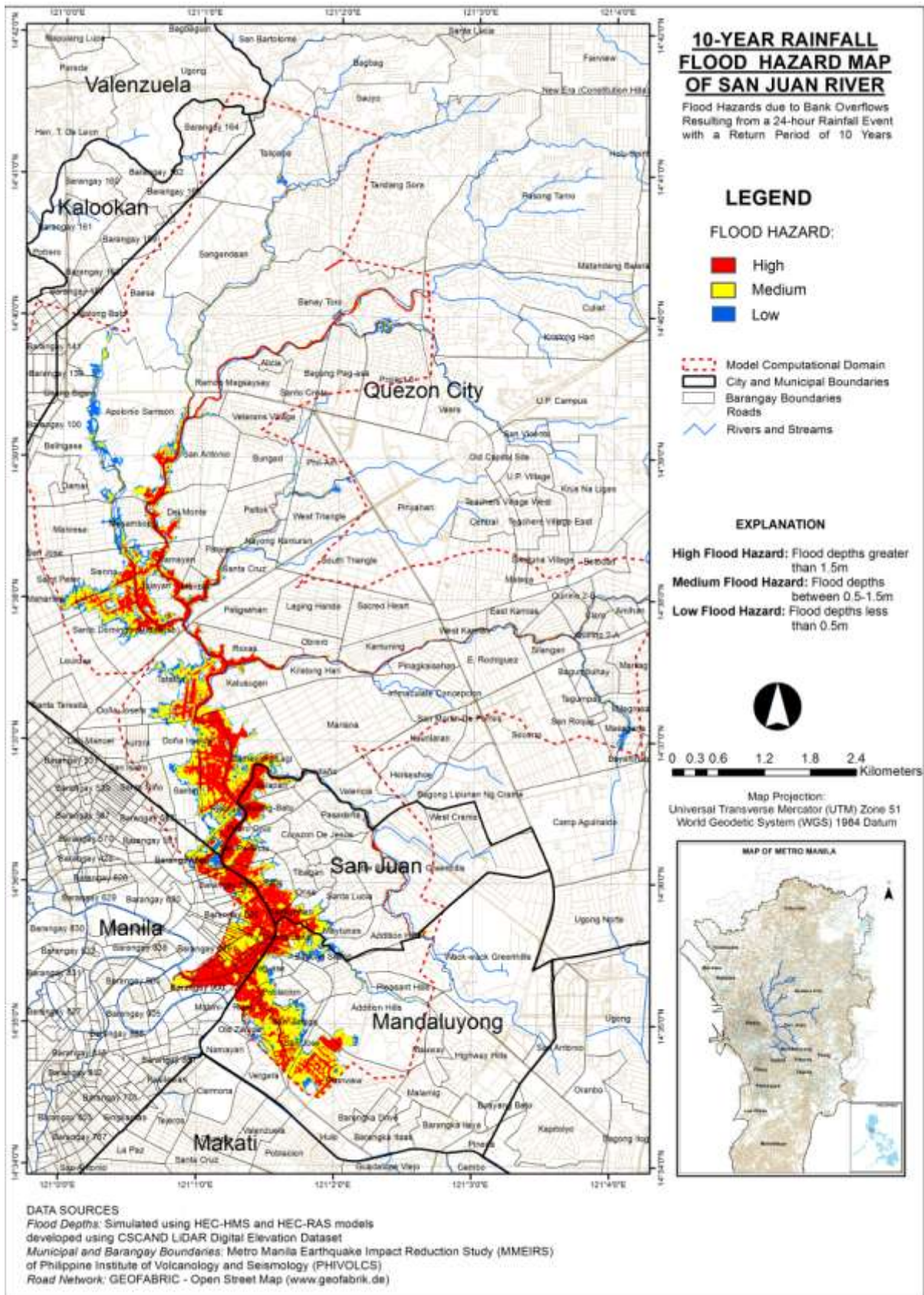
Figure 156. Simulated flood hazard map of San Juan River Basin for a 5-year rainfall event.
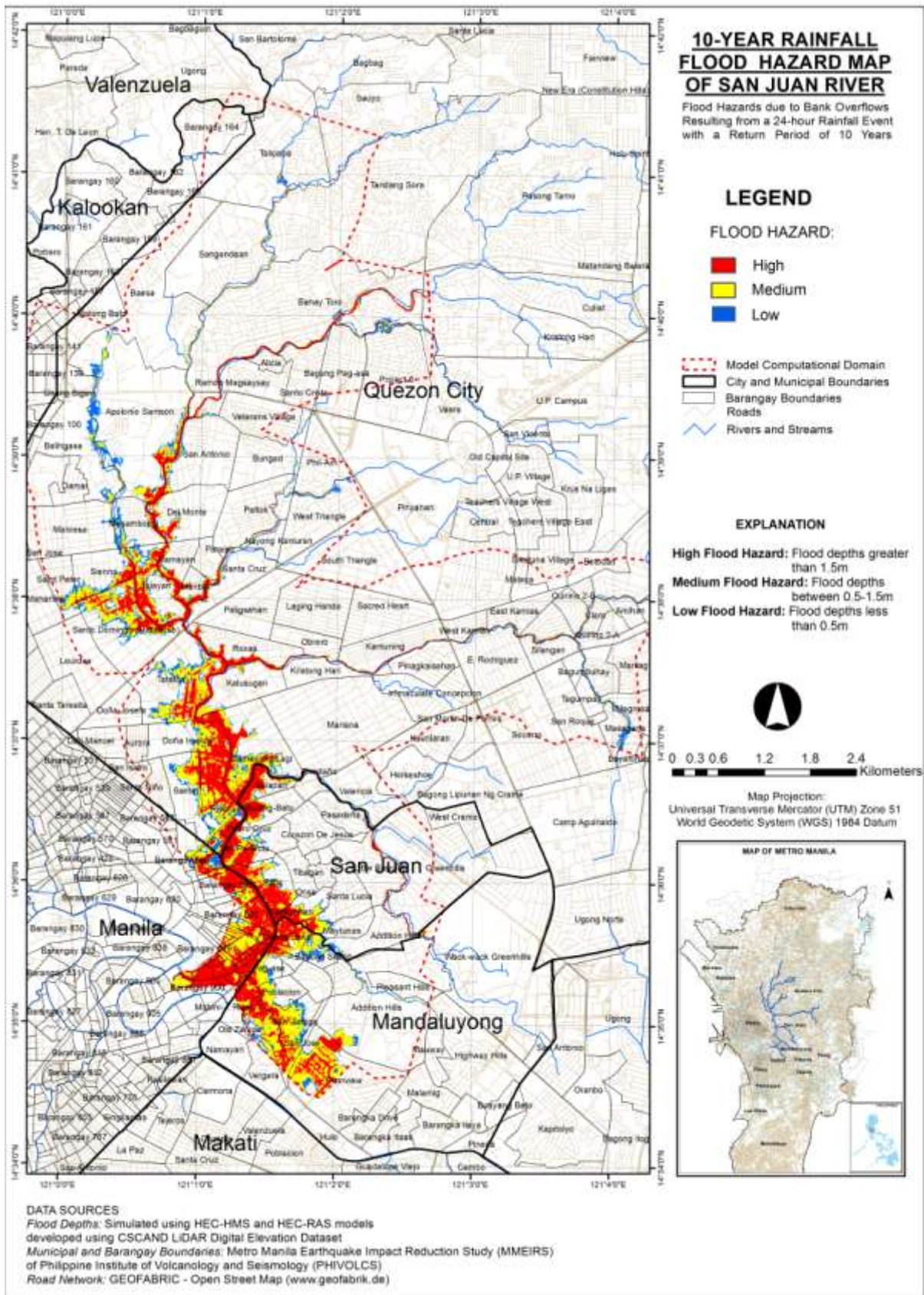
Figure 157. Simulated flood hazard map of San Juan River Basin for a 10-year rainfall event.
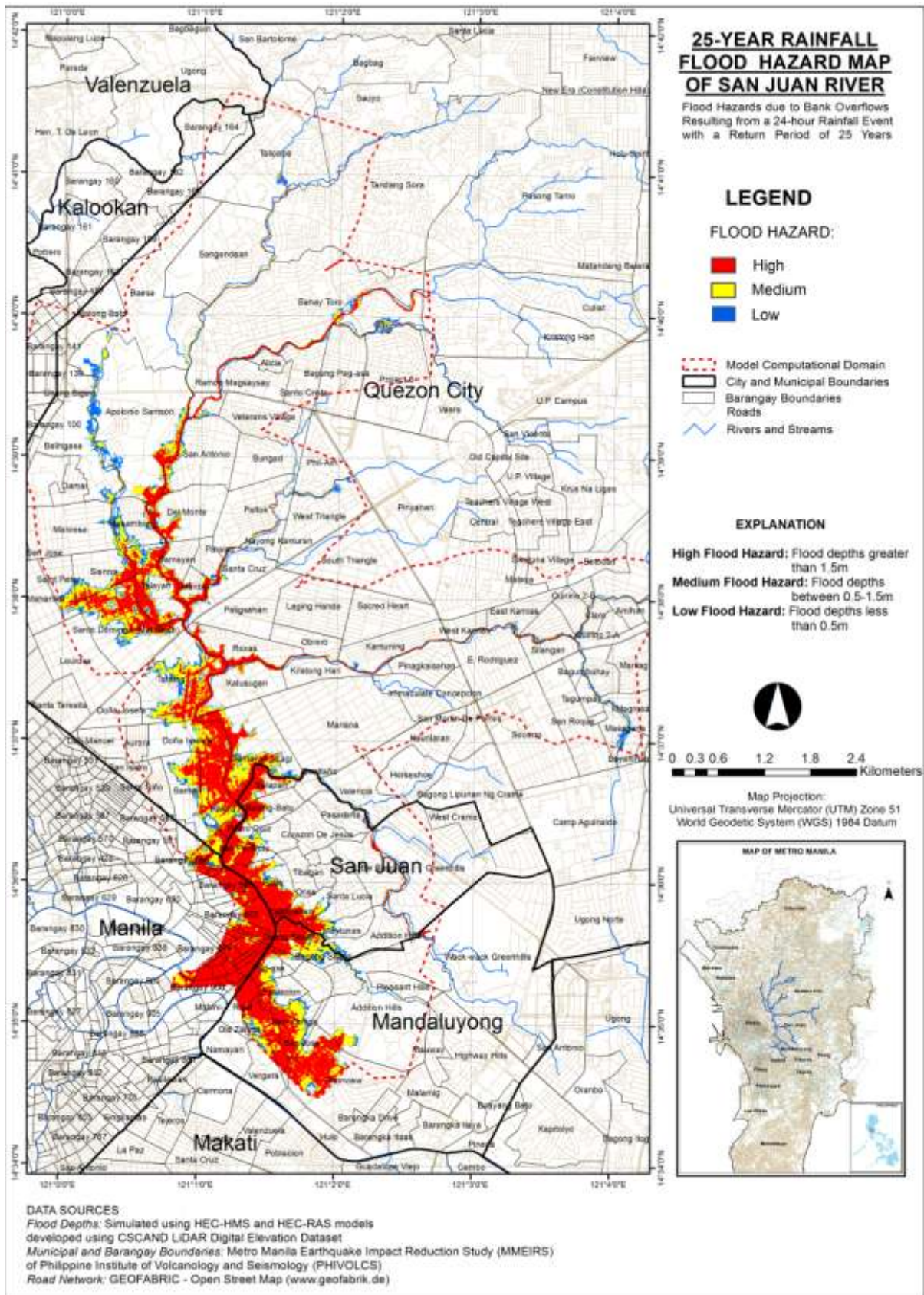
Figure 158. Simulated flood hazard map of San Juan River Basin for a 25-year rainfall event.
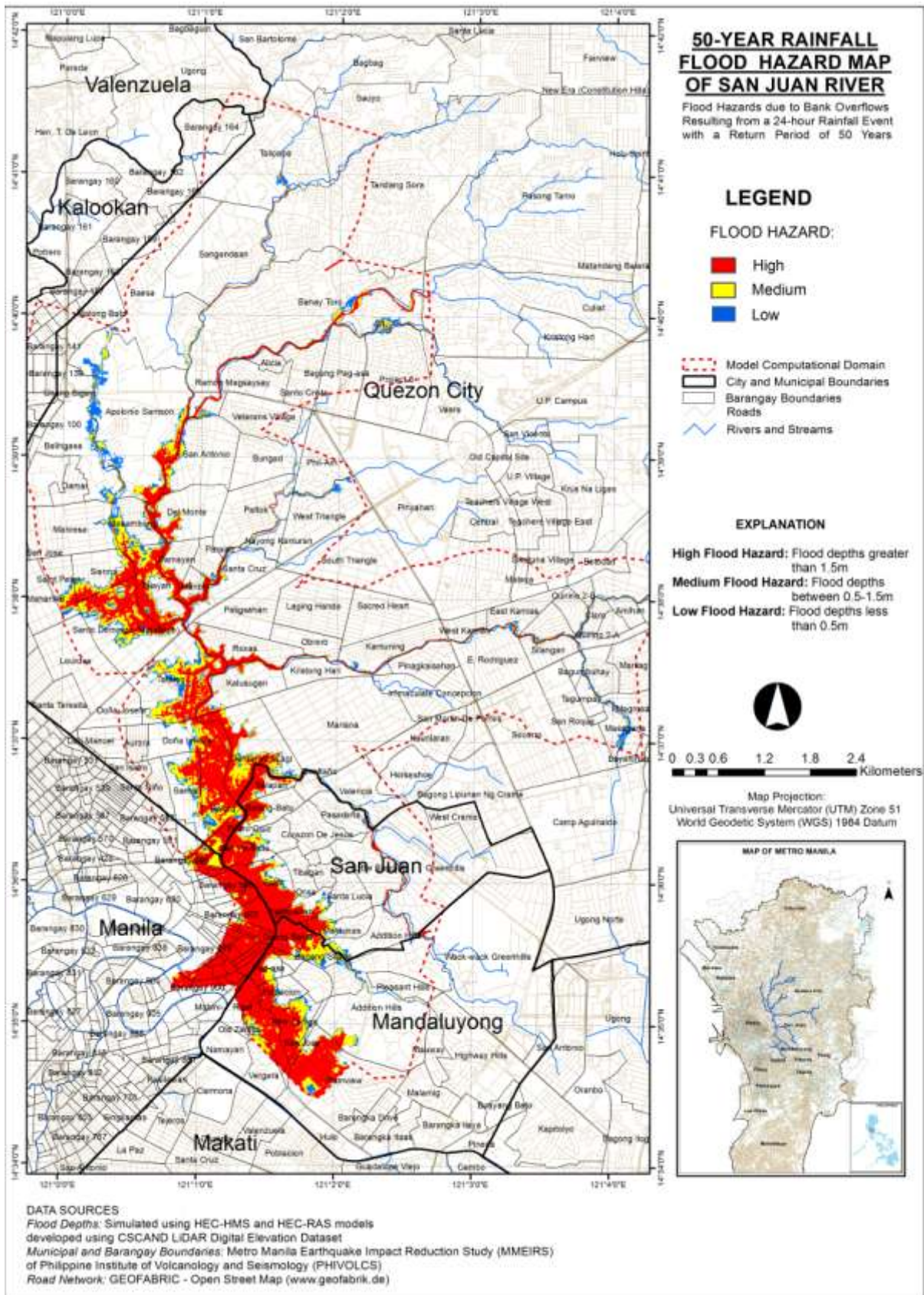
Figure 159. Simulated flood hazard map of San Juan River Basin for a 50-year rainfall event.
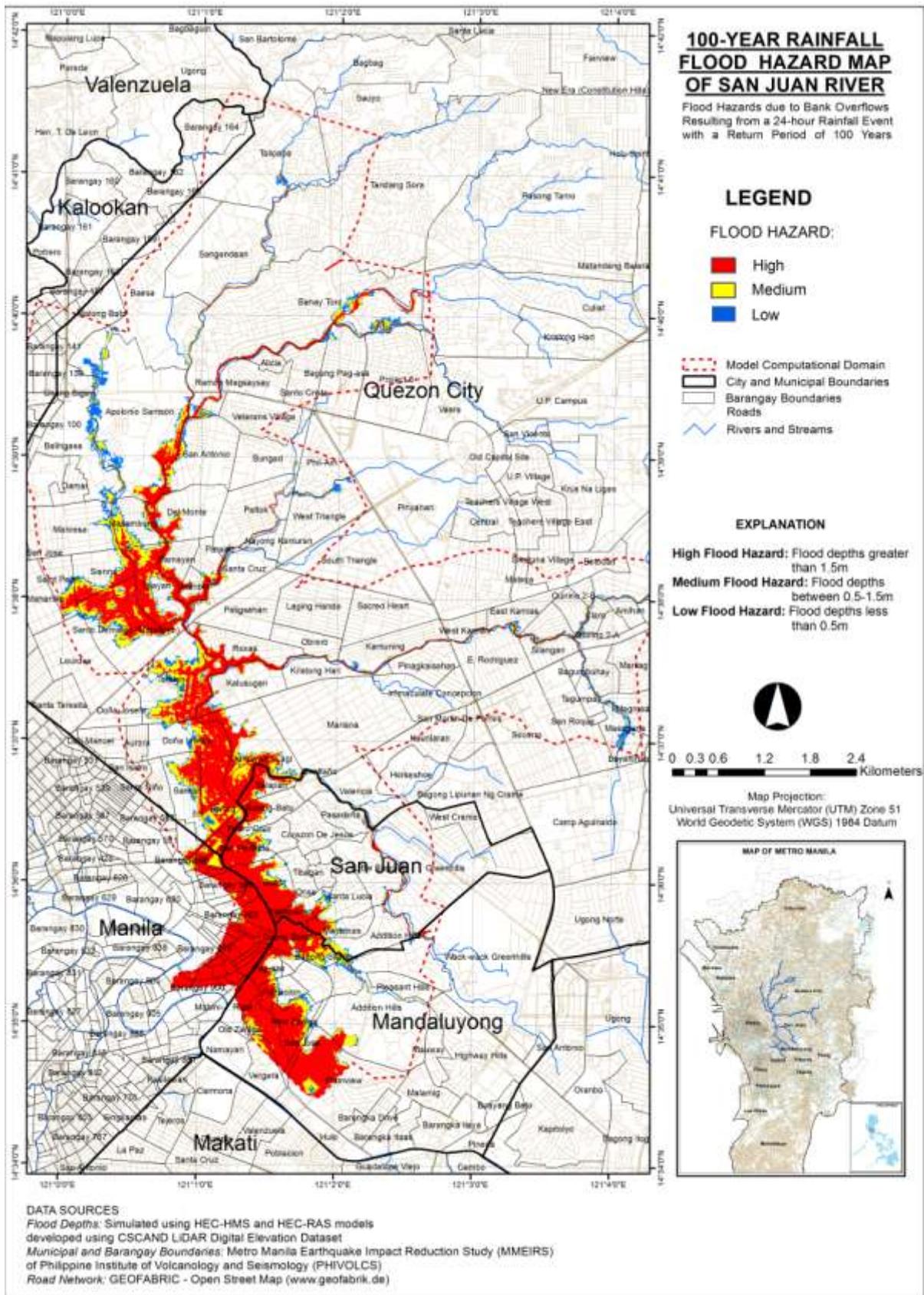
Figure 160. Simulated flood hazard map of San Juan River Basin for a 100-year rainfall event.

Chapter Summary and Conclusions

In this chapter, the development, calibration and validation of HEC HMS model of San Juan River Basin was presented. The model was found to have "good" performance in predicting discharge hydrographs at two upstream stations namely Quezon Avenue and E. Rodriguez, although the model simulated hydrographs did not perfectly matched those of the observed data.

One of the limitations during the calibration of the model was the effects of tide in the downstream portion of the model, especially at those sub-basins and reaches downstream of E. Rodriguez station. These parameters of these model elements were not subjected to optimization.

The calibrated model was then used to simulate discharge hydrographs of actual and hypothetical flood events. From the discharge hydrographs, peak flows were extracted and used as input to the HEC RAS model to create flood depth maps and flood hazard maps.

In general, the flood hazard maps indicate increase in areas affected by high hazards as rainfall events becomes extreme (e.g., from 2-year to 100-year). The areas most affected by high hazards are along San Juan River, San Francisco River, and Talayan Creek.

Should flood events similar in magnitude to the events simulated in this study occur again in the future, the flood hazard maps would provide important information for preparation, evacuation, and damage estimation. Essentially, the flood hazard maps generated show which areas are to be avoided if such flood events are expected to occur.

Chapter 9. Water Level Forecasting and Near-real Time Inundation Monitoring in Marikina, San Juan and Pasig Rivers: the I aM AWaRE app

This chapter presents the development of an automated system called I aM AWaRe - **I**nund**a**tion **M**onitoring **A**nd **W**ater Level Foreca**s**ting in **R**iv**e**rs. The system utilized the HEC HMS models presented in the previous chapters and HEC RAS models of the main sections of Marikina, San Juan and Pasig Rivers.

Design concept

During a flood event, there are two levels of information that are needed:

- information on the current extent of flooding along the river and the areas that are presently flooded; and
- forecasts on how water level will rise (or recede) at different locations along the river as rainfall events occur in the watersheds.

Usually, the first information can be obtained by direct observation (i.e., visiting the areas affected, taking pictures) but this is often difficult and risky. Alternatively, numerical models (i.e., flood models) can be used to estimate the current extent of flooding ("inundation") by utilizing water level recorded by monitoring stations in a river. Given that the geometry of the river is known before hand, the model can compute the level of water all throughout the river if the water level at the upstream and the downstream are known. Through GIS analysis, this can be converted to inundation extent.

The second information can be known by use of numerical models (i.e., watershed hydrologic models) that can compute how much runoff or "flood water" will be generated and goes down the river when a rainfall event occur. Since the effect of a rainfall event in making water level rise in rivers is not immediate (usually takes hours before it is felt downstream especially if much of the flood water will come from upstream watersheds), it is then possible to make a forecast on how water will rise or recede at different locations along the river.

Based on these concepts, it is very possible to generate these two levels of information during a flood event. And through the use of web geo-visualization technologies (Google Map, Google Earth), this information can be relayed through the internet for easy access by the public – this is what **I aM AWaRe** is all about.

Purpose

I aM AWaRe is developed with the aim to increase awareness and responsiveness of the public during flooding events by providing answers to the following questions:

- Is the river in my community have already overflowed?
- Where are the flooded areas?
- How large is the extent of flooding?
- Has the flooding receded?
- It is raining very hard right now. How high will the water level in the river be in the next hours?

Providing this kind of information during a heavy rainfall event is useful in informing the public as to the current extent and depth of flooding in rivers. It may assist in preparation for evacuation; and it may aid in identifying areas that need immediate action, in identifying areas that should be avoided; and in estimating the severity of damage as flooding progresses.

Framework

I aM AWaRe is built upon the framework (Figure 161) that numerical models must first be developed that can generate the needed information. The development of the model is crucial and requires data from several sources. Once the information is generated, it can then be uploaded to a web server. The user can access this information online through the use of third party application (Wordpress+Google Map).

Figure 161. I aM AWaRe framework.

Area of Application

I aM aWaRe covers three major rivers of Metro Manila, Philippines (Figure 162): Marikina River, San Juan River, and Pasig River. However, for water level forecasting, only Marikina River is covered at the moment. Although forecasts are generated for different locations along this river, the generation of this information is actually obtained by considering the whole Marikina River Basin.
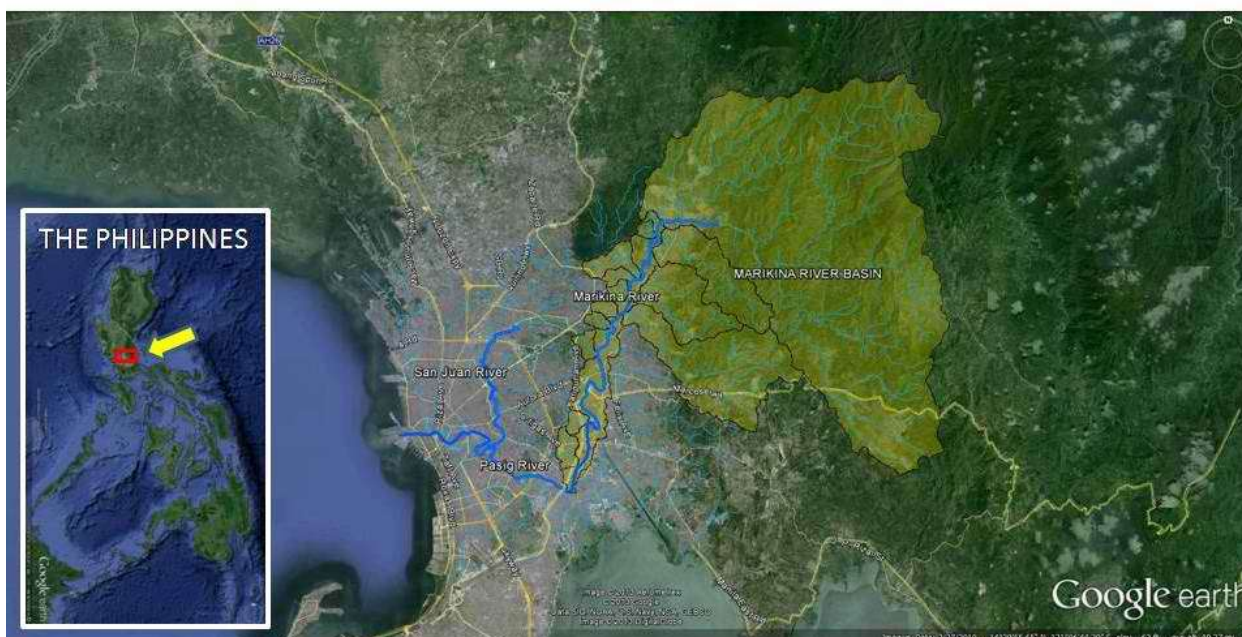
Figure 162. The area of application for I aM AWaRe.

Development of I aM AWaRe: system requirements, set-up and implementation

I aM AWaRe consists of three components:

- **Information Generation Component (IGC)** – computers running the models and upload new information to the server
- **Information Storage Component (ISC)** – a web server installed with Apache. The latest information (flood inundation extent and water level forecasts, in Keyhole Markup Language format) is uploaded here and accessed by the user through the online visualization component
- **Online Visualization Component (OVC)** – this is the I aM AWaRe web app (http://iamawareph.wordpress.com)

Information Generation Component

Three computers (one computer for each river) are used to run numerical models in order to generate information on the latest flood inundation and water level forecasts. The outputs from these computers are KML files. Each computer has the following specifications:

- CPU: Intel Core 2 Quad, 2.66 GHz
- RAM: 4 GB
- Windows 7 Professional OS

The following free software/programs necessary to generate the information are installed in the computers:
- HEC RAS 4.1 – used to generate flood inundation extent
- HEC HMS 3.5 – used to generate the water level forecasts

- HEC DSS Vue – used for the conversion of text files of water level and rainfall into a format recognizable by the HEC programs; also used to generate the forecast graphs
- FW Tools – a binary distribution of GDAL (Geospatial Data Abstraction Library – gdal.org) libraries and utilities that includes the OGR Simple Features Library for shapefile to KML conversion
- Python 2.7 – used to reformat text files, update model parameters; implement OGR's ogr2ogr.exe to do shapefile to KML conversion; and uploading of information to the server
- AutoIT – used to automate the HEC RAS program
- GNU wget – used to automatically download water level and rainfall data files

The flood inundation information is generated by HEC RAS models of the three major rivers. HEC RAS stands for "Hydrologic Engineering Center – River Analysis System". It is a one-dimensional flood model that utilizes river and flood plain geometric data (from topographic and hydrographic surveys and LiDAR digital elevation model-DEM), land-cover and surface roughness (from remotely-sensed images), and the latest water level data at specific locations of the river (e.g., at the upstream and downstream of a river) in order to compute water levels all throughout the river. Once these water levels are computed, the flooded or inundated areas along the river and in the floodplains are estimated by intersecting the water surface profiles into a high resolution LiDAR DEM. This is done through the "RASMapper", the GIS module of HEC RAS.

The interfaces of the three HEC RAS models of the main rivers are shown in Figure 163 to Figure 165.

In order to provide the latest inundation information, the HEC RAS simulation was completely automated starting from the input of latest water level data from the monitoring stations, to running the model and generating a GIS shapefile of inundation extents, to the conversion of this shapefile to KML, until it is uploaded to the data server and displayed in the I aM AWaRE app. The automation was done through the use of automation scripts (wget, python, AutoIT) while the conversion of shapefile to KML was done through python implementation of OGR (ogr2ogr.exe) based upon FW Tools' libraries and utilities. The output of the automated HEC RAS models are KML files of inundation extent (one KML per river). This whole process, summarized in Figure 166, is repeated every 10-minutes through Windows Task Scheduler.
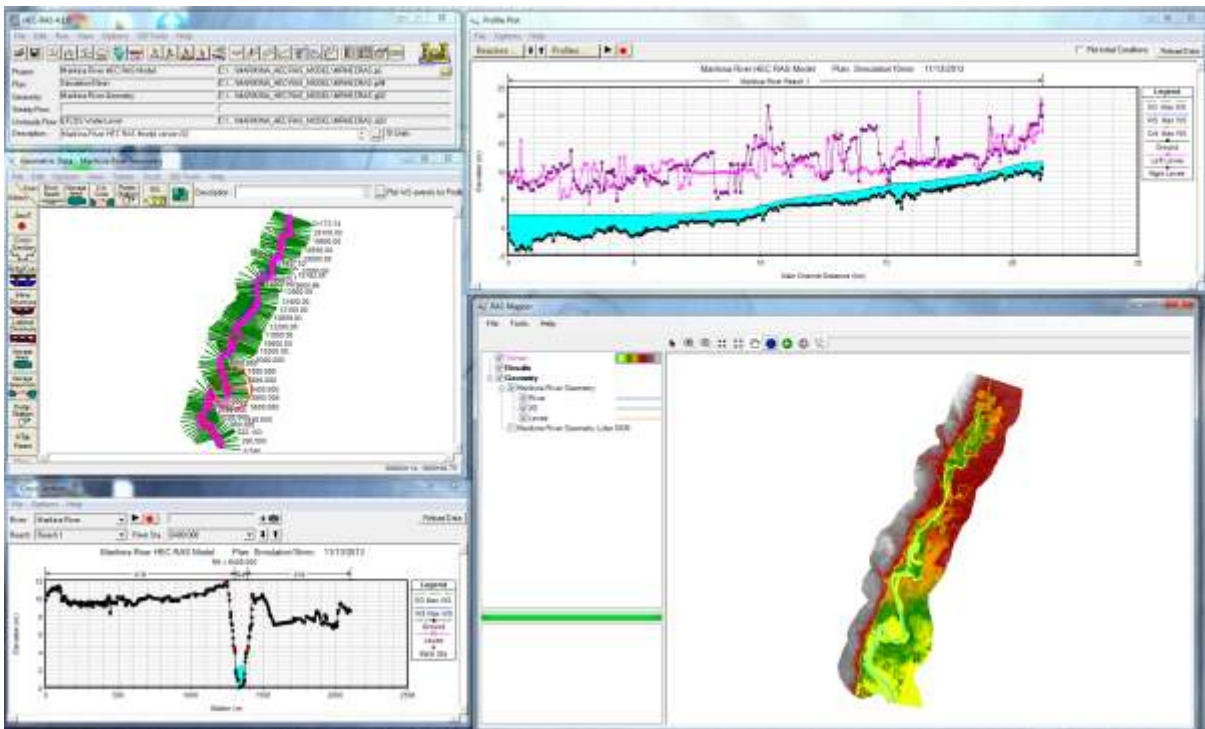
Figure 163. Interface of the Marikina River near-real time HEC RAS model.
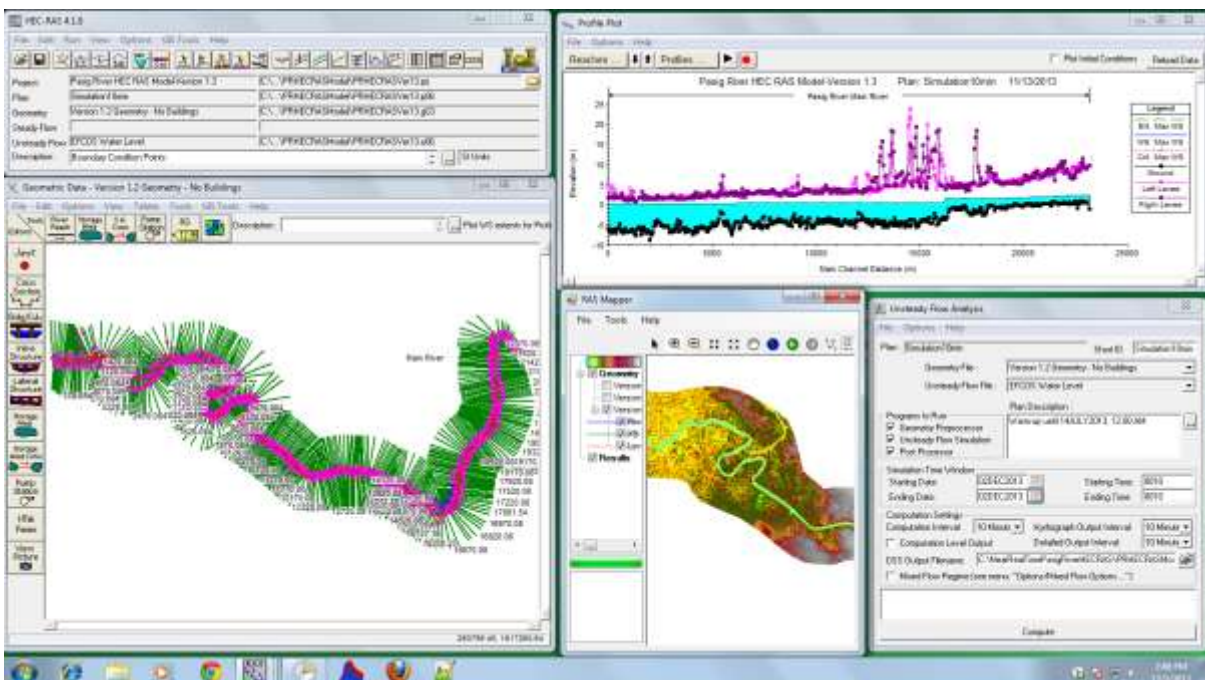
Figure 164. Interface of the Pasig River near-real time HEC RAS model.
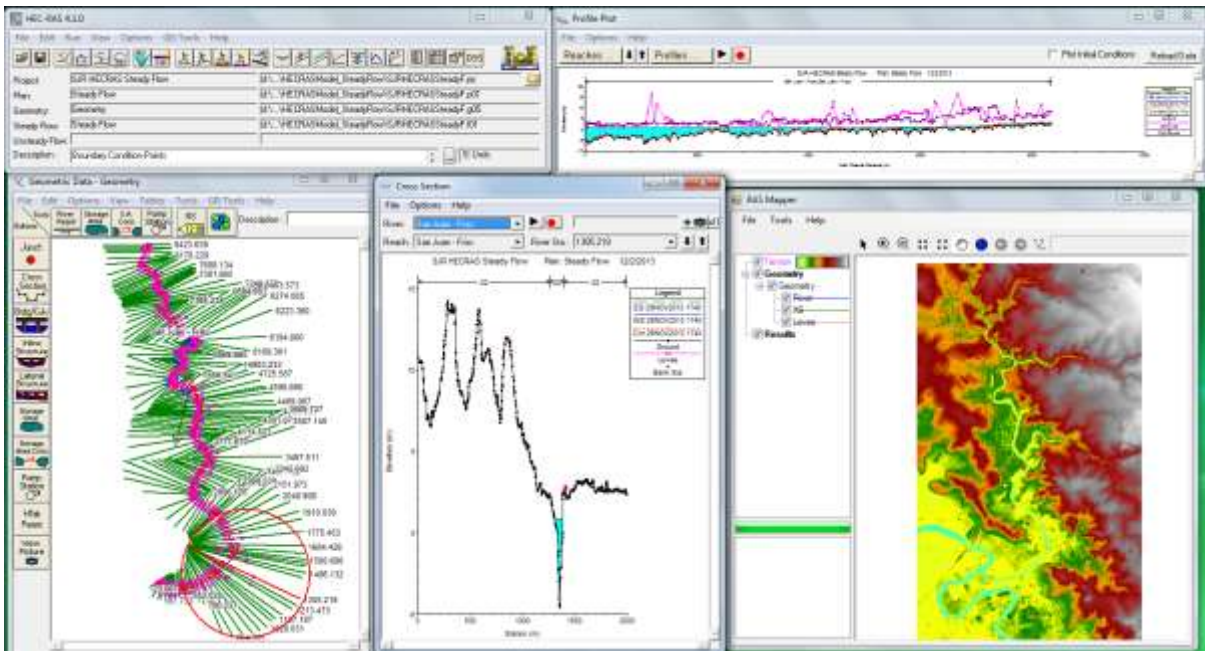
Figure 165. Interface of the San Juan River near-real time HEC RAS model.
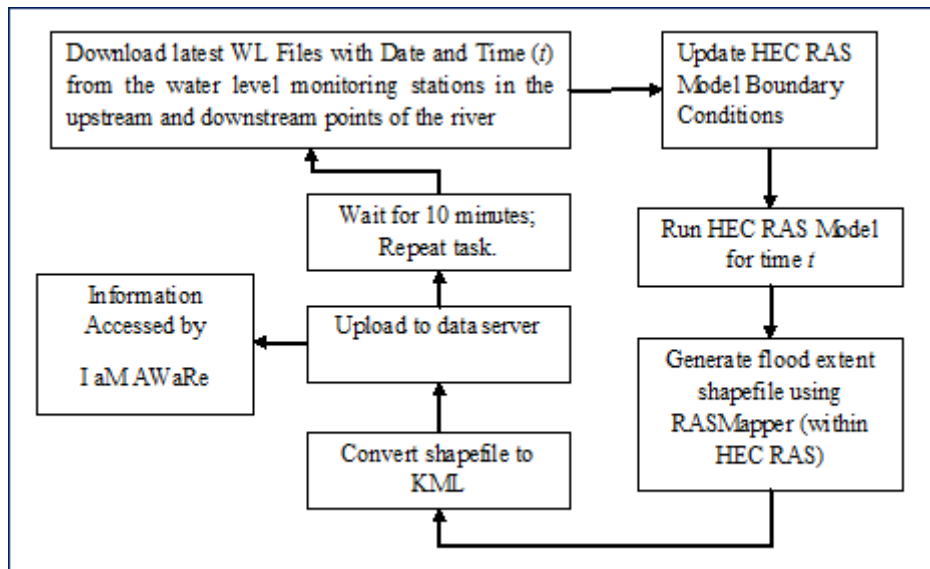
Figure 166. The process flow for generating flood inundation extents. The whole process is automated.

On the other hand, water level forecasts for Marikina River are results of model simulation of basin hydrology as well as river and flood plain hydraulics, using recorded data of rainfall events 3 days ago to present time as primary input of the models. This means that

water levels at specific locations along Marikina River (MONTALBAN, STO. NINO, ROSARIO) for the next 48 hours are computed using the model to estimate the effect of rainfall events, if there are any, that have occurred 3 days ago to present time in the Marikina River Basin. The effects of possible rainfall events in the next 24 or 48 hours are not simulated, although it is possible to incorporate rainfall forecasts into the model. Each time the model generates a forecast (i.e., every 5 minutes), rainfall data from nearest active rainfall stations are utilized using an inverse-distance approach. The starting water level for the forecast is computed based on the latest water level data from the monitoring stations which are also downloaded. The forecast model (which has been calibrated and validated, as presented in Chapter 5) is based on the United States Corps of Engineers (USACE) Hydrologic Engineering Center – Hydrologic Modeling System (HEC HMS). The model was completely automated (from data input to output) using a combination of wget, Python, Jython and native HEC HMS scripts. The outputs of the automated HEC HMS are tabular files of water level forecasts which are then plotted into forecast graphs through HEC DSSVue. The forecast graphs are then uploaded to the server using a python script. This whole process, summarized in Figure 167, is repeated every 10-minutes through Windows Task Scheduler.
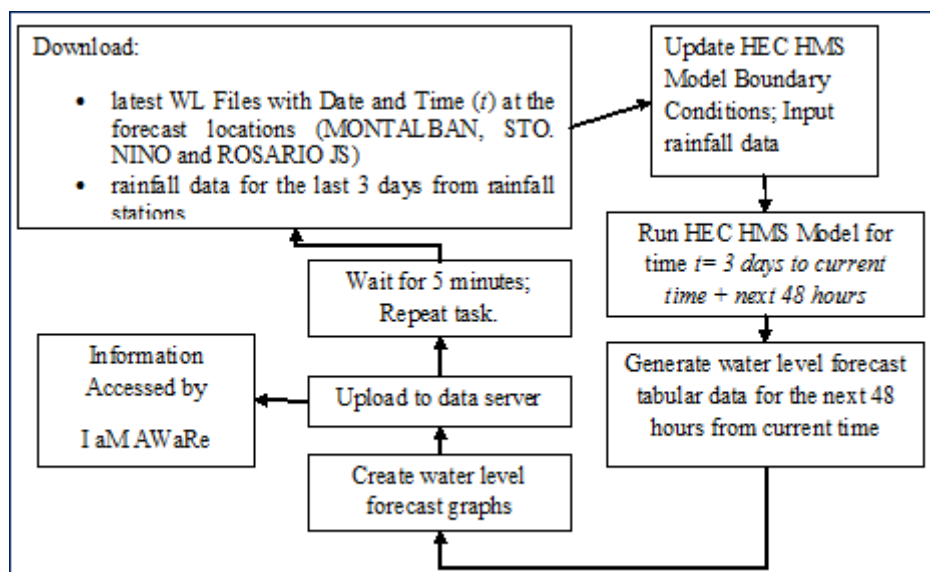
Figure 167. The process flow for generating water level forecasts. The whole process is automated.

The development of I aM AWaRe was actually started by the **Marikina RELiEF web application** (http://mrbforecast.wordpress.com/). I aM AWaRe can be said to be an upgraded version of Marikina RELiEF because flood inundation information is already included in the I aM AWaRe app.

Information Storage Component

A data server (HP Z800, Intel Xeon, 32GB RAM installed with Apache) which is connected to the internet is used to store the KML files of inundation extents and JPEG files of water level forecast graphs. In order for this files to be viewable in a web browser, a

"mother" KML file is created wherein the three KML files and the JPEG files are "network-linked" (i.e., KML files within a KML file, linked to their source files in the data server). This mother KML file is the one called by the I aM AWaRe app in order to display the inundation extents and forecast graphs. Note that only the KML files of inundation extents and the JPEG files are updated every 10-minutes not the mother KML file.

Online Visualization Component

The OVC consist of Google Map embedded in a WordPress.com free web site (http://iamawareph.wordpress.com, Figure 168). The HTML codes for the embedded Google Map was generated by calling the mother KML file in map.google.com (i.e., putting the link to the mother KML file in Google Map's search button), and then using available tools in Google Map to set the map size to 800 x 800 resolution. The application is best viewed in the latest version of Mozilla Firefox.

There are advantages in using Google Map and WordPress as hosts for I aM AWaRE:

- there is no need to develop and maintain a geodata server (like MapServer, GeoServer and the like) because everything needed is already provided, and for free
- there is no need to maintain hardware of the website; the app rides on WordPress which is accessible all the time
- fast delivery of information — the end-user's browser only needs to download the KML files from the data server; other information are provided by Google Map
- Google Map has the basemap and background information necessary to supplement the information delivered by I aM AWaRe such as, but not limited to:
    - Road network
    - Placemarks
    - High resolution satellite imagery showing built-up areas and other land-cover classes that can be used to assess/estimate areas affected and the amount of damage during flood events
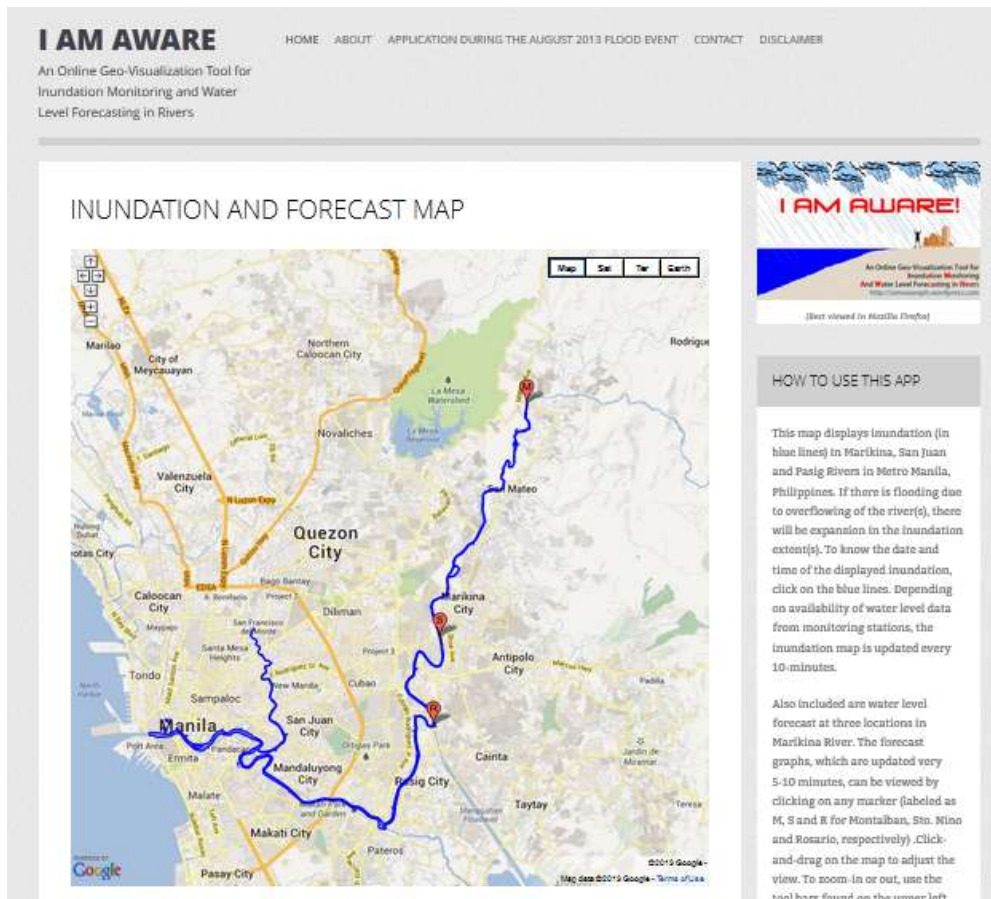
Figure 168. The interface of I aM AWaRe as accessed online via http://iamawareph.wordpress.com

Functions of I aM AWaRe

The app is very easy to use. The map displays inundation (in blue lines) in Marikina, San Juan and Pasig Rivers in Metro Manila, Philippines. If there is flooding due to overflowing of the river(s), there will be expansion in the inundation extent(s). To know the date and time of the displayed inundation, one just need to click on the blue lines. Depending on availability of water level data from monitoring stations, the inundation map is updated every 10 minutes. Also included are water level forecast at three locations in Marikina River. The forecast graphs, which are updated every 5-10 minutes, can be viewed by clicking on any marker (labeled as M, S and R for Montalban, Sto. Nino, and Rosario, respectively).

Default Google Map buttons are available for use in the I aM AWaRe web app. This includes:

- Zoom-in
- Zoom-out
- Pan
- Option to view a larger map of the app in map.google.com ("View Larger Map" button is available)
- Options to view different backgrounds:
    - Street Map View ("Map")
    - Satellite Imagery View ("Sat")

- Street Map with Terrain ("Ter")
- 3D Imagery View ("Earth")

Application of I aM AWaRe during the August 2012 Flooding in Metro Manila

Starting August 17, 2013, heavy to torrential rains were pouring over Metro Manila and nearby provinces. Raining continued for more than 3 days and caused flooding in different areas, most especially in the vicinity of Marikina, San Juan and Pasig Rivers. During these times, the flood inundation and water level forecasting models are providing inundation extents and water level forecast in near-real time at an interval of 10 minutes. Figure 169 shows a snapshot of the application of I aM AWaRE during this kind of events. This is also available in the online application.
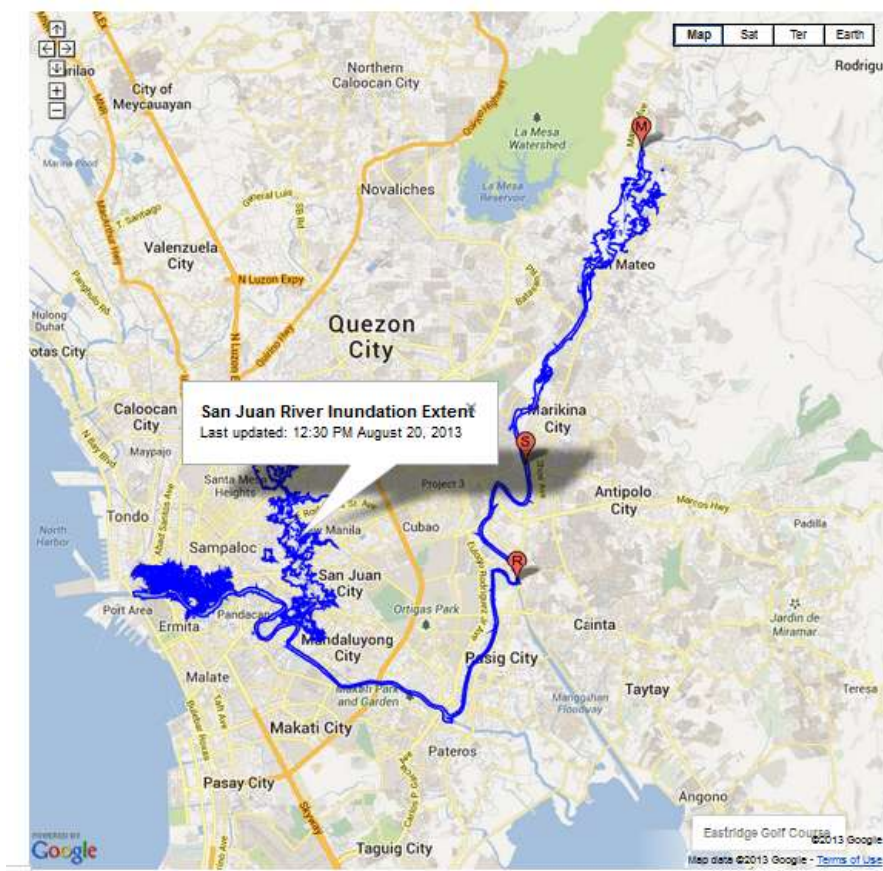
Figure 169. A snapshot of the application of I aM AWaRE during the August 2013 flooding in Metro Manila. This is also available online.

Availability of Flood Inundation Information in Project Noah

The flood inundation extent information generated for the three rivers have been contributed to the Project NOAH (Nationwide Operational Assessment of Hazards) of the Philippine's Department of Science and Technology at http://noah.dost.gov.ph. The information is accessed by clicking on *Flood Map –> Flood Inundation Monitoring*.

Although it is already made available in Project NOAH, a more dedicated app just like I aM AWaRe is necessary especially if we only wanted to get informed about current inundation condition in rivers as well as forecast of water levels.

Limitations

I aM AWaRe can only provide flood inundation extents and water level forecasts based on available water level and rainfall datasets:

- o If a water level monitoring station (at the upstream or downstream or both) have stopped recording water level data, latest flood inundation information will not be generated and only the last generated information will displayed
- o The water level forecasting model will continue to provide forecast even if one or more rainfall stations have stopped recording data. When this happens, the model will utilize rainfall data from other "active" rainfall stations. This may lead to inaccurate forecast as rainfall data may be incomplete.
- o Also, the water level forecasting model will continue to provide forecast even if one or more water level monitoring station have stopped recording data. In this case, water level data used to "initialize" the model will use the last recorded data. This may lead to inaccurate forecast as the starting water level data for the forecast is not based on "current" conditions of the river.

At the moment, only flood inundation extents are displayed in I aM AWaRe. The next updates will include the display of flood depths (both for current conditions and for forecasted conditions.)

Chapter 10. Two-dimensional Approach in Modeling Floods in Marikina River

The combined HEC HMS-HEC RAS flood developed and presented in the previous chapters showed acceptable performance in simulating actual and hypothetical flood events in Marikina River. However, since HEC RAS is a 1-D flood model, it cannot portray very well the evolution of flooding, especially as water from the upstream watersheds enters Marikina River, its overflow from the river banks, and the flood propagation from the banks towards the floodplain. Also, a 1D model does not provide details on velocity distribution, for instance across flood plains . It may also falsify reality especially in the case when flooding waters leave the main channels, reaching floodplains, with no returning to the rivers, having their own ways over the watershed. These limitations can be addressed by the use of 2D hydraulic model. 2D models provide a higher order representation of river hydraulics more consistent with known processes, include a continuous representation of topography and require no secondary processing step to determine the flood inundation [62].

In this chapter, a two dimensional approach of modeling floods in Marikina River is presented. The HEC HMS model is still used to generate upstream watershed discharge hydrographs as model boundary condition data. For hydraulic modeling, a 2D model based on the Environmental Fluid Dynamics Code (EFDC) is used instead of HEC RAS. The model domain and upstream boundary condition locations are the same as that of HEC RAS.

EFDC Model Development

The Environmental Fluid Dynamics Code (EFDC) [63] is a state-of-the-art hydrodynamic model that can be used to simulate aquatic systems in one, two, and three dimensions. It has evolved over the past two decades to become one of the most widely used and technically defensible hydrodynamic models in the world [64]. EFDC uses stretched or sigma vertical coordinates and Cartesian or curvilinear, orthogonal horizontal coordinates to represent the physical characteristics of a water body. It solves three-dimensional, vertically hydrostatic, free surface, turbulent averaged equations of motion for a variable-density fluid. Dynamically-coupled transport equations for turbulent kinetic energy, turbulent length scale, salinity and temperature are also solved. The EFDC model allows for drying and wetting in shallow areas by a mass conservation scheme.

In this study, only the 2D hydrodynamic module of EFDC was used. EFDC solves the shallow water equations (with the hydrostatic and Boussinesq approximations) using a combination of finite volume and finite difference techniques on curvilinear structured grids in the horizontal. For the theoretical and computational aspects of the EFDC model, the reader is referred to [63] and [65].

EFDC model development and parameterization was done using EFDC_Explorer 7.1, a Windows-based pre- and post-processor of EFDC [**66**].

The development of the 2D EFDC model for Marikina River involves subdividing the model domain into square cells of 20 x 20 m resolution (total of 147,903 cells). A better resolution of less than 20 x 20 m is also possible but due to computational constraints (e.g., very long computation time), this was not done.

The average elevation of each cell was obtained from the 1-m updated LIDAR DEM. Each cell was also assigned spatially distributed surface roughness values using the roughness map derived from the ALOS-AVNIR 2 satellite image.

Model boundary condition (BC) data consisting of HEC HMS-simulated discharge hydrographs at the upstream BC points (inflows) and time series of water level elevations at the outlet were then fed into the model. Unlike in HEC RAS, internal flow boundary condition data was not set in the EFDC model. In this way, the evolution of water from the upstream watersheds can be modelled realistically as they enter Marikina River.

Using the EFDC model, the *September 2009 Ondoy*, the *September 2011 Pedring* and the *August 2012 Habagat* were simulated at 1-second time step. Flooding due to hypothetical rainfall events of varying return periods (2, 5, 10, 25, 50 and 100) were also simulated.

2D Flood Simulation Results

Shown in Figure 170 to Figure 174 are snapshots of the 2D simulation of actual flood events.

The results illustrate the usefulness of the 2D model in the reconstruction of flooding that had occurred in Marikina River, especially that of the *September 2009 Ondoy* event. In Figure 170, the evolution of flooding from the start of the *Ondoy* event (5:20 PM, Sep 25) is clearly manifested by the EFDC model. At the start, there is already minimal flooding in areas downstream of San Jose Bridge, in San Mateo Rizal. At 12:00 AM, Sep. 26, increase in flood depth is already visible although the extent of flooding has not yet started to increase. Simultaneous increase in flood depth and extent became visible starting 3:00 AM. At 12:00 PM, Sep. 26, larges areas in the upstream of Marikina River, specifically in Rodriguez and San Mateo, Rizal, has already been flooded. Flooding in areas downstream (e.g., Marikina City) is still minimal at this time. But after just an hour (1:00 PM, Sep. 26), the whole stretch of Marikina River, from Rodriguez to Pasig City has already overflowed. Overflowing of Marikina River continued and already reached portion of Cainta, Rizal by 4:00 PM. Overflowing water continued to travel and has inundated portions of Antipolo City by 5:00 PM, and this continued even until 12:00 PM of Sep. 29.

The results of the 2D flood simulation is very informative as it appears that overflowing water from Marikina River also contributed to flooding in areas more than 2 kilometers from the banks of Marikina River (e.g., Antipolo City and Cainta. The magnitude

of the event is therefore extreme. It was also shown by the simulation that although significant volume of water has overflowed downstream, flooding in the upstream (e.g., Rodriguez and San Mateo, Rizal) is still significant.

Compared to the flooding extent due to *Pedring 2011* and *Habagat 2012*, the extent due to Ondoy 2009 is very large.
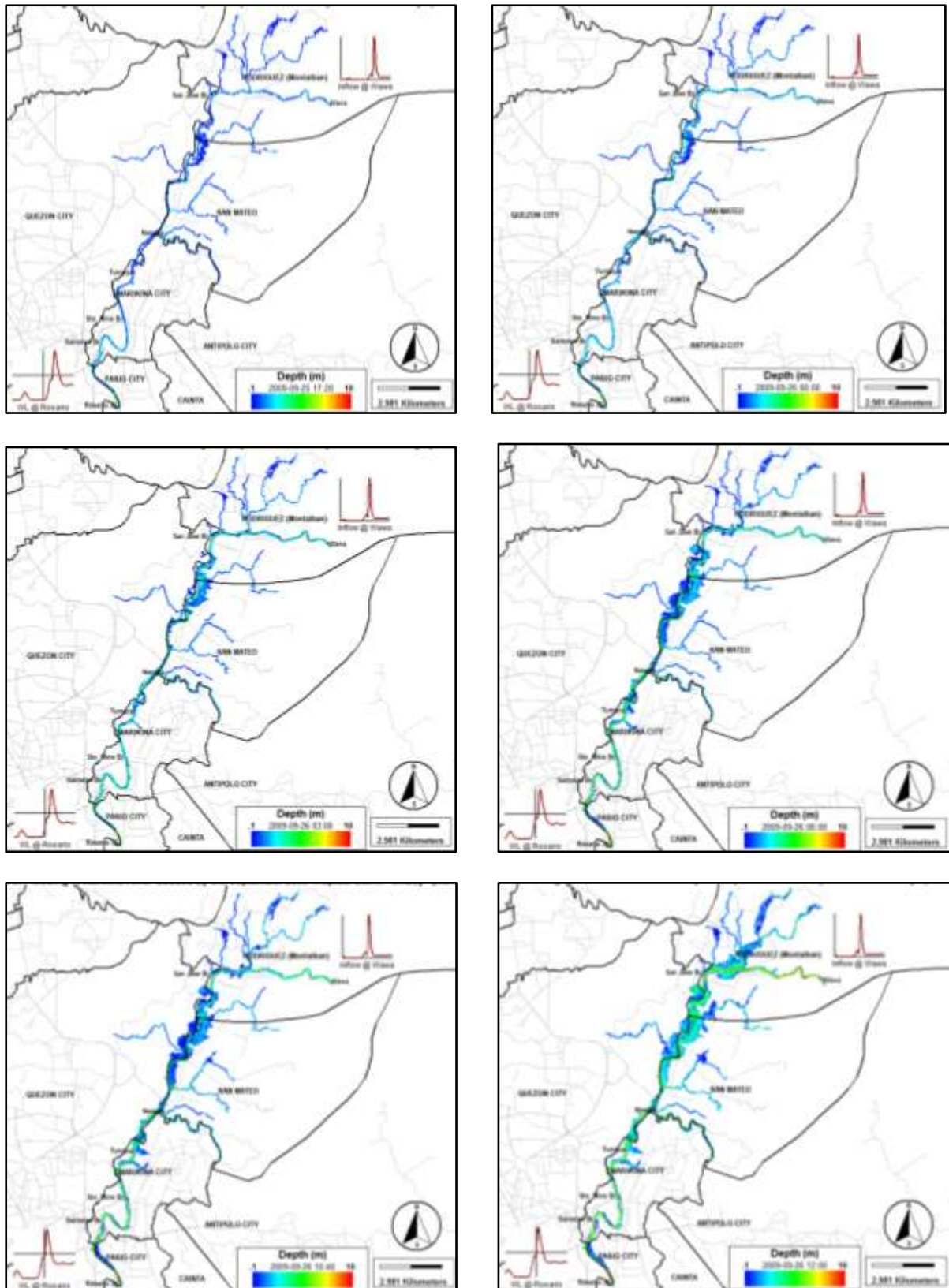
Figure 170. Snapshots of the evolution of flooding during the *September 2009 Ondoy* event in Marikina River and tributaries as simulated by the 2D EFDC model. The figure shows depths during the start of rainfall event (5:20 PM, Sep. 25) until 12:00 PM of Sep. 26.
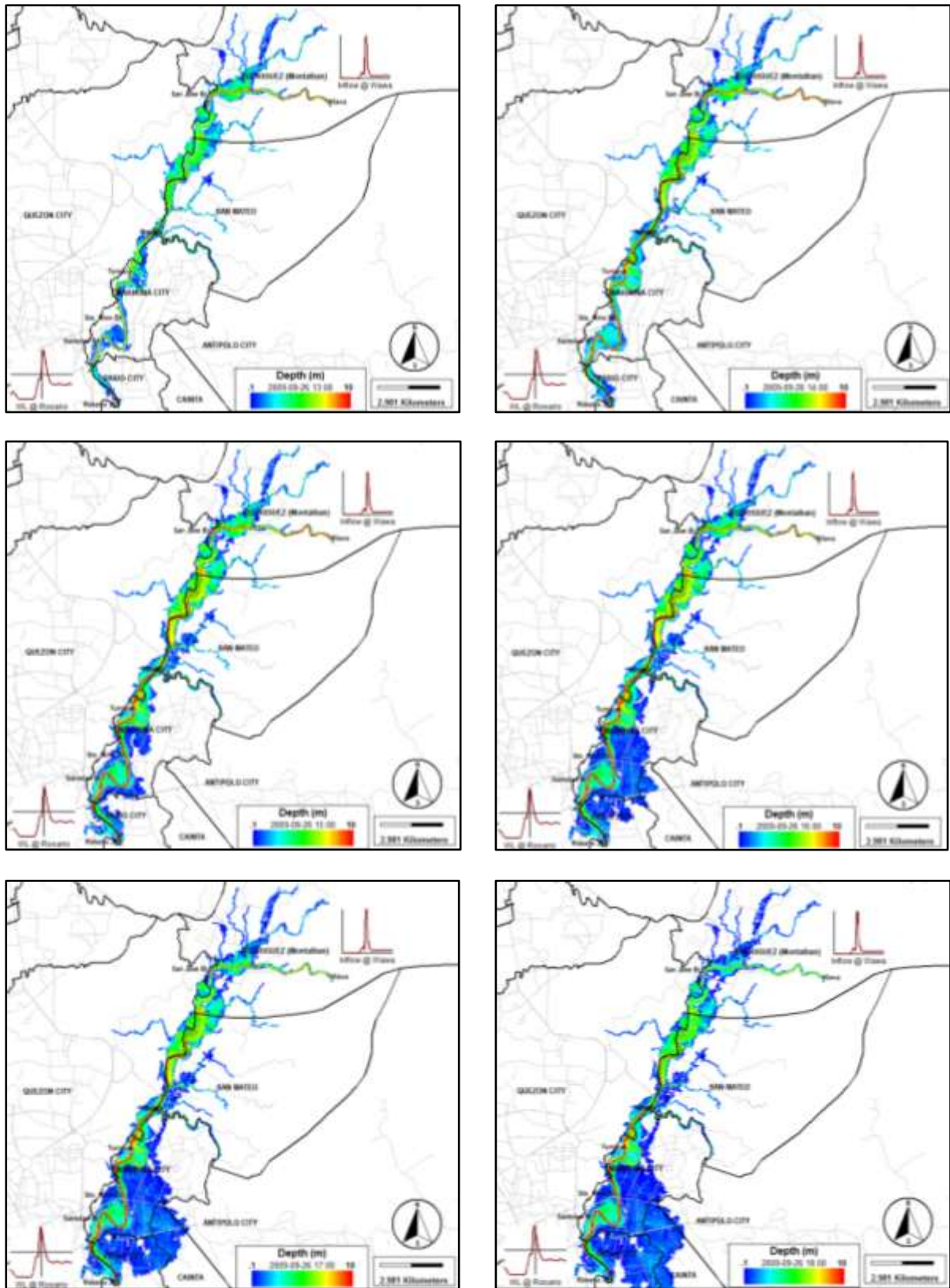
Figure 171. Snapshots of the evolution of flooding during the *September 2009 Ondoy* event in Marikina River and tributaries as simulated by the 2D EFDC model. The figure shows flood depths from 1:00 PM until 6:00 PM of Sep. 26.
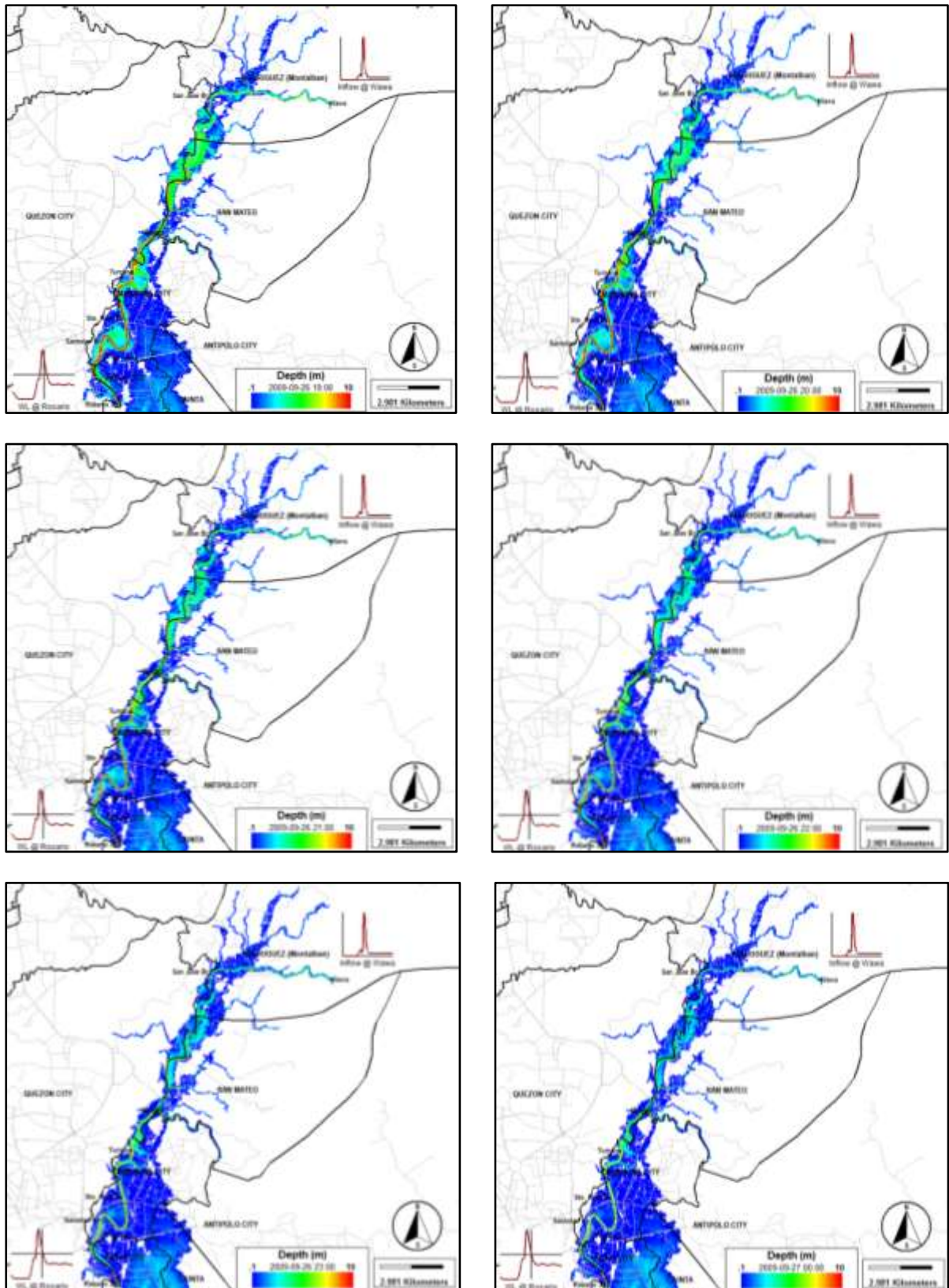
Figure 172. Snapshots of the evolution of flooding during the *September 2009 Ondoy* event in Marikina River and tributaries as simulated by the 2D EFDC model. The figure shows flood depths from 7:00 PM of Sep. 26 until 12:00 AM of Sep. 27.
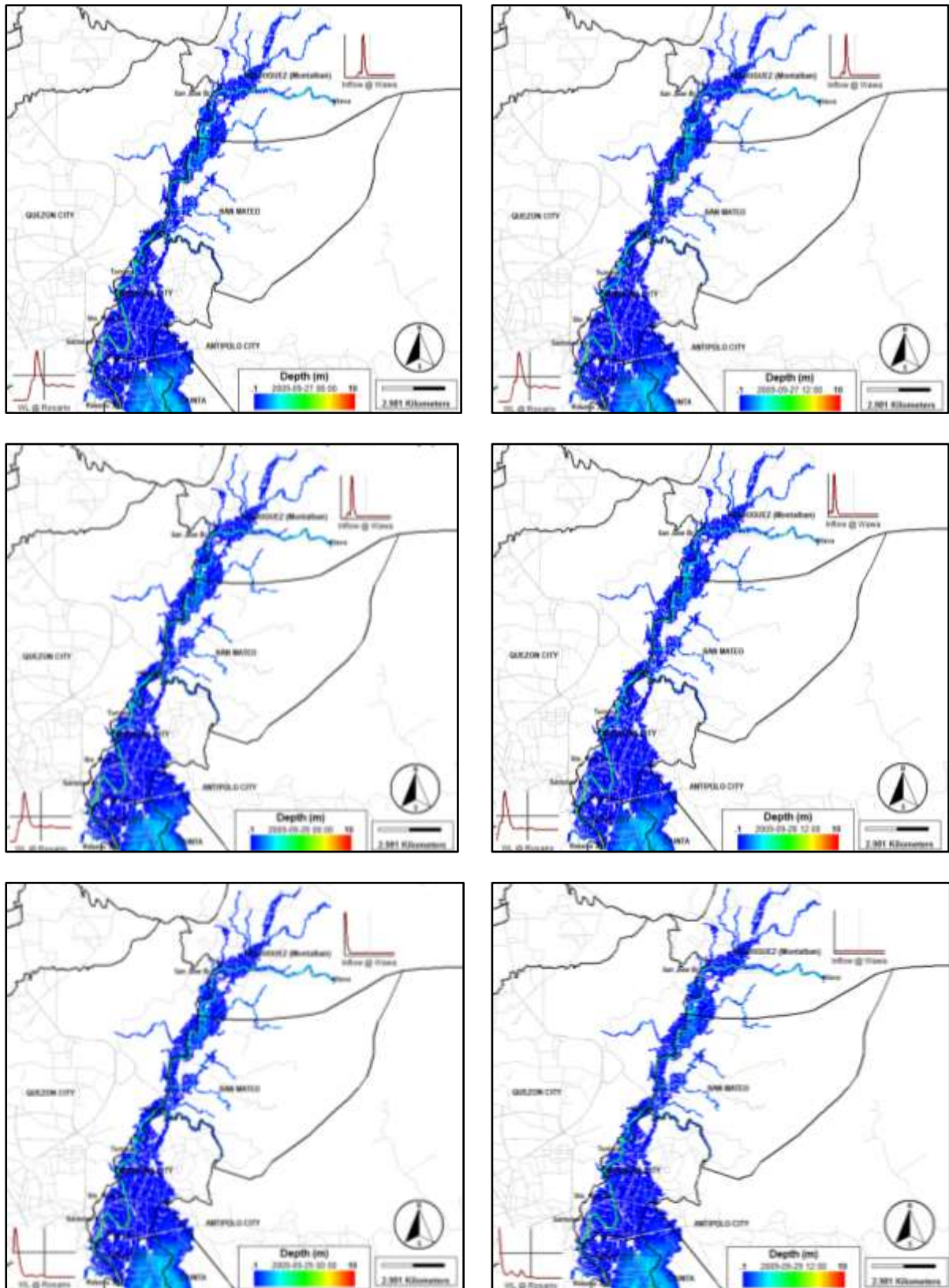
Figure 173. Snapshots of the evolution of flooding during the *September 2009 Ondoy* event in Marikina River and tributaries as simulated by the 2D EFDC model. The figure shows flood depths from 6:00 PM of Sep. 27 until 12:00 PM of Sep. 29.
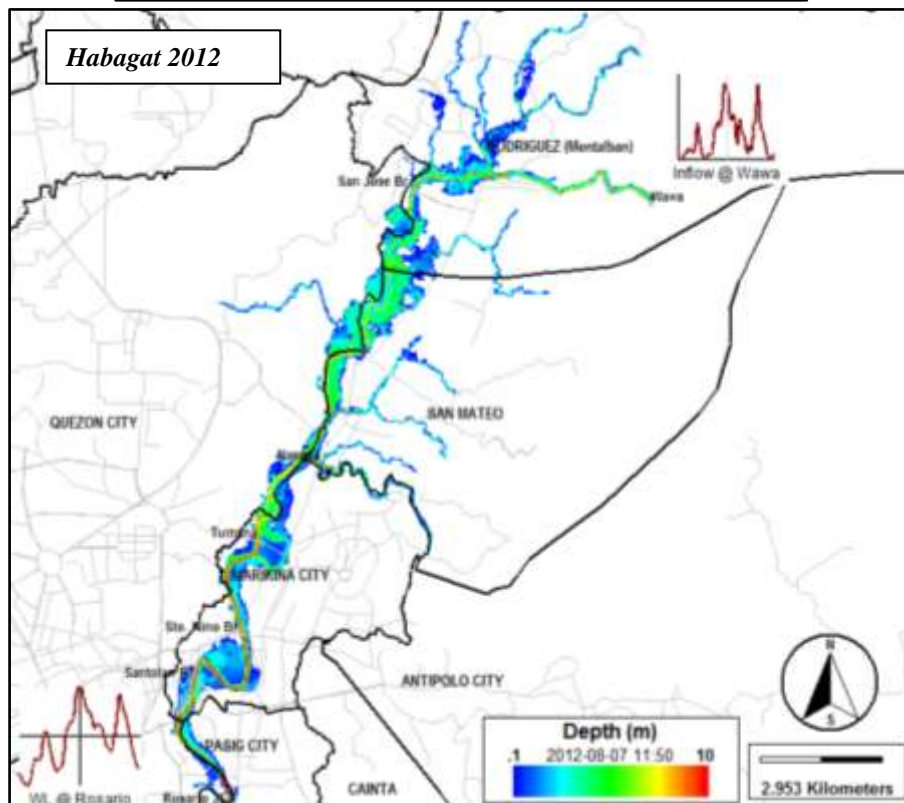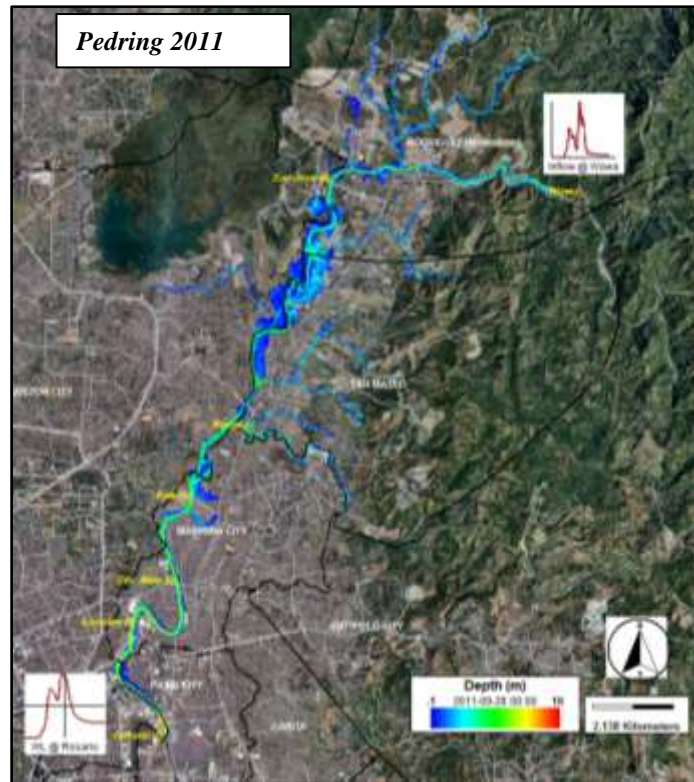
Figure 174. Snapshots of flooding simulated by the 2D EFDC model for *Pedring 2011* and *Habagat 2012* events.

Chapter Summary

In this chapter, actual flood events such as the September 2009 Typhoon Ondoy, the September 2011 Typhoon Pedring, and the August 2012 Habagat events were reconstructed through the use of watershed hydrologic models (HEC HMS) combined with a 2-dimensional flood model (EFDC). The reconstruction was done by:

- Inputting rainfall data of above events that were recorded by different rainfall stations into a calibrated HEC HMS model to compute for the volume per unit time at which runoff or flood water goes into Marikina River from different locations (upstream watersheds) in Marikina River Basin.
- The computed volume per unit time (also called "infows" or "discharge") at each point of entry into the Marikina River is then used as inputs into the 2-dimensional flood model of Marikina River. The 2D model determines the movement and depth of water as it passes into Marikina River, including how it overflows from the river.

Although not shown, simulation of flooding due to hypothetical, extreme rainfall events were also done using the same approach for the simulation of actual flood events. However, instead of actual rainfall events Rainfall Intensity Duration Frequency (RIDF) data of rainfall events with 2, 5, 10, 25, 50 and 100-year return periods was used.

All the 2D flood simulations (actual and hypothetical events) are available for viewing at Project 3's website (http://dge.upd.edu.ph/proj3/). To better appreciate the 2D flood simulation results, they were converted into video/animations.

Chapter 11. Summary of Findings, Conclusions and Recommendations

In this project, flood models consisting of HEC HMS and HECRAS models for two major river basins in Metro Manila namely Marikina River Basin and San Juan River Basin, were developed through utilization of data obtained from field observations, Remote Sensing (RS), Geographic Information System (GIS), and hydrological and hydraulic simulations.

The basic inputs of the models of MRB and SJRB such as river and floodplain topography, land-cover, soil information, actual flood information, and hydrological data were generated from different sources such as remotely sensed images, surveying and cartographic data, and rainfall and water level monitoring stations.

GIS was found to be very important in this project as it made possible the incorporation of all components for the modeling, simulation, and analysis. The role of GIS as information retrieval tool for disaster response and prevention is exemplified by the I aM AWaRe application that was developed in this project.

Marikina River Basin Flood Model

Based on the results of independent validations using observed data, it was shown that the MRB HEC HMS model has more than satisfactory performance in simulating discharge due to rainfall events. Its coefficient of model efficiency E ranges from 0.77 to 0.88. On the other hand, the results of the comparison of the simulated water levels with observed data indicates that the use of the calibrated HEC HMS model to simulate discharge and converting this discharge into water levels using rating curves provides a fast and relatively accurate way of forecasting water levels at MONTALBAN and STO. NINO stations. The average water level errors are relatively low, while the RMS errors indicate sub-meter accuracy of the predicted water levels. The HEC HMS model was also found to simulated peak flows ahead of the observed peaks flows by 40 minutes to 1 hours and 10 minutes. For flood inundation mapping in Marikina River and tributaries, the combined HEC HMS-HEC RAS models can predict flood extent during rainfall with accuracy ranging from 64-79%, which is relatively good and comparable to results of other studies. With these results, the MRB flood model can be utilized for water level forecasting, reconstruction of actual flood events, and for simulation of flooding due to hypothetical and extreme rainfall events.

Discharge hydrographs and maps of depths and hazards were generated for the *Ondoy* 2009, *Pedring* 2012 and *Habagat* 2012 flood events through the use of the calibrated and validated HEC HMS and HEC RAS models. The flood depth and flood hazard maps show the magnitude and extent of flooding due to bank overflows. Should similar flood events occur again in the future, the flood hazard maps would provide important information for preparation, evacuation, and damage estimation.

One of the important findings is the results of the simple analysis on the potential of the calibrated HEC HMS model as an early warning system during extreme flood events in Marikina River. It was shown that should an extreme rainfall event with intensity similar to that of the *Ondoy* event occurred again, there is a lag time of at least 5 to 7 hours before the effect of the extreme rainfall event is felt downstream areas such as Wawa, Montalban, Nangka, Tumana, Sto. Nino and Rosario JS. This number of hours can be utilized to prepare for evacuation provided that the peak intensity is known together with the accumulated rainfall.

The flood hazard maps generated for Marikina River and tributaries indicate increase in flood affected areas as the rainfall return period increases. The areas most affected in all type of events are in the upstream portion of the domain, specifically the barangays of San Mateo, Rizal (e.g., Maiy, Guinayang, Malanday, Dulong Bayan, Gitnang Bayan) and portions of barangays of Quezon City (e.g., Bagong Silangan).

In the downstream where Marikina and Pasig Cities are located, flooding due to 2-year rainfall is found to be not significant. But for rainfall events with return period greater than 2 years, the hazard due to flooding is found to be significant, especially in Nangka, Tumana, Concepcion Uno, Malanday, Sto. Nino, Jesus dela Pena, Santa Elena, Industrial Valley, and Calumpang. All these barangays have medium to high flood hazard levels.

San Juan River Basin Flood Model

The HEC HMS model for San Juan River Basin was found to have "good" performance in predicting discharge hydrographs at two upstream stations namely Quezon Avenue and E. Rodriguez, although the model simulated hydrographs did not perfectly matched those of the observed data.

One of the limitations during the calibration of the model was the effects of tide in the downstream portion of the model, especially at those sub-basins and reaches downstream of E. Rodriguez station. These parameters of these model elements were not subjected to optimization.

The calibrated model was then used to simulate discharge hydrographs of actual and hypothetical flood events. From the discharge hydrographs, peak flows were extracted and used as input to the HEC RAS model to create flood depth maps and flood hazard maps.

In general, the flood hazard maps indicate increase in areas affected by high hazards as rainfall events becomes extreme (e.g., from 2-year to 100-year). The areas most affected by high hazards are along San Juan River, San Francisco River, and Talayan Creek.

Near-real Flood Extent Monitoring and Water Level Forecasting

Aside from the flood depth and flood hazards maps that the project has generated for Marikina River and San Juan River Basins, another major output of the project is an online application called I aM AWaRe. The app is a online geo-visualization tool for monitoring flood inundation and forecasting of water levels in rivers as applied to the Marikina, San Juan

and Pasig Rivers in Metro Manila, Philippines. I aM AWaRe provides near-real time information (at 10-minute interval depending data availability) on the current extent of flooding along the river and the areas that are presently flooded, as well as forecasts on how water level will rise (or recede) at different locations along the river as rainfall events occur in the watersheds.

The flood inundation extent information generated by I aM AWaRe for the three rivers have been contributed to the Project NOAH (Nationwide Operational Assessment of Hazards) of the Philippine's Department of Science and Technology at http://noah.dost.gov.ph. The information is accessed by clicking on Flood Map –> Flood Inundation Monitoring.

Although it is already made available in Project NOAH, a more dedicated app just like I aM AWaRe is necessary especially if we only wanted to get informed about current inundation condition in rivers as well as forecast of water levels.

2D Flood Modeling

A two dimensional approach of modeling floods in Marikina River was also conducted by coupling the HEC HMS with the 2D hydraulic model based on the Environmental Fluid Dynamics Code (EFDC). Actual flood events such as the September 2009 *Ondoy*, the September 2011 *Pedring*, and the August 2012 *Habagat* events were reconstructed. Simulation of flooding due to hypothetical, extreme rainfall events were also done using the same approach for the simulation of actual flood events. However, instead of actual rainfall events Rainfall Intensity Duration Frequency (RIDF) data of rainfall events with 2, 5, 10, 25, 50 and 100-year return periods was used.

The results illustrated the usefulness of the 2D model in the reconstruction of flooding that had occurred in Marikina River, especially that of the *September 2009 Ondoy* event. The 2D model portrayed very well the evolution of flooding, especially as water from the upstream watersheds enters Marikina River, its overflow from the river banks, and the flood propagation from the banks towards the floodplain.

All the 2D flood simulations (actual and hypothetical events) are available for viewing at Project 3's website (http://dge.upd.edu.ph/proj3/). To better appreciate the 2D flood simulation results, they were converted into video/animations.

Conclusions and Recommendations for Future R&D Work

The HEC HMS and HEC RAS models developed in this project can be eventually applied at an operational scale by the flood forecasting and warning system (FFWS) program of PAGASA and the flood control offices in the Marikina River Basin and in the San Juan River Basin. It has been presented that the models are capable of providing the details necessary for the development of an accurate and reliable forecasting for assessing disaster risks, especially for extreme rainfall scenarios. Examples of which are estimated extent, duration and degree (depths) of the flood that is about to occur at any given amount of rainfall. This is exemplified by the flood depth and hazard maps. On the other hand, the 2D

simulation results can help us analyze and understand the characteristics of floods caused by torrential rainfall, its risk implications for the community and its effects to the environment.

One of the activities that was not undertaken is the use of the generated flood hazard maps in estimating the impacts of flooding to land-cover, infrastructures such as buildings, and population, including areas of barangays in the project areas. This is important especially if flooding of magnitudes similar to those of *Ondoy* 2009, *Pedring* 2012 and *Habagat* 2012, or if flooding of similar nature to those simulated using hypotherical rainfall scenarios will happen in the near future.

The purpose of estimating impacts of flooding to land-cover is to identify how much built-up areas, vegetated areas, and uninhabited areas within the model domain could be affected by flooding. The land-cover data that can be used in the analysis is the same land-cover map that was derived from the ALOS AVNIR-2 satellite image. The classes could be aggregated as follows to simplify the analysis: vegetated areas correspond to portions of the model domain covered by grassland and shrubs and trees; uninhabited areas are those whose land-cover classes are bare soil, excavations, exposed river beds and water bodies. The result of this analysis can help us determine the degree of exposure of land-cover types to flooding (e.g., if flooding will have more impact to uninhabited areas than built-up areas, then this uninhabited areas must not be converted to built-up areas).

The number of buildings that could be affected by flooding according to type of hazard can also be identified by overlaying building footprints to flood hazard layers.

The number of population and the area of barangays within the model domain that could be affected by flooding according to type of hazard can also determined through overlay analysis of barangay boundaries. Barangay boundaries and recent population data (e.g., 2010) can be obtained from the National Statistic Office (NSO). To estimate the number of affected population per barangay, the area affected by flooding is determined by intersecting the boundaries with the flood hazard layers. Population is then estimated by multiplying the barangay's population density (derived from total population and barangay area) with the area affected by flooding.

Bibliography

[1] E Morin, Y Jabocy, S Navon, and E Bet-Halachmi, "Towards flash-flood prediction in the dry Dead Sea region utilizing radar rainfall information," *Advances in Water Resources*, vol. 32, pp. 1066-1076, 2009.

[2] C C Abon, C P David, and N B Pellejera, "Reconstructing the Tropical Storm Ketsana flood event in Marikina River, Philippines," *Hydrology and Earth System Sciences*, vol. 15, no. 4, pp. 1283-1289, 2011.

[3] M H Cheng, "Natural disasters highligh gaps in preparedness," *The Lancet*, vol. 374, no. 9698, pp. 1317-1318, 2009.

[4] M Heistermann et al., "Using the new Philippine radar network to reconstruct the Habagat of August 2012 monsoon event around Metropolitan Manila," *Natural Hazards and Earth System Science*, vol. 13, no. 3, pp. 653-657, 2013.

[5] P A Burrough, *Principles of Geographical Information Systems for Land Resources Assessment*.: Oxford University Press, 1986.

[6] American Meteorological Society. (2013) Glossary of meteorology. [Online]. http://glossary.ametsoc.org/wiki/Flood

[7] Wikipedia. (2013) Wikipedia. [Online]. http://en.wikipedia.org/wiki/Flood

[8] United Nations. (2004) Guidelines for reducing flood losses. [Online]. http://www.unisdr.org/

[9] UN ESCAP, "Guidelines and manual on land-use planning and practices in watershed management and disaster reduction," 1997. [Online]. http://www.unescap.org/enrd/water_mineral/pubs/watershed/GUIDELINE-6-97.pdf

[10] C A Doswell, H E Brooks, and R A Maddox, "Flash flood forecasting: an ingredients-based methodology," *Weather Forecast*, vol. 11, pp. 560-581, 1996.

[11] J A Ramirez, "Prediction and modeling of flood hydrology and hydraulics," in *Inland Flood Hazards: Human, Riparian and Aquatic Communities*.: Cambridge University Press, 2000.

[12] R A Badilla, "Flood modelling in Pasig-Marikina river basin," Enschede, The Netherlands, 2008.

[13] USACE HEC. (2013) HEC HMS. [Online]. http://www.hec.usace.army.mil/software/hec-hms/

[14] Z Yusop and A Katimon, "Runoff characteristics and application of HEC-HMS for modelling stormflow hydrograph in an oil palm catchment," *Water Science and Technology*, vol. 56, no. 8, pp. 41-48, 2007.

[15] X Chu and A Steinman, "Event and continuous hydrologic modeling with HEC-HMS," *Journal of Irrigation and Drainage Engineering*, vol. 135, no. 1, pp. 119-124, 2009.

[16] E Abushandi and B Merkel, "Modelling rainfall runoff relations using HEC-HMS and IHACRES for a single rain event in an arid region of Jordan," *Water Resources Management*, vol. 27, no. 7, pp. 2391-2409, 2013.

[17] C Chang and W Huang, "Hydrological modeling of typhoon-induced extreme storm runoffs from Shihmen watershed to reservoir, Taiwan," *Natural Hazards*, vol. 67, no. 2, pp. 747-761, 2013.

[18] M De Silva, S Weerakoon, and S Herath, "Modeling of event and continuous flow hydrographs with HEC-HMS; a case study in the Kelani River Basin, Sri Lanka," *Journal of Hydrologic Engineering*, vol. 10.1061/(ASCE)HE.1943-5584.0000846, 2013.

[19] J Santillan, M Makinano, and E Paringit, "Integrated Landsat image analysis and hydrologic modeling to detect impacts of 25-year land-cover change on surface runoff in a Philippine watershed," *Remote Sensing*, vol. 3, no. 6, pp. 1067-1087, 2011.

[20] S G Catane, C C Abon, R M Saturay Jr., E P Mendoza, and K M Futalan, "Landslide-amplified flash floods—the June 2008 Panay Island flooding, Philippines," *Geomorphology*, vol. 169, pp. 55-63, 2012.

[21] C C Abon, C C David, and G Q Tabios III, "Community-based monitoring for flood early warning system: An example in central Bicol River basin, Philippines," *Disaster Prevention and Management*, vol. 21, no. 1, pp. 85-96, 2012.

[22] G W Brunner, "HEC RAS River Analysis System Hydraulic Reference Manual," Davis, California, 2010.

[23] F E Hicks and T Peacock, "Suitability of HEC-RAS for flood forecasting," *Canadian Water Resources Journal*, vol. 30, no. 2, pp. 159-174, 2005.

[24] M S Horritt and P D Bates, "Evaluation of 1D and 2D numerical models for predicting river flood inundation," *Journal of Hydrology*, vol. 268, no. 1, pp. 87-99, 2002.

[25] M R Knebl, Z L Yang, K Hutchison, and D R Maidment, "Regional scale flood modeling using NEXRAD rainfall, GIS, and HEC-HMS/RAS: a case study for the San Antonio River Basin Summer 2002 storm event," *Journal of Environmental Management*, vol. 75, no. 4, pp. 325-336, 2005.

[26] E Pedzisai, "Rainfall-runoff modelling for Flashfloods in Cuong Thinh Catchment, Yen Bai Province, Vietnam," Enschede, The Netherlands, 2010.

[27] F Fotopoulos, C Makropoulos, and M A Mimikou, "Flood forecasting in transboundary catchments using the Open Modeling Interface," *Environmental Modelling and Software*, vol. 25, pp. 1640-1649, 2010.

[28] R J Moore, V A Bell, and D A Jones, "Forecasting for flood warning," *Comptes Rendus Geoscience*, vol. 337, pp. 203-217, 2005.

[29] J Sanyal and X X Lu, "Application of remote sensing in flood management with special reference to monsoon Asia: a review," *Natural Hazards*, vol. 33, no. 2, pp. 283-301, 2004.

[30] C R Yang and C T Tsai, "Development of a GIS-based flood information system for floodplain modeling and damage calculation," *Journal of the American Water Resources Association*, vol. 36, no. 3, pp. 567-577, 2000.

[31] E T Engman, "Remote sensing applications to hydrology: future impact," *Hydrological Sciences*, vol. 41, pp. 637-647, 1996.

[32] H Bach, M Braun, G Lampart, and W Mauser, "Use of remote sensing for hydrological parameterisation of Alpine catchments," *Hydrology and Earth System Sciences*, vol. 7, pp. 862-876, 2003.

[33] A M Melesse and S F Shih, "Spatially distributed storm runoff depth estimation using Landsat images and GIS," *Computers and Electronics in Agriculture*, vol. 37, pp. 173-183, 2002.

[34] A Pandey, V M Chowdary, B C Mal, and M Billib, "Runoff and sediment yield from a small agricultural watershed in India using the WEPP model," *Journal of Hydrology*, vol. 348, pp. 305-319.

[35] S J Bhuyan, J K Koelliker, L J Marzen, and J A Harrington, "An integrated approach for water quality assessment of a Kansas watershed," *Environmental Modelling and Software*, vol. 18, pp. 473-484, 2003.

[36] P D Bates, M S Horritt, C N Smith, and D Mason, "Integrating remote sensing observations of flood hydrology and hydraulic modelling," *Hydrological Processes*, vol. 11, no. 14, pp. 1777-1795, 1997.

[37] P D Bates, "Remote sensing and flood inundation modelling," *Hydrological Processes*, vol. 18, no. 13, pp. 2593-2597, 2004.

[38] G Schumann, P D Bates, M S Horritt, P Matgen, and F Pappenberger, "Progress in

integration of remote sensing-derived flood extent and stage data and hydraulic models," *Reviews of Geophysics*, vol. 47, no. 4, 2009.

[39] P A Townsend and S J Walsch, "Modeling floodplain inundation using an integrated GIS with radar and optical remote sensing," *Geomorphology*, vol. 21, no. 3, pp. 295-312, 198.

[40] K Takeuchi, "Closing the gap between science and practice to reduce human losses in hydro-meteorological disasters," in *Geophysical Hazards*, T Beer, Ed. Netherlands: Springer, 2010, pp. 105-114.

[41] J C Felizardo, "Reducing disasters in the densely populated Manggahan floodway and the adjoining Laguna Lake shoreline in Metro Manila," in *9th International River Symposium*, Brisbane, Australia, 2006.

[42] D B Zoleta-Nantes, "Differential impacts of flood hazard among the street children, the urban poor and residents of wealthy neighborhoods in Metro Manila, Philippines," *Mitigation and Adaptation Strategies for Global Change*, vol. 7, no. 3, pp. 239-266, 2002.

[43] H Madsen and C Skotner, "Adaptive state updating in real-time river flow forecasting - a combined filtering and error forecasting procedure," *Journal of Hydrology*, vol. 308, pp. 302-312, 2005.

[44] E C Paringit, C Cruz, and G Tumanda, "Surveys and Measurement Technologies for Flood Control, Mitigation and Management System: Project 2: Establishment of spillover elevation along flood prone river systems - Marikina-Pasig River," UP Training Center for Applied Geodesy and Photogrammetry, Quezon City, 2010.

[45] N K Pavlis, S A Holmes, S C Kenyon, and J K Factor, "The development and evaluation of the Earth Gravitational Model 2008 (EGM2008)," *Journal of Geophysical Research: Solid Earth (1978-2012)*, vol. 117, no. B4, 2012.

[46] M Bouvet, P Goryl, G Chander, R Santer, and S Sauiner, "Preliminary radiometric calibration assessment of ALOS AVNIR-2," in *Proceedings of the IEEE International Geoscience and Remote Sensing Symposium – IGARSS 2007*, 2007, pp. 2673-2676.

[47] A Elumnoh and R P Shrestha, "Application of DEM data to Landsat image classification: evaluation in a tropical wet-dry landscape of Thailand," *Photogrammetric Engineering & Remote Sensing*, vol. 66, no. 3, pp. 297-304, 2000.

[48] P Watanachaturaporn, M K Arora, and P K Varshney, "Multisource classification using support vector machines: an empirical comparison with decision tree and neural network classifiers," *Photogrammetric Engineering and Remote Sensing*, vol. 74, pp. 239-246,

2008.

[49] K Fitzpatrick-Lins, "Comparison of sampling procedures and data analysis of a land-use and land-cover map," *Photogrammetric Engineering and Remote Sensing*, pp. 349-366, 1981.

[50] Digital Globe, "The Benefits of the 8 Spectral Bands of WorldView-2," Digital Globe White Paper 2009.

[51] ITT - Visual Information Solutions. (2010) ENVI 4.8 Help.

[52] X Gong, L G Markluing, and S Tsuji, "Land Use Classification," in *14th Meeting of the London Group on Environmental Accounting*, Canberra, Australia, 2009.

[53] NCRS, *Urban Hydrology for Small Watersheds TR-55*. Washington DC, USA: Natural Resources Conservation Service, Conservation Engineering Division, US Department of Agriculture, 1986.

[54] USACE, "Hydrologic Modeling System HEC-HMS Technical Reference Manual," United States Army Corps of Engineers, Hydrologic Engineering Center, Davis, California, 2000.

[55] USACE, "Geospatial Hydrologic Modelling Extension HEC-GeoHMS User's Manual, Version 1.1. ," United States Army Corps of Engineers, Hydrologic Engineering Center, Davis, California, 2003.

[56] NCRS, "Chapter 7 Hydrologic Soil Groups," in *National Engineering Handbook, Part 630 Hydrology*.: Natural Resources Conservation Service, US Department of Agriculture, 2007.

[57] V T Chow, D R Maidment, and L W Mays, *Applied Hydrology*. New York: McGraw-Hill, 1998.

[58] PAGASA, "Rainfall-Intensity Duration Frequency (RIDF) Curve for PAGASA-Science Garden Station Based on 41 Years of Data," Hydrometeorological Data Applications Section, Hydro-Meteorology Division, Philippine Atmospheric, Geophysical and Astronomical Services Administration, Quezon City, Philippines, 2012.

[59] J R Santillan et al., "Near-real time flood extent monitoring in Marikina River, Philippines: model parameterisation using remotely-sensed data and field measurements," in *Proceedings of the 33rd Asian Conference on Remote Sensing*, Pattaya, Thailand, 2012.

[60] D N Moriasi et al., "Model evaluation guidelines for systematic quantification of accuracy in watershed simulations," *Transactions of the ASABE*, vol. 50, pp. 885-900,

2007.

[61] V M Ponce. (2011, November) Unsteady flow with HEC-RAS. [Online]. http://ponce.sdsu.edu/unsteady_flow_with_hec_ras.html

[62] P D Bates and A P De Roo, "A simple raster-based model for flood inundation simulation," *Journal of Hydrology*, vol. 236, no. 1, pp. 54-77, 2000.

[63] J M Hamrick, "A three-dimensional environmental fluid dynamics computer code: Theoretical and computational aspects," Virginia Institute of Marine Science, School of Marine Science, College of William and Mary, Virginia, 1992.

[64] USEPA. (2013, January) Environmental Fluid Dynamics Code (EFDC). [Online]. http://www.epa.gov/athens/wwqtsc/html/efdc.html

[65] S N Chan and J H Lee, "Impact of river training on the hydraulics of Shenzhen river," *Journal of Hydro-environment Research*, vol. 4, no. 3, pp. 211-223, 2010.

[66] Dynamic Solutions International. (2013) EFDC_Explorer 7.1.

Appendix 1. Publishable and Published Reports